Study of Physics and Mathematics Principles of Cuff-Based Blood Pressure Measurement Methods

by

Mariana Alvarado Alvarez

A thesis submitted in partial fulfillment of the requirements for the degree of

Doctor of Philosophy

Department of Physics

University of Alberta

Abstract

The two most important methods used to measure blood pressure, the cuff-based methods of oscillometry and auscultation, are analyzed in this work. The goal is to understand the principles and shortcomings of each method in order to suggest some improvements that can be immediately implemented in the devices used in their application, or in the development of an improved technique.

The discussion on the oscillometric method is approached by a study on the Maximum Amplitude Ratio Algorithm, believed to be one of the most common options that automated devices use to estimate blood pressure. The study includes analyzing different options of data representation and how this affects the accuracy of the method.

Blood pressure measurement through auscultation is boarded from the perspective of psychoacoustics to understand how the human operator perceives the Korotkoff sounds that define the measurement. A study on the masking of these sounds serves as the foundation for a proposed algorithm to automate the procedure.

Finally, physics-based mathematical models of the phenomena involved in each cuff-based measurement are derived based on models found in the literature. The equations obtained are compared to measured data by means of a non-linear least squares regression analysis, to determine which model most effectively represents the observed phenomena.

Acknowledgements

My first and most important acknowledgement, as well as the biggest thank you I can give, go to my husband for all his patience and help with this thesis. He unofficially became my co-co-supervisor, therapist, and editor, and is probably my biggest cheerleader to date. Without his support I'm sure this chapter of my life would have had quite a different ending.

I am also infinitely grateful to my supervisors, Dr. Wayne Hiebert and Dr. Raj Padwal, for all their teachings, guidance and support throughout the duration of this project. I'm sure it must have been hard at times, given the extraordinary conditions we found ourselves in, but all your ideas, contributions and feedback were very well received and very much appreciated.

The gratitude also extends to the members of my committee, Dr. Frank Hegmann and Dr. Mark Freeman, for gifting me with some of your time for meetings and thesis readings, and also offering valuable feedback and ideas.

My friends and family were also equally important pillars of my life during these times, especially the friends I met in Edmonton that made my stay so much better. I am thankful to them for turning Canada into my second home.

Finally, I would like to acknowledge and thank the institutions that made the completion of this PhD possible: the University of Alberta, for allowing me to learn and grow as a person and as a scientist, and to CONACyT (Consejo Nacional de Ciencia y Tecnologia) in Mexico, for giving me this opportunity and providing the necessary means so that I could fully focus on my studies and do my best.

Thank you!

Contents

List of Tables

List of Figures

List of Abbreviations

ABPM	Ambulatory Blood Pressure Measurement
APW	Arterial Pressure Waveform
BCG	Ballistocardiography
BIHS	British and Irish Hypertension Society
CVD	Cardiovascular Diseases
DBP	Diastolic Blood Pressure
DL	Difference Limen
DR	Diastolic Ratio
ECG	Electrocardiogram
ERB	Equivalent Rectangular Bandwidth
FEM	Finite Element Modelling
FFT	Fast Fourier Transform
FS	Fourier Series
IL	Intensity Level
KS	Korotkoff Sound
LHSM	Latin Hypercube Sample Matrix
MAP	Mean Arterial Pressure
MAR	Maximum Amplitude Ratio
ME	Mean of the Errors
MS	Maximum Slopes
NLLS	Non-Linear Least Squares
NN	Neural Networks
OBPM	Oscillometric Blood Pressure Measurement
OMW	Oscillometric Waveform
OMWE	Oscillometric Waveform Envelope
PP	Pulse Pressure
PPG	Photoplethysmography
PTT	Pulse Transit Time
PWV	Pulse Wave Velocity
SBP	Systolic Blood Pressure
SD	Standard Deviation
SDE	Standard Deviation of the Error

SNR	Signal-to-Noise Ratio
SPL	Sound Pressure Level
SR	Systolic Ratio

Declaration of Authorship

Some of the research conducted for this thesis forms part of a research collaboration between the Departments of Medicine and Physics of the University of Alberta, and the National Research Council, Canada. This work, included in chapter 2, has been published as M. Alvarado Alvarez, R. Padwal, J. Ringrose, A. Jalali and W. Hiebert, "Optimum waveform envelopes and amplitude ratios in oscillometric blood pressure estimation", *Blood Pressure Monitoring*, 2021, **26**:53–59. The data collection was done by the collaborators in the Department of Medicine, Drs. J. Ringrose and R. Padwal, and the filtering and processing of the data was done by A. Jalali. I was responsible for the final analysis of the data under the supervision of Dr. W. Hiebert.

Chapter 1

Introduction

Blood pressure (BP) is one of the four vital signs used to assess a person's health and quality of life. It is commonly measured in any routine physical examination, although simple and inexpensive devices allow for this vital sign to be measured in practically any location of convenience. Blood pressure is the measure of the amount of pressure blood exerts on the arterial walls during a cardiac cycle. It is expressed as a ratio of two quantities: the numerator is the pressure on the vessels during systole, when the heart contracts and expels blood to the system. This is known as systolic blood pressure (SBP). The denominator is the pressure on the vessels when the heart relaxes and fills with blood, or diastole, and it is known as diastolic blood pressure (DBP). These pressures are expressed in units of millimetres of mercury, or mmHg.

Maintaining a record of BP over time is important, since abnormalities or deviations from average values are good indicators of underlying conditions and other more serious diseases. For instance, hypertension, or raised blood pressure, presents no symptoms and is otherwise almost impossible to detect without periodic BP measurements, yet is the most important risk factor for cardiovascular diseases (CVD). The World Health Organization reports CVD as the leading cause of death in the world in 2019, with ischaemic heart disease in the first place [8].

Hypertension is also associated to other CVD, such as intracerebral haemorrhage, aneurysms, myocardial infarction and peripheral arterial disease [9], and has a strong correlation to chronic kidney disease and brain atrophy [10, 11]. Recent studies have also found that hypertension is one of the most common comorbidities in patients with COVID-19. While there is no evidence that hypertension is a risk factor for this disease, patients with hypertension were most likely to be more severely affected by it, particularly those who were not managing

this condition [12–15].

Hypertension affects approximately 1 in 5 Canadian adults and represents a significant burden in the national healthcare costs, which were estimated to be close to $14 billion CAD in 2010 ($1.4 billion in the province of Alberta) [16]. In 2014 the prevalence of hypertension in US adults over the age of 20 was 34%, and projections estimate that by 2030 approximately 41.4% of US adults will have hypertension [17].

It is evident, thus, that BP measurement is an important practice. The accuracy of the measurement is also critical, given that a systematic error of under/overestimating BP by 5 mmHg could misclassify millions of people and prevent them from getting necessary care, or exposing them to the burden of needless treatment [18].

The gold standard for BP measurement for many years has been auscultation with a mercury manometer, and this is the reference method against which all others must be compared. However, this was not the first method used, nor the only one. In the following section we briefly introduce some of the different BP measurement methods used, to give the reader a broader scope of the status of this research topic, its progress and complications.

1.1 Blood Pressure Measurement Methods

The most accurate, and one of the first ever used, method of obtaining beat-to-beat BP variations is through the invasive intra-arterial method. A cannula is inserted in the artery and, in modern times, a transducer converts the pressure variations in the artery into an electric signal that can be viewed in a monitor. Besides requiring special equipment and trained personnel, this method is painful and has the potential for infections and blood loss if there is an accidental disconnection of the tubing. For these reasons this method is usually reserved for patients in Intensive Care Units (ICUs), or in cases where an indirect method of measuring BP is not possible. In the earlier studies on BP measurement this method was used as the standard to compare the accuracy of indirect methods.

Methods to measure BP departed from invasive techniques with the discovery that the application of counter pressure to a limb could be used towards this end. The French physiologist E. J. Marey was responsible for the first experiments in 1876 that applied this concept. He realized that by applying counter pressure to the arm immersed in a water reservoir he could observe oscillations in the pressure inside the reservoir. At a critical counter pressure,

oscillations ceased and the arm blanched, indicating blood was no longer flowing through it [19].

The first sphygmomanometers, which are practical applications of this concept, developed by Marey and others were cumbersome and impractical for routine clinical use. A revolutionary advance in this technique came with the advent of pneumatic arm-encircling devices, which could be filled with water or inflated with air to apply counter pressure to a section of the arm or leg. Precursors to present-day cuffs are the devices proposed by Riva Rocci and Hill and Barnard. Using these cuffs and Marey's observations BP could be practically measured in the clinic, although at first only systolic pressure and mean arterial pressure (MAP) could be measured. Mean arterial pressure is the average pressure on the arteries during a cardiac cycle.

In 1907 the Russian surgeon Nikolai Korotkoff discovered that BP could be measured by auscultation using a pneumatic cuff and a stethoscope. He discovered the Korotkoff sounds, named in his honour, which are the basis of this method. The greatest advantage of auscultation over its precursors is that it was the only method available to measure both SBP and DBP.

The development of microprocessors and electronic transducers made it possible to revisit Marey's concept and develop a simplified, portable, and automated version of what is known as the oscillometric technique. This is another method that requires the use of a cuff and relies on the observed pressure oscillations inside the cuff to estimate BP. Automated BP measurement devices that operate under this method have become increasingly popular and are slowly replacing the auscultation method in most clinics.

Other methods to estimate BP that do not require a cuff have been developed in more recent years, although their accuracy is not as good as that of cuff methods. One example is arterial tonometry, which consists of flattening a superficial arterial wall against an underlying structure, preferably bone, and using a sensor plate to detect the force produced by blood pressure on the artery [20]. Tonometry delivers satisfactory results when compared against invasive BP measurements in normotensive subjects and in patients with uncomplicated hypertension [21], however it does not always provide accurate values of SBP and DBP. It depends on proper sensor positioning and is very susceptible to motion artifacts.

Another example is that of the volume clamp method, which consists of using a small cuff around a finger with a diode on one side of the finger and a photodetector on the opposite

side. Light transmitted from the diode and detected on the other side is proportional to the volume of tissue it passes, which changes each cardiac cycle with the passage of blood. Using this relationship, the small cuff is inflated and deflated accordingly to maintain a constant volume, and the variations in pressure in the cuff can be detected and correlated to arterial pressure. This is often referred to as the Peñaz method, given that Dr. J. Peñaz was the first to describe this device with a feedback loop to control cuff volume [22].

This type of device is also very susceptible to motion artifact, given that its meant to be applied to the fingers. Another disadvantage is that SBP and DBP estimated at this location are different to those measured at the upper arm, where cuff methods measure them. BP at the peripheral arteries is usually greater than at the central arteries given that reflection sites are closer at these locations and that these arteries are stiffer. Estimates of BP at both locations are not usually directly correlated and accuracy can be greatly compromised.

A popular method in cuff-less BP estimation is the use of pulse wave velocity (PWV) or pulse transit time (PTT), which essentially measure the propagation rate of pressure pulses to determined locations of the arterial tree. This is done by detecting pressure pulses at two different locations of the body, like the wrist and the leg, for instance, and measuring the time difference between peaks or troughs of these two pulses with the use of a third signal as reference to correlate them. This third signal is generally one of the peaks from an electrocardiogram (ECG). These measures have been found to relate to BP and the presence of hypertension [23–26], although results may not be consistent depending on the site of measurement in the case of PTT in particular [27]. Other major drawbacks of this method are the need for additional equipment to obtain the ECG, and the difficulty in making an accurate estimate of the distance between the measurement sites.

1.1.1 State of the Art

An important part of current research dedicated to BP measurement is related to improving existing methods. For instance, novel techniques that were not easily available in the past, such as neural networks and artificial intelligence, are used to process the information obtained with the current measurement techniques. On the other hand, different features of the data obtained with current methods that were not previously considered are also extensively researched in the hopes of obtaining a parameter that better correlates to BP. Such is the focus of the work presented in this thesis.

The other topic of interest in current BP measurement research is the development of new devices with a very important feature: the ability to continuously monitor BP without inconveniencing the user. The importance of this feature is perhaps better appreciated in the case of the diagnosis of hypertension. The gold standard for hypertension diagnosis is the ambulatory blood pressure measurement (ABPM), which consists of tracking BP for a period of 24 hours to observe its progression during everyday activities and sleep. This ABPM is particularly important since it reveals a broad picture of a subject's BP profile instead of a single specific moment in an uncharacteristic situation, such as the physician's office. It is also an ideal method to reveal nocturnal BP patterns, where preferably mean BP should "dip" to values 10% lower than awake mean BP. Evidence of the contrary is associated with elevated risk of heart, brain, and kidney injury, and CVD [28].

Currently, ABPM is done with specialized oscillometric devices consisting of a cuff worn on the upper arm and a monitor attached to a strap that can be worn around the neck or fastened to the belt. These devices collect BP measurements every 30 to 60 minutes during the day, and at least every 60 minutes during the night. Needless to say, these devices are cumbersome and uncomfortable, and can make the user self-conscious, purposefully modifying normal daytime activities. There is also some evidence that the use of these monitors affects the sleep BP patterns, which prevents from making an adequate assessment of the occurrence or absence of dipping in mean nighttime BP [29].

For this reason, the newly developed devices are intended to be cuff-less and wearable, or at least easily accessible. A popular approach is to design wearable technology that estimates BP based on PTT. Some of these new devices make use of photoplethysmography (PPG), which consists in detecting light absorption/reflection in tissues, to detect the blood volume waveform where the timing of the pulses can be measured. This is because photodiodes and photodetectors can be easily implemented in strap-based [30] or watch-based [31] configurations, which can also include an ECG as an additional strap or as part of the watch.

Fibre optic technology is another candidate for cuff-less watch-based devices [43]. Fibre Bragg gratings are highly sensitive to strain variations, which in principle makes them a good candidate to detect the faint pulsations of the radial artery at the wrist. However, they are a costly alternative to other strain-sensing technology, and the main issue with such sensitive transducers is the removal of motion artifact.

Ballistocardiography (BCG), which is the measurement of the reaction forces of the body

in response to the ejection of blood from the heart to the aorta, has received renewed attention as an alternative to the ECG reference in PTT [32] or as a separate method of estimating BP. This can be done either by relating the timing between the BCG and the PPG waveforms to BP [33] or by relating specific features of the BCG waveform to BP [34]. The advantage of BCG is that sensors can be easily implemented in simple everyday objects, such as seat cushions, mattresses or weight scales.

Neural networks have also been an important tool in the development of wearable technology. An example is their use in the analysis of certain features in the PPG signal to derive BP estimates [35, 36].

Smartphone technology has also been exploited in the search of a convenient method to estimate BP, given that this is the technology that perhaps the vast majority of people is most familiar with. Heart sound signals measured with the smartphone's microphone or a stethoscope attachment have been analyzed in their frequency domain [37] or with respect to pulse signals recorded by the smartphone's camera [38].

Finally, an interesting development in sensors that has great potential in the measurement of BP is the incorporation of flexible display technology in the design of photodiodes and detectors for PPG that can be worn in a smart bandage-style configuration [39], and the development of the called "epidermal electronics", which consist of stretchable strain sensors that can be adhered to the skin similar to stickers or temporary tattoos [40–42]. While this technology has not yet been tested for BP estimation, they show promise as wearable, durable technology.

1.2 Objectives

Naturally, the most appealing topic of research, based on the introduction given above, is the development of cuff-less technology for ambulatory BP measurement. Large companies have entered the race to develop an accurate method of estimating BP that can also be implemented in devices as simple as smart watches, for instance. However, the most challenging hurdle this technology needs to overcome first is ensuring cuff-less BP estimates correspond to BP measurements obtained through traditional methods.

The BP measurements cuff-less devices should aim to replicate are those obtained through manual auscultation, which we have pointed out previously, is the gold standard in BP

measurement. Unfortunately, manual auscultation requires specific conditions and trained personnel in order to be performed correctly. This can slow down the progress of device development and even introduce unwanted sources of error, which we'll discuss in following chapters. The most convenient solution is to use automated devices, although there exist few automated devices that estimate BP through auscultation, and furthermore, there is no guarantee that they can faithfully reproduce the results of manual auscultation.

Therefore, the first approach of most research groups to test and calibrate novel ambulatory devices is by comparison to automated oscillometric devices. This is a reasonable option, given the convenience of using these oscillometric devices which, as we shall see, require no training or specialized background for use. However, it should be noted that oscillometry is not the ideal reference because of some accuracy issues it has compared to the gold standard (auscultation) that will also be subject of commentary in the following chapters.

The author believes, thus, that before continuing the discussion of ambulatory devices, the two basic cuff-based methods of auscultation and oscillometry, and their particular challenges, have to be addressed first.

As is generally the case, unexpected issues and complications arising in any physical system can be overcome with a deeper understanding of the phenomena and processes involved. Physics-based mathematical analyses of these cuff-based BP measurement systems, however, are not of the highest priority in recent literature. The oscillometric method relies on empirical results that currently do not have a well-defined theoretical background and the phenomenon of Korotkoff sounds that define the method of BP measurement through auscultation, and that will be discussed in detail in the following chapters, has not been fully explained either. Some of the available models have been derived from *in vitro* experiments, while others from general principles of fluid dynamics and linear mechanics. Although these models seem to reproduce ideal case measurements, to the author's knowledge, they have not been tested in an inverse-problem scenario to verify whether they can be applicable to real data.

The main objective of this work is, thus, to focus on these two cuff-based BP measurement methods, from understanding the most general principles of their operation, to studying the phenomena and processes discussed above. To achieve this, three specific paths will be explored:

1. The method of oscillometry and the algorithms automated oscillometric devices use

for BP estimation will be reviewed first, following the observation that this is the first reference for ambulatory device development, and the method that is set to replace manual auscultation in the clinic. The aim is to understand the importance of this method and the reasons why the algorithms established are at times deficient. In particular, we will focus on the most used algorithm for BP estimation, the maximum-amplitude-ratio algorithm, and propose some modifications that can be practically implemented in automated devices to improve their accuracy. Another objective is to verify the applicability of the method to individual subjects. This last objective will serve as commentary on the use of this method as reference for cuff-less device development.

2. The next step is to analyze the method of auscultation to try and propose a solution to the concerns mentioned above. Particularly, the fact that since this method is part of the gold standard for BP measurement, there should be an effective way to use it as reference for all other device development. The author believes that this can be done with an analysis of the Korotkoff sounds from a psychoacoustical perspective. The advantage of following this approach is that the topic of psychoacoustics deals with human perception of sound. The goal is to address the lack of an automated auscultation device that reproduces the measurements of manual auscultation. The objective of this section, in particular, is to be able to design an algorithm based on the results of the psychoacoustical study that will estimate BP similar to a human observer. This, additionally, will benefit the completion of the second part of the thesis, simplifying the processing of the data and optimizing the computation of results.

3. Finally, having established the basics of the two methods and having developed an automated auscultation method, we focus the second half of the thesis on the physics-based mathematical analysis of the phenomena. Separate mathematical models for each method will be derived based on previous models found in the literature and each will be tested on measured data by means of non-linear least squares regressions. One of the goals is to validate these models and to determine which is the better candidate to describe the observed phenomena. Another goal is to take advantage of the results of the regressions themselves to obtain more information on the main components of the cuff-based methods, namely the underlying brachial artery and the cuff itself.

The overall goal of this thesis is, naturally, to contribute in the advancement of BP measurement methods for improved healthcare and quality of life. The contributions in the first part of this thesis can be directly applied on the existing methods and on the development of new technologies. The analyses in the second part of this thesis, although based on simple models, will hopefully pave the way for other analyses of this nature, with improved models and computational techniques. The procedures described in this second section can also be potentially applied to existing technology to obtain a broader scope of a subject's health, so that physicians and other healthcare providers can make better informed decisions on diagnosis and treatment.

This thesis is organized as follows:

- Chapter 1 is the present introduction, where the importance of BP measurement is stated, and a brief review of the different methods is given with some historical context. The objectives are stated in this chapter as well.
- Chapter 2 is devoted to describing the implementation of the oscillometric method, its advantages and disadvantages. The algorithms used in the automated devices that use this principle are discussed, and some improvements are suggested based on the results of a study performed on one of these algorithms. The study discussed here culminated in a publication, which is included in the Appendix section.
- In chapter 3 we go into more detail on the method of auscultation. Psychoacoustics and how their principles can be exploited in the accurate measurement of BP through auscultation are discussed here. Evidence found in the literature is used to propose a study on how to automate this measurement and an original algorithm is proposed and implemented. Results of this study are presented and discussed.
- The first mathematical model is presented in chapter 4. This is a model of oscillometry, and its functional equation is applied to a set of measurements in a regression analysis. Results and implications of this procedure are discussed.
- The second mathematical model is developed in chapter 5. This is a model of auscultation and the generation of Korotkoff sounds. Similar to the work described in chapter

4, a regression analysis is also performed on a set of measured data with the equation resulting from the model, and the results of the analysis are discussed.

- The final chapter, chapter 6, summarizes the findings of this thesis. The overall project is discussed and the conclusions derived from it are presented here, as well as some suggestions for future work.

Chapter 2

Oscillometric Blood Pressure Measurement

The Oscillometric Blood Pressure Measurement (OBPM) is currently the most popular method used to estimate blood pressure (BP). It pre-dates the auscultatory method by almost 30 years and was initially demonstrated in 1876 by the French physiologist E. J. Marey. Its premise is that BP can be estimated from a series of pressure oscillations that are observed when a limb is enclosed by a device that can apply counterpressure, if a pressure transducer is connected to this device. In Marey's case, the bare arm was placed in a closed cylinder filled with water and connected to a water reservoir that could be elevated to induce a change in pressure. In modern times an inflatable cuff is used as the means to apply pressure, usually to the upper arm.

Oscillometry was not widely used when it was first demonstrated. The only correct prediction it could make related to BP was that of the point of Mean Arterial Pressure (MAP), which was found to correspond to the counterpressure at which the oscillations reached a maximum amplitude. There was no agreement for a long time on the correct estimation of systolic and diastolic blood pressures. This was particularly difficult since at the time the available devices were hard to implement in a clinical setting, and manual analysis of the data was cumbersome. Major breakthroughs on the characterization of the oscillometric method would come until the 1970s, when microprocessors and miniature pressure sensors provided a means of automating the process. For instance, Maynard Ramsey III published and filed some of the first patents about automated devices that determined MAP from an OBPM [44].

Modern oscillometry is now a fully automated process that is able to estimate systolic

blood pressure (SBP) and diastolic blood pressure (DBP) in addition to MAP. While auscultation is still the gold standard for clinical estimation of BP, some medical guidelines have recognized the advantages of switching to these automated oscillometric devices for clinical practice [45]. The Canadian Hypertension guidelines fully recommend the use of automated (oscillometric) methods to measure BP instead of auscultation [46].

Oscillometric devices are preferred over the more traditional method of auscultation because they prevent many of the human-sourced errors inherent to auscultation, require less training to operate, can collect multiple readings for averaging, and reduce the incidence of white-coat hypertension and white-coat effect. White-coat hypertension is defined as persistent hypertensive BP estimates in clinical recordings for an individual with otherwise normal BP outside the physician's office. White-coat effect is the spurious rise in BP that occurs when BP is measured in the presence of a physician or in a clinical setting for a hypertensive individual that normally has controlled levels of BP (with the use of medication). While these last two conditions do not appear to have negative effects in a subject's overall health, they may lead to an incorrect diagnosis of hypertension and to the prescription of unnecessary medication [47–49].

Another important advantage of automated oscillometric devices is their application to out-of-office BP measurements, such as at-home or ambulatory blood pressure measurement (ABPM). ABPM is the gold standard for diagnosing hypertension. It allows the observation of BP fluctuations throughout a 24-h period, and the presence of conditions not measurable in the office, such as white-coat effect, masked hypertension (which is the opposite of white-coat hypertension), and nondipping or reverse-dipping BP during nighttime. This last condition refers to the absence or reversal of the usual decrease in BP that occurs during sleep. ABPM along with home BP measurements have been shown to be stronger predictors of cardiovascular events compared to office measurements [45, 50–52].

Automated devices are also advantageous in the prevention of the transmission of highly contagious diseases, such as COVID-19. Proximity to a physician is not required and many devices currently have storage and bluetooth transmission capabilities. This allows patients to easily share their at-home measurements with their physician remotely to ensure continued care and disease management when in-person consultations present a health risk to the patient.

It is evident, thus, that with such widespread use the accuracy of these devices is a

primary concern. Unfortunately, the oscillometric method has a number of disadvantages that affect it. It has been found that the accuracy of oscillometric devices can be lower in the elderly, in patients with diabetes, and in those with increased arterial stiffness [53–56]. Special considerations must be made for BP measurement in children and pregnant people and there are less recommended devices for these populations compared to those intended for average users. The use of oscillometry is also challenging in subjects with abnormal heart-rates, such as those with atrial fibrillation.

The methods of data collection, filtering and subsequent processing of most automated devices are usually proprietary. There is no regulation of the algorithms used in these devices, therefore devices are not interchangeable, even if they come from the same manufacturer. Even though devices are required to undergo strict validation procedures before they are recommended for use[1], there are several cheap devices in the market that have not met these requirements.

As a reminder, in this chapter we intend to understand these different processes followed during an OBPM: how the data is collected, filtered and presented before an estimate of BP can be made. At the same time, commentary on how variations in these steps can affect a device's accuracy are offered. The goal is to analyze the most widely used algorithm for BP estimation by means of an extensive study of the method using measurements collected from a large number of volunteers. In particular, the objective of this study was to verify if certain modifications in the data presentation could be beneficial to the accuracy of the method, and if they had any implication on the applicability of the method to individual subjects.

Therefore, in the following sections we first review oscillometry in more detail, how data is collected and filtered, and what are its most important components. At the same time, we show some examples of how different processing of the data may change the final outcome. Second, we discuss the main methods used in the literature and, possibly, in automated devices to estimate BP. The focus is then centred in the algorithm of interest, and in following sections we discuss the study mentioned above: the experimental procedure followed, the results, and finally the discussion and conclusions derived from this work. Some results of this study are also part of a published article, a copy of which is included in Appendix A.

[1] A list of recommended devices is available at *www.dableducational.org*

2.1 Data Processing in OBPM

The oscillometric process is fairly simple: an inflatable cuff is wrapped around the upper arm and air is pumped into the cuff until the pressure inside is above estimated SBP. A valve then slowly releases the air until the pressure inside the cuff is below DBP. A pressure sensor is connected to the cuff to register pressure variations in the cuff. This information is filtered and processed to obtain what is known as the oscillometric waveform (OMW), from which BP is estimated using a choice of algorithms that take certain features of this OMW into consideration. The process generally takes around a minute to complete.

At this point we can already encounter some potential sources of error that are not related to the device's processing algorithms. If the measurement is not collected in the appropriate conditions the BP estimate will likely be inaccurate. It is recommended that prior to a BP measurement the subject not consume any type of food or beverage, particularly caffeine or alcohol, and that they perform no strenuous physical activity. The measurement should also be performed in a quiet room with controlled temperature, since cold temperatures cause the peripheral arteries to contract. The subject should be seated in a comfortable position with their back supported and the arm on which the cuff will be placed should be resting on an elevated support so that the cuff is at heart level. Talking or sudden movements during the measurement are to be avoided as well.

An important consideration that is often overlooked when measuring BP at home is the choice of a cuff of the correct size (width). This decision depends on the subject's arm circumference, and many of the commercial devices will not provide recommendation or guidance, but will instead include a single standard cuff. Narrow cuffs require higher pressures to completely occlude the artery and therefore give higher estimates of SBP and DBP. Geddes and Tivey found that a recommended cuff width was that measuring 38% of the arm's circumference [57], so the general recommendation is to use a cuff width that is close to 40% of the subject's arm circumference [58]. Overcuffing, which is the opposite procedure of applying a larger cuff, has also been found to negatively impact oscillometry, resulting in lower estimates of BP [59]. A study by Palatini *et al* also suggests that obese patients with upper arms of a conical shape would benefit from the use of cuffs that follow this conical shape [60].

Once these external details of the procedure are taken care of, we can turn to the process that happens inside the device. To collect data some devices use the inflation sequence while

others the deflation. In this work we shall only consider those that record pressure signals during deflation. These type of devices have the advantage of providing a cleaner signal since often during inflation the pump's operation adds a significant amount of noise. Among the devices that measure BP during deflation there are those that deflate at a constant rate, and those that use a step deflation, where cuff pressure is maintained constant for a few seconds and then lowered a few mmHg where the process repeats. The former type of device is considered in this work.

As mentioned above, the cuff is inflated to suprasystolic pressures in order to completely collapse the artery that runs inside the upper arm, that is, the brachial artery, and to prevent the flow of blood towards the lower part of the limb. Once the cuff is slowly deflated, ideally at a constant rate of 3 to 5 mmHg/s, the artery is able to reopen and allow a progressively increasing amount of blood to flow past the length of the cuff. As the cuff is being deflated two distinct features can be appreciated in the pressure signal recorded by the sensor: the overall signal decreases monotonically and there are periodic oscillations present in the signal. The constant decrease in overall pressure corresponds to the slow release of air from the cuff. The periodic oscillations are caused by blood volume pulsations that occur at each cardiac cycle.

2.1.1 The Oscillometric Waveform

The oscillations in the pressure signal are observed to begin at suprasystolic cuff pressures. Their amplitude increases as cuff pressure approaches SBP, reaches a maximum when cuff pressure equals MAP, and finally decreases as cuff pressure reaches DBP. The oscillations can also be observed at subdiastolic pressures where they are of smaller and mostly constant amplitude. These oscillations make up the oscillometric waveform mentioned above, and are one of the most important components of the OBPM. They can be separated from the main signal by means of band-pass or high-pass filters that remove the lower frequency signals of the constant deflation signal, or by fitting a curve to the deflation signal and subtracting it from the total pressure signal. The manner in which the OMW is obtained may affect BP estimates: filters can modify the shape of the individual pulses in the OMW [61] or can alter the values assumed to correspond to the decreasing pressure signal and give an incorrect estimate of the pressure in the cuff at a given time [62].

To extract the OMW by fitting a curve to the deflating signal a few different approaches can be considered. A polynomial function can be fitted to the signal, for instance. High order polynomials provide a good fit, although one must take care when fitting a curve with high order polynomials. Due to their oscillatory nature and their tendency to approach $+/-$ infinite values at a rate proportional to their order, unwanted oscillations at the data endpoints can appear.

Another option is to construct a curve that passes through specific points of the signal. These points can be a location related to the cardiac cycle as indicated by an electrocardiogram (ECG), or a choice of the highest or lowest points of each individual pulse, for example. The first option relates heart activity to a point in the pressure signal and will benefit from a consistent location not affected by noise in the signal. The main problem is that it requires additional equipment that cannot be incorporated into the cuff. The second option requires sectioning the signal into individual pulses to locate the highest/lowest points. Noise in the signal will affect these locations, particularly noise derived from motion artifact or irregular oscillations.

An example of a raw pressure record from an OBPM is shown in figure 2.1, which comes from a measurement taken from a volunteer. In this case, the deflating signal was obtained by an asymmetric least squares fit to the lowest points in each pulse. The dotted red line shows the fit, or *baseline*, and the horizontal blue lines mark the location of SBP and DBP.

Subtracting this baseline from the signal results in the OMW shown in figure 2.2. Depending on the effectiveness of the baseline estimation the OMW can be presented as the absolute magnitude of the pulses, with the lowest values coinciding with zero. Otherwise additional steps can be taken to ensure this levelling of the data, which is useful in some of the BP estimation algorithms described in the following section. It is customary to present the OMW as a function of the baseline as it progresses in time, that is, from highest to lowest pressure to represent cuff deflation. The changes in pulse amplitude mentioned previously are better appreciated with this representation as well.

SBP, DBP and MAP are marked by the vertical lines in figure 2.2. To the left of the red SBP line one can verify the existence of suprasystolic oscillations, and to the right of the blue DBP line the existence of subdiastolic oscillations. In this case there was no simultaneous measurement of MAP to verify that it corresponds to the point of maximum amplitude, so the magenta line that marks MAP in figure 2.2 was drawn after the fact, assuming the

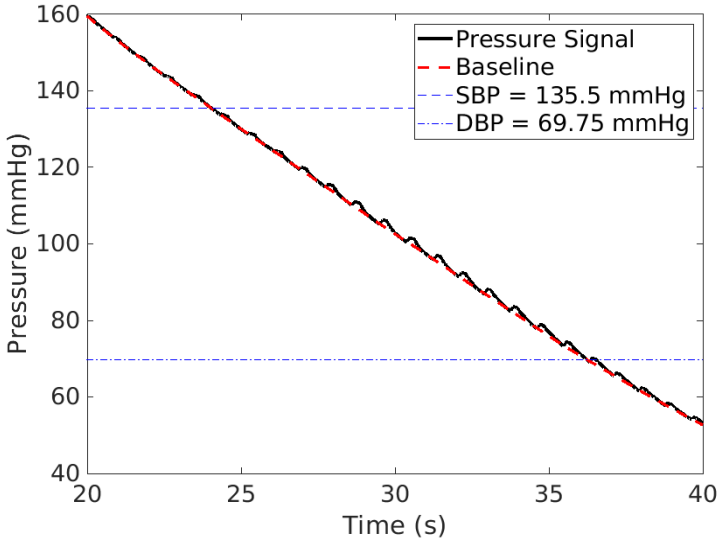

FIGURE 2.1: Pressure detected by the pressure sensor and estimated baseline. BP = 135.5/69.75 mmHg is marked by the horizontal blue dashed lines.

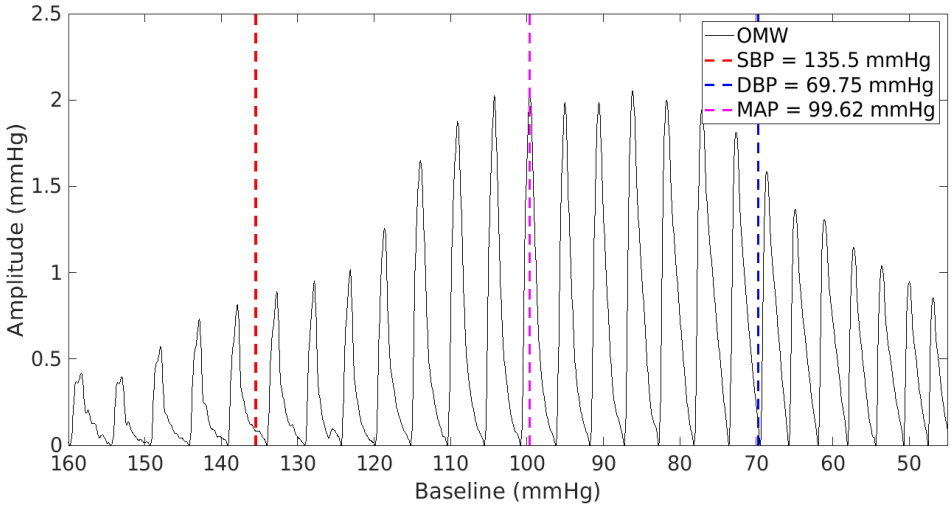

FIGURE 2.2: Oscillometric Waveform with locations for SBP, DBP and MAP marked by dashed vertical lines.

relationship is correct. It was previously stated that studies in the past have confirmed this relationship, however in this case we can not assert this statement for reasons that will be explained in the following section.

Using the maximum amplitude approach, MAP = 99.62 mmHg for the example in figure 2.2. A popular formula for calculating an approximate MAP is: $MAP = DBP + \frac{1}{3}(SBP - DBP)$. In this case SBP = 135.5 mmHg and DBP = 69.75 mmHg, which results in a MAP = 91.66 mmHg with the use of this formula. There is a difference of almost 8 mmHg in these two estimates, however this formula is a very simplified method of obtaining a quick estimate of MAP. We can not conclusively state that the maximum amplitude approach in this case is incorrect on the basis of this calculation alone.

2.1.2 The Oscillometric Waveform Envelope

SBP and DBP are estimated by empirical relationships derived between the amplitude of the pulses and the location of these pressures in relation to the OMW. To simplify analysis it is common to use the oscillometric waveform envelope (OMWE) instead of the OMW to estimate BP. Depending on the shape of the extracted OMW, the OMWE will be obtained in a few different ways, but its purpose is always to showcase the absolute amplitude of the pulses with no regards to their individual shape.

Two examples of an OMWE obtained for the same OMW following different procedures are shown in figure 2.3. The top row corresponds to the OMW obtained by fitting a ninth-order polynomial function to the deflation pressure signal and subtracting the approximated function from the original signal. The bottom row is the OMW obtained from fitting a baseline (fit of a curve to the lowest points of the oscillations) as described in the previous section and exemplified in figures 2.1 and 2.2.

Here we can appreciate the advantage of fitting a baseline instead of a polynomial function to the pressure signal. In the top row case (figure 2.3a) a piecewise cubic interpolation was done for the highest points of each oscillation (marked in red) and another for the lowest points (marked in blue). The lower envelope (blue) was subtracted from the upper envelope (red) and the result is the OMWE in figure 2.3b. In the bottom row case (figure 2.3c) the subtraction of the baseline already results in the data expressed as absolute amplitudes and only some minor adjustments are needed to make sure all the lowest points of the

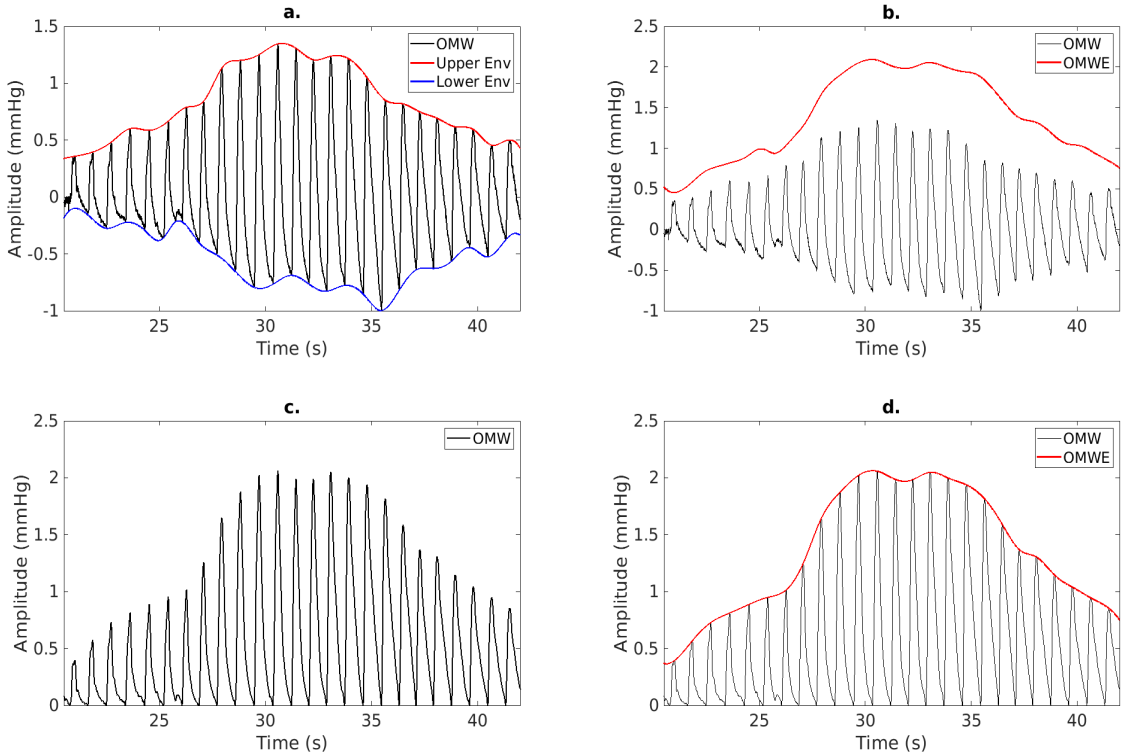

FIGURE 2.3: Different presentations of the OMW and the OMWEs obtained from each. a.OMW obtained from subtracting a 9^{th}-order polynomial to the pressure signal with cubic interpolations to the highest (red) and lowest (blue) points in the oscillations. b.OMWE obtained from subtracting the interpolations in a. c.OMW obtained from subtracting a baseline to the pressure signal. d.OMWE obtained from a cubic interpolation to the maximum amplitudes of the OMW in c.

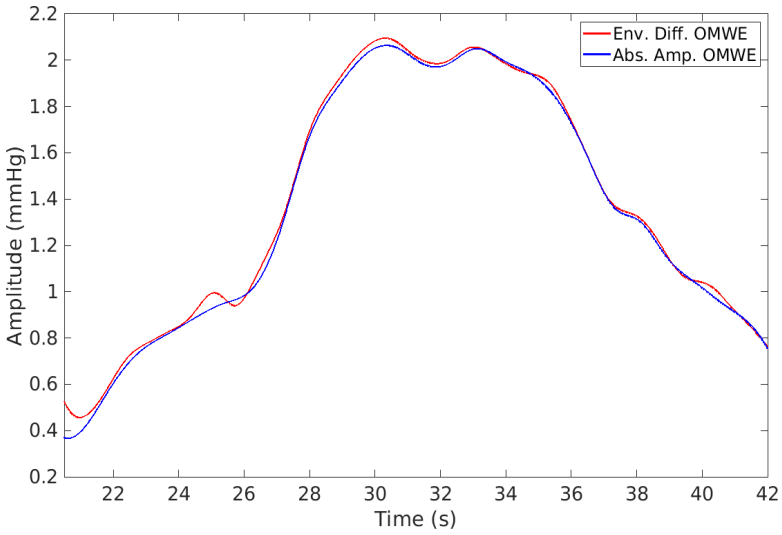

FIGURE 2.4: Comparison of the OMWEs obtained from the different representations of the OMW from figure 2.3.

oscillations coincide with zero. The OMWE in this case (figure 2.3d) is a single piecewise cubic interpolation to all the maximum amplitude points in the OMW of figure 2.3c.

Both OMWEs are plotted together in figure 2.4. The OMWE obtained from the OMW in figure 2.3a was labeled as "Env. Diff. OMWE" in relation to its origin from a difference of envelopes. The OMWE obtained from the OMW in figure 2.3c was labeled as "Abs. Amp. OMWE" in reference to the interpolation of the absolute amplitudes. We can readily appreciate that there is a difference in the magnitude of the maximum amplitude of the envelopes and some differences in their shapes.

It is clear, thus, that each step of the data processing in oscillometry can introduce a certain amount of error to the BP estimate. The effect that the filtering of the data has on the accuracy was already described above. Figure 2.4 gives us an example of how following different steps to obtain the OMWE contribute another source of inaccuracy. Furthermore, differences in the shape of the OMWE can also affect the measurement's accuracy [61, 63, 64]. Figure 2.5 shows four OMWE representations of the OMW in figure 2.3c.

In the following sections we will discuss how using these different OMWE affects the BP estimate. Figures 2.5a and 2.5d are two common fits to the maximum amplitude points:

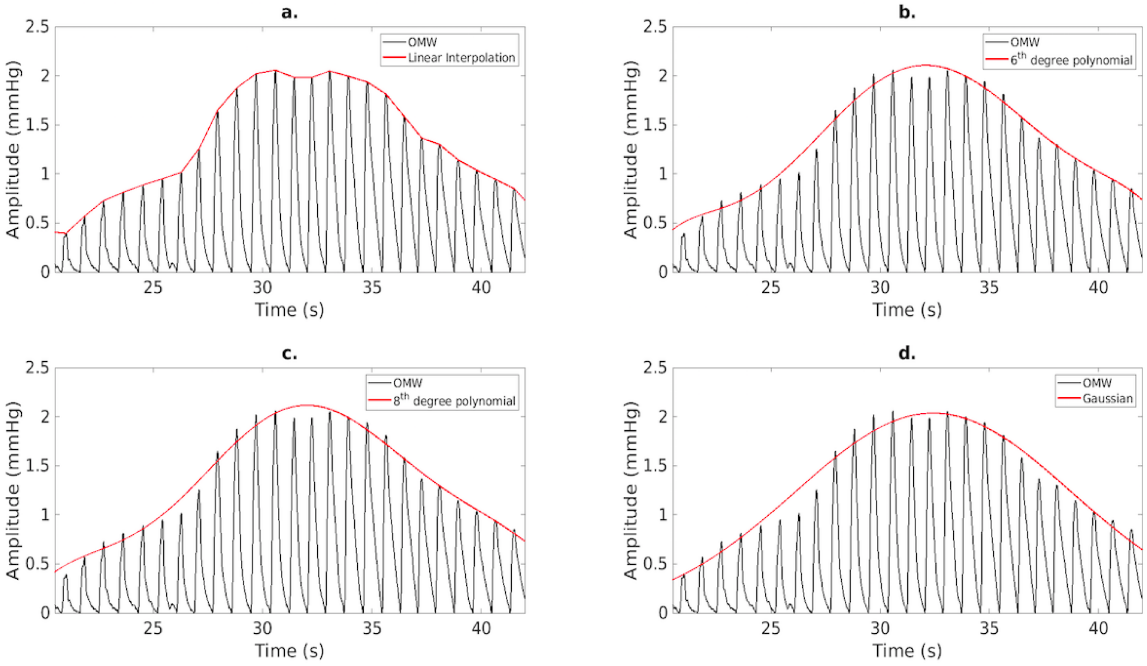

FIGURE 2.5: OMWEs obtained from different curve fits to the maximum amplitude points. The same OMW is used for all and OMWE are marked with red lines. a.Linear interpolation, b.6^{th} degree polynomial, c.8^{th} degree polynomial, and d.Gaussian function.

a linear interpolation and a Gaussian function, respectively. The 6^{th} and 8^{th} degree polynomials shown in figures 2.5b and 2.5c, respectively, are not a common approach to fitting the envelope, but were analyzed after a suggestion from Dr. Alexander Kobryn, a Senior Research Officer at the National Research Council Canada.

2.2 Blood Pressure Estimation Methods

The methods used to estimate BP from an OMW or an OMWE are usually one of four methods, or a combination of any of them: pulse morphology, maximum slopes, maximum amplitude ratios, or envelope modelling. Currently, all of these methods use empirical references to estimate BP and there is no formal physical reasoning behind these references. The most effective and well established method is that of maximum amplitude ratios (MAR) and, even though the processes followed by commercial devices are unknown, it is likely that most of them use a version of this method. The maximum slopes (MS) method is similar in application to the MAR method but it is not as robust, and is probably only used as a complement to MAR, if at all. Pulse morphology and envelope modelling are BP estimation methods that have gained more interest in recent years, although they are apparently not yet considered as viable replacements to the MAR method. A brief description of each method is given below.

Pulse Morphology. This method looks at the shape of individual pulses and tries to relate observed temporal and amplitude features of the pulses to arterial mechanics and wave transmission in the arterial tree. Under normal conditions (in the absence of a cuff) the pressure pulse can be obtained from either intra-arterial measurements or with the use of a tonometer. An immediate observation is that the shape and maximum amplitude of the pulse change depending on the site where it is measured. Amplitude increases at the periphery due to the proximity of reflection sites in the arterial tree. At peripheral arteries waves are reflected sooner and forward and backward waves will superimpose at the systolic phase of the pulse resulting in the observed amplitude increase. For this reason, BP values are higher when measured at the wrist when compared to those measured at the upper arm, for instance. The timing of the reflected waves also gives a measure of arterial stiffness.

In general, the pressure pulses are rich in information. MAP can be obtained, as well as pulse pressure, duration of systolic and diastolic phases, and other parameters closely related to heart activity if the pulses are measured at the ascending aorta [65]. During an OBPM the pulses are modified by the interaction of cuff and arterial mechanics. Unfortunately, unlike auscultation (discussed in Chapter 4), specific features that a pulse must meet in order to assign one particular pulse of the OMW to either SBP or DBP haven't yet been determined. Some recent approaches to estimating BP from pulse morphology include relating temporal features of the pulse, such as the timing between the foot and the maximum amplitude of the pulse, to SBP [66], or using neural networks to identify temporal relations between successive pulses [67], or teaching them to identify certain characteristics in the pulses to relate them to auscultation data [68].

Maximum Slopes Algorithm. As its name indicates, this algorithm relates SBP and DBP to maximum slopes found in the OMWE. It is assumed that the locations where there is a maximum change in pulse amplitude correspond to these pressures. When the OMWE is presented as a function of decreasing cuff pressure, SBP is estimated where there is a maximum positive slope on the rising phase of the OMWE, before the location of the maximum amplitude. DBP is estimated where there is a maximum negative slope on the descending phase of the OMWE, past the location of the maximum amplitude.

A look a the envelopes in figure 2.5 already gives an idea of how the OMWE representation will affect the location of these maximum slopes. Figure 2.6, a measurement obtained from a different volunteer, shows the BP estimates obtained with the MS algorithm for two envelope representations, and compared to true BP. One of the envelopes, that obtained from the linear interpolation in figure 2.6a, contains more inflexions, while the other, obtained from a fit to a Gaussian function in figure 2.6b, presents a smooth profile.

The dashed vertical red lines indicate the location of true BP. The locations of the dashed vertical blue lines were obtained using the MS method. A numerical first derivative is applied to the envelope and its minimum and maximum values correspond to the locations of SBP and DBP, respectively.

True BP was estimated as 128.00/76.25 mmHg, while that obtained with the MS algorithm was estimated as 120.90/80.52 mmHg for the linearly interpolated envelope, and as 123.18/79.06 mmHg for the Gaussian envelope. The errors in the MS algorithm (measured

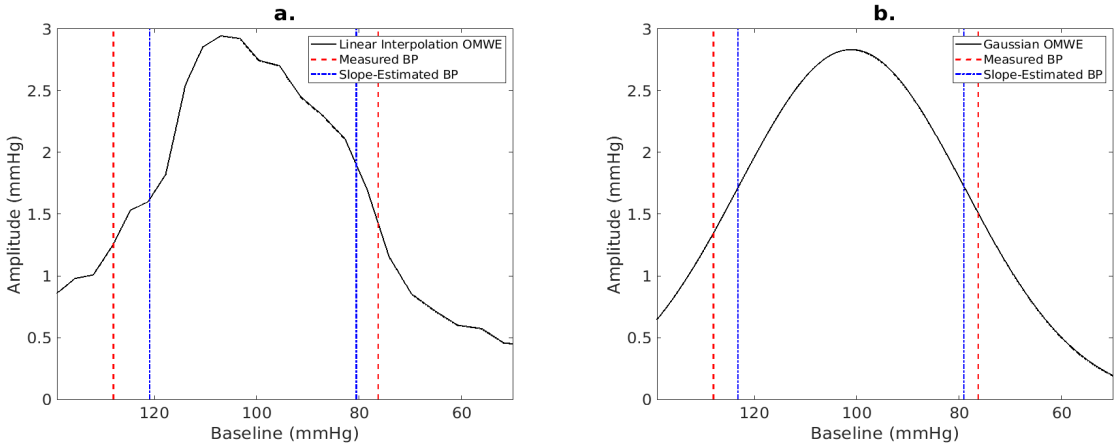

FIGURE 2.6: Comparison between the true BP (red) and the estimate from MS algorithm (blue) for two envelope representations. True BP = 128.00/76.25 mmHg. a.Linearly interpolated OMWE. MS algorithm BP = 120.90/80.52 mmHg. b.Gaussian function OMWE. MS algorithm BP = 123.18/79.06 mmHg.

values minus algorithm values) are $+7.1/-4.27$ mmHg and $+4.82/-2.81$ mmHg, respectively, which means SBP was underestimated and DBP overestimated in both cases. Sudden variations in pulse amplitude can also affect the estimate by giving false maximum and minimum slopes.

Maximum Amplitude Ratio Algorithm. This algorithm was formally established by the work of Geddes *et al* in the early 1980s [69]. This group measured the amplitudes of the maximum oscillations (those corresponding to MAP), and of the oscillations corresponding to SBP and DBP. These amplitudes were labeled A_M, A_S, and A_D, respectively. They then noticed that for a data set of 3 measurements obtained for each of 23 subjects, the ratios A_S/A_M and A_D/A_M would consistently fall within the limits 0.45-0.57 and 0.75-0.86, respectively. This means that SBP can be located on the rising phase of the OMWE where its amplitude is approximately 50% of the maximum amplitude. DBP on the other hand, can be located on the descending phase when the OMWE's amplitude is approximately 80% of the maximum amplitude. The authors, however, made sure to point out that these percentages depend on BP.

The method is exemplified in figure 2.7. Several studies have confirmed the repeatability

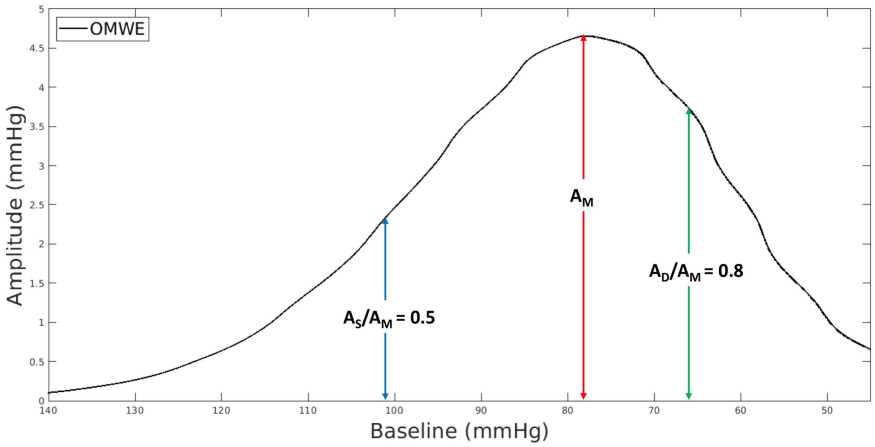

FIGURE 2.7: Location of the maximum amplitude A_M and the ratios $A_S/A_M = 0.5$ and $A_D/A_M = 0.8$ on an OMWE.

of these ranges of percentages or ratios. For this reason, the MAR algorithm became the most implemented method on automated devices for BP estimation. In cases of BP outside of normotensive ranges, such as in hypertension or hypotension, the ratios may fall outside of the expected ranges and a simple MAR algorithm becomes less effective. In these cases, a multicomponent algorithm that uses a variable ratio or adjusts for BP level is used.

Mathematical models have been developed to identify the possible sources of error of the MAR ratio. Studies agree that the oscillometric ratios are mainly affected by arterial stiffness and the amplitude of the pressure pulse (PP) [6, 70, 71]. These findings are helpful in explaining why the method fails for hypertensive and older subjects. These populations will, in general, have increased arterial stiffness and an amplification of the pulse pressure due to the higher prevalence of isolated systolic hypertension in the particular case of older subjects.

Envelope Modelling. To avoid a deterministic selection of ratios that may not apply to all populations equally, recent studies have turned to modelling the envelope with mathematical functions that often stem from measured functions of arterial mechanics [72–74]. These models include several parameters that can be adjusted as the mathematical function is fitted

to measured data. Some of these procedures essentially require a form of least squares curve fitting, and the resulting parameters are expected to be unique for every measurement.

This method of BP estimation proposes a patient-specific and measurement-specific approach, which may circumvent the sources of error of the MAR algorithm discussed above. The challenges this type of approach faces are similar to the rest, particularly the processes of data extraction and filtering. The effectiveness of the mathematical models will depend on how closely they represent the OMWE, provided the OMWE is properly obtained in the first place. Another constraint that this method has is the complexity of the models used to fit the OMWE. The model must be simple enough to be computationally economical, but sophisticated enough to properly describe the shape of the OMWE.

Certainly other methods have been developed that do not fall within these four categories, but most are related to extracting features from the OMWE, or approaching one of these methods with a different technique.

2.3 Results of a Study on the MAR Algorithm

A study on the popular algorithm of maximum amplitude ratios to measure BP through oscillometry was completed and published in a collaboration of the departments of Physics and Medicine of the University of Alberta and the National Research Council, Canada. Data were collected and partially processed at the Department of Medicine. The resulting article was published in the journal *Blood Pressure Monitoring* [75] and a copy is included in Appendix A. The purpose of the study was to verify optimum ranges of maximum amplitude ratios for a custom-made automated oscillometric device, as well as the influence that different representations of the OMWE have on the accuracy of the MAR algorithm. In this section we shall discuss the findings of this study in detail, including some results that were not published.

2.3.1 Experimental Method: Data Collection

Data were collected from 74 subjects by the group from the Department of Medicine of the University of Alberta with approval from the University of Alberta Research Ethics Board. BP measurements were performed in a manner similar to that of validation protocols and

following the International Standard Organization (ISO) 2013 protocol [76]. The procedure is as follows: subjects are seated in a quiet, temperature-controlled room on a chair with back support and the measurement arm propped up to heart level. Cuff size was selected according to arm circumference and cuffs could be interchangeably connected to a mercury sphygmomanometer and to a custom made oscillometric device.

Three observers were present for data collection: two would perform auscultation simultaneously using a dual-headed stethoscope while being blinded from each other's results. The third observer collected their BP estimates and ensured they were within 4 mmHg from each other. A total of five auscultatory measurements and four oscillometric measurements were taken in alternating fashion beginning with auscultation. The first measurements of each method were discarded and not considered for analysis. An auscultatory measurement was equal to the mean of the measurements from the two observers. "True" BP is that assumed to correspond to the oscillometric measurement; this was calculated as the mean of the auscultation measurements taken immediately before and immediately after. Therefore, a total of 3 oscillometric measurements were obtained for each patient. Data from one subject were discarded since they had an underlying health condition. In total, there were 219 measurements of oscillometry.

Subject ages ranged from 19 to 79 years, (mean $\pm$ SD: 51 ± 18 yrs), and 63% were female. SBPs ranged from 82 to 155 mmHg (115 ± 16 mmHg), DBPs from 51 to 93 mmHg (69 ± 8 mmHg), and PPs from 24 to 88 mmHg (46 ± 14 mmHg). Age, SBP, DBP and PP distributions are given in figures 2.8 through 2.11, respectively.

2.3.2 Experimental Method: Data Processing

The initial processing of the collected pressure data was done by the collaborators in the Department of Medicine. From their description of the procedure, the data was processed as follows.

The complete data set was processed on Matlab (The MathWorks, Inc., Natick, Massachusetts, USA). The signal obtained from the custom oscillometric device is filtered and arranged by their algorithm to look like what is shown in figure 2.1. The baseline for each measurement was obtained as described in previous sections, by fitting a curve to the lowest points in each oscillation. Subtracting the baselines from the original signals resulted in OMWs that were adjusted to present absolute amplitudes similar to the one shown in figure

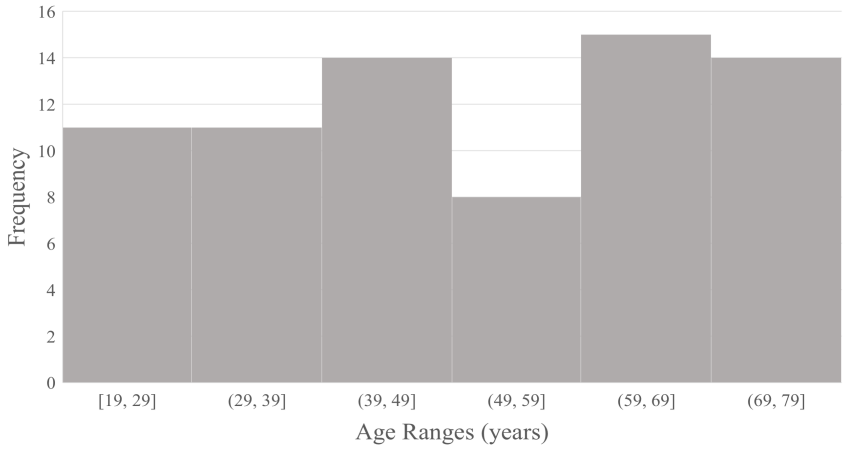

FIGURE 2.8: Age distribution for the 73-subject sample.

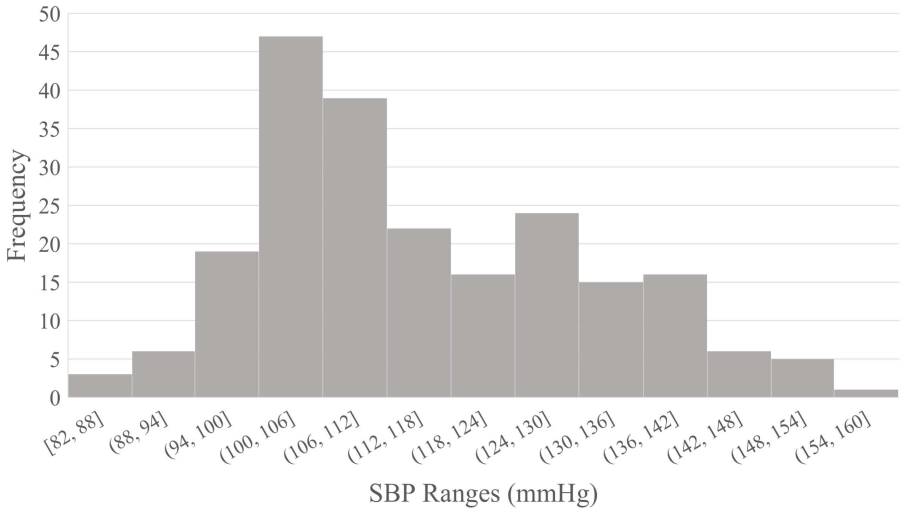

FIGURE 2.9: SBP distribution for the 219-measurement dataset.

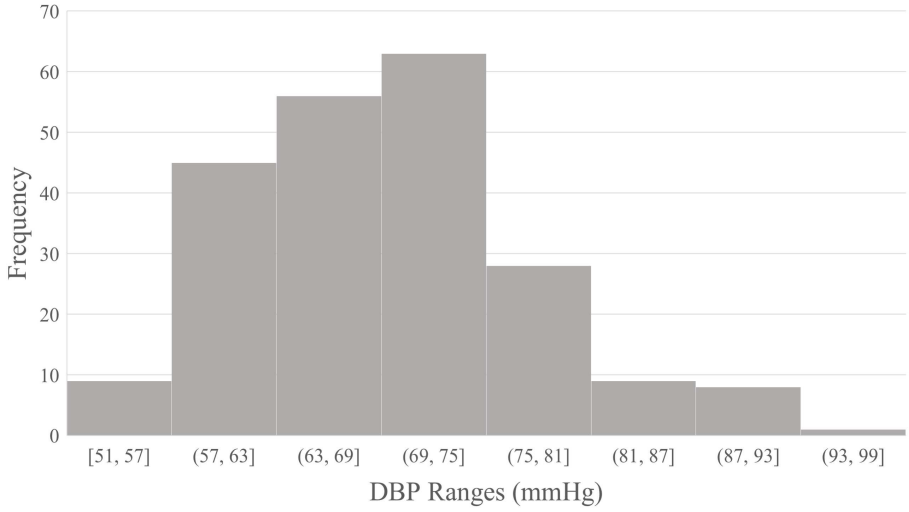

FIGURE 2.10: DBP distribution for the 219-measurement dataset.

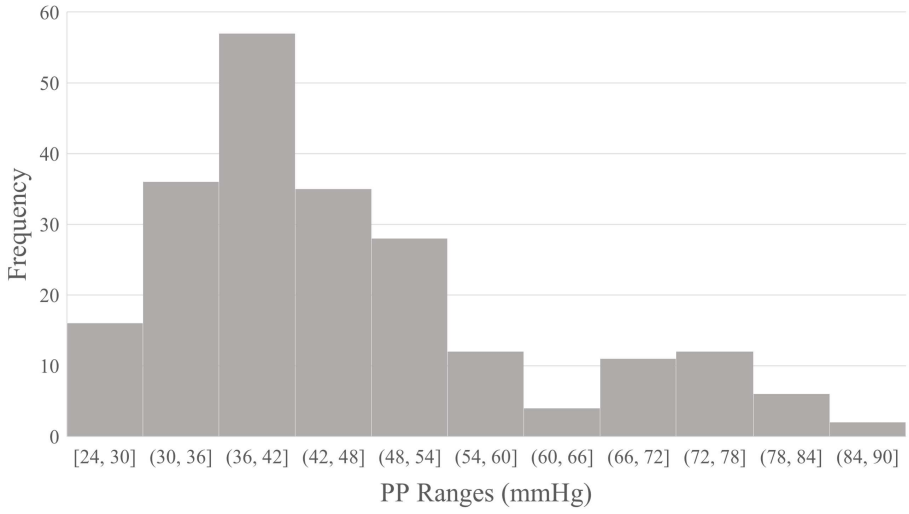

FIGURE 2.11: PP distribution for the 219-measurement dataset.

2.2. The OMWs were further processed to remove outliers from motion artifact. The points of maximum amplitude in each oscillation were selected and outliers were identified as points of much higher or much lower amplitude than the neighbouring ones by means of a function that uses statistics of a seven-point window. They were then replaced by a point that was the result of a linear interpolation between the points located before and after.

These OMWs were the final product that the author made use of for the envelope and MAR algorithm study. As mentioned at the start of this section, one of the objectives of this study was to verify the influence the OMWE's shape has on the MAR algorithm. For this reason, four different fits to the peak points of each oscillation were used to model the OMWE. These fits are the same ones shown in figure 2.5: a linear interpolation between the peaks, polynomials of 6^{th} and 8^{th} order, and a Gaussian function.

The linear interpolation has the advantage of exactly following each data point and providing real amplitude information at these locations. Its main disadvantage is that the removal of outliers is a necessary step in the process, otherwise it will follow those locations as well and introduce a potential error in the measurement. Polynomials of 6^{th} and 8^{th} order as well as Gaussian functions have a smoother profile. While they may affect the estimate of MAP to some degree, the appearance of outliers does not significantly affect the fit, unless they are higher than the maximum amplitude. This is usually not the case, since any outliers of this size represent a significant amount of motion artifact and the measurement as a whole is discarded.

2.3.3 Results

One of the first observations done in this published work is how the amplitude ratios do not depend exclusively on a subject's BP. Geddes *et al* reported a systolic ratio ($SR = A_S/A_M$) of 0.55 and a diastolic ratio ($DR = A_D/A_M$) of 0.82 for what was considered a "typical" BP of 120/80 mmHg [69]. Using these ratios to estimate BP from a measurement where BP = 118/80 mmHg resulted in underestimation of both SBP and DBP for all four representations of the OMWE. The highest differences came from the SBP estimate, of up to 13 mmHg. This result provides an initial confirmation to the studies that found that arterial mechanics play an important role in the correct selection of amplitude ratios. Even if BP is the same in a number of individuals, each will have different artery configurations.

The second step in the analysis was to estimate BP using a range of amplitude ratios applied to each of the four representations of OMWE to determine which combination resulted in the lowest mean error. For SRs the range between 0.28 and 0.89 was used in increments of 0.01. For DRs the range between 0.3 to 0.99 was likewise sampled in steps of 0.01. The BPs that resulted from the application of each of these ratios to each of the OMWEs were compared to the estimates of true BPs. The error in the measurement was calculated as true BP minus BP obtained from the algorithm. Ratios that were considered accurate for this sample population where those where the mean of the errors (ME) was $\leq \pm 5$ mmHg and the standard deviation of the error (SDE) was < 8 mmHg. These limits are of clinical relevance for diagnosis and treatment and considered in device validation recommendations.

Accurate SRs were found to fall on average between 0.44 and 0.66 for the linear interpolation and the polynomial functions, and were shifted to higher ratios for the Gaussian function, between 0.5 and 0.74. These ranges extend to higher ratios than those reported originally by Geddes *et al*, but are consistent with those reported by other groups. In the case of DRs the accurate ratios fall between 0.56 and 0.83 on average from all OMWE representations, with no significant shift for the Gaussian function. Here the ratios extend to lower values than those reported by Geddes *et al*, but are also consistent with other reports.

The optimal ratios from each OMWE representation were chosen as those that had the lowest values of ME $\pm$ SDE. These ratios and their statistics are shown in table 2.1. On average, optimal SRs are close to 60% of the maximum amplitude and optimal DRs to 70%. The SR for the Gaussian function is slightly shifted to a higher value compared to the other fits, in accordance with the shift observed for the ranges of accurate ratios. This shift is directly related to how each function represents the OMWE. The ME and the SDE for all four representations are significantly small, although the best results are obtained in the SBP estimates for the 6^{th} degree polynomial envelope, and in the DBP estimates for the 8^{th} degree polynomial envelope.

We can appreciate in figure 2.12 a comparison of the different fits for a measurement. In this case we can observe how the maximum amplitudes of the polynomial and Gaussian envelopes are lower with respect to the linear interpolation, and their location shifted towards lower pressures. The mean and standard deviations of these amplitude differences and location shifts were calculated using the linear interpolation as reference. The results are shown in table 2.2.

TABLE 2.1: Systolic and diastolic amplitude ratios with lowest values of ME±SDE for each envelope function.

Envelope Function	SR	ME ± SDE (mmHg)	DR	ME ± SDE (mmHg)
Linear interpolation	0.54	0.0 ± 6.6	0.64	-0.1 ± 6.9
6^{th} degree polynomial	0.57	0.0 ± 6.2	0.71	-0.1 ± 6.8
8^{th} degree polynomial	0.56	0.2 ± 6.5	0.68	0.0 ± 6.5
Gaussian	0.62	-0.2 ± 5.7	0.74	0.2 ± 7.3

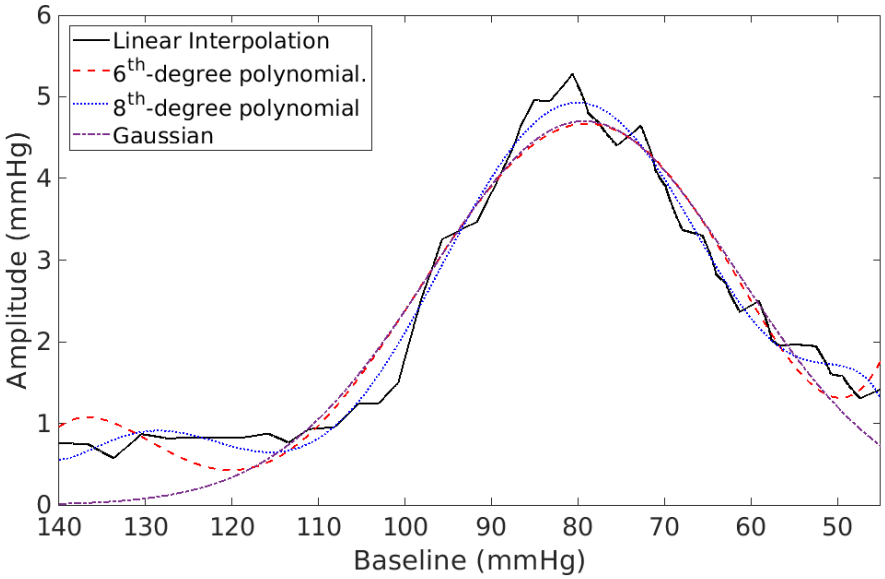

FIGURE 2.12: Comparison of the different representations of the OMWE used in the author's published study.

TABLE 2.2: Mean and SD of the amplitude differences and shifts in peak locations resulting from polynomial and Gaussian functions using linear interpolation data as reference.

Envelope Function	Amplitude difference Mean±SD (mmHg)	Peak location shift Mean±SD (mmHg)
6^{th} degree polynomial	0.16 ± 0.17	-0.50 ± 5.48
8^{th} degree polynomial	0.08 ± 0.24	0.40 ± 6.77
Gaussian	0.27 ± 0.19	-2.09 ± 6.22

The Gaussian function results in lower amplitudes and in larger shifts towards higher pressures compared to the polynomial functions. The Gaussian function envelope will, on average, overestimate MAP more so than the polynomial functions. These differences reflect the overall higher ratios required for a better accuracy using a Gaussian function to fit the OMWE.

A final important result discussed in the publication was the percentage of volunteers that had BP estimates that fall within the acceptable accuracy limits of ME $\leq \pm$ 5 mmHg. To verify this the absolute values of the errors of the three BP estimates for each subject, obtained with the optimal ratios for each envelope, were averaged. This average is considered a measure of the performance of a device for a specific subject that operates based on the most accurate ratios for the population, and for each OMWE function. The results for all volunteers are shown in figure 2.13, and in figures 2.14 and 2.15 the same results are now divided by age groups.

The numbers atop each bar are the percentages that each one represents. Results in figures 2.13 through 2.15 show that the device would be recommendable for about 70% of the subjects regardless of OMWE function. When related to the age of the subjects, those aged between 41 and 62 years have lower accuracy in SBP estimates, and those aged 63 and above have lower accuracy for DBP estimates.

2.4 Discussion and Conclusion

In this chapter we reviewed the basic operation of the OBPM, its advantages and disadvantages, and the different processes followed in order to obtain an estimate of BP. The

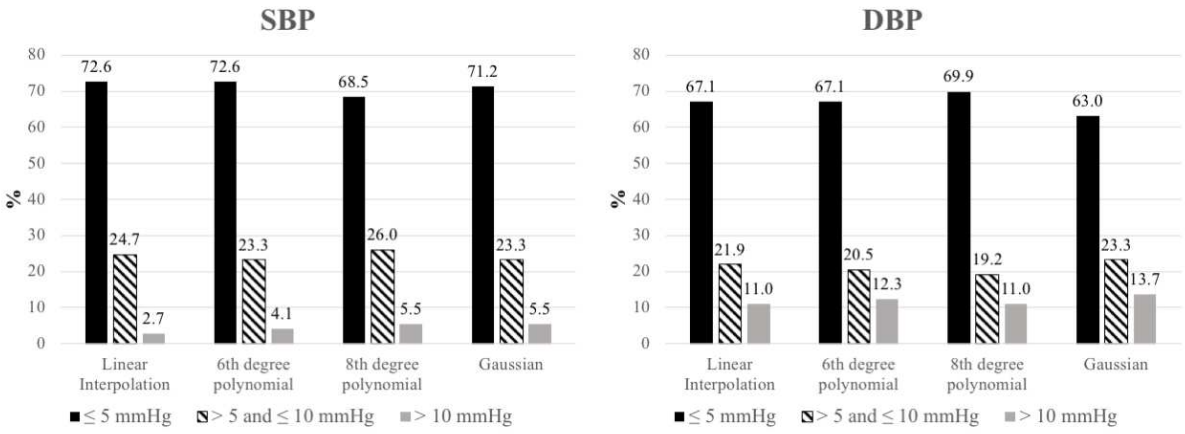

FIGURE 2.13: Percentage of volunteers with BP estimates within three ranges of accuracy depending on envelope representation.

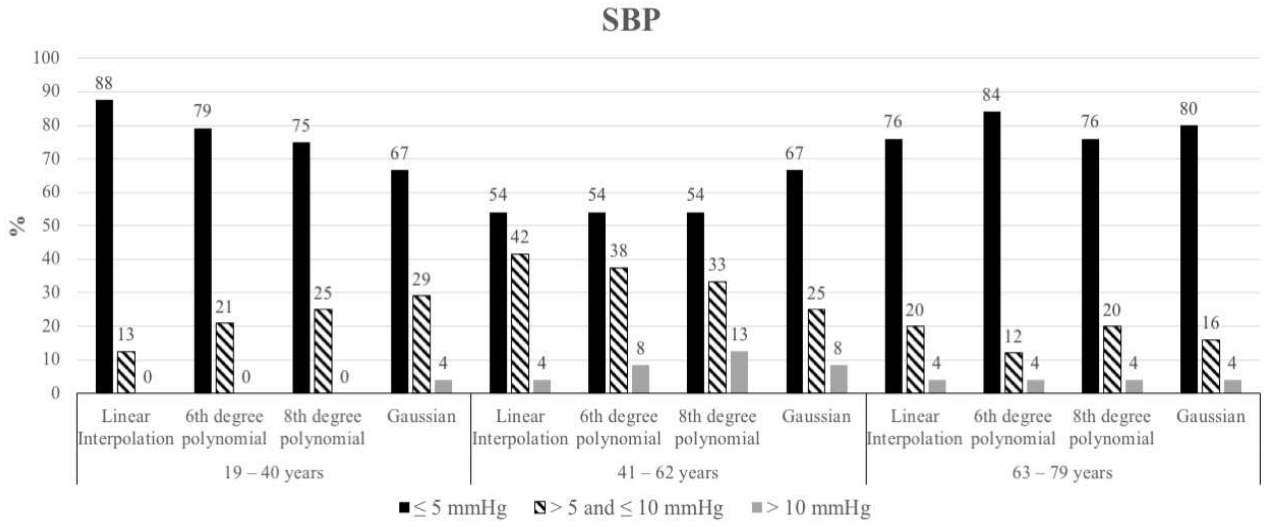

FIGURE 2.14: Percentage of volunteers with SBP estimates within three ranges of accuracy and divided by age group, depending on envelope representation.

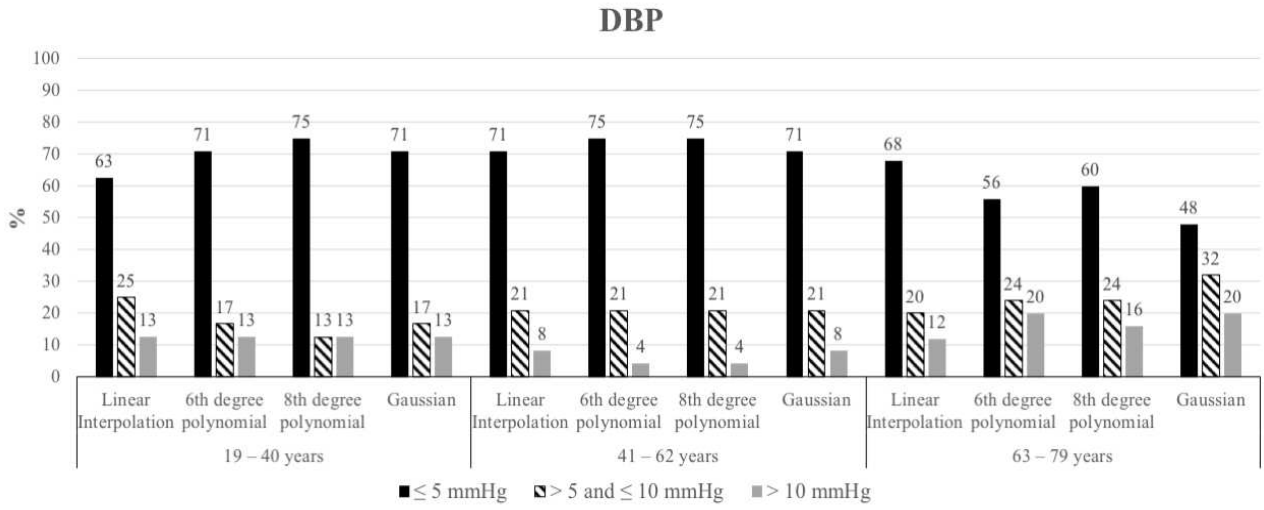

FIGURE 2.15: Percentage of volunteers with DBP estimates within three ranges of accuracy and divided by age group, depending on envelope representation.

practicality of the automated oscillometric devices often supersedes their limitations, and they are slowly but surely set to replace the method of auscultation altogether. Their poor performance on some target populations makes this replacement challenging.

Errors in the measurement usually come from three different sources: subject/operator (human-based), procedure (cuff size selection, adequate environmental conditions), and device operation (filtering and algorithms). Human-based and procedural errors can introduce large inaccuracies, but are addressable with proper technique, although this is not easy to ensure in a busy clinical environment. The most difficult issues to resolve are those based on device operation. The black-box quality that most commercial devices have makes this task particularly difficult.

The most important components of the OBPM related to data processing are the baseline or estimated cuff pressure, the oscillometric waveform, which is a collection of periodic oscillations present in the pressure signal, and the oscillometric waveform envelope, which is the representation of the amplitude of these oscillations. Several steps must be followed to obtain these components, and unfortunately each step carries a potential source of error.

The OMW is rich in information. It is probably the most important part of the OBPM and it is a reflection of how cuff and arterial mechanics modify the pressure pulse. The OMWE is a simplification of this OMW and BP is estimated from empirical constants derived from relating this envelope to intra-arterial or auscultation BP measurements. Unfortunately, there is an extensive number of options and combination of procedures to obtain these two components, and there is no single ideal set that will equally benefit all types of populations. Adaptive solutions to this problem have been proposed in recent years, however these methods have not yet been validated.

Currently the best option for BP estimation is the method of maximum amplitude ratios. Many commercial devices that have been validated are likely to use this algorithm, and their statistics show that they have consistently accurate results. The ratios that some commercial devices use have been approximately derived [77] and have been confirmed to be different from each other. The results of the study published by the author show that there is a significant range of ratios that will yield accurate results, and a device will probably have favourable statistics if the ratios fall anywhere within this range.

Another contribution of this publication is the confirmation that there are several other physiological factors affecting the measurement apart from BP. A major advantage of this

study was the wide range of ages and pressures from the subjects available. This allows comparisons of the effects of arterial stiffness and PP on the MAR algorithm. The sample did not include subjects with underlying health conditions, therefore it was not possible to quantify the effect that these might have on the procedure and on the selection of ratios and envelope function.

An important result of the publication was the demonstration of how population statistics don't represent individual requirements. When individual cases are considered more than a quarter of the sample had inaccurate BP estimates with errors greater than 5 mmHg. In other studies oscillometry has been found to be persistently unreliable for some subjects that don't necessarily have underlying health conditions [78]. The results of said studies were obtained over the course of several visits to the physician's office. It would be interesting to see if, were the subjects discussed in this thesis to return for another set of measurements, the same effect is observed.

Perhaps most surprising was the fact that the most affected population was that aged between 41 to 62 years, and that the most unreliable result was that of their SBP estimation in all OMWE representations. Only about 54 to 67% of the individuals in this age bracket had SBP estimates with an error < 5 mmHg. It was expected that this would be the case in older individuals, however the method overall performed well in the age bracket of 63 to 79 years, with only lesser accuracy in the DBP estimate when functions other than the linear interpolation were used.

One of the objectives established at the beginning of this document was to offer suggestions for the overall improvement of the OBPM method. The first suggestion for improvement is the use of envelopes with smoother profiles than a linear interpolation. Even though the linear interpolation may better reflect the value of pressure at each instant, the different features of such a function may confound the algorithm and lead to incorrect amplitude choices if there are unexpected rises or dips in the signal that an initial filter may have not been able to correct. This suggestion is backed by the better statistics obtained with the polynomial functions.

A second suggestion is the use of a combination of envelopes and ratios during the measurement. Figure 2.13 further confirms the results from table 2.1, showing how the percentage of subjects with better estimates increases when using these envelope functions. However, it is important to mention that, once the age group is considered, the definition of ideal choice

of envelopes and ratios changes. Overall, the potential improvements can be summarized as considering the possibility of having a device that allows customizable settings. Said device can be calibrated for the intended user by their healthcare provider, and the selection of envelope with its corresponding ratio would be set according to this calibration. Even if the device is not calibrated by a professional, the device could offer recommended settings in its user manual.

The author is unaware of the existence of such customizable devices, although there is a high probability that they exist in the market. It is also very likely that these devices won't disclose their method of operation, as is common with automated devices, so it is possible that the results offered in this chapter offer a novel approach to this possibility of customization.

The final important comment done on this method, and established in the objectives of the thesis, is the applicability of automated oscillometric devices as reference to calibrate newly developed cuff-less devices. Based on the results presented here we can confirm that there is good reason why this is a preferred first approach to test these new devices. It is evident that good accuracy in automated oscillometric devices is easily achievable with a wide range of amplitude ratios in the MAR algorithm. However, we have also confirmed that users and research groups must be cautious when relying on this method, considering the results of figures 2.13 to 2.15. Testing of devices, particularly those under development, must consider not only the type of population, but also the age bracket of the population. Once again, the suggestion of a customizable device may greatly benefit research as well, broadening the options of testing conditions.

As an overall conclusion, the OBPM method surpasses other BP measurement methods in terms of convenience and reach. It is unfortunate, however, that currently we have been unable to exploit the full extent of the information contained in its components. We instead rely on a set of empirical constants that have been repeatedly found to render the method unreliable for a majority of the population. In this chapter some suggestions have been offered to minimize the errors incurred in the procedure that are simple and easy to apply. The author firmly believes, however, that the most valuable contribution that can be done to the method requires a deeper understanding of the physical phenomenon, and an effective comparison between the theories that describe it and measured data. One of these possible theories and its subsequent comparison will be the subject of a later chapter.

Chapter 3

Auscultation for Blood Pressure Measurement

Auscultation is one of the most ancient procedures used to evaluate a subject's condition. In essence, it is the act of listening to the internal sounds of the human body, ideally with a stethoscope. The use of auscultation for BP estimation came about in 1905 when the Russian surgeon Nicolai Korotkoff discovered the series of periodic sounds now called Korotkoff Sounds in his honour.

Korotkoff realized that, when compressing a limb with a cuff to occlude the flow of blood through an artery towards the periphery, the method of palpation alone was not enough to verify that the artery was completely occluded. If only partial occlusion was achieved, a small volume of blood could still flow through the length of the cuff, yet the pulse would not perceptibly transmit to the surface. Instead, Korotkoff correctly concluded that sound was a more efficient marker of total occlusion. He noticed that when pressure in the cuff was high enough to completely collapse the artery no sounds would come through the stethoscope, but as pressure decreased in the cuff and flow of blood was slowly restored, what he described as "clapping sounds" could be heard, even before the reappearance of pulsations in the periphery of the limb [79].

Korotkoff sounds (KS) were later found to be an efficient method to estimate BP in a non-invasive way. Korotkoff himself theorized that the appearance of sounds marked the point where the arterial pressure wave initially surpassed the point of occlusion, that is, the instant when the artery first reopens, and thus indicates the point of SBP. As the cuff continues to be deflated and the pressure it applies on the artery decreases, there comes a point where the KS disappear. Korotkoff assigned the location of DBP to this event, assuming that at

this moment the pressure pulse wave was free to pass under the cuff. Comparisons of intra-arterial pressure measurements and the appearance/disappearance of KS later confirmed these associations to SBP and DBP.

Currently, blinded, two-observer manual auscultation to estimate BP is considered the gold standard. Definitions of the thresholds of BP that correspond to reduced risks of cardiovascular disease are based on statistical data obtained initially from standardized single observer auscultation (and later from oscillometric measurement). Two-observer auscultation is also recommended to validate any type of automated device.

However, as mentioned in the previous chapter, use of auscultatory BP measurement for clinical care or population surveillance purposes is slowly being phased out and replaced with automated devices for the following reasons:

1. Proper auscultation is ideally, and most accurately, performed using a mercury sphygmomanometer; however, due to concerns regarding mercury toxicity, many jurisdictions have banned the use of mercury sphygmomanometers.

2. Auscultation is more operator dependent than automated measurement, underscoring the need for training and periodic recertification. This means that subjective decisions made by the operator are a source of error and inaccuracy. For instance, terminal digit preference, such as consistent rounding of the values to the nearest zero or to a specific value of BP commonly occurs. As an example, a study found that when a target BP (SBP = 150 mmHg) was set for a particular hypertensive group under treatment, reported values in follow-up measurements would repeatedly fall on the same value (148 mmHg), potentially overestimating the number of subjects that achieved the goal [80]. A most important source of error, and one that is sought to be addressed in this work, is the ability of the operator to properly identify the sounds that are the basis of the method. Often times the sounds that signal the location of SBP and DBP are faint and easy to miss, resulting in an under/over-estimation of the respective pressures. The DBP estimate is particularly difficult with this method. Hearing acuity of the operator may be a factor to consider, although hearing loss from aging or from damage occurs first at high frequencies [81] which, as will be discussed in the next sections, does not necessarily affect KS perception. Instead, it is considered in this work that the effect

known as masking of sounds has a greater impact in this source of error. The principles of this effect will be discussed in depth and how they relate to auscultation below.

3. Auscultation requires the observer to be next to the subject, which leads to prevalence of white-coat effect and white-coat hypertension.

Automated devices for BP measurement that use auscultation and sound processing are available, but in a much smaller proportion compared to oscillometry based devices. These devices use certain features of the KS, like amplitude and frequency content, to determine SBP and DBP. However, similar to the empirical ratios in oscillometry, the exploited features often come from results observed for certain populations that vary from one study to another.

As pointed out in the introduction, the author firmly believes that in order for an automated auscultation device for BP measurement to be successful, it must reproduce the results of its true definition: measurement of BP based on human judgement of the sounds heard through the stethoscope. Therefore, in this chapter the goal is to address this need for a device that can estimate BP in a similar way that a human operator would.

The most useful approach we can take, thus, is analyzing the method under a psychoacoustical perspective. Psychoacoustics studies sound perception, and the effect that sound characteristics such as frequency and amplitude have on human interpretation of it. For this reason, the author theorizes that a psychoacoustical analysis of the KS in particular is the key to an automated auscultation algorithm and subsequent device.

In this chapter, a review of the characteristics that define the KS is presented first. By doing so, we can narrow the broad subject of psychoacoustics to those concepts that will be of use for the study. Next, the basic concepts of psychoacoustics will be defined in detail, specifically the effect known as masking of sounds which will be central to the development of the algorithm. Finally, this theory will be applied to a set of digitized auscultation sounds, and the results and discussion of this study will serve as basis to develop the proposed automated auscultation algorithm.

The implications of these results, and how they align with the objectives set in the introduction will be discussed in detail in the final section of the chapter. Particularly, the possibilities this algorithm represents, as well as the challenges that need to be addressed before it can be implemented in a device.

3.1 The Korotkoff Sounds

The procedure followed to estimate BP through auscultation is initially similar to that followed in oscillometry. The same considerations of optimum measurement conditions (room temperature, body and arm position, etc.) and proper cuff selection followed in an oscillometric BP measurement (OBPM) are observed for an auscultation measurement. Just as in an OBPM, an inflatable cuff is wrapped around the upper arm of the subject, although in this method the transducer is now a stethoscope. The head-piece of the stethoscope is placed on top of the brachial artery at the distal end of the cuff, usually on the diaphragm side.

The cuff is inflated until the pressure transmitted to the arm reaches suspected suprasystolic levels and the brachial artery is fully occluded, which can be verified with the stethoscope by the absence of sounds. Air in the cuff is released to decrease cuff pressure, preferably at a rate of 2-3 mmHg/s, which is a lower rate than that used in oscillometry. Inflation and deflation are usually done manually and this requires practice to be able to achieve the ideal deflation rate. The cuff is connected to a mercury or aneroid sphygmomanometer to keep track of the pressure inside.

As cuff pressure reaches SBP the first KS appears, and these tapping sounds continue in a periodic fashion following the cardiac cycle. As the measurement progresses and cuff pressure continues decreasing KS change their intensity and quality. When cuff pressure reaches DBP, the sounds disappear. KS are categorized into five different phases according to these changes:

- **Phase I** marks the onset of KS and the pressure corresponding to SBP. In some cases they are faint, easy to miss sounds. At least two consecutive beats should be heard to be categorized as SBP; in some cases sporadic single beats (or artifact from movement of the stethoscope or arm) can be heard at suprasystolic pressure levels but these are not considered part of phase I.

- **Phase II** sounds are more defined than in phase I and there may be a rumble following the initial tap.

- **Phase III** sounds have the highest intensity. A murmur or rumble may also follow the initial tap, but of shorter duration than in phase II.

- **Phase IV** is usually known as the muffling phase. Sounds become abruptly softer and appear to be muffled.
- **Phase V** marks the complete disappearance of sounds. The general consensus is to measure DBP at this phase as "the first sound that is not heard"[1].

There is an additional phenomenon called the auscultatory gap where the sounds disappear for a couple of beats between phases I and III, after SBP has been identified without doubt. If the cuff has not been inflated to a BP level that is above systolic, the end of the auscultatory gap can be mistaken for systole. Phases II and III have no clinical significance to date. In some individuals there is no phase V, or it appears at extremely low cuff pressures. In these cases, for DBP measurement the onset of phase IV is recorded along with phase V, if present.

Measurement of DBP had been a contentious issue for some time until phase V was generally accepted as its location. Phase V often underestimates intra-arterial DBP, yet phase IV clearly overestimates it. In general, however, cuff BP measurements have been found to underestimate intra-arterial SBP and overestimate intra-arterial DBP, regardless of the method used [82].

3.1.1 Time and Frequency Description of the KS

Korotkoff sounds have been closely analyzed since their discovery in 1905. An interesting and extensive qualitative description was published by McCutcheon and Rushmer in 1967 that includes a description of the degree of collapse of the arteries, and of the flow velocity and arterial wall movements at each of the phases described above [83].

The total duration of a KS has been reported to range between 41 and 127.5 ms [84]. Durations were found to increase as cuff pressure decreases, until they reach a maximum probably around phase II, and then decrease until they disappear [85]. The author of the present work has encountered KS of durations potentially as short as 14 ms and as long as 300 ms, although this was not part of a controlled experiment with a large number of samples, and the start and end points of individual KS are difficult to identify from noise present in the signal. What is certain is that the increase and decrease pattern in their duration as measurement progresses was definitely observed.

[1] From Drs. Ringrose and Padwal's most useful instructions on how to measure blood pressure.

Description of the most energetic frequencies present in KS varies from one publication to the next. However, there are two fundamental results that all research agrees on: *1.* there are no characteristic fundamental frequencies or the presence of harmonics, and *2.* there is no significant content in frequencies above 400 Hz.

The change in sound quality from one phase to the other has prompted frequency analysis of each phase as a whole in hopes of identifying representative frequencies. The greatest content has been found, in general, at frequencies below 250 Hz, sometimes as low as < 10 Hz, below the human hearing spectrum [86]. There is some discrepancy on which frequency bands characterize each phase.

Results by Geddes *et al* indicate that the first three phases have lower frequencies, between 40 - 60 Hz, and that the last two phases see an increase to frequencies between 50 and 70 Hz [87]. On the other hand, Allen *et al* found that phases I through III have most of their frequency content below 280 Hz, and that this decreased to below 100 Hz in phases IV and V [88]. Ware and Anderson reported that in phase I higher energy is predominant at frequencies below 50 Hz, and that during phases II and III higher-frequency components appear near 200 Hz, which disappear once again in phases IV and V [89]. They also found that strenuous exercise significantly increases the energy of the high-frequency components in all phases.

In the case of BP estimation, these types of analysis have been applied towards the design of frequency filters that single out KS from the rest of the signal. Maurer and Noordegraaf proposed a bandpass filter ranging from 50 to 160 Hz for this purpose [90]. Golden Jr. *et al* chose a set of more specific narrow-band filters to specifically identify SBP and DBP. They found that at SBP there was a maximum spectral amplitude increase between 18 - 34 Hz, and a maximum decrease at 40 - 60 Hz at DBP [91]. These results were later used to develop and automated auscultation BP measurement device [92].

3.1.2 Theories on the Origin of KS

One of the reasons why developing accurate automated auscultation devices (and oscillometric devices as well, for that matter) has been challenging is the difficulty researchers have encountered in satisfactorily describing the physics of the method. Estimates of SBP and DBP would be more accurate if there was a better understanding of the mechanisms responsible for the sounds that mark the location of these pressures.

A wealth of theories have been proposed since the discovery of the KS. Due to the nature of the phenomenon these theories are inevitably related to flow rate phenomena, pressure differential effects, or the properties of the arterial walls.

Korotkoff himself initially proposed that the section of the artery distal to the compression was fully collapsed and the Korotkoff sounds originated because the pulse wave front forced the arterial walls apart causing vibration and sound production [93]. In reality, the artery is not fully relaxed past the distal end of the cuff, therefore there is no forceful opening of the artery at this point.

An observed property of the transmitted pressure waves, namely the steepening of the ascending limb of the pulse wave, preceded by smaller waves, whenever the artery was compressed by the cuff, led to the shock wave theory [94, 95]. This phenomenon is not always present, so this theory was dismissed as well.

Another interesting observation was the potential presence of the Bernoulli effect in the arteries. This effect could originate due to an increased flow velocity in the semi-compressed arteries that would cause a drop in lateral pressure that further constricts the artery. The artery would then suddenly expand as flow velocity comes close to zero, causing a "fluttering" effect [96, 97]. The viscosity of the medium in which the artery is immersed may, however, provide enough damping to render the energy of this fluttering as insufficient for the production of sound.

A natural later conclusion was that flow turbulence was responsible for the origin of KS. It was proposed that the blood that flows through the constriction becomes turbulent, and in turn releases energy that transforms into acoustic energy [98, 99]. Others proposed that a combination of this turbulence along with a sudden separation of the arterial walls gave origin to the tapping sounds and the rumbling sounds that accompany some of them [83, 100].

Theories related to arterial wall properties propose that cuff pressure interacts with arterial mechanics to generate instability and cause vibrations [101–103]. This is made possible due to the nonlinear compliance of the artery, which is a topic that will be discussed in the following chapters.

Finally, improved computational equipment and modelling techniques have made it possible to combine and analyze fluid dynamics and arterial mechanics. For instance, simulations of the flow and pressure differentials, and how arterial wall mechanics change by the presence

of cuff pressure, are now possible for the generation of artificial KS [3, 103]. These improved models may eventually lead to a more efficient description of the phenomena that gives origin to the KS.

3.2 The Stethoscope

Before approaching the subject of the human perception of sound and how this affects the detection of KS, it is important to briefly comment on one of the most important components of auscultation: the stethoscope. In the case of manual auscultation, the stethoscope acts as the transducer that detects vibrations at the surface of the skin and transforms their energy into acoustic waves.

The acoustic stethoscope was invented in 1816 by the French physician Rene Theophile Hyacinthe Laënnec, and it consisted of a hollow wooden tube. Modern stethoscopes, exemplified in the diagram in figure 3.1, consist of a chest-piece that can be used in two modes, bell and diaphragm, of hollow rubber tubing that connects the chest piece to the earpieces, and of earpieces that should fit comfortably inside the ears and fully seal the ear cavity. The diaphragm of the stethoscope has a circular membrane that conducts the skin's vibrations. The bell, on the other hand, is a hollow piece that uses the skin as the membrane. The stethoscope provides a closed acoustic system for sound conduction through a column of air.

The difference between bell and diaphragm modes of a stethoscope is related to their transfer functions. A transfer function is defined as the ratio of sound pressure delivered at the ears to the sound pressure detected at the chest piece as a function of frequency. The dimensions and materials of the bell and diaphragm modes influence their resonant or fundamental frequencies. Maximums in their transfer function are usually located near these frequencies.

These differences in transfer functions were thoroughly demonstrated in a 1966 study by Ertel *et al* where they compared the transfer functions of four different types of bell chest-pieces and three diaphragm chest-pieces that were manufactured at the time that had different features and dimensions [104]. The majority of the bell chest-pieces had a maximum transmission ratio near 100 Hz and attenuated most of the frequencies above 200 Hz. The diaphragms on the other hand acted mostly as filters, attenuating lower frequencies while leaving higher frequencies almost undisturbed.

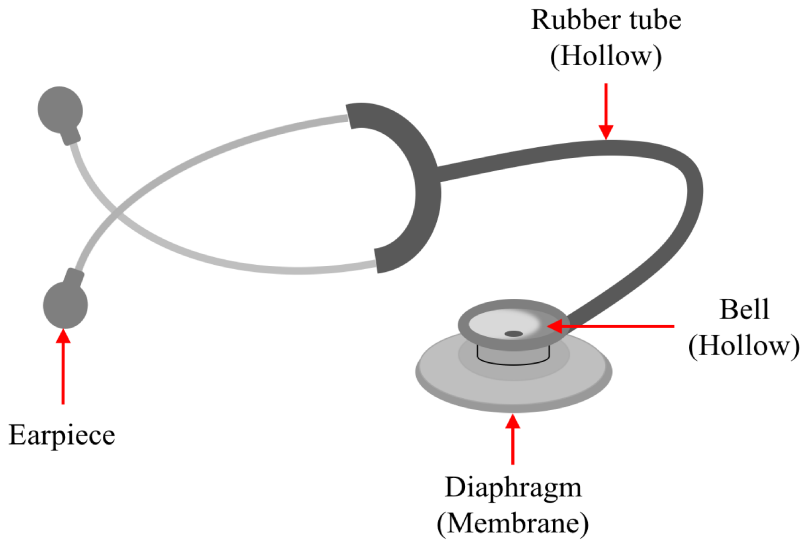

FIGURE 3.1: Diagram of the components of an acoustic stethoscope.

More recent studies have found that in modern acoustic stethoscopes there is no significant difference between bell and diaphragm modes, and that for the purpose of BP measurement both modes can be used interchangeably [105–107]. The diaphragm of the stethoscope is often preferred in BP measurements because it is easier to hold in place. Also, its fundamental mode of vibration is dependent on the stress applied to the diaphragm, which makes it possible to "manually select" which frequencies are attenuated/amplified by applying more or less pressure on the chest-piece.

Electronic stethoscopes offer certain advantages over acoustic stethoscopes. Their operation is based on different principles: the chest-piece is a microphone that converts the vibrations of the underlying body part into electric signals. Each electronic stethoscope uses a different type of electroacoustic transducer, such as electret microphones, piezoelectrics or capacitor-based microphones. The electric signals are then transmitted to headphones or speakers.

One of the advantages these electronic stethoscopes offer is sound amplification. Softer sounds or sounds below audible ranges can be made distinctly perceptible by controlling the output "volume" of the stethoscope. This, however, is also one of their disadvantages. The use of electronic components adds a certain amount of electronic noise to the signal, and

amplifying sounds of interest also amplifies this noise. Manufacturers often include digital or analog filters to remove this noise and to simulate bell and diaphragm modes of operation of the acoustic stethoscope. These filters selectively amplify certain ranges of frequencies that are supposed to correspond to each mode.

A study that compared four different electronic stethoscopes to an acoustic stethoscope found significant differences in the transmitted frequencies [108]. This means that the filters implemented in the electronic stethoscopes hardly mimic the output of an acoustic stethoscope, and there is an evident difference in the sound quality between one type of stethoscope and another.

Of these four stethoscopes one was found to have the closest resemblance to an acoustic stethoscope. The study does not mention brands, but from the description of its features it was easy to deduce that the stethoscope in question was the One Digital Stethoscope (Thinklabs Medical LLC, CO, USA). This stethoscope is essentially a capacitor, with the diaphragm acting as a movable plate. It includes five filters that span different frequency ranges, two of which are supposed to mimic bell and diaphragm mode, two that slightly shift the frequency ranges of the first two filters to higher frequencies, and a wideband mode that has an extended frequency range, between 20 and 2000 Hz.

This digital stethoscope was chosen as the ideal option for the analyses in this work. The response of its wideband mode is flat over a wide range of frequencies, including those of interest for KS auscultation, as shown in figure 3.2, which was reproduced based on the information found in the One Digital Stethoscope webpage [109].

3.3 The Effective Detection of Korotkoff Sounds for BP Measurements

The problem of correctly identifying the sounds that determine BP was already stated in the introductory part of this chapter. Phase I and phase V sounds are often difficult to identify because of their low intensity. A couple of possible solutions to this low intensity problem are offered by electronic stethoscopes: the volume of the sounds coming through the earpieces or headphones can be adjusted to the preference of the user, or the sounds can be recorded and played back on a computer, for instance, where audio editing software can be used to improve the quality of the sound.

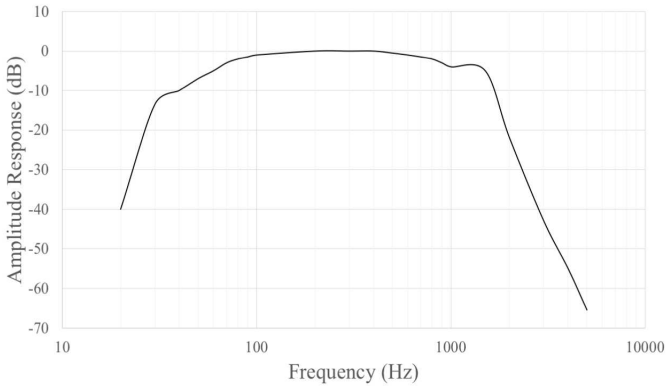

FIGURE 3.2: Approximate reproduction of the One Digital Stethoscope amplitude response as a function of frequency.

One would be inclined to believe that the frequency transmission differences between acoustic and electronic stethoscopes discussed above may affect the usefulness of these solutions. However, in the case of BP measurements this is not necessarily a relevant issue since the only requirement is that the sounds are present at the proper timing, regardless of their frequency composition.

Still, it is important to keep in mind the fact that sound cannot be modified in acoustic stethoscopes, save for the limited selection of fundamental vibration mode in a diaphragm. Sound recorded with electronic stethoscopes should not be substantially adjusted because this may cause large discrepancies from acoustic results and compromise the accuracy of the measurement.

In order to be able to propose an algorithm to automate KS identification, solving to this problem is of immediate interest, considering that any automated device developed in the future will have to make use of an electronic stethoscope. Additionally, in the following chapters analysis is performed on a number oscillometric and auscultation BP measurements simultaneously recorded, the latter of which was done with an electronic stethoscope. Auscultation with an acoustic stethoscope in this situation was not possible, yet accurate estimates of BP are necessary for the analyses. Applying an oscillometry algorithm is not an ideal solution, as stated before, therefore the recorded KS were relied on to accurately estimate

BP in each measurement.

A method to identify KS from these digital measurements that has a similar selection process as that of a certified operator will also benefit, in this case, the completion of the rest of the objectives in this thesis.

3.3.1 Psychoacoustics

Human hearing is dependent on the amplitude and the frequency of the sound pressure waves, and this relationship is by no means linear. Humans can detect very small pressure variations and a wide range of frequencies. The hearing threshold is defined as an RMS pressure of 20 μPa at a frequency of 1000 Hz, and the hearing spectrum extends from 20 Hz to 20 kHz.

The relationship of human hearing sensitivity to the frequency of the sound is presented in Figure 3.3. The y-axis in this figure represents the Sound Pressure Level (SPL). This quantity expresses the difference in pressure between any sound and a reference value, which in this case is the auditory threshold of 20 μPa. Large differences in pressures are involved, so it is customary to express this quantity in logarithmic scale and its units are denoted by "dB SPL". Each line, or contour, in figure 3.3 represents the dB SPL required for pure tones of the corresponding frequencies to be perceived at the same level of loudness, the unit of which is called the phon.

It is customary to also refer to a sound's *intensity level*. Most experimental results related to human sound perception are expressed in reference to this intensity level, so the discussion that follows will be based on sound intensity levels, unless specified otherwise. This quantification of sound is not too different from SPL. The concept is the same: it is a logarithmic ratio of a sound's intensity to a reference intensity. The only difference is that instead of pressure, the energy per unit area is now measured. The reference intensity is also that of the auditory threshold, which in this case equals 10^{-12} Watt/m^2.

The intensity level (IL) and sound pressure level (SPL) of a plane or spherical progressive wave are related by the following equation:

$$IL = SPL + 10log_{10}\frac{p_{ref}^2}{\rho_0 c I_{ref}} \tag{3.1}$$

where p_{ref} and I_{ref} are the reference pressure and intensity given above, respectively, ρ_0 is the density of air at a specific temperature and barometric pressure ($\rho_0 = 1.18$ kg/m^3 at a

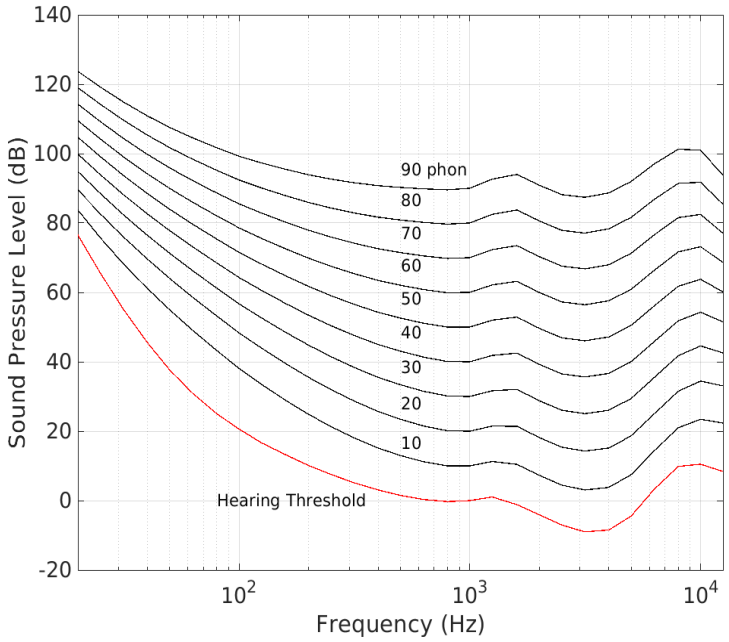

FIGURE 3.3: Equal-loudness contours for pure tones obtained from ISO 226:2003(E) [2].

temperature of 295 K and a pressure of 1 atm), and c is the speed of sound in air, which is also dependent on temperature ($c \sim 344.8$ m/s at a temperature of 295 K).

One of the reasons why KS are sometimes difficult to identify can be inferred from the information in figure 3.3. The human ear is more sensitive to higher frequencies, around 3-4 kHz, and requires increasingly larger pressure variations to be able to detect sounds of lower frequencies. It was already established that KS are mainly composed of frequencies below 250 Hz. This represents a difference of at least 20 dB SPL in their hearing threshold compared to those frequencies to which the ear is more sensitive.

An interesting effect is that the hearing threshold can shift to higher or lower dB SPL values for a number of factors. Auscultative BP measurements are directly affected by this shift in threshold for the following reasons:

1. Binaural thresholds are lower than monaural thresholds [110, 111].

2. When sound is delivered by headphones, the auditory threshold of low frequencies is displaced upwards by about 10 dB SPL relative to the threshold of a sound produced by a loudspeaker located at least 1 m away from the subject. This is believed to be due to irregular twitching of the muscles near the ears where the headphones rest [110]. In the case of auscultation with an acoustic stethoscope the effect may not be as evident, but a similar occurrence is possible depending on the tightness of the earpieces of the stethoscope. The extent to which this tightness affects the threshold of audibility is yet unknown.

3. Audibility thresholds vary from person to person. The graph shown in figure 3.3 represents statistical averages of various publications that reported on otologically normal people[2]. Depending on long term exposure to loud sounds, a person's threshold may be lower or higher compared to that of others. Exposure to moderate sound pressure levels also has an immediate temporal shift in auditory thresholds. For example, if the operator performing auscultation was listening to music through a set of earphones right before the measurement their auditory threshold might have shifted at that moment, potentially impacting their BP estimate.

[2]Defined as a "person in a normal state of health who is free from all signs or symptoms of ear disease and from obstructing wax in the ear canals, and who has no history of undue exposure to noise, exposure to potentially ototoxic drugs or familial hearing loss" by the International Standard with reference number: ISO 226:2003(E) [2].

4. Audibility thresholds depend on the duration of the sound. For sounds lasting longer than 200 ms the dependence of threshold on duration is constant. However, for sounds of durations $<$ 200 ms thresholds increase with decreasing duration at a rate of 10 dB per decade [112]. KS durations are within these ranges, with the shortest ones occurring at the diastolic end. This shift in threshold may be one of the main reasons why the last KS are harder to identify.

This gives further explanation as to why KS identification is challenging, and why there can be significant differences in results between individuals, or even between measurements done by a same individual on different occasions. Determination of the average auditory threshold of KS could potentially help standardize the method, however this is not a simple procedure. Measuring SPL or IL at the earpiece of an acoustic stethoscope is understandably difficult and, although there exist calibrated microphones that assign a value of SPL to their voltage output, this is not the case in electronic stethoscopes, and this is hardly a topic of interest for companies that manufacture them.

Another factor that affects auditory threshold, which was not listed above, is the masking effect. This is present in day-to-day interactions as the difficulty to hear any sound over another, sometimes louder, sound. The auditory threshold of any sound is raised in the presence of another masking sound. A clear example of how this affects KS identification is observed if the measurement is collected in a busy location, with noise occurring in the background. However, even in the ideal case of a measurement performed in a completely silent room there will be a degree of masking present, and it is proposed in this chapter that this effect will be of use in deriving an automated method to detect KS.

This procedure does not require knowledge of the auditory thresholds shown in figure 3.3, only of the manner in which sounds interact with each other. The phenomenon of masking and experimental results relevant to its application in the proposed method will be described below and in the following section.

Masking

Masking is the effect that a sound has of reducing the ability to perceive another sound when they are (usually) simultaneously present. Different masking effects are observed depending on the spectral nature of the sounds, that is, whether they are pure tones, complex tones

(sounds composed of more than one harmonic), narrow-band noise, or wide-band noise. A way to quantify the masking effect is to determine the new auditory threshold of a test sound in the presence of a masker. In other words, the minimum signal-to-noise ratio (SNR) of these two sounds required to identify the test sound from the masker.

Harvey Fletcher determined that only frequencies lying near the spectrum of the test sound are effective in masking it. He proposed the existence of critical bands, the width of which depend on the frequency of the masked tone. Fastl and Zwicker determined that these critical bands had a constant bandwidth of 100 Hz for centre frequencies up to 500 Hz. Past this frequency the bandwidth increases at a rate of $0.2f_c$, where f_c is the centre frequency [112]. The bandwidths proposed can be calculated using the following approximation:

$$\Delta f_{FZ} = 25 + 75[1 + 1.4(f_c/1kHz)^2]^{0.69}. \tag{3.2}$$

Glasberg and Moore proposed a different definition of critical bandwidths. They called them the Equivalent Rectangular Bandwidth, or ERB, which approximates the bandwidths as simple rectangular band-pass filters [81]. The bandwidths can be calculated by the expression:

$$\Delta f_{GM} = 24.7 + 0.108 f_c[kHz], \tag{3.3}$$

where the centre frequency is expressed in units of kHz, and are only valid for 100 Hz $< f_c <$ 10 kHz. This definition by Glasberg and Moore results in narrower bandwidths than those of Fastl and Zwicker. For example, at a centre frequency of 100 Hz the bandwidth is of 35.5 Hz, and for a centre frequency of 500 Hz, 79 Hz.

In the present case it is believed that each KS acts as an individual test sound, and that the noise in the signal is the masking sound. The masking sound in this case will be limited to noise present in the signal by virtue of the use of electronic components. The presence of intrinsic masking sounds has not been explored in the context of acoustic stethoscopes, yet one might argue that they are still present in this type of measurement. The noise in this case is not electronic in nature, but rather noise produced by sounds resonating within the acoustic cavity produced by inherent bodily processes from both ends of the measurement.

Once more, the critical bandwidths discussed here apply to pure tones. An example of a single KS is shown in figure 3.4a. This figure contains a 1-s long segment of sound, and the sudden deflection in voltage observed is the KS. A 400 ms window was selected around the

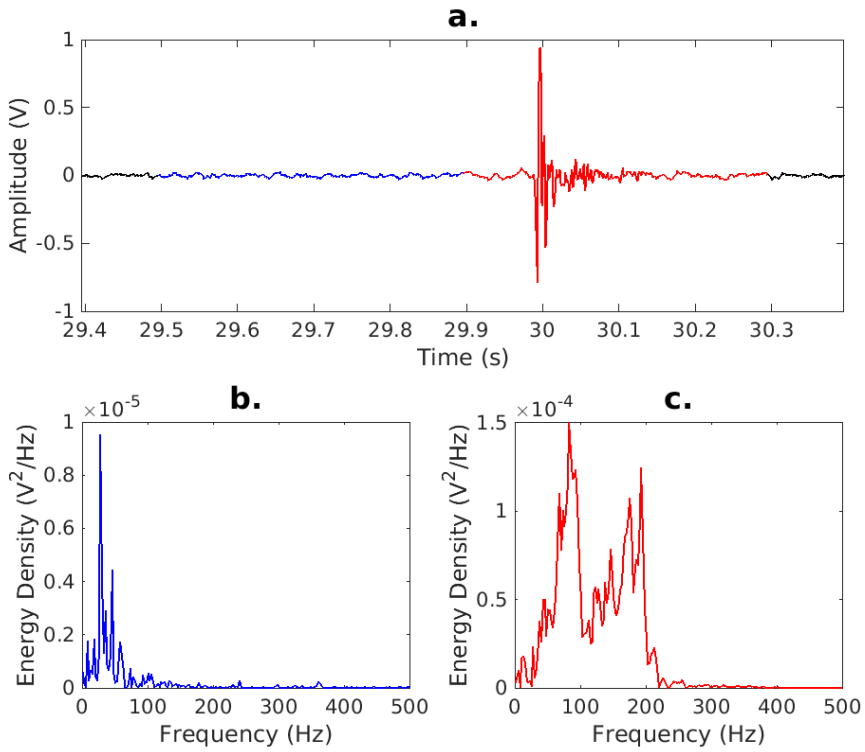

FIGURE 3.4: a.Single Korotkoff sound segment marked in red with immediately preceding noise segment marked in blue. b.Energy density spectrum of the noise segment. c.Energy density spectrum of the KS segment.

KS, spanning 100 ms before the point of maximum positive amplitude of the KS, and 300 ms after; this selection is marked in red and consists of the "test sound". The selection in blue consists of another 400 ms window selected to end immediately before the KS window. This window is considered to be a representation of the masking sound or background noise.

The energy density spectrums of the noise and test sound are given in figures 3.4b and 3.4c, respectively. The maximum energy of the noise segment is an order of magnitude smaller than that of the KS segment. This sample has not been filtered or altered in any way. From these figures one can immediately discard masking effects related to pure or complex tones, and the immediate application of either of the above equations to calculate their critical bandwidths.

The background noise is also clearly not the white noise signal present in many electronic devices. White noise is defined as a sound with constant spectral density independent of frequency spanning the whole range of audible frequencies.

The most obvious conclusion derived from figure 3.4 is that KS can be considered a case of narrow-band noise masked by another narrow-band noise. Bos and de Boer studied this case, in which test and masking sounds were narrow-band noises of the same bandwidth [1]. What they found was that there is a minimum *SNR*, or intensity difference between the two sounds, required for a human to be able to perceive the test sound above the masking sound. This minimum intensity difference is known as the Difference Limen, *DL*.

The *DL* has been found to decrease with increasing intensity and to be independent of frequency [113]. Bos and de Boer found that in the case of narrow-band sounds the *DL* depends on their bandwidth. They also confirmed that it may also be independent of central frequency, but it is subject-dependent. In their work they present results for the *DL* of the two authors for test sounds of different bandwidths and centred at different frequencies. An approximation of their results for a centre frequency of 500 Hz is presented in table 3.1. Their results were obtained through binaural listening and with test sounds of 250-ms duration, which is a similar situation in KS listening.

The bandwidths shown in table 3.1 were chosen from results in [1] for being the ones most closely related to the critical bandwidths discussed above for pure tones centred at frequencies below 500 Hz. The results of table 3.1 also show how the *DL* depend on the subject, as there is a mean difference of approximately 1 dB between the two observers.

In the following section the results of a study of the *SNR* between KS and noise segments

TABLE 3.1: Difference limens obtained from [1].

Δf [Hz]	Difference Limen [dB]	
	Observer CEB	Observer EdB
20	5.1	6.6
40	4.2	5.6
80	3.5	4.4
100	2.9	3.4

like the one shown in figure 3.4 are presented. This was calculated at the four different bandwidths in table 3.1 in an attempt to identify which one better represents the KS and the extent to which noise in the signal is capable of masking them. The observed results are later used in combination with the *DL* from Bos and de Boer to propose an automated method to detect KS, and to potentially estimate BP, that mimics human response.

3.4 Study on the Identification of KS above Noise in a Digital Auscultation Measurement

3.4.1 Data Collection

For this study digital auscultation measurements were collected by the author from 9 volunteers at the National Research Council Canada, including staff and students. Measurements were taken in two rounds, the first including 4 volunteers, and the second including the remaining 5. All volunteers were instructed to abstain from ingesting food and caffeinated beverages for at least 30 minutes prior to the measurement, as well as from performing strenuous physical activity.

Volunteers were seated with their back supported and their measurement arm propped up so the cuff would be approximately at heart level. Unfortunately, the temperature of the room could not be controlled in the measurement and it was lower than recommended ($\sim 20°C \pm 1°C$), however, since the purpose of this study was not strictly determining the true BP of each volunteer, this fact may be overlooked.

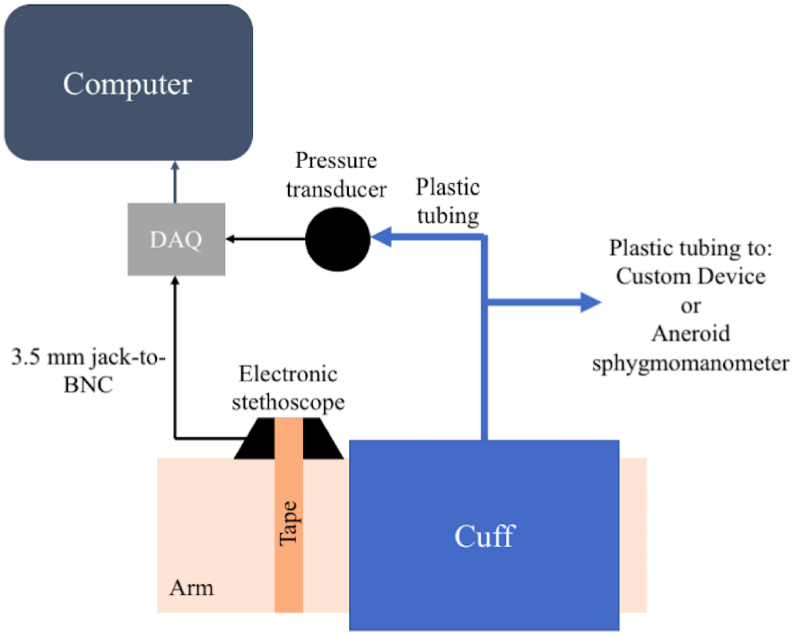

FIGURE 3.5: Diagram of the setup used to record both oscillometric and digital auscultation data.

In all measurements simultaneous oscillometric and auscultation data were recorded with the setup represented in figure 3.5. The One Digital Stethoscope, described in a previous section, was placed on top of the brachial artery and secured to the arm of the volunteer with the aid of medical tape. The wide-band mode of the available stethoscope's filters was selected, which passes frequencies between 20 Hz and 2 kHz. It was connected to a DAQ through a 3.5-mm-jack-to-BNC cable, which in turn was connected to a computer, where data were recorded as *txt* and *wav* files with a LabVIEW (National Instruments Corp.) code written by Derek Weiler, a co-op student collaborating with Dr. Hiebert's group during 2019. The data saved in the *txt* files were vectors of voltage as functions of time.

For the first round of measurements the rubber tubing of the cuff was connected to a custom oscillometric device borrowed from the Department of Medicine of the University of Alberta, which controlled inflation and deflation of the cuff. Data in this round were sampled at a rate of 1 kSps. For the second round the measurement was entirely manual and the tubing was connected to an aneroid sphygmomanometer that includes a dial, a bulb and a valve. Inflation and deflation were controlled by the operator (the author) and sampled at a rate of 10 kSps.

To collect the pressure data the tubing attached to the cuff was connected through a "T" connector to a pressure transducer (MPX5050GP, Freescale Semiconductor, Inc.), which in turn was also connected to a DAQ. The computer received the data from the DAQ in the form of voltage as a function of time, which was then converted to pressure as a function of time following the transducer's specifications for data conversion.

At least three consecutive measurements were collected per volunteer each session, with a rest period of at least one minute between measurements. The group in Round 1 had BP measurements taken in at least two occasions except for one volunteer, while the group in round 2 participated only once. Of these, two representative measurements were selected per volunteer for analysis, for a total of 18 measurements. None of the volunteers indicated having underlying health conditions. Pressures in this set of 18 measurements ranged from $90.08 - 138.71$ mmHg for SBP, with mean $\pm$ SD of 114.71 ± 12.78 mmHg; DBP ranged from $47.07 - 100.74$ mmHg, with mean $\pm$ SD of 66.35 ± 13.55 mmHg.

3.4.2 Experimental Procedure and Data Processing

Simultaneous measurement of BP with an acoustic stethoscope was not possible due to space constraints, because the electronic stethoscope was required to be placed in the antecubital fossa, leaving no room for another stethoscope head. For this reason, there is no estimate of BP as determined by traditional manual auscultation with an acoustic stethoscope. Instead, BP had to be determined by listening to the digital audio track. This was done on the free audio editing software Audacity.

As mentioned above, the wide-band mode of the One Digital Stethoscope was used to measure this set. As a reminder, its frequency response is maximally flat between the frequencies of 100 - 1000 Hz, and frequencies below 100 Hz are attenuated, with the highest attenuation rate occurring below 40 Hz (see figure 3.2 for reference). For this reason, to keep the data that was least modified by the stethoscope, in the software Audacity all audio was high-pass filtered with a cutoff frequency of 50 Hz, and then low-pass filtered with a cutoff frequency of 400 Hz, both filters at the same roll-off rate of 36 dB/octave.

The audio was played back on at least three separate occasions for the author to identify as many audible sounds as possible. All files were listened to at the same volume, raised until most of the fainter sounds at the diastolic end were perceptible, yet the louder sounds were not uncomfortable to hear. Phase I was easier to identify, with only a few differences in some measurements, where it could be identified as commencing a beat sooner or later. Phase V was often harder to identify, particularly because it appeared to extend to the end of the measurement in some volunteers. SBP and DBP locations were thus estimated at the locations most consistently identified on each separate occasion. Their pressure values were obtained by relating their timing to the corresponding oscillometric data.

The *txt* files were processed using Matlab (The MathWorks, Inc., Natick, Massachusetts, USA). The DC bias of the signal was removed first by subtracting the mean of the signal. Then, a 6^{th} order Butterworth band-pass filter was applied to the data between the limits of 50 - 400 Hz. This bandpass filter is the equivalent of the combination of low- and high-pass filters applied in Audacity, and an example of how this filter alters the frequency spectrum of the measurements is given in figure 3.6. The black trace is that of the frequency spectrum of a complete auscultation measurement, with only the DC bias removed from it and no filters applied. The red trace is the section of the frequency spectrum that remains after the Butterworth band-pass filter discussed above is applied to the original signal.

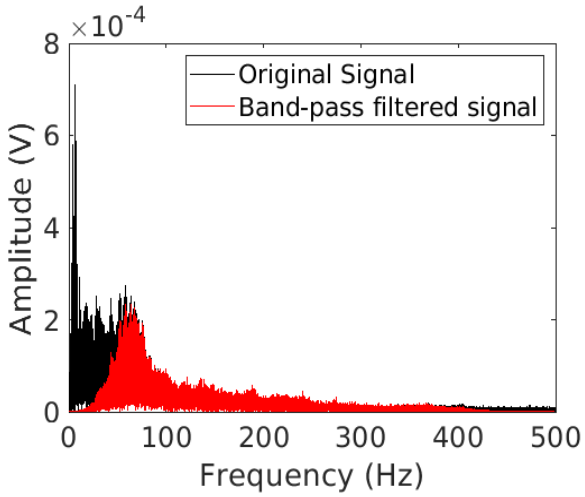

FIGURE 3.6: Frequency spectrum of a full auscultation measurement. In black is the spectrum of the original signal and overlaid in red is that of the band-pass filtered signal.

Several measurements were found to have significant energy peaks at the mains frequency and some of its harmonics, as well as others believed to be carrier frequencies. To prevent these frequencies from affecting the results they were attenuated with a 4^{th} order Bandstop Chebyshev Type II filter with edge frequencies $\pm$ 2.5 Hz from the central frequency. The frequencies that were to be attenuated were manually selected from visual inspection of the single-sided amplitude spectrum of the complete sound signal.

The procedure that follows is summarized in the flow diagram in figure 3.7. The sound signal was divided in windows 700 ms long, equivalent to a heartbeat period of 85 bmp. Windows with content of amplitude $\geq$ 0.5 mV were selected for further processing and analysis. Each of these selected windows were identified as the windows containing the test sound and are numbered in part 1 of the flow diagram.

The point of highest amplitude in each was identified, and the windows were re-centred using this point as reference, extending 100 ms before and 300 ms after this point. A second 400-ms window was selected as that containing the masking sound for each test sound window. This noise segment was chosen to end immediately before the test sound. An example of these segment selections was given in figure 3.4 and is represented in part 2 of the flow diagram, where the blue trace corresponds to the masking sound and the red trace to the test sound.

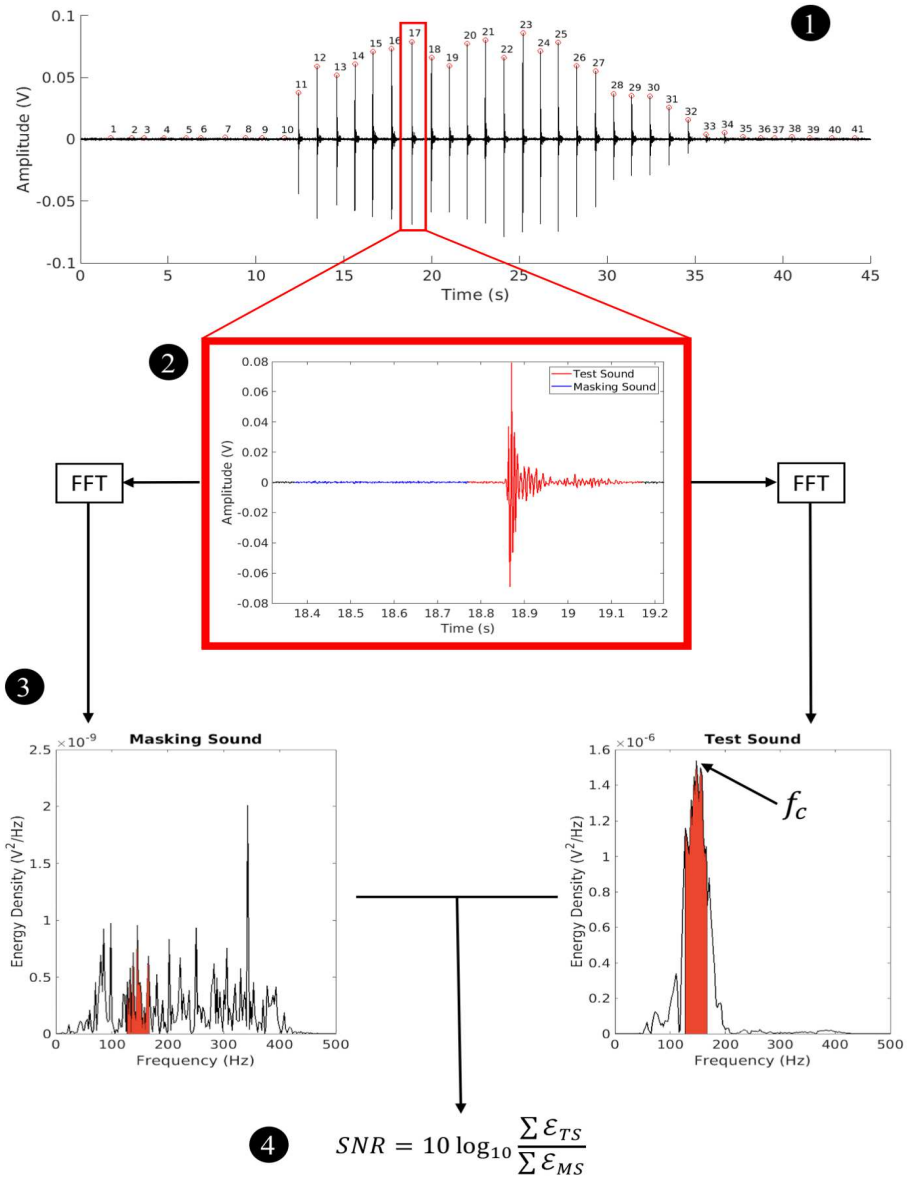

FIGURE 3.7: Flow diagram of the calculation of the *SNR* between test and masking sounds.

To select the central frequencies for critical bandwidth determination, the spectral energy density of the test and masking sound segments was obtained by means of a Fast Fourier Transform (FFT). The frequency with the highest energy density in the test sound was selected as the central frequency, f_c. The four critical bands of widths 20, 40, 80 and 100 Hz were centred around this frequency. These steps are exemplified in part 3 of the flow diagram, and the coloured areas correspond to the critical bandwidth.

Finally, the *SNR* was calculated as the ratio of the sum of energy over the critical bands, which in part 4 of the flow diagram is indicated by the equation

$$SNR = 10\log_{10}\frac{\sum \varepsilon_{TS}}{\sum \varepsilon_{MS}} \tag{3.4}$$

where ε_{TS} is the energy of the test sound and ε_{MS} of the masking sound.

3.4.3 Results

An example of one of the measurements is given in figure 3.8. Figure 3.8a is the sound signal after having the bandpass filter applied to it. Figure 3.8b is the single-sided amplitude spectrum of the measurement, and figure 3.8c is the single-sided amplitude spectrum of the same measurement after the Chebyshev filters for different frequencies were applied.

The example in figure 3.8a has clear extraneous frequency peaks of higher amplitude than the adjacent frequencies centred at 30, 45 and 60 Hz. These higher amplitude frequencies were attenuated by 10 dB, the result of which is shown in figure 3.8c. The 60 Hz frequency is the mains frequency that appeared because the measurement setup was powered by a power source connected to the electrical outlet. In some measurements the harmonics 120, 240 and 360 Hz are also present. The frequencies of 30 and 45 Hz may be carrier frequencies originating from one of the measurement setup components.

The test sounds selected can be divided in three categories: inaudible sounds, KS, and audible sounds that are not KS, but rather noise artifact or sporadic beats resembling KS that do not follow the periodicity of the rest of the KS. These categories are expected to be differentiable by the overall frequency content or *SNR* of the sounds belonging to each. If this is the case, these differences will be particularly important in identifying the points of SBP and DBP.

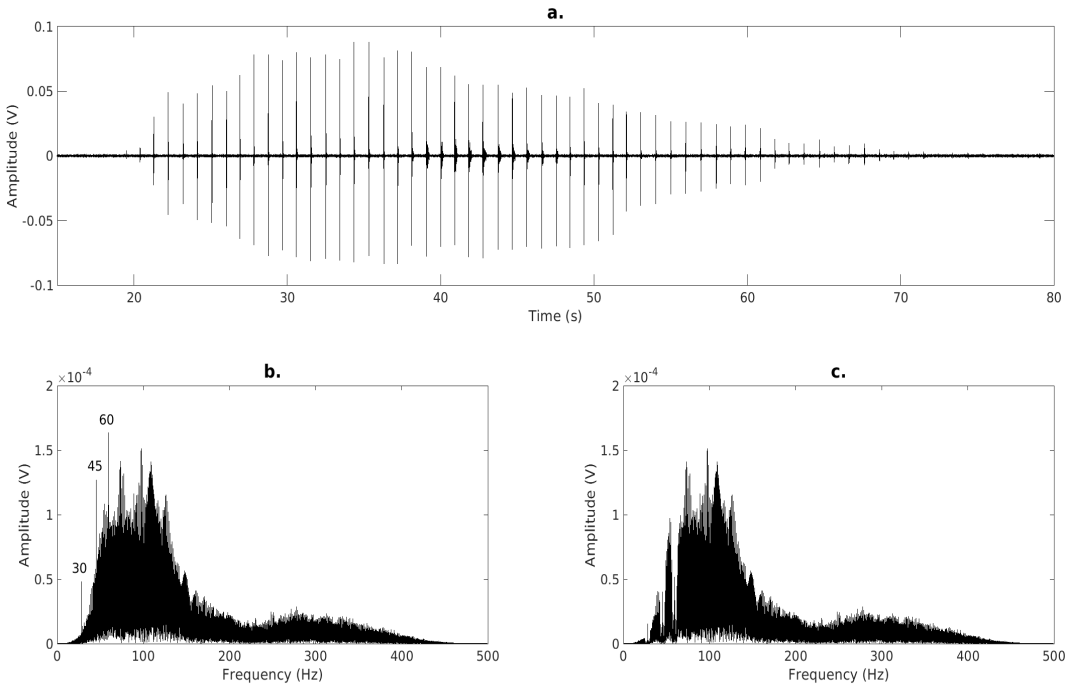

FIGURE 3.8: a.Sound measurement from a volunteer in the first round of measurements. b.Amplitude spectrum of a. with extraneous frequency peaks at 30,45 and 60 Hz. c.Amplitude spectrum of a. after 10 dB attenuation of the frequencies marked in b.

TABLE 3.2: Mean and standard deviation of the central frequencies found for each type of test sound.

Test-Sound Type	Round 1 Mean ± SD [Hz]	Round 2 Mean ± SD [Hz]
KS	75.8 ± 12.8	102.4 ± 20.8
Inaudible	141.8 ± 50.0	94.2 ± 27.3
Noise Artifact	71.7 ± 9.5	110.6 ± 37.5

TABLE 3.3: Mean and standard deviation of the *SNR* of KS test sounds for each critical bandwidth.

Bandwidth $\Delta f_c[Hz]$	Round 1 Mean ± SD [dB]	Round 2 Mean ± SD [dB]
20	24.8 ± 2.2	32.9 ± 4.9
40	23.7 ± 2.2	31.7 ± 5.2
80	22.6 ± 2.1	30.0 ± 4.8
100	22.2 ± 2.0	29.4 ± 4.5

To verify if these differences exist the mean ± SD of the central frequencies for each type of test sound and for each set is shown in table 3.2. The mean ± SD of the *SNR* of the sounds identified as KS are shown in table 3.3 for both rounds and for the four bandwidths considered. Those of the sounds classified as inaudible are given in table 3.4 and those of noise artifact in table 3.5. Each of these results are divided into the two rounds of measurement collection to verify if there was any difference when using automated *vs* manual deflation, or lower and higher sampling rates.

Figures 3.9 through 3.12 show how the *SNR* changes in the vicinity of SBP and DBP, when it is calculated from bandwidths of 20, 40, 80 and 100 Hz, respectively. The markers are the mean value of the *SNR* of all the measurements and the error bars represent ± 1 standard deviation. The corresponding *DL* from each observer in table 3.1 are indicated by the horizontal dashed lines.

In all four figures the red trace indicates the sound segments near SBP and the blue trace the sound segments near DBP. On the systolic end the KS that marks SBP identified with

TABLE 3.4: Mean and standard deviation of the *SNR* of inaudible test sounds for each critical bandwidth.

Bandwidth	Round 1	Round 2
$\Delta f_c[Hz]$	Mean ± SD [dB]	Mean ± SD [dB]
20	2.2 ± 0.9	1.6 ± 1.1
40	1.6 ± 0.6	1.5 ± 0.9
80	1.1 ± 0.5	1.2 ± 0.5
100	1.0 ± 0.4	1.2 ± 0.5

TABLE 3.5: Mean and standard deviation of the *SNR* of noise artifact test sounds for each critical bandwidth.

Bandwidth	Round 1	Round 2
$\Delta f_c[Hz]$	Mean ± SD [dB]	Mean ± SD [dB]
20	9.1 ± 2.7	18.0 ± 2.7
40	7.7 ± 2.6	17.5 ± 2.2
80	6.9 ± 2.4	16.7 ± 2.4
100	6.6 ± 2.4	16.6 ± 2.4

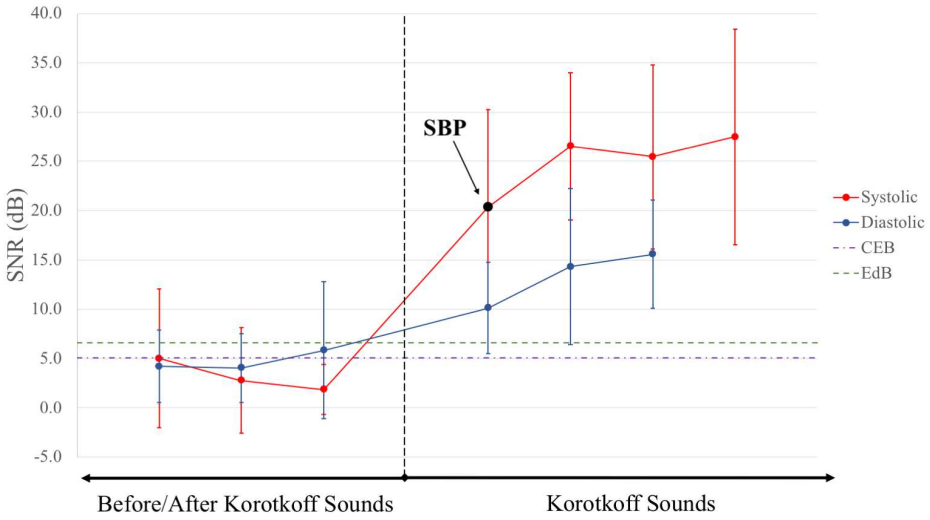

FIGURE 3.9: Mean of the *SNR* of the sounds in the proximity of SBP and DBP calculated for a bandwidth of 20 Hz. The *DL* for 20-Hz bandwidth for each observer in [1] are indicated with horizontal dashed lines. The diastolic plot is inverted in time.

Audacity is highlighted in black, to its left are the three preceding sound segments, and to its right the next three KS. On the diastolic end there is no specific marker for DBP, but rather the last three audible KS identified with Audacity are plotted to the right of the vertical dashed line, and the sound segments that come after are plotted to its left. That is, the plot that corresponds to the diastolic end is inverted in time, with the last sound being the first point on the left. Another way to interpret these plots is the fact that all inaudible sounds are to the left of the dashed vertical line, and all audible sounds to its right.

3.4.4 Discussion

The ability to record and visualize auscultation data is without doubt a significant advantage electronic stethoscopes have over their acoustic counterparts. Recordings such as these can potentially facilitate training and enable less experienced operators to acquire necessary practice. They are particularly ideal for research purposes, such as what is presented in this work. However, a significant drawback of utilizing electronic recordings of auscultation

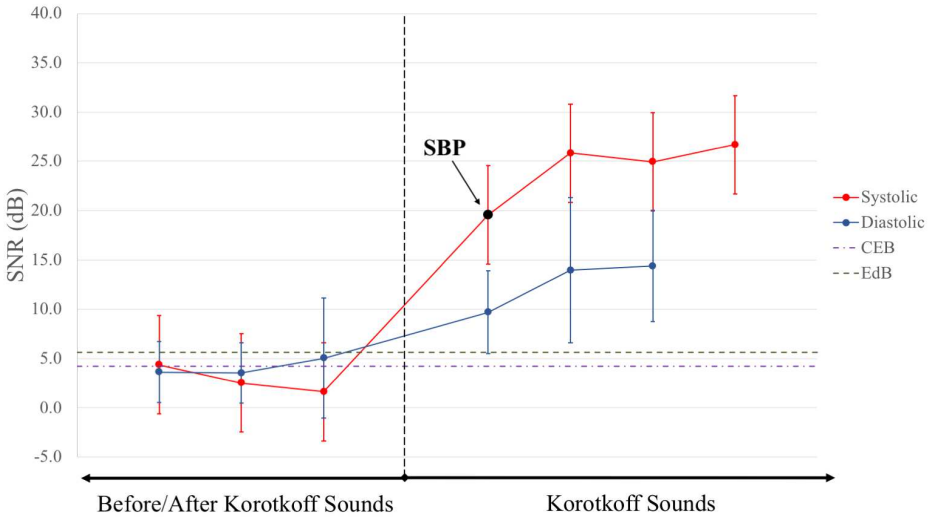

FIGURE 3.10: Mean of the *SNR* of the sounds in the proximity of SBP and DBP calculated for a bandwidth of 40 Hz. The *DL* for 40-Hz bandwidth for each observer in [1] are indicated with horizontal dashed lines. The diastolic plot is inverted in time.

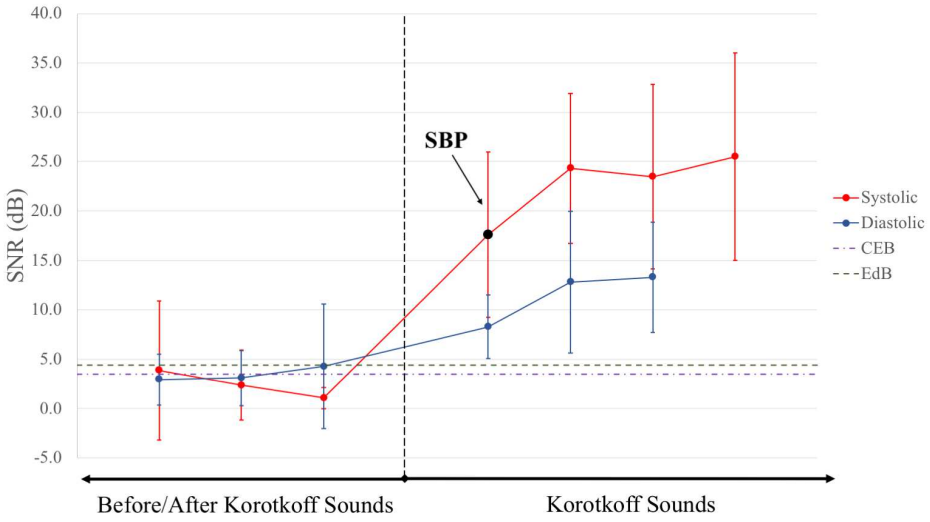

FIGURE 3.11: Mean of the *SNR* of the sounds in the proximity of SBP and DBP calculated for a bandwidth of 80 Hz. The *DL* for 80-Hz bandwidth for each observer in [1] are indicated with horizontal dashed lines. The diastolic plot is inverted in time.

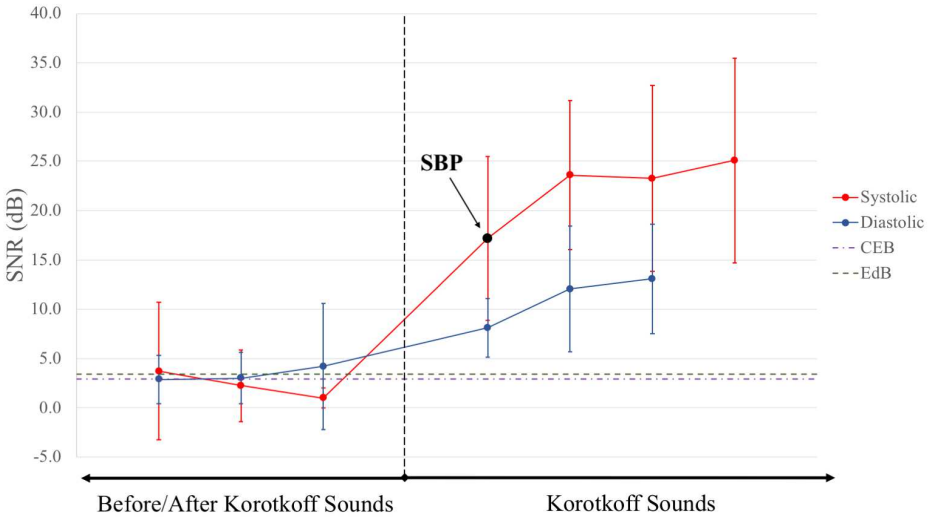

FIGURE 3.12: Mean of the *SNR* of the sounds in the proximity of SBP and DBP calculated for a bandwidth of 100 Hz. The *DL* for 100-Hz bandwidth for each observer in [1] are indicated with horizontal dashed lines. The diastolic plot is inverted in time.

measurements, particularly in the case of BP estimation, is found in defining which sounds are truly relevant to obtain the correct result.

This was of significance in the development of this research, given that one of the features electronic stethoscopes have is the option to increase the volume of the sound. As a result, the operator now has the ability to identify the faintest sounds at the diastolic end that may otherwise not be perceived with acoustic stethoscopes. The dilemma is then whether these new sounds, if present, should be considered part of the measurement or not if they are not identified with the traditional method.

The use of visual aids can also be misleading in trying to identify the relevant sounds. As an example, we have Figure 3.8 at the diastolic end of the measurement, past the 70 s mark. If each vertical line in the measurement, or spike in voltage, is associated with a KS, then the smaller, yet visible, lines at the final seconds of the measurement can be interpreted as KS. One of the purposes of this study is to verify if said lines do correspond to a KS, based on whether a person would be able to perceive them in a measurement above the masking sound.

Unfortunately, the appearance of external frequencies, such as the mains and carrier

frequencies and their harmonics, introduces a certain amount of error to the procedure. Attenuating these frequencies with the use of stopband filters offers a simple and immediate solution. However, the power contained in each frequency is not uniform, therefore selecting the attenuation level for each is not a straightforward decision. Additionally, using a stopband filter also reduces the amplitude of all the frequencies included in the bandwidth of the filter, as can be observed in figure 3.8c. Noticeable dips in the frequency spectrum can be observed where the troublesome frequencies are attenuated.

It should be noted that a smaller range of frequencies can be selected in the stopband filter, depending on the frequency resolution of the original signal. However, the sound segments selected in the next steps of the procedure are limited to a resolution of 2.5 Hz. This means that selecting a bandwidth for the stopband filter that is smaller than the 2.5-Hz resolution will result in an attenuation that will most likely not have any effect on the data of interest.

Despite these issues, the attenuation of these frequencies did prove to be beneficial for the overall algorithm. Before the application of the stopband filters the mains or carrier frequencies were sometimes more energetic than the rest of the spectrum, particularly at the diastolic end. This greater energy of externally sourced frequencies would hinder the process and result in an incorrect classification of the test sound. For example, in figure 3.13 we can appreciate the frequency spectrum of one of the measurements collected, before the attenuation with stopband filters. We can clearly see how the line corresponding to 45 Hz dominates over those next to it. Its effect can be observed in figure 3.14, which is the energy density plot of one of the KS of this measurement near the diastolic end, and its corresponding masking sound.

The frequency with the highest energy in both test and masking sounds is near 45 Hz, and the masking sound actually has a higher energy level than the test sound. When using a critical bandwidth of 40 Hz, the resulting SNR in this case was of 3.15 dB, which would classify the sound as inaudible with either DL. As a reminder, this test sound is an audible KS.

After the stopband filters are applied, we encounter a situation that looks instead like figure 3.15, where the critical frequency of the test sound has been shifted to 52.5 Hz and the energy of the masking sound has been reduced. This is a clear example of why the use of the stopband filters was important to the procedure. In this case, with a critical bandwidth of

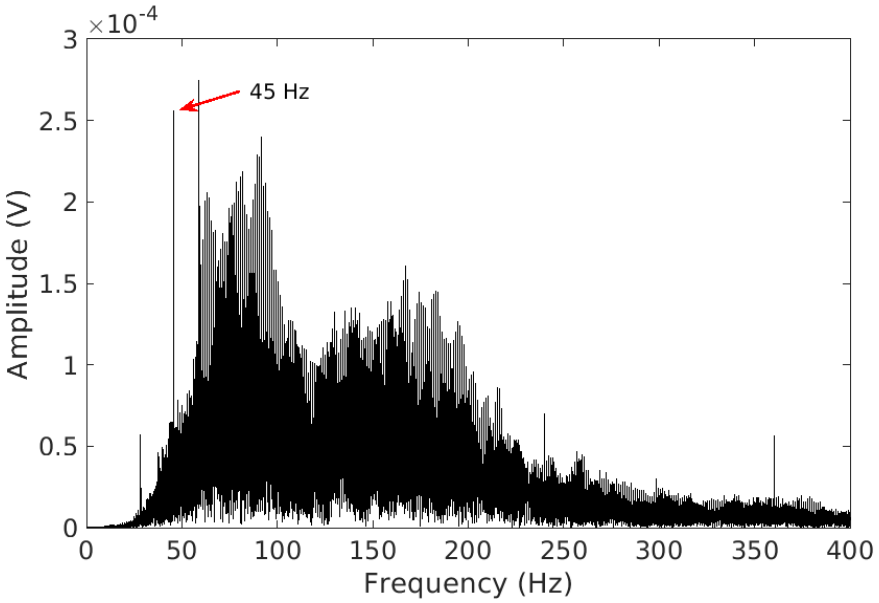

FIGURE 3.13: Amplitude spectrum of a sound measurement after it has been bandpass filtered, but not stopband filtered at the mains and carrier frequencies. The line corresponding to 45 Hz is signalled.

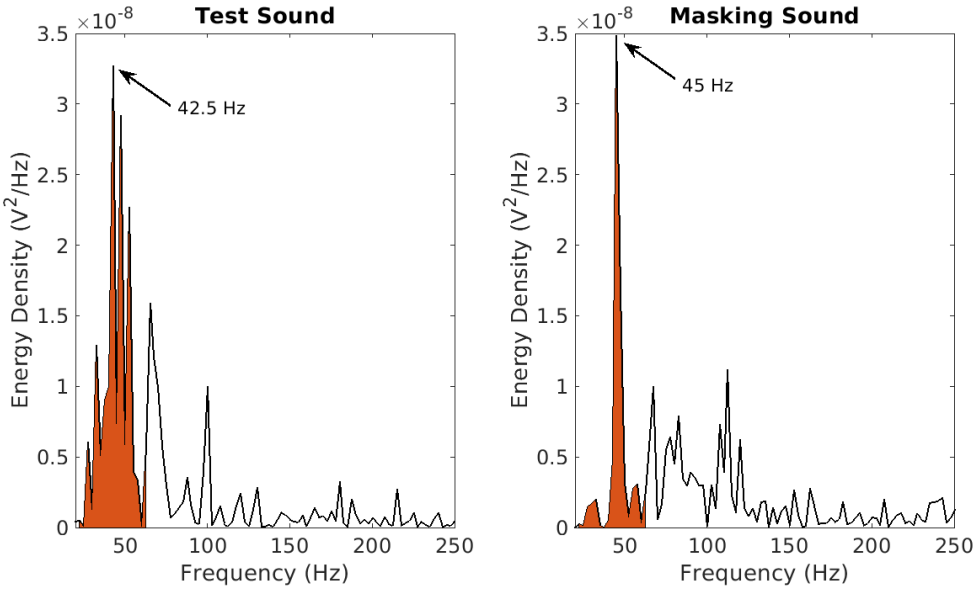

FIGURE 3.14: Energy density of test (left) and masking (right) sounds of a single KS segment without stopband filter application. Coloured area represents a bandwidth of 40 Hz used to calculate a $SNR = 3.15$ dB.

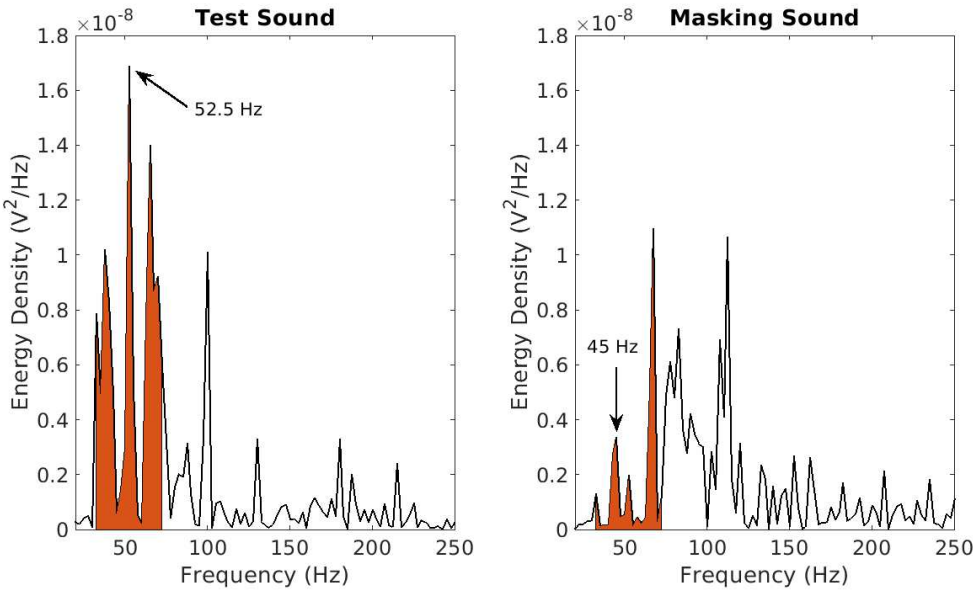

FIGURE 3.15: Energy density of test (left) and masking (right) sounds of a single KS segment after stopband filter application. Coloured area represents a bandwidth of 40 Hz used to calculate a $SNR = 5.65$ dB.

40 Hz once more, the *SNR* is now 5.65 dB, which allows us to correctly classify the segment as containing an audible sound, independent of which *DL* is used for this classification.

Another interesting observation that can be made related to the central frequencies is that, as expected, there are no characteristic frequencies for KS. From table 3.2 we can verify that they are on average located below 200 Hz as reported in previous research, but they are not significantly different from the centre frequencies of noise artifact. There is a shift in the mean of the centre frequencies for all types of sounds between both rounds of measurements. It is not possible to conclude that this was due to the measurement procedure or the sampling rate, since the large SD in all cases points to this being only a statistical matter. Another possibility is that the troublesome frequencies had a more negative impact on one case than on the other.

The results of the mean *SNR* for KS show that there is a significant difference in energy between the test sound and the masking noise. This difference in energy is significantly higher on average for KS than it is for noise artifact. This may be a useful result for filtering out unwanted sounds in the signal that may affect the estimate of BP. This observation is

limited, however, to the case where noise artifact is not particularly intense, for instance a sound coming from tapping on the stethoscope headpiece or considerable movement from the limb. These situations are preferably avoided in BP measurements, so this criterion could be applied to any measurement. In the case of inaudible sound segments the *SNR* is close to zero, meaning there is little to no difference between the segment selected as the test sound and the segment of masking noise as expected.

It is important to mention that there were occasions of incorrect sound classification that were not related to the previous discussion of application of stopband filters. That is, there were still inaudible sounds with a *SNR* higher than the mean, or KS identified from the audio track that had a *SNR* considerably smaller than the mean. This was particularly observed at the diastolic end, but not exclusively. Two reasons for these deviations from the mean have been identified. The first reason is the presence of the mains and carrier frequencies and their harmonics in the audio tracks. These were not removed in Audacity before listening to the audio and could have masked some lower intensity sounds. The second reason is the overlap of the masking sound segments with intermediate vibrations. This happens because the algorithm selects the vibrations with the highest amplitude as the test sound, but within the window there might be another smaller vibration. Once the test sound and masking sound windows are selected, the smaller vibration may fall within the masking sound's range, contributing to the energy of this segment.

Figures 3.9 through 3.12 demonstrate how the *DL* reported in [1] are related to the measurement of BP. The *DL* in said publication refer to the difference in sound intensity of the test and masking sounds, which as mentioned before is a measure of the power of sound. In this case the *SNR* was calculated from the power spectrum of the data, which is why the *DL* can be directly applied to the results.

The sounds identified as corresponding to SBP by listening to the audio tracks, and those that follow, are several dB above both *DL*, independent of the critical bandwidth. This indicates that KS belonging to the first phases have enough energy to not be masked by nearby frequencies. There is also a large jump in *SNR* between the sound marking SBP and that preceding it, which is also usually below the limits of perception. The sound corresponding to SBP, however, has a lower *SNR* on average than the following sounds, sometimes even close to the *DL*. This confirms that the onset of the KS may be a softer sound compared to the ones that follow, explaining why this sound is easy to miss or to be misinterpreted on

occasion.

By contrast, the sounds that were assumed to be the last three audible sounds in the signal when the audio was listened to are much closer to the *DL*. An important observation is that the sound that comes immediately after (the third marker from left to right) in all cases is between or above both limits, and the following two are not too far from them. This is a clear example of how sound perception is subject dependent. In the cases of 20 and 40-Hz bandwidths one observer would "correctly" estimate DBP, while the other would underestimate it. For wider critical bandwidths both observers would likely have greater difficulty in accurately estimating DBP.

This observation may very well apply to the author's assumptions of where the last audible sounds are located. However, two important points must be made in favour of the author's definition of last audible sounds. The first is that, while KS effective frequency bandwidths may not be constant, the sounds in phases IV and V are neither as complex nor as energetic as those in the preceding phases. This may point to a narrower bandwidth of the last KS, and thus to only a narrow noise bandwidth contributing to the masking effect. The second observation is that the three sounds assumed to be inaudible all have approximately similar values of *SNR*. If the blue plots in each figure are read from right to left (in correct temporal order) one can identify a gradual decrease in *SNR* until it reaches an almost constant value in the final three sounds.

These observations may indicate that the author's estimate of audible sounds is accurate, and that narrower critical bandwidths may be more effective in studying the masking of KS.

The possibility also exists that, because mains and carrier frequencies were not removed from the audio track before playback, these could influence the location of the last audible sounds. However this effect would likely be the equivalent of the situation represented in figures 3.9 and 3.10, where in some instances the sounds are perceived and, in some instances, not, depending on the subject.

Finally, it is important to point out that, to the author's knowledge, this is the first analysis of KS done from the psychoacoustics topic of sound masking and difference limens. Other KS research related to psychoacoustics and human hearing threshold exists in the literature [114], however, a significant advantage of this method in comparison is that no information on the microphone's pressure-to-voltage conversion is necessary, and the gain of the apparatus will not affect the results. Another important advantage is that the method

is self-sufficient in the sense that there is no need for an external reference, given that all comparisons are done within a single measurement. From this, the natural progression is to attempt the development of an algorithm to automate auscultation based on the results of this section.

3.5 Proposed Method to Automatically detect KS

The method was applied initially to the 18 measurements described in the previous section so they could serve as a "training" set of data. Once the method was fully established with these measurements, it was applied to a larger set including most of the measurements collected.

In what follows the processing of the data and the selection criteria are described. The effectiveness of the method will be determined by the correct location of the sounds that mark SBP and the last audible KS. Some comment on the accuracy of a hypothetical device is included at the end of this section.

An important caveat in the validity of BP estimation and the accuracy of the method is the fact that BP was estimated to the best of the author's ability. The author is by no means an expert in auscultative BP estimation, so the results are based on instruction received by more capable personnel and the limited amount of experience acquired through the completion of this work.

The data were in general processed in a very similar manner to what is described in the previous section, only adjusted to make the method applicable to sets containing a larger number of measurements. The DC bias is removed as a first step from the original signal by subtracting the mean, and a 6^{th} order bandpass Butterworth filter is applied to the data. The same criterion is used as in the previous section for the filter: the bandpass ranged between the frequencies of 50 - 400 Hz.

In the previous section the external frequencies were visually identified and specifically filtered in each measurement. For a larger number of measurements this individual selection becomes a time-consuming task. For this reason, it was decided that a set of defined frequencies would be filtered based on those that appeared most often in all measurements. In this case the frequencies 30, 45, 60, 120, 240 and 360 Hz, were all equally attenuated 10 dB for all measurements.

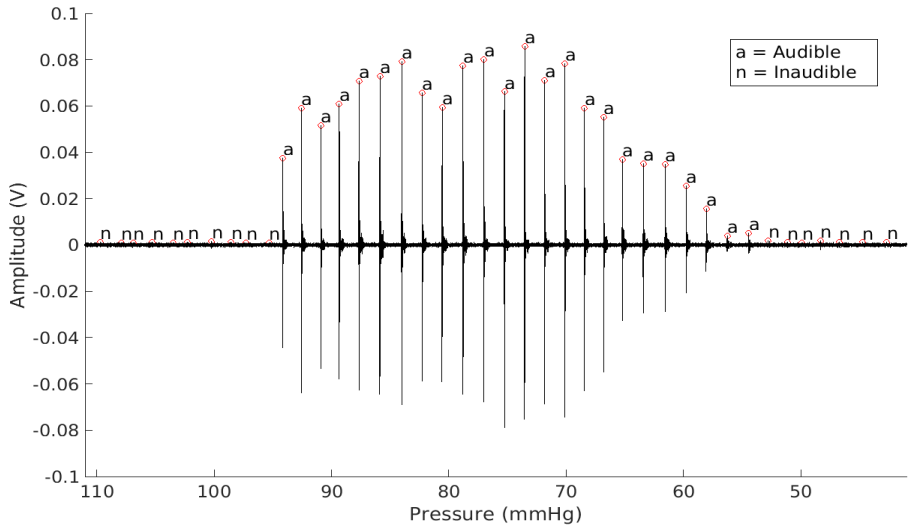

FIGURE 3.16: Visual example of the classification of audible and inaudible sounds by the proposed algorithm. "a" is the label for audible sounds and "n" the label for inaudible sounds.

The rest of the procedure is the same as that described in the previous section. The signal was divided in windows of 700-ms length, test sounds were selected from windows with content ≥ 0.5 mV, and the windows recentred and shortened to 400-ms length. Their corresponding masking segments were selected immediately preceding each test sound. Central frequencies were identified from the amplitude spectrum, and *SNR* was calculated for each within one of the four bandwidths under study.

The first objective of the algorithm is, of course, to differentiate the audible sounds from the inaudible ones. A visual example of this is given in figure 3.16, where a sound measurement is plotted as a function of cuff deflation pressure and the segments are labeled according to their classification. For this purpose, the *DL* from table 3.1 were used as cut-off values. In the training set both *DL* were used for each bandwidth to determine the optimum limit.

An important relationship between KS that was not extensively discussed in the previous section was their periodicity. For subjects with regular heartbeats, KS are spaced by an approximately constant period of time. Clearly, audible sounds that are separated by a length of time greater than the average heartbeat period do not correspond to the set of KS.

This spacing in time was the next criteria to filter out sounds that are not of interest.

To further narrow down the selection of audible candidates to KS only, other results from the previous section can be applied. In the case of SBP, it is observed that the *SNR* of the KS that marks SBP is considerably higher than that of the preceding segment, which is usually an inaudible test sound. Therefore, part of the selection criteria for SBP includes considering this difference.

The case of DBP is far more complicated, since there don't appear to be other relevant characteristics that separate one phase from another. After the *DL* criteria is considered to determine the last few audible sounds, the last KS is identified as that occurring within a temporal separation lower than a couple of standard deviations from the mean of the heartbeat period.

In the training set the most effective combination for BP estimation was obtained with a bandwidth of 40 Hz and the lowest of the two *DL*, that is, 4.2 dB. Of all the sound segments selected by the algorithm in the training set, 852 were identified to be audible sounds, and 365 to be inaudible sounds. This combination had a classification accuracy of 99% for audible sounds (847/852) and of 88% for inaudible sounds (324/365). SBP was accurately estimated 88% of the time (16/18) and DBP 55% of the time (10/18). These values of critical bandwidth and *DL* were thus applied to the complete set of measurements collected by the author. A visual example of the results of the algorithm is given in figure 3.17, which corresponds to the same measurement as in figure 3.16.

A total of 60 measurements is considered for the overall measure of the algorithm's performance, including the 18 measurements of the training set. In these measurements SBP ranged from $90.08 - 138.71$ mmHg, with mean $\pm$ SD of 110.53 ± 13.18 mmHg; DBP ranged from $44.49 - 100.74$ mmHg and mean $\pm$ SD of 63.60 ± 11.61 mmHg.

Of the 60 SBP measurements, 53 were exactly determined by the method. Of the remaining 7, three were incorrectly estimated because there was a gap in the sounds, which shifted the selection to lower pressures where there were uninterrupted occurrences of the KS, as exemplified in figure 3.18. The gap could be an auscultatory gap or the result of poor contact between the stethoscope and the skin caused by movement. The other four incorrect estimates missed the SBP mark by a single vibration.

Of the 60 DBP measurements, 23 were exactly determined by the method. 16 measurements of the 60 missed the DBP mark by a single vibration, 12 missed it by 2 vibrations,

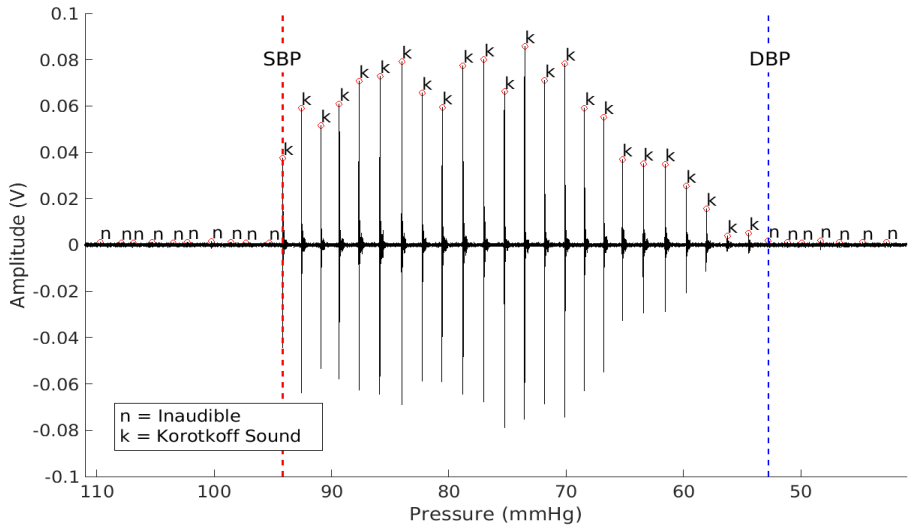

FIGURE 3.17: Visual example of the estimate of BP obtained with the proposed algorithm corresponding to the measurement in figure 3.16. The intermediate sounds between SBP and DBP are marked as "k", corresponding to Korotkoff sounds.

and 9 by 3 or more vibrations. On 22 instances of these errors, however, it was observed that the cause was the periodicity selection criteria, not the *DL* criterion, as shown in figure 3.18. That is, the sound segments were correctly identified as audible/inaudible sounds, but the second filter used to select the point of DBP based on their temporal separation was insufficient. This second filter depends on the mean and SD of the period of the sounds, however in some instances sounds are separated by more than one or two SD.

As a BP measurement method, the resulting mean ± SD of the errors for the set of 60 measurements was 0.19 ± 1.18 mmHg for SBP and 0.02 ± 2.81 mmHg for DBP. This is below the limits of clinical relevance. Overall, only one of the SBP estimates was beyond this limit of clinical relevance and only 3 of the DBP estimates.

3.5.1 Final Remarks

The results presented here provide some evidence for the effective bandwidth containing the main frequency components of the KS, and that exploiting the available knowledge of

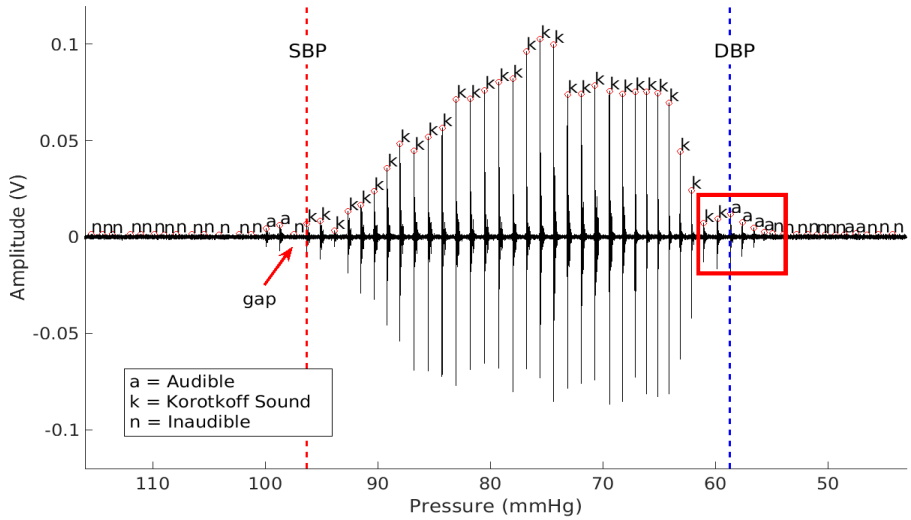

FIGURE 3.18: Example of a measurement with incorrect BP classification containing both a gap at the systolic end, and audible sounds not classified as KS at the diastolic end framed in red.

the masking phenomenon is useful to explain how these sounds are perceived by a human operator. They confirm some of the findings of Bos and de Boer and set a precedent on how to establish critical bandwidths for masked short-duration sounds with frequency content in the lower frequency end of the auditory spectrum.

It should be noted that some disadvantages in this study are the limited number of measurements and that strict protocols were not followed to collect such measurements. Unfortunately, a real estimate of BP through simultaneous auscultation with an acoustic stethoscope was also not possible.

Nevertheless, BP measurement through auscultation relies on correctly identifying the start and endpoints of the KS, regardless of the conditions of the measurement. These points were identified by real human response, that is, by listening to the sounds as they were recorded, and the method proposed here appears to effectively mimic these observations.

It is important to emphasize the fact that this is an original method proposed by the author based on the observations and results obtained above. The main purpose of such a method was to address the need of an automated auscultation device that could faithfully reproduce the results of manual auscultation. The other objective was to develop this method

to optimize the computations of the following sections. These objectives were successfully accomplished, considering of course that the method can still be improved, although the algorithm presented has far more important implications for BP measurement and future device development.

A potential automated device that uses this algorithm, based on auscultation rather than oscillometry, would be of particular importance considering that manual auscultation is part of the gold standard for estimating BP, and that its application is entirely reliant on human perception of sound. The author believes that, if any automated auscultation device is to be developed, the ideal one would be one that can apply psychoacoustic principles into its selection algorithm.

It is also the author's belief that this device based on psychoacoustics would have greater accuracy in BP estimates compared to devices based on oscillometry. The reason behind this is that, as we have discussed in the previous chapter, oscillometric devices are most likely based on empirical constants whose accuracy depends on the individual; a device operating under the proposed algorithm would, instead, rely on the well-established definition of BP measurement. This definition of BP measurement, while having some exceptions for certain cardiovascular conditions, applies to more types of populations.

A potential disadvantage this proposed method could have compared to oscillometric devices, is its application to noisier environments. So far, the discussion above has been limited to masking by electronic noise from the stethoscope. The possibility exists of the stethoscope detecting external sound from the measurement setting, such as a busy clinic, adding to the noise masking the KS. In this case, however, if we were to design an algorithm that is capable of performing accurately in these situations, further analysis of the interaction between KS and other types of background noise is necessary. As we should recall, the method proposed here is based on the assumption that a narrow-band sound in masked by another narrow-band sound. Depending on the type of background external noise the stethoscope is able to detect during a measurement, the possibility exists that we would now have to consider white noise or complex tones masking the narrow-band KS. The effect these type of sounds have on KS could force us to modify the algorithm in order to define new DL and a new set of steps to identify SBP/DBP in the measurement.

An example of these cases of other types of external noise detected by the stethoscope is given in Appendix B. In these cases no further analysis of the psychoacoustics has been done;

the algorithm designed here is tested "as is". The purpose of this exercise is to confirm the need for more analysis on specific types of background noise, and to verify how a potential device based on this original principle would perform in other less than ideal situations.

Despite this disadvantage the algorithm has compared to oscillometric devices, we should not overlook the fact that there are still a large number of applications where a device operating under this algorithm would excel above other automated devices by virtue of its greater accuracy. At-home measurements, for instance, would be greatly benefited since they are usually performed in quieter settings where additional background noise is not a significant concern. If a patient were to share measurements collected with this device with their physician, diagnosis and treatment decisions would have the added confidence of being based on results that the physician would have obtained themselves.

Another advantage of this device, and one that was set to be addressed in the introduction of this text, is its use as reference for other devices. Cuff-less ambulatory devices could now be calibrated with this potential device and the added uncertainty in BP estimation through oscillometric devices can be avoided altogether. Research groups would now have direct "gold-standard type" estimates to calibrate their devices, increasing the confidence in the results obtained with their own devices.

A final important example of another application of this proposed algorithm/device, that cannot be addressed by other automated devices, is the validation of automated devices. This procedure is costly and time-consuming, requiring certified operators and a large number of participants. The algorithm proposed here could replace one or all of the required operators, translating in potentially large savings in human and economic resources. Other devices that are also based on auscultation have been proposed previously to aid in this validation [115, 116], however, they require the verification of their results by a trained operator. The algorithm proposed here dispenses with the need of this additional verification.

There are, certainly, several other instances of automated devices available in the market based on auscultation. Older patents use a simple approach to identify KS based on content detected at certain frequency ranges [92, 117–119], or at certain predetermined amplitudes [120]. These criteria are, as discussed previously, not ideal, considering that the frequencies contained in KS are not consistent, and any intensity (or amplitude) threshold would be arbitrary with the potential of selecting sounds not related to KS, or eliminating fainter sounds at the diastolic end. The method proposed here has a significant advantage on that

front, considering that it adapts the frequency "filters" to the components of each individual sound, and that there must be a clear separation between KS and masking sounds, not just an arbitrary intensity level.

Other interesting applications of digital auscultation make use of the sound data as a visual aid to determine BP [115, 116, 121]. The user can see the auscultation measurement in a computer or a smartphone, and it looks just as the data shown here in figure 3.8a. The disadvantage in doing this, which was mentioned in the previous sections, is that this visual aid may be misleading, particularly in the diastolic end, especially if the user is not familiar with KS or is properly trained to identify them. The method proposed here can go a step further and visually indicate which voltage spikes are audible, inaudible, or KS, like what is shown in figures 3.16 and 3.17.

Next Steps

Before implementing the proposed method in a device that can fulfill all the potential applications discussed above, necessary next steps include improving the KS selection algorithm, particularly on the diastolic end, and to implement a decision process that can deal with auscultatory gaps and arrhythmias. In the future it will also be important to increase the number of measurements and observers to properly calibrate the method, particularly enlisting the aid of an expert in KS identification. Real-time auscultation is possible with the type of stethoscope used here with an audio splitter, so the *DL* of the KS can be better characterized, and the method further improved to mimic human response. The greatest disadvantage is that this characterization would not be possible with acoustic stethoscopes, although an electronic stethoscope can be calibrated to a certain extent so that the audio output is as close as possible to that of the acoustic counterpart.

With the objective of further developing the algorithm, tests have been done on a separate set of auscultation measurements collected by the British and Irish Hypertension Society (BIHS) that are publicly available on the internet. Some preliminary results from those tests are included in Appendix C. These results indicate that the procedure can independent of the equipment used to record the sound, as long as certain considerations are made about the noise contained in the signal and its frequency components. It has also become evident that some improvements are necessary to be able to apply the method to different cardiovascular conditions.

In recent years Artificial Intelligence (AI) and Neural Networks (NN) have seen increased application in the medical field. This is also true in the case of auscultation. NN are taught to identify certain features of the KS, such as temporal relations and energy or frequency content [122, 123], in order to estimate BP. Perhaps the features identified here can also be implemented in a NN in the future.

Chapter 4

Physics-Based Mathematical Model and Regression Analysis of the Oscillometric Method

Up to this point, the reader is now hopefully familiar with the oscillometric blood pressure measurement (OBPM) method, and its advantages and shortcomings. The method was qualitatively described in chapter 2, and the discussion in that chapter centred on the filtering processes and the algorithms used to estimate BP. As one might recall, these algorithms are based on empirical evidence and their accuracy is often compromised in populations that deviate from average cardiovascular conditions.

It was pointed out in the introduction of this thesis that, to date, there is no formal theoretical background that explains the particular choice of features used to estimate BP with the OBPM method. To understand the influence that various factors have on these estimates, detailed mathematical description of the physical phenomena involved has been derived by a few research groups. These mathematical models take into consideration fluid dynamics, cuff and arterial mechanics, and may become increasingly more elaborate if other factors are included, such as mechanics of the tissue surrounding the artery or the influence of veins and capillaries. Often, these models consist of several equations that must be solved by elaborate numerical methods.

These models are useful to visualize the effect that certain parameters have on the expected result. Their result is a synthetic representation of the observed oscillations that resembles the overall features of measured data. For instance, the work of Ursino and Cristalli has revealed that arterial mechanics play a significant role on the definition of the MAR

algorithm to estimate BP [6]. However, these models are not usually directly verified on measured data.

The goal of this chapter, as set in the introduction, is to approach this challenge, and preferably to do so in a practical manner. This means deriving a simple, yet effective, mathematical description of the physics behind the generation of the oscillometric waveform (OMW), so that it can be readily compared to data typically obtained during a cuff measurement. This comparison between mathematical model and measured data is intended to validate the model in question, or at least reveal potential improvements that can be made to the model, and at the same time provide information about parameters directly related to the components of the system.

The chapter begins with the derivation of the mathematical functions that make up the model in question. As we shall see, there are several possible expressions for the component of the model that describes arterial mechanics. These have been formulated from experimental data obtained in settings different to those of an oscillometric measurement. The comparison performed in this chapter will also help identify which one of these formulations may be better suited to describe arterial mechanics in a cuff-based measurement.

Once the necessary equations have been established, these will be fitted to oscillometric data collected from the volunteers mentioned in the previous chapter by means of a non-linear least squares regression. The resulting parameters will be analyzed to verify if their values are representative of the phenomena under study.

4.1 Mathematical Model of the Oscillometric Waveform

The model derived below is based on a derivation by Charles F. Babbs included in this publication [4]. This derivation was followed because it allows us to obtain a simple mathematical expression for the OMW, as we shall see in the text below. The pressure signal where the oscillometric information is extracted from is a monotonically decreasing function of time that contains small oscillations (see figure 2.1). The small oscillations correspond to the OMW, and one of the methods described in chapter 2 to extract this information from the original signal consisted of fitting a baseline to the signal and subtracting it. Mathematically the combination of the OMW and the baseline can be described as:

$$P(t) = P_{base}(t) + OMW(t) \tag{4.1}$$

where *P(t)* is the total pressure signal as recorded by the pressure sensor. The function $P_{base}(t)$ is assumed to be the mean pressure inside the cuff that decreases in time as air is slowly being released by the valve, that is, $P_{base} = P_c$.

One thing that was not discussed in chapter 2 is that the small oscillations in the signal, or the OMW, originate from the changes in blood volume flowing through the arterial tree during each cardiac cycle. These volume changes are also periodic oscillations and when expressed as a function of time they form what is know as the blood volume waveform.

When the pressure in the cuff is above SBP blood cannot flow towards the distal end of the cuff and the lower extremity. The blood volume pulses impact on the proximal edge of the cuff and the variations are minimally transmitted to the cuff, which is why we observe small oscillations in the pressure signal even at suprasystolic cuff pressures. As pressure in the cuff decreases the artery slowly reopens and allows increasing amounts of blood to flow across the whole section of the artery that is under the cuff. Once cuff pressure is below diastolic pressure the artery remains open and blood flows freely as it would under normal (cuffless) conditions.

This interaction between cuff pressure and the oscillating blood volume waveform is responsible for the varying amplitude of the pulses in the OMW. The relationship between blood volume and the pressure pulses in the OMW is not exactly linear. To describe the connection between the blood volume waveform and the OMW we make use of Boyle's law assuming an isothermal system:

$$P_1 V_1 = P_2 V_2. \tag{4.2}$$

If we consider $P_2 = P_1 + \Delta P$ and $V_2 = V_1 + \Delta V$, where ΔP and ΔV are small pressure and volume variations, respectively, occurring after a change in time, Δt:

$$PV = (P + \Delta P)(V + \Delta V) \tag{4.3}$$

where the indices are dropped and P and V are understood to be the absolute pressure and total volume of the air in the cuff.

If the variations are sufficiently small, we can obtain

$$PV \approx PV + P\Delta V + V\Delta P \tag{4.4}$$

and thus,

$$\frac{V}{P} \approx -\frac{\Delta V}{\Delta P}. \tag{4.5}$$

The ratio V/P is defined as the cuff's compliance. In the strict sense of the definition, this ratio refers to the compliance of the air inside the cuff, not to the material the cuff is made of. However, to simplify the discussion and to avoid confusion, we shall refer to it as cuff compliance. Drzewiecki *et al* studied cuff mechanics and derived an expression for this compliance [7]. Their findings indicate that the Pressure-Volume relationship of a cuff is non-linear at low cuff pressures, but can be approximated as a linear function as cuff pressure increases. This approximation is most effective at pressures beyond the range of what is normally used in a BP measurement. However, we can still assume a linear behaviour, or constant compliance, at pressures measured during a BP measurement.

From equation 4.1 we know that total cuff pressure in an OBPM is the sum of two components. Therefore, if there exist variations in total cuff pressure, ΔP, there will naturally exist variations in each of these components:

$$P + \Delta P = (P_{base} + \Delta P_{base}) + (OMW + \Delta OMW). \tag{4.6}$$

and eliminating terms with the equality in equation 4.1 we thus conclude that the variation in cuff pressure is the sum of the variation in each component: $\Delta P = \Delta P_{base} + \Delta OMW$. Likewise, the total volume variation in the cuff is the result of variations in both baseline and oscillating components ($\Delta V = \Delta V_{base} + \Delta V_{osc}$). The baseline component of the volume function is the steady decrease in cuff volume as the cuff is deflated; the oscillating component of the volume function is the direct and opposite result of the blood volume variations, or $-\Delta V_{osc} = \Delta V_a$, where V_a is the arterial blood volume.

Substituting these definitions in equation 4.1 we obtain an expression that relates variations in volume to the variations in pressure through cuff compliance. If compliance is assumed constant we can also assume that the variations in the linear component of the volume are directly responsible for the variations in the linear component of the pressure. Likewise, variations in the oscillating component of the pressure are a result of the variations

in the oscillating component of the volume, that is, variations in blood volume. With these considerations in mind, for the oscillometric waveform we have:

$$\Delta OMW = \frac{1}{C_c}\Delta V_a, \tag{4.7}$$

This last equation shows that the relationship between the OMW and the blood volume waveform is approximately linear only to the extent that cuff compliance can be considered constant. The quantity V_a is rarely measured, so the next step now is to relate the OMW to the variable of interest, that is, blood *pressure*.

4.1.1 Arterial Compliance

We assume the OMW variations, and thus the blood volume variations, in equation 4.7 happen over a small fraction of time, Δt, which in the limit when $\Delta t \to 0$ can be expressed as the derivative

$$\frac{d}{dt}OMW = \frac{1}{C_c}\frac{d}{dt}V_a. \tag{4.8}$$

Under normal hemodynamic conditions (no cuff) the only pressure applied on the arterial walls is that of regular blood pressure on the internal side of the arterial wall. During an OBPM there is an additional pressure applied by the cuff acting on the external side of the arterial wall. Therefore, the difference between these two pressures will be the "net" effect perceived by the artery. This difference is called the transmural pressure, P_t, and is defined by,

$$P_t = P_a - P_c \tag{4.9}$$

where P_a is the internal, or arterial, pressure, and P_c is the external, or cuff pressure.

At the start of the measurement the artery is collapsed because the pressure in the cuff exceeds the highest pressure attained in the circulatory system (SBP), and $P_t < 0$. Blood flow is occluded and at this point there is minimal blood volume variation under the cuff. As the measurement progresses and cuff pressure descends past SBP there is a continuous shift on which side of the artery "feels" the highest pressure. That is, transmural pressure will oscillate between negative and positive values. When pressure inside the artery is greater,

that is $P_t > 0$, the artery is able to open and there is an increased flow of blood under the cuff.

At cuff pressures higher than SBP the blood volume is observed to pulsate against a point of occlusion at the proximal end of the cuff, which is why there is minimal volume variation, even at high cuff pressures. When cuff pressure is below, yet close to, SBP transmural pressure is positive for a small fraction of time and minor variations in the volume V_a occur under the cuff. As cuff pressure continues decreasing there comes a point where it is in the vicinity of MAP. This means that the pressure outside the arterial wall is, on average, equal to the pressure inside most of the time, and the mean value of P_t is equal to zero. At this point the artery is collapsed the same amount of time that it is open, causing the largest variations in blood volume of the measurement. Once the pressure in the cuff is past MAP and is closer to, or below, DBP the influence of the pressure on the outside of the arterial wall will be minimum and blood flow conditions eventually return to normal.

From these interactions it is clear that arterial volume is a function of transmural pressure, that is, $V_a = V_a(P_t)$. Expanding the time derivative of V_a in equation 4.8 results in

$$\frac{d}{dt}OMW = \frac{1}{C_c} \cdot \frac{dV_a}{dP_t} \cdot \frac{dP_t}{dt} = \frac{1}{C_c} \cdot C_a \cdot \frac{dP_t}{dt}. \tag{4.10}$$

The term C_a is the arterial compliance defined as $C_a = dV_a/dP_t$ or as $C_a = dA/dP_t$, where A is the artery's cross-sectional area. Finally, if we expand the definition of P_t we obtain a complete expression for the time derivative of the OMW:

$$\frac{d}{dt}OMW = \frac{C_a}{C_c} \cdot \left(\frac{dP_a}{dt} - \frac{dP_c}{dt} \right). \tag{4.11}$$

With this final equation we arrive at a simple model that potentially describes the measured OMW and that also contains information about arterial mechanics. The use of this model is further simplified by the fact that one of its variables is information easily obtained from a cuff measurement, that is, P_c. The arterial pressure waveform, P_a, is a variable that is only faithfully obtained through an invasive measurement, however it can be modelled with the use of a Fourier series following a few approximations that will be described in following sections.

The only parameters that are left for consideration are the compliances. Since cuff compliance is assumed constant, we only need to estimate its order of magnitude. Models of

arterial compliance are discussed in what follows.

Models of Arterial Compliance

Obtaining an accurate expression for arterial compliance, C_a, is perhaps the most challenging part of equation 4.11. This parameter is difficult to measure during a cuff measurement and most of the information available has been obtained from *in vitro* experiments. Arterial properties change significantly when excised from the body, and the changes are more pronounced the longer it remains outside *in vivo* conditions.

Some Pressure-Volume or Pressure-Area relationships for the artery have nevertheless been derived from experiments with rubber tubbing and excised animal arteries. The main observation is that this function follows a sigmoidal shape to account for the observed behaviour at different transmural pressures. Namely, the minimal variations in volume at negative and positive transmural pressures, and the large variations near zero transmural pressure.

Figure 4.1a shows an example of a few models of these relationships found in the literature, each labeled with the last name of the first author in the publication they were obtained from [3–6]. The plots were drawn using the same parameters reported in each publication, except for [6], where an artery of a smaller radius was considered. In all cases a 1-cm-long segment of artery was assumed.

The models shown in figure 4.1, and many others in the literature, make different considerations for each side of P_t in the P-V or compliance function. The region where $P_t > 0$ is often modelled as an exponential [4, 70, 124] or logarithmic [5, 125] function. The region where $P_t < 0$ is also often modelled as an exponential function [4, 70], or as a hyperbolic function [5]. Some authors have instead described the relationship as $P_t = f(A)$, where the function is usually a polynomial or power function of the area (or volume), and different formulations of these functions are used to model each region [3, 6, 126].

To complete the formulation for the OMW stated in equation 4.11 two of the models plotted in figure 4.1 were selected to represent arterial compliance. The other two models, unfortunately, are the type of models that describe P_t as a function of the cross-sectional area, and they are complex functions that cannot be rewritten in terms of the transmural pressure. In the case of a cuff measurement like the one we are considering here, the information we have available is that of P_t.

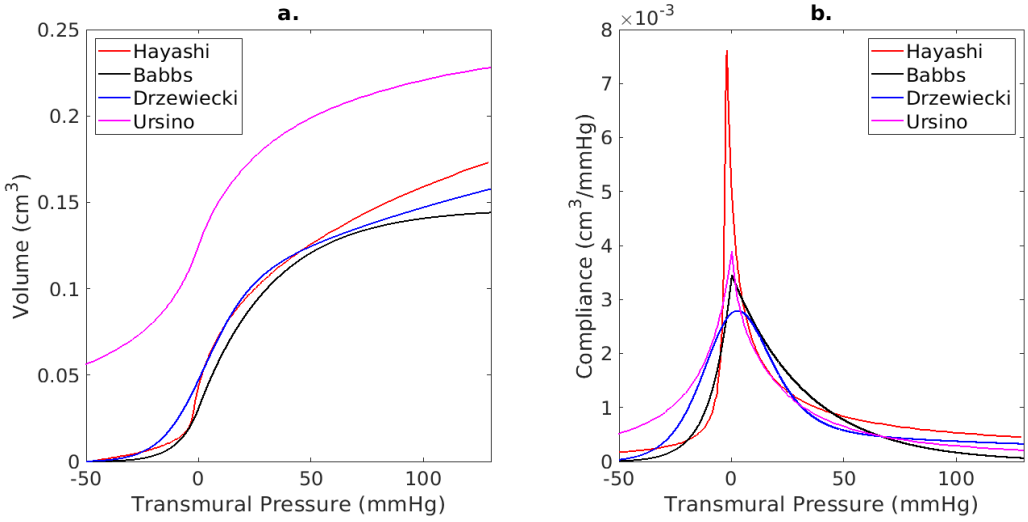

FIGURE 4.1: a.Pressure-Volume relationship models for a human arterial wall. b.Arterial compliances derived from these models. Each model is labeled by the first author's last name from [3–6].

The first model selected is the one formulated by Drzewiecki *et al* in [5], which combines the observations of arterial distention following a logarithmic function, and collapse a hyperbolic relationship:

$$A = d\frac{ln(aP_t + b)}{1 + e^{-cP_t}} \tag{4.12}$$

where A is the lumen (cross-sectional) area and a, b, c, d are empirical constants, which in Drzewiecki's case were obtained from a fit to measured data from a canine carotid. The constant d acts as a scaling parameter, so the function can be rewritten in terms of arterial volume by assuming that the multiplication times the length dimension is included in this constant.

The second model selected makes an explicit separation between positive and negative transmural pressures, and assumes that both sides behave exponentially. The differences in the behaviour at both sides are accounted for in the constants of each exponential function. The formulation for this P-V function was taken from Babbs' publication [4], which is a simplified version of the equation used by Baker *et al* [70]:

$$V = \begin{cases} V_0 e^{a_B P_t} & \text{for } P_t < 0, \\ V_0 \left[1 + \frac{a_B}{b_B}(1 - e^{-b_B P_t})\right] & \text{for } P_t \geq 0. \end{cases} \tag{4.13}$$

The constants a_B and b_B are also empirical constants that can be derived from experiments and V_0 is the zero pressure volume.

In equation 4.13 it is always assumed that the maximum arterial compliance occurs at $P_t = 0$, while in equation 4.12 this point can be adjusted with the constants. Deriving these expressions with respect to transmural pressure will give the function of arterial compliance that can be substituted in equation 4.11. For the purpose of comparison, both functions will be used in the OMW model.

4.1.2 Arterial Pressure Waveform

The arterial pressure waveform (APW) is a periodic signal that shows the pressure changes in a given artery at each cardiac cycle. Its shape and amplitude vary depending on the location of the arterial tree where it is being measured, mostly due to the proximity of reflection sites to this location. It oscillates between SBP and DBP, meaning its maximum amplitude is the pulse pressure (PP), defined as the difference between these two pressures, or $PP = SBP - DBP$.

Like any periodic signal, it can be synthesized with a Fourier Series (FS), and the constant term in the series can be related to an arterial pressure parameter. Mean Arterial Pressure (MAP) was briefly mentioned in chapter 2 and an approximate definition of this pressure was given as

$$MAP = DBP + 1/3PP. \tag{4.14}$$

However, as MAP is the mean pressure recorded in a patient's arteries during a cardiac cycle, we can also use the following equation to determine its value:

$$MAP = \frac{1}{T}\int_0^T P_a(t)dt \tag{4.15}$$

where T is the period of the cycle and P_a the arterial pressure waveform. This integral is reminiscent of the definition of the constant term in the FS:

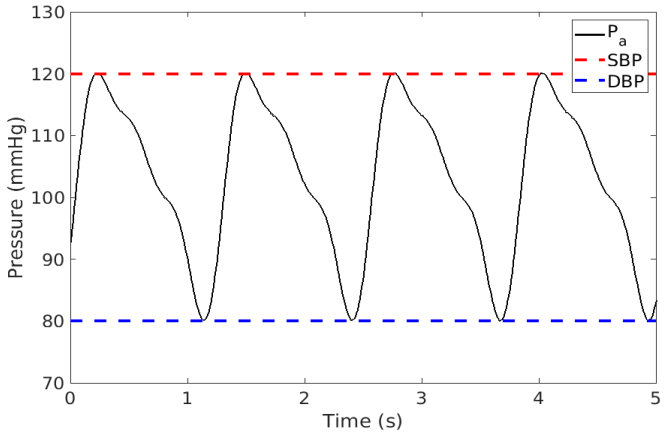

FIGURE 4.2: Simulated arterial pressure waveform for BP = 120/80 mmHg.

$$a_0 = \frac{2}{T}\int_{-T/2}^{T/2} f(t)dt \tag{4.16}$$

from where we can conclude that $MAP = a_0/2$. Therefore, the APW can be expressed by the following FS:

$$P_a(t) = MAP + \sum_{n=1}^{3}\left[a_n \cos(2n\pi ft) + b_n \sin(2n\pi ft)\right] \tag{4.17}$$

where for simplicity only three harmonics are considered. An example of this is shown in figure 4.2, where the FS coefficients are: MAP = 102.9, $a_1 = -6.285$, $a_2 = -2.989$, $a_3 = -0.935$, $b_1 = 14.594$, $b_2 = 5.981$, and $b_3 = 2.926$, all measured in mmHg.

4.2 Model Fitting to Oscillometric Data

4.2.1 Non-Linear Least Squares Regression

A simple method to fit an equation to measured data is by means of a Non-Linear Least Squares (NLLS) regression, which can be stated as an optimization process that seeks to minimize the function

$$S = \sum_{i=1}^{N} \varepsilon_i^2 = \sum_{i=1}^{N} [y_i - f(x_i, \vec{\beta})]^2. \tag{4.18}$$

The measured variable y_i is compared to the function $f(x_i, \vec{\beta})$, which is the output of the equation used to describe the observed phenomenon when an independent variable x_i, measured at the same time as y_i, is used as input. Multiplying the independent variable are a number of unknown parameters listed in the vector $\vec{\beta}$. The function S is the sum of the square of the errors or residuals, ε, which are the differences between measured variables and function-generated variables. This function is minimized when the ideal combination of parameter values is found.

In the present case, the measured variable y_i corresponds to the OMW obtained from the oscillometric measurement. The function $f(x_i, \vec{\beta})$ will be obtained from using equation 4.11 along with equations 4.17, which has a time dependency, and 4.12 or 4.13, which depend on transmural pressure, that ultimately also depends on time. Therefore, the independent variable x_i in this case is the time, and the parameters in vector $\vec{\beta}$ are all the constants included in the equations mentioned above that have not yet been accounted for, such as the constants in the FS that represents the APW, and the empirical constants in the arterial P-V functions.

NLLS requires the use of an iterative procedure. An initial parameter estimate vector, $\vec{\beta}_0$, is provided for an initial computation of the function S. The values of the parameters are then adjusted in each iteration depending on whether the function S is minimized with respect to the previous iteration or not. For this reason, NLLS is unfortunately very sensitive to the initial estimate. This must be reasonably close to the real parameter estimates, otherwise the function may not converge, or it may converge to a local minimum rather than a global minimum [127].

Limits and constraints can be set for this type of optimization problem to narrow down the search region of parameter values. Given that the parameters in this case are related to the two functions P_a and C_a, the limits and constraints can be easily visualized by the properties of these functions.

In the case of P_a the MAP and the heartbeat frequency, f, can be limited to reasonable values. The other series constants are harder to limit, but the overall maximum and minimum points of the waveform can be expected to have values close to SBP and DBP, respectively.

The parameters in the C_a functions are assumed to be positive real numbers. Additionally, since the C_a function originates from the P-V relationship of the artery, it should be expected that if the resulting parameters are used to generate a function of the type $V = V(P_t)$, this function should be positive for all the range of transmural pressures. In the case of equation 4.13 the requirement of positive real values is sufficient to ensure this condition. However, in the case of equation 4.12, the logarithm in the expression requires that

$$ln(aP_t + b) \geq 0$$

or that the parameters be constrained as

$$a \leq \frac{1-b}{P_t} \text{ for } P_t < 0.$$

Including these limits and constraints into the optimization algorithm will help ensure that the resulting parameter values are a good estimate of their true values. Given that we have little to no knowledge on the parameters that define arterial mechanics, we must make use of the knowledge we have available to make sure the chosen solution best represents the measured data.

Observations from Synthetic Data

In order to establish the algorithm and to ensure the NLLS regression will be effective with measured oscillometric data, the regression was first applied to a few synthetic cases created with equations 4.11, 4.12 or 4.13, and 4.17. One can think of this regression to synthetic data as an exercise in numerical modelling to get familiarized with the functions available in the computational language of choice, their requirements according to the model in question, and the nuisances or errors that may arise during the procedure. This exercise will also help in giving an idea of what are the expected results and how to interpret them.

The first step was to generate the synthetic data, which was done by creating an APW with equation 4.17, a cuff pressure function, P_c, and using these to create the transmural pressure waveform to be used in the compliance functions. The APW generated was that shown in figure 4.2, for a BP of 120/80 mmHg, and the cuff pressure was assumed linear, deflating at a constant rate of 3 mmHg/s from a maximum pressure of 140 mmHg. Differences in OMW were obtained by setting different values of the constants a through d in equation

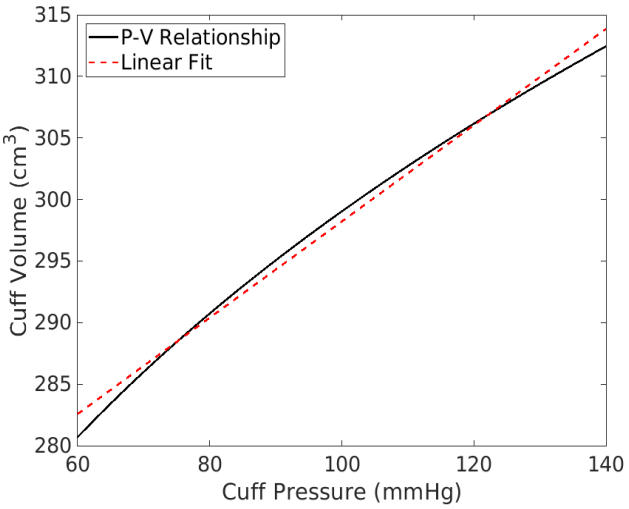

FIGURE 4.3: Cuff P-V relationship obtained from the results in [7] in the range 60 – 140 mmHg. A linear function fit to the data is shown by the dashed red line.

4.12, and constants V_0, a_B, and b_B in equation 4.13. Cuff compliance was approximated from Drzewiecki's work on cuff mechanics, which is reproduced in figure 4.3 for cuff pressures between 60 and 140 mmHg. The dashed red line represents a simple linear fit to the data performed with a Matlab function. The result is the linear function $V = 0.39P_c + 259.1$, from which we can obtain a cuff compliance of ~ 0.4 cm^3/mmHg.

The data were generated for a total duration of 30 s, and sampling frequencies of 100 and 1000 Sps were assumed. Equation 4.11 was numerically integrated by a simple Euler method, the step size of which was required to be the inverse of the sampling frequency, and three different OMW were generated per compliance model. An example of one of these synthetic OMW is shown in figure 4.4, obtained from using equation 4.12 in the model and the constants used by Drzewiecki in his publication ([5]).

The NLLS regression to these sets of synthetic data was performed with the *lsqcurvefit* function in Matlab. Several initial estimate vectors, $\vec{\beta}_{0,m}$, were tried to verify if the regression returned the original set of parameters independent of initial estimate, or if several solutions to the problem existed. The initial estimate vectors were generated with the aid of a Latin hypercube sample matrix (LHSM), which in the case of Matlab creates a matrix of size

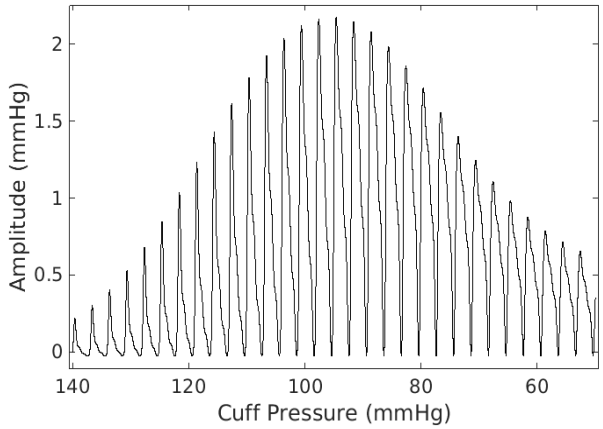

FIGURE 4.4: OMW obtained by integrating equation 4.10 with the compliance model from equation 4.12. The value of the constants are: $a = 0.03$ mmHg^{-1}, $b = 3.3$, $c = 0.1$ mmHg^{-1}, and $(d \times L)/C_c = 2$ mmHg.

$m \times n$ and randomly distributes the elements in each column with one from each interval $(0, 1/n), (1/n, 2/n), ..., (1 - 1/n, 1)$, and then randomly permutes them. Each column in this case corresponds to a parameter, and each row to an initial guess vector.

A few observations from the obtained results, which are applicable to both compliance model sets, are:

1. The regression is possible regardless of sampling frequency (time step).

2. Some initial guess vectors did not lead to any result because the search could not converge to a solution.

3. The cases that did lead to a solution were not always sensible results, which could be confirmed by plotting the OMW function (eq. 4.11) obtained with the parameter estimates in question. These resulted in oscillations that had no resemblance to the original OMW.

4. The correct answer to the parameter estimates, considered to be that which returned the original values used to generate the synthetic OMW, was always the one corresponding to the lowest value of the function S, as expected, which was usually of the order of 10^{-5}.

5. Results with function S values within the approximate limits of $1 \times 10^{-4} < S < 1$ were also close estimates of the original OMW (confirmed visually). As the function S approached smaller values, the corresponding estimates approached the values of the correct solution.

6. If the APW was used as input to the model instead of including the FS constants as part of the parameter vector, the regression was more effective. That is, the regression would return less correct estimates if the FS constants were also sought during the regression.

These observations indicate that, in our experimental cases, we should expect to obtain several resulting combinations of parameters that do not correspond to any sensible solution, and that the best way to filter these cases out is via visual confirmation (plotting the solution). Once these cases are removed, the best solution is then expected to be that with the lowest value of function S.

4.2.2 Experimental Procedure

The oscillometric data used in this analysis were the same collected simultaneous to the KS data as in chapter 3 with the setup in figure 3.5. As a reminder, in this setup pressure from the cuff was detected with a pressure transducer (MPX5050GP, Freescale Semiconductor, Inc.) connected to the inflatable cuff, and converted from a voltage signal to a pressure signal according to the transducer's specifications. For the first round of measurements (4 volunteers) a custom oscillometric device was borrowed from the Department of Medicine of the University of Alberta. This device controlled inflation and deflation of the cuff. The data were sampled at a rate of 1 kSps. For the second round (5 volunteers) inflation and deflation were done manually. The cuff used in this round was connected to an aneroid gauge that had a rubber bulb and a valve. In this case the data were sampled at a rate of 10 kSps.

Given that the regression is effective even at low sampling rates, to simplify the procedure and to save computational time all data were decimated to a sampling rate of 100 Sps. The OMW was obtained from the original pressure signal using the same procedure described in chapter 2. As a reminder, the baseline, or P_c, is obtained from fitting a curve to the lowest value of each oscillation in the decreasing pressure signal. When this baseline is subtracted the result is the OMW.

From the observation that excluding the FS in the synthetic cases led to better results, two trials were performed on the data for each compliance equation. The difference between these trials is summarized in the schematic in figure 4.5. The measured OMW corresponds to the variable y_i in equation 4.18 and the mathematical model corresponding to function $f(x_i, \vec{\beta})$ is the integration of equation 4.11. The two cases discussed are derived from the two different compliance equations, obtained from the derivative of the P-A and P-V equations, correspondingly. The two trials, furthermore, correspond to the number of parameters included in vector $\vec{\beta}$ and how the APW is considered, which is described below.

The first trial consisted of the original idea of including the constants in the FS as part of the parameter vector. This meant that the frequency, MAP, and the other six constants in the FS were part of the vector (denoted by K_{FS} in figure 4.5) along with the constants in each compliance equation (K_C in figure 4.5). Similar to the synthetic case, several initial guess vectors were sampled in the NLLS regression. The parameters in K_{FS} in all these initial guess vectors were set as follows: the frequency of the FS was set as the mean frequency of the oscillations of the measured OMW; the MAP was calculated with equation 4.14; the rest of the constants in the FS were all set to zero. The constants in the compliance equations (K_C) were randomly generated with the aid of a LHSM. The values for each constant in the LHSM took on values within the limits of 0.1 to 10 multiplied by their respective order of magnitude, to allow the initial guess vectors to constitute a wide range of values. 300 different combinations of initial guess vectors were sampled.

Equation 4.11 was integrated with the Euler method, and the result compared to the measured OMW in the regression. This problem was solved using Matlab's *fmincon* function which, unlike the function *lsqcurvefit*, allows the problem to be constrained in addition to having limits imposed on the value of the parameter estimates. During a first test it was observed, however, that if the values of the constants were limited to any small range of values, then the regression would not succeed. Thus, the FS constants were allowed to take any positive or negative value, and only an additional limit was imposed on the overall FS, that required that the maximum and minimum values were within ± 20 mmHg of the measured BP. The compliance related constants were limited to only positive values. These changes fixed the issue and the regression could perform normally.

Resulting values of the function S were of a high order after a first regression. In hopes of obtaining a better estimate, a second regression was performed based on the results obtained.

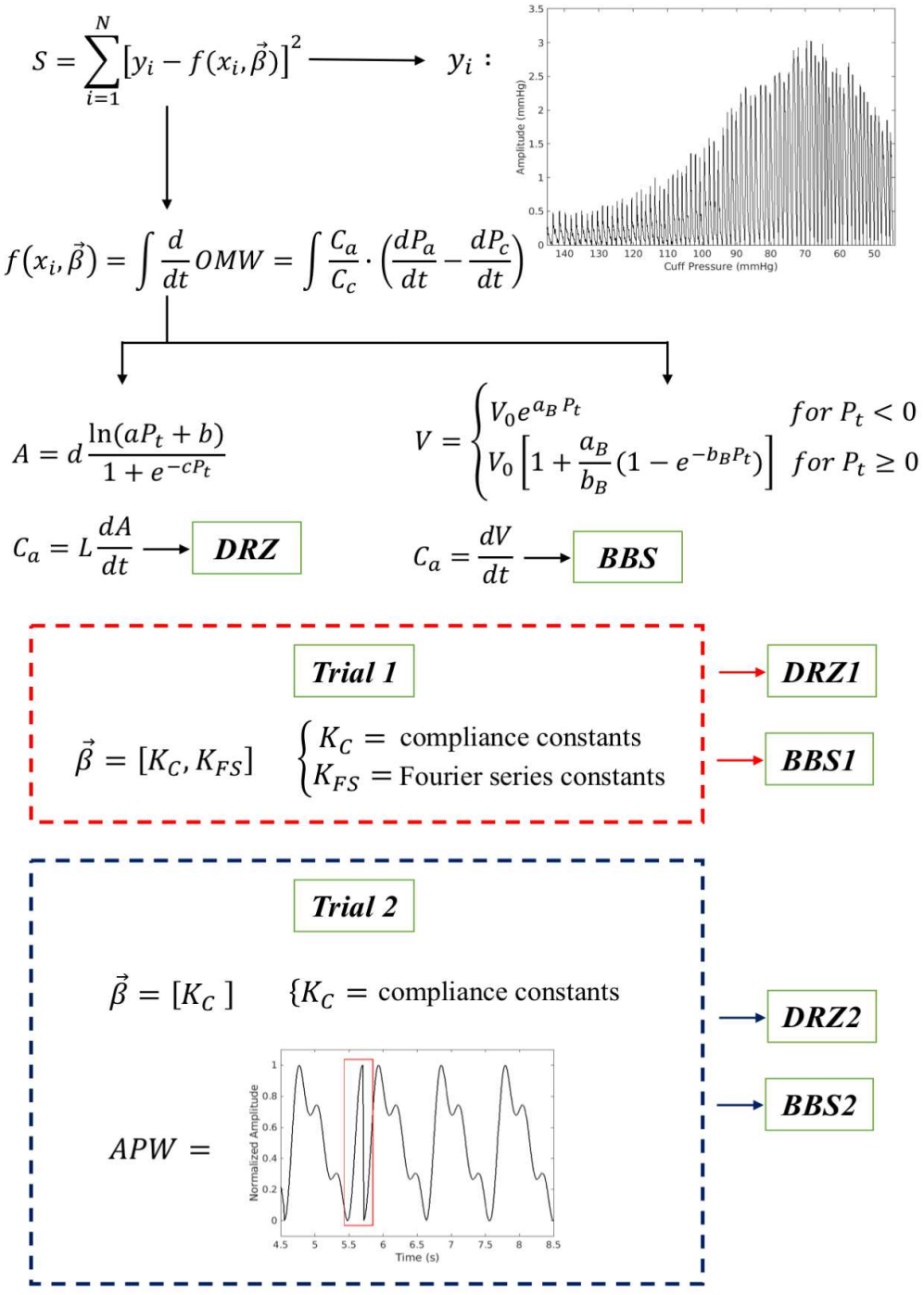

FIGURE 4.5: Schematic of the trials used in the NLLS or oscillometric data.

From the first regression all the results that were associated to values of $S \leq S_{min} + \frac{1}{2}S_{min}$, where S_{min} is the lowest value of S obtained, were selected and the mean of the compliance related parameters was calculated from all these results. A new initial guess matrix was generated, but this time the guesses had these constants limited to values within $\pm 20\%$ of the calculated means, a percentage that was arbitrarily chosen. This second matrix was 200 rows in length. Results from this second regression were also selected based on those associated to values of $S \leq S_{min} + \frac{1}{2}S_{min}$, and saved along with the results of the initial regression.

In the second trial, the attempt to model the APW as a FS was removed from the equation. The conclusion is that, as in the case of the synthetic data, the inclusion of the FS in the model affects the regression to a higher extent than expected. On closer observation, this was determined to be the most likely reason why the function S cannot go below certain values, particularly owed to the fact that the model of APW can only account for a fixed oscillation frequency. The oscillations in the measured OMWs do not have a fixed frequency and, while the variation is not drastic, it is persistent and not constant throughout the whole measurement. This means that assuming an APW (or FS) with a fixed frequency will eventually cause the modelled OMW to shift its phase with respect to that of the measured OMW, aggravating the error in the fit.

Unfortunately, the most ideal solution to this problem is to measure the APW directly and simultaneous to the OBPM. The most accurate way of doing so is by invasive means, which would completely defeat the purpose of this study that intends to be as practical as possible. In an attempt to circumvent this issue a different approach is proposed in the second trial: to construct an APW with the same frequency variations in its oscillations as those observed in the measured OMW.

This was done by isolating a single oscillation in the OMW, generally the last oscillation measured, at P_c values below DBP, normalizing it to an amplitude of 1, and fitting to it a FS of three harmonics, as shown in figure 4.6. The last oscillation was selected given that past the point of DBP the oscillations have a smoother shape and the fit to the FS would be significantly easier. Once the parameters of this FS were obtained, the APW was constructed by creating individual oscillations with the parameters of the FS, but with frequencies adjusted to the individual oscillations of the measured OMW. That is, a sequence of oscillations was created based on the single FS, and then pieced together in sequence to

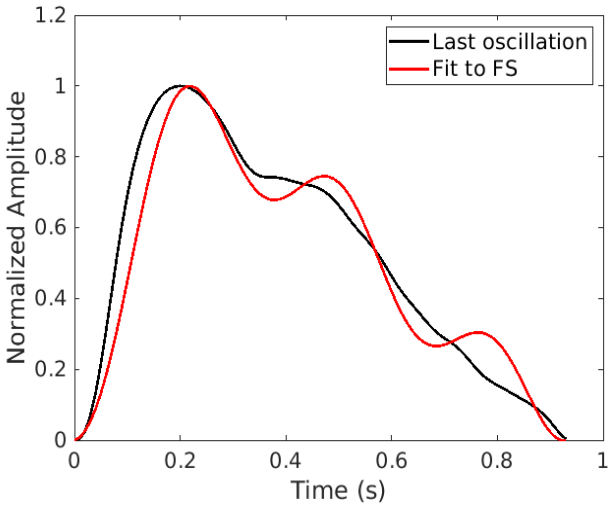

FIGURE 4.6: Last oscillation of the OMW of a volunteer (black), with an approximation to a FS (red).

create a train of oscillations that had the same shape, but different frequencies.

The result of doing this is shown in figure 4.7. Naturally, this is not the most ideal solution to the problem of the varying frequencies. While there is little discontinuity in most of the generated waveform, given that most of the oscillations have the same frequency, there are some oscillations where the difference in frequency results in a significant variation in the oscillation. An example of such a variation is marked after the first oscillation in figure 4.7, where the FS fit does not match the frequency of that particular oscillation, and a drastic drop in the amplitude occurs. These drops do not occur often, and in most cases are not as large as the one shown in figure 4.7. Therefore, it is expected that they will not significantly affect the regression, and that the benefit of having a waveform with similar frequency variations as that of the measured data will far outweigh any error these amplitude variations may induce.

With an APW of this form as an input to the model we can now reduce the amount of parameters by eliminating those related to the FS, and instead having two parameters that will adjust the APW to its expected values: the DBP which adjusts the bias, and the PP which adjusts the amplitude. It was also found to be more effective if the parameter estimates related to BP were not limited to specific values and only conditioned to be positive real numbers. It was also found that the regression would work better if the function *lsqcurvefit*

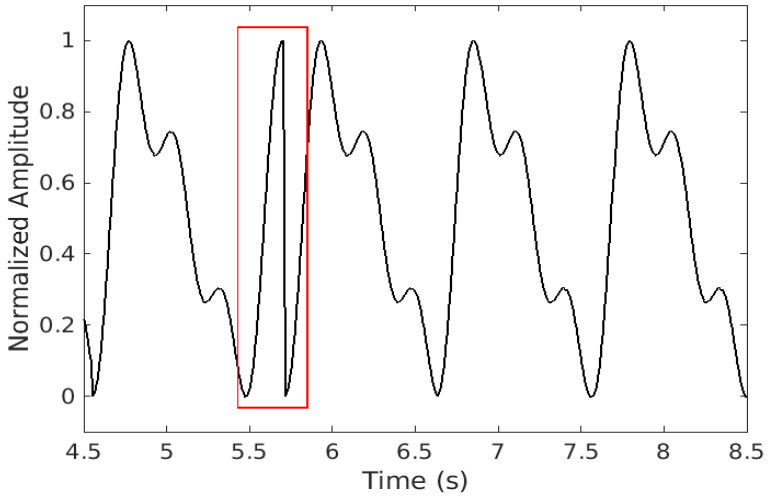

FIGURE 4.7: A 2-s long section of APW created by joining oscillations generated from the fit to FS of a single oscillation (figure 4.6) from the measured OMW. The discontinuity framed by the red rectangle is due to the mismatch in frequencies in the original OMW.

from Matlab was used instead. Unfortunately this function does not allow constraints to be imposed on the parameters as does *fmincon*, so the results for the model using equation 4.12 for arterial mechanics will have to be selected after the fact to include only those that comply with the required constraint.

In this trial only one regression was considered necessary. The results were selected first on the basis of those that produced $S \leq S_{min} + \frac{1}{2}S_{min}$. A second filter required that only those results with reasonable values of DBP and PP were finally selected. This second filter was necessary since the parameters were unbound, and DBP and PP estimates of the result with the lowest value of S were not always sensible.

4.2.3 Results

Of the measurements available, 40 were kept for analysis and the rest were discarded. This was because in some of the measurements that were discarded there was no solution obtained in at least one of the four regressions performed. To make a better comparison, only those measurements that had a complete set of solutions are considered.

As mentioned above, the first regression trial required two rounds of regressions performed, the second of which was done with the initial guess vectors limited to a region defined the parameter estimates obtained in the first round, and that were associated to the lowest values of S. This procedure was found to be effective in some of the measurements; in all cases the resulting estimates had a lower value of S, yet only in some cases did these new results produce a fit that resembled the OMW. This means that, even though there are parameter estimates that somehow produce a model with low value of S, the plot of this model is a line that in no way approximates measured data, or even synthetic data like the one shown in figure 4.4. Despite the filters placed to select an appropriate solution, the results still had to be filtered manually to remove the incorrect estimates. The final solution was selected from the remaining parameter estimate vectors as the one with the lowest value of S.

Figures 4.8 and 4.9 are an example of one of such solutions obtained from the same measurement, where the function f was constructed with equations 4.12 and 4.13, respectively, and fitted to the measured data. Since these results are from the first trial, the APW was approximated in conjunction to the compliance constants. The subject in this case had BP = 93.77/60.81 mmHg. The measured OMW is plotted in black as a function of deflating cuff pressure, and the result of the fit is plotted in red.

Figures 4.10 and 4.11 represent the arterial mechanics of the vessel from the same data in figures 4.8 and 4.9. Figures 4.10a and 4.10b are the P-V relationship and arterial compliance, respectively, obtained from substituting the parameters estimates found from the fit in equation 4.12 and its derivative with respect to P_t. Figures 4.11a and 4.11b contain the same information, but substituting the parameter estimates in equation 4.13 and its derivative, respectively.

The APW obtained in both cases is plotted in figure 4.12, where model "DRZ" refers to the results obtained from using equation 4.12 in the regression and is related to the results in figures 4.8 and 4.10, and model "BBS" refers to the results obtained from using equation 4.13 and is related to the results in figures 4.9 and 4.11. The dashed horizontal lines correspond to the measured BP of 93.77/60.81 mmHg. The shape of the FS is not significantly different, and both cases resulted in an estimated frequency of 1.02 Hz. MAP for model DRZ was estimated to be 70.96 mmHg, and for model BBS it was estimated to be 78.38 mmHg. When calculated with equation 4.14 MAP = 71.80 mmHg.

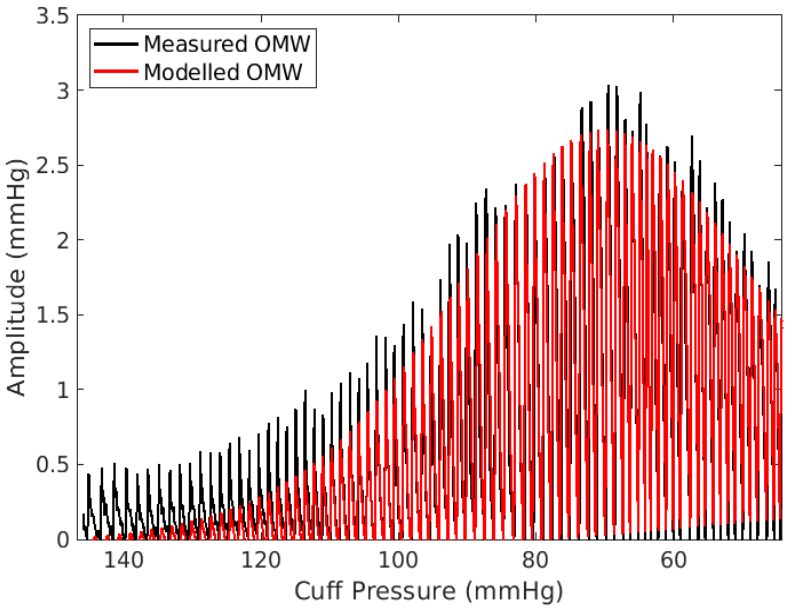

FIGURE 4.8: Measured data (black) with a result for function $f(x_i, \vec{\beta})$ (red) obtained from equation 4.12 during the first trial.

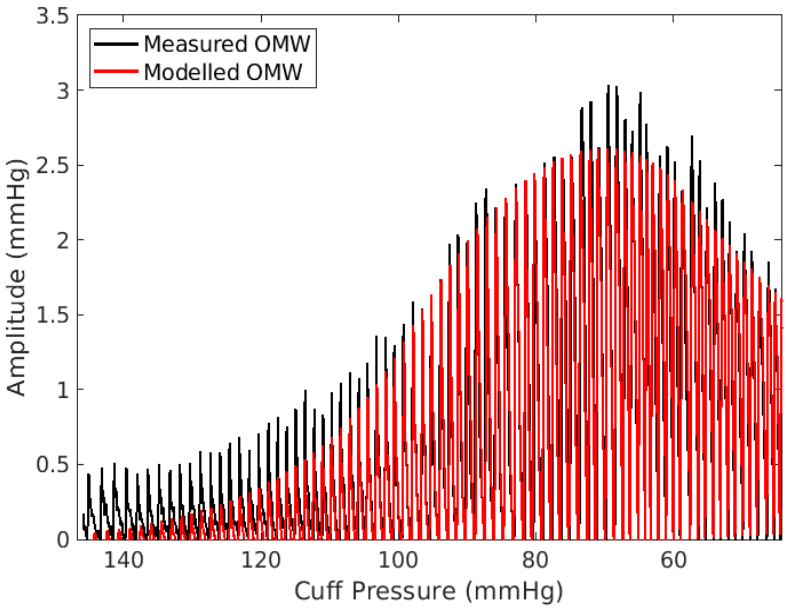

FIGURE 4.9: Measured data (black) with a result for function $f(x_i, \vec{\beta})$ (red) obtained from equation 4.13 during the first trial.

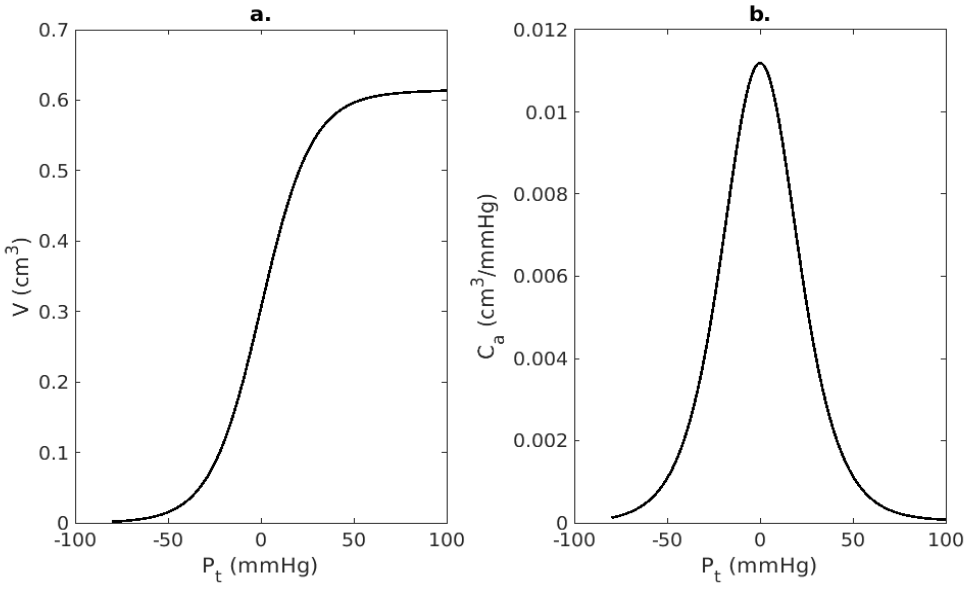

FIGURE 4.10: a.Pressure-Volume function obtained from equation 4.12 with the parameter estimates obtained from the fit. b.Arterial compliance obtained from the derivative of equation 4.12 and the parameter estimates obtained from the fit. Results obtained from the first trial.

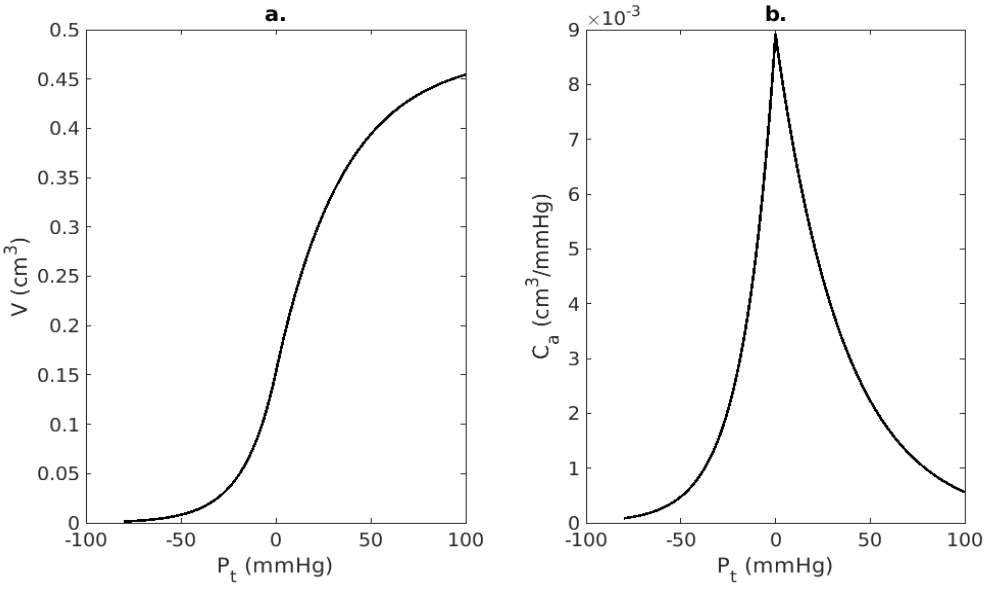

FIGURE 4.11: a.Pressure-Volume function obtained from equation 4.13 with the parameter estimates obtained from the fit. b.Arterial compliance obtained from the derivative of equation 4.13 and the parameter estimates obtained from the fit. Results obtained from the first trial.

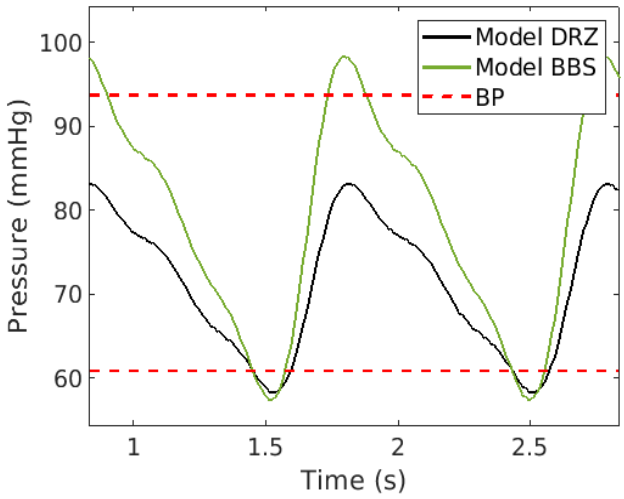

FIGURE 4.12: Modelled APW obtained with the FS constant estimates from the regressions in the first trial. Model DRZ refers to the use of equation 4.12 and model BBS refers to the use of equation 4.13. The dashed lines correspond to the measured BP = 93.77/60.81 mmHg.

BP in this case is estimated from the maximum and minimum values of the FS obtained. The difference in the BP estimate, calculated as measured BP minus estimated BP, is 10.60/2.48 mmHg for model DRZ, and −4.64/3.35 mmHg for model BBS. The value of function S obtained with model DRZ was 668.51 mmHg^2, and that obtained with model BBS was 697.18 mmHg^2.

In the second trial, on the other hand, there were just as in the first trial a few cases where the results associated to the lowest value of S were not correct, so these results had to be manually removed until a satisfactory result was obtained. In this second trial, however, there were fewer of these cases than in the first. Figures 4.13 and 4.14, show the results corresponding to the same measurement discussed above, now obtained from the second regression trials. Figures 4.15 and 4.16 represent the P-V function and the C_a function obtained, and figure 4.17 is a section of the APW that results from multiplying the waveform used as input times the estimated PP, and adding the estimated value of DBP to it, as obtained by the regression.

In this case of the second trial, the APW has the same shape for both models, and the same varying frequency as the measured OMW. MAP was not estimated in this case, but

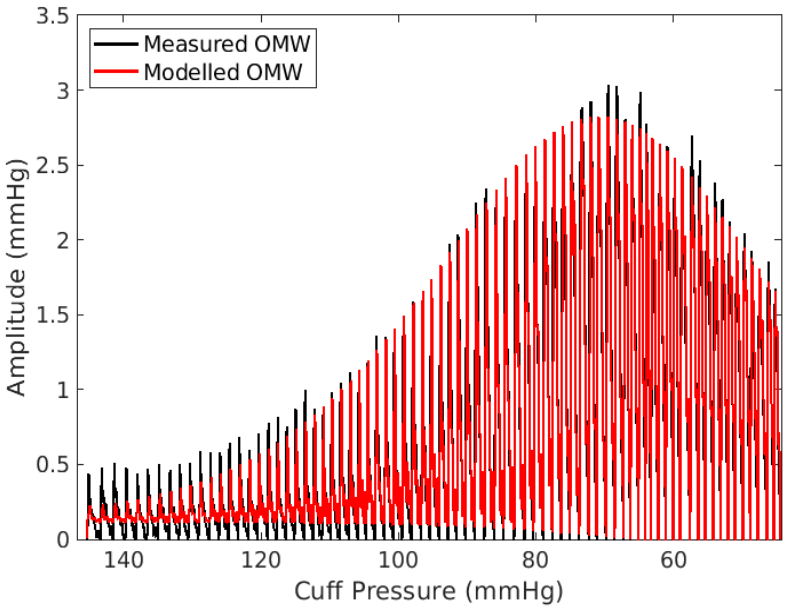

FIGURE 4.13: Measured data (black) with a result for function $f(x_i, \vec{\beta})$ (red) obtained from equation 4.12 during the second trial.

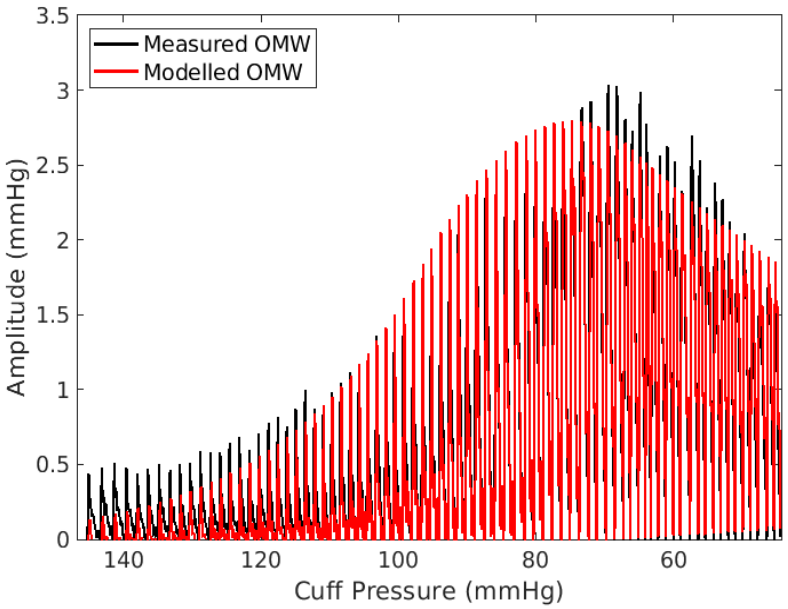

FIGURE 4.14: Measured data (black) with a result for function $f(x_i, \vec{\beta})$ (red) obtained from equation 4.13 during the second trial.

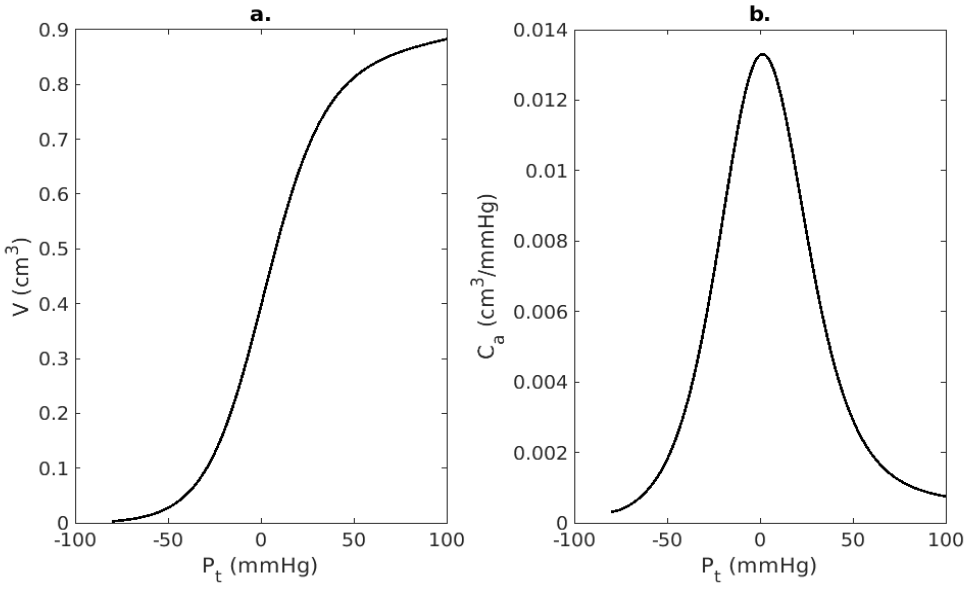

FIGURE 4.15: a.Pressure-Volume function obtained from equation 4.12 with the parameter estimates obtained from the fit. b.Arterial compliance obtained from the derivative of equation 4.12 and the parameter estimates obtained from the fit. Results obtained from the second trial.

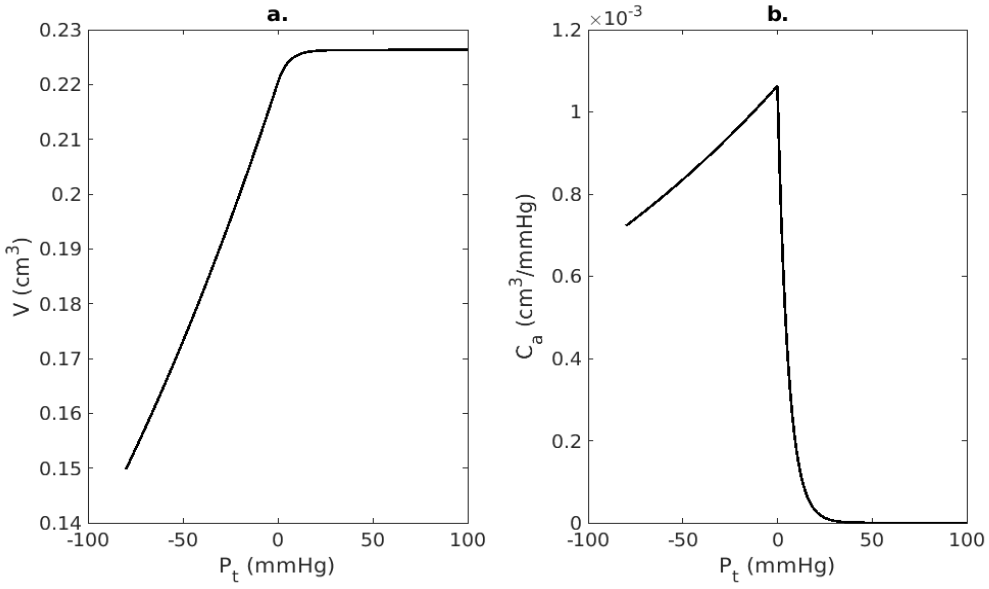

FIGURE 4.16: a.Pressure-Volume function obtained from equation 4.13 with the parameter estimates obtained from the fit. b.Arterial compliance obtained from the derivative of equation 4.13 and the parameter estimates obtained from the fit. Results obtained from the second trial.

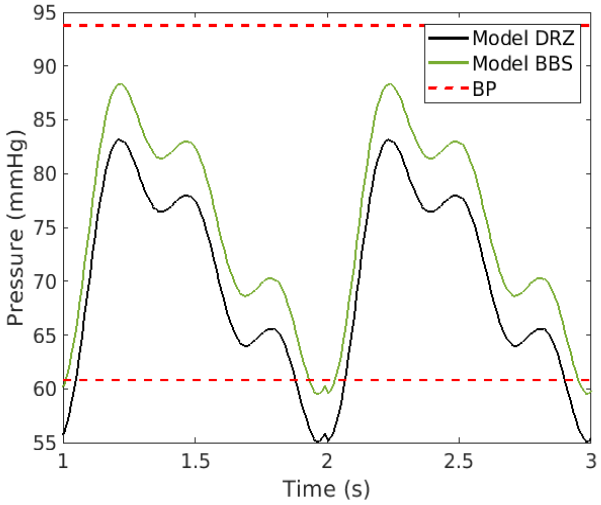

FIGURE 4.17: Modelled APW obtained with the PP and DBP estimates from the regressions in the second trial. Model DRZ refers to the use of equation 4.12 and model BBS refers to the use of equation 4.13. The dashed lines correspond to the measured BP = 93.77/60.81 mmHg.

DBP is directly obtained as a parameter, and SBP is calculated by adding to this value the estimated PP. The difference in BP values for the DRZ model are 10.57/5.63 mmHg, while those for the BBS model are 5.44/1.22 mmHg. The values of function S were 605.72 mmHg^2 and 630.42 mmHg^2 for the DRZ and BBS model, respectively.

Figure 4.18 shows a comparison of the arterial mechanics obtained in all cases and table 4.1 gives a summary of the constant estimates for this particular measurement. The labels DRZ1 and DRZ2 correspond to the results from using equation 4.12 in the first and second trials, respectively, and BBS1 and BBS2 from using equation 4.13 in the first and second trial, respectively. For each case the maximum value of the arterial compliance, $C_{a,max}$, was calculated, and this value is shown in table 4.2 along with the value of function S and the difference in BP vales, BP_{Δ}.

The results presented in figure 4.18 and in tables 4.1 and 4.2 correspond to a single measurement. However, the relationship between parameter estimates and the other calculated values is considered to be representative of how they relate in most of the cases. For instance, we can observe how the value of the function S is lower for the regressions where the constants of the APW were not part of the parameter vector, and the BP estimate is closer

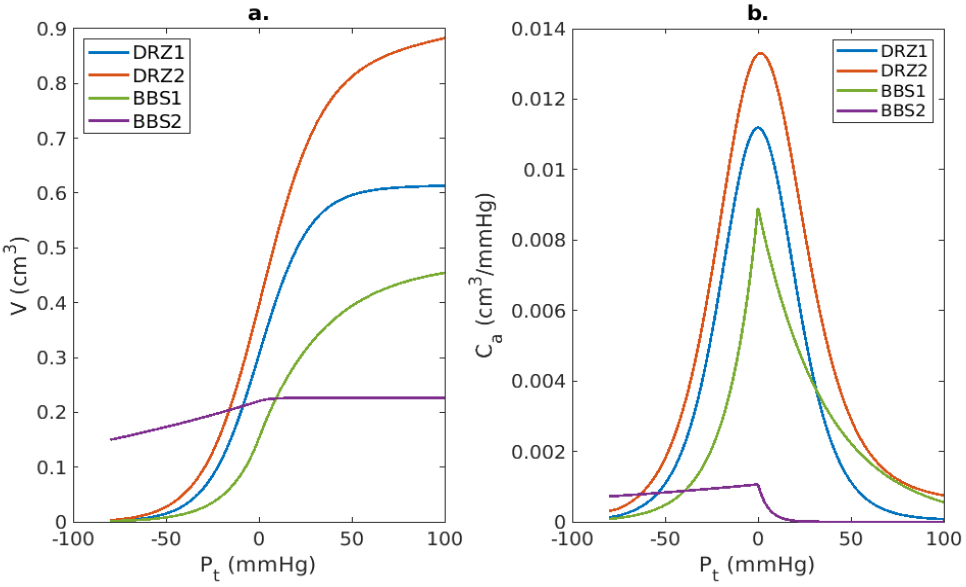

FIGURE 4.18: a.Comparison of the Pressure-Volume function obtained from using both compliance equations and after both regression trials. b.Corresponding comparison of the arterial compliance. DRZ1 and DRZ2 correspond to first and second trials using equation 4.12, and BBS1 and BBS2 to the first and second trials using equation 4.13.

TABLE 4.1: Summary of the estimated parameter values obtained for each regression for the case discussed in figures 4.8 through 4.18.

Model	Parameter Estimates			
	a [mmHg^{-1}]	b	$c \times 10^{-2}$ [mmHg^{-1}]	$(d \times L)/C_c$ [mmHg]
DRZ1	7.14×10^{-5}	1.71	7.33	11.31
DRZ2	7.47×10^{-1}	67.34	7.68	1.34
	a_B [mmHg^{-1}]	b_B [mmHg^{-1}]	V_o/C_c [mmHg]	
BBS1	5.86×10^{-2}	2.77×10^{-2}	1.52	
BBS2	4.66×10^{-3}	0.24	2.62	

TABLE 4.2: Values of maximum arterial compliance, $C_{a,max}$, S, and difference in the BP values, BP_Δ, calculated for each regression for the case discussed in figures 4.8 through 4.18.

Model	$C_{a,max} \times 10^{-3}$ [cm^3/mmHg]	S [mmHg^2]	BP_Δ [mmHg]
DRZ1	11.19	668.51	10.60/2.48
DRZ2	11.59	605.72	10.57/5.63
BBS1	8.92	697.18	−4.64/3.35
BBS2	1.22	630.24	5.44/1.22

TABLE 4.3: Population mean ± SD of the difference between measured values of SBP and DBP and their estimates according to regression type and trial. SBP difference = SBP_Δ, and DBP difference = DBP_Δ.

Model	SBP_Δ [mmHg]	DBP_Δ [mmHg]
DRZ1	14.79 ± 6.37	0.08 ± 8.07
DRZ2	10.80 ± 5.59	11.24 ± 11.55
BBS1	4.41 ± 6.12	-0.27 ± 5.59
BBS2	7.79 ± 5.64	4.85 ± 10.43

to the measured value for the regressions performed using equation 4.13.

Figure 4.19 confirms that, overall, the value of S is lower for the regressions that did not include the FS in the parameter estimates. The results presented in table 4.3 represent the population mean ± SD of the difference in systolic and diastolic estimates compared to the measured values. The regressions where equation 4.13 was involved, or model BBS, have BP estimates closer to the measured values and smaller SD, particularly the first one.

An effect that was expected to be observed was consistency between the estimated parameters related to arterial mechanics of an individual. That is, in a short period of time the values of the constants that define arterial P-V or C_a functions should not differ significantly for a single individual. Tables 4.4 and 4.5 show the mean ± SD of the parameter estimates of four volunteers who had at least three measurements where all four regressions were successful.

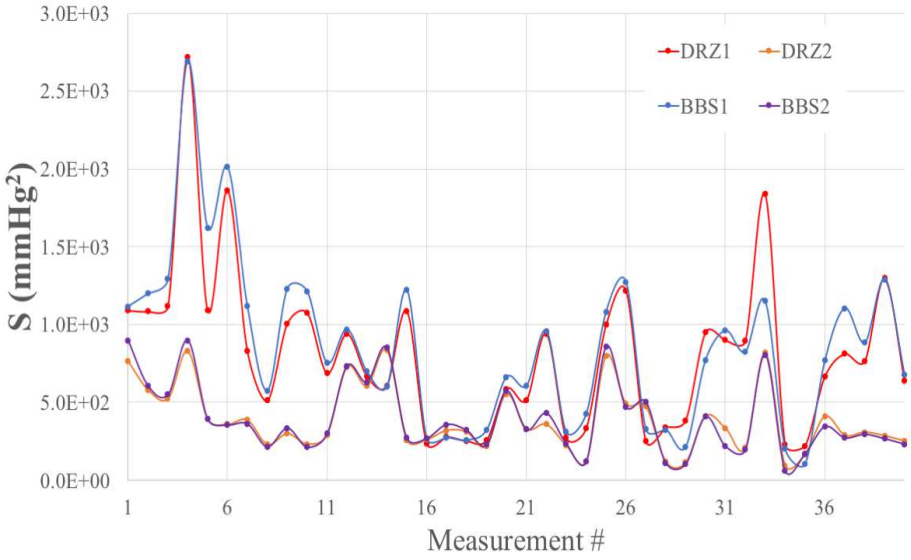

FIGURE 4.19: Comparison of the value of function S for all 40 measurements according to the regression, where DRZ stands for those performed using equation 4.12, BBS for those using equation 4.13, and the numbers relate to the first or second trial.

TABLE 4.4: Mean ± SD of the arterial mechanics constants found for 4 volunteers during a session using equation 4.12 in the two trials.

ID	Model	a [mmHg^{-1}]	b	$c \times 10^{-2}$ [mmHg^{-1}]	$(d \times L)/C_c$ [mmHg]	$C_{a,max} \times 10^{-3}$ [cm^3/mmHg]
V1	DRZ1	$4.41 \pm 3.07 \times 10^{-4}$	5.41 ± 3.07	8.75 ± 0.88	3.87 ± 1.62	11.21 ± 0.46
	DRZ2	$8.32 \pm 8.50 \times 10^{-1}$	76.25 ± 77.67	8.08 ± 0.86	1.70 ± 1.03	10.13 ± 1.61
V2	DRZ1	$6.85 \pm 1.95 \times 10^{-4}$	7.85 ± 1.95	9.12 ± 1.87	2.27 ± 0.23	10.36 ± 0.65
	DRZ2	$2.29 \pm 1.90 \times 10^{-2}$	100.51 ± 88.26	6.23 ± 0.70	1.67 ± 0.61	8.54 ± 1.80
V3	DRZ1	$3.29 \pm 5.49 \times 10^{-3}$	34.05 ± 54.70	7.16 ± 0.94	3.79 ± 2.55	8.04 ± 1.50
	DRZ2	$2.65 \pm 3.48 \times 10^{-1}$	719.72 ± 1168.93	6.29 ± 1.53	1.01 ± 0.44	7.06 ± 1.19
V4	DRZ1	$8.82 \pm 19.57 \times 10^{-2}$	1367.27 ± 3039.37	13.21 ± 1.58	2.23 ± 1.26	13.65 ± 4.28
	DRZ2	$7.72 \pm 17.19 \times 10^{-2}$	617.62 ± 1169.25	9.16 ± 0.83	1.70 ± 1.92	9.20 ± 1.22

TABLE 4.5: Mean ± SD of the arterial mechanics constants found for 4 volunteers during a session using equation 4.13 in the two trials.

ID	Model	$a_B \times 10^{-2}$ [mmHg^{-1}]	$b_B \times 10^{-2}$ [mmHg^{-1}]	$V_o/C_c \times 10^{-1}$ [mmHg]	$C_{a,max} \times 10^{-3}$ [cm^3/mmHg]
V1	BBS1	5.82 ± 1.32	13.26 ± 8.96	14.61 ± 2.04	8.37 ± 1.38
	BBS2	0.46 ± 0.04	24.80 ± 3.22	24.89 ± 5.35	1.14 ± 0.21
V2	BBS1	8.31 ± 2.65	4.85 ± 4.28	9.43 ± 2.86	7.33 ± 0.61
	BBS2	0.41 ± 0.06	51.65 ± 43.53	24.66 ± 8.31	0.99 ± 0.29
V3	BBS1	7.25 ± 0.10	5.77 ± 2.85	11.61 ± 0.78	8.42 ± 0.65
	BBS2	0.44 ± 0.03	28.52 ± 1.88	20.25 ± 1.35	0.89 ± 0.07
V4	BBS1	8.96 ± 0.86	6.79 ± 0.86	12.98 ± 2.75	11.56 ± 2.25
	BBS2	0.53 ± 0.08	50.52 ± 14.44	21.84 ± 4.57	1.12 ± 0.16

For an additional analysis of consistency in the arterial mechanics parameters, the author collected measurements of a single individual over an extended period of time. These results are shown in tables 4.6 and 4.7 and represent the compliance constants and maximum compliance obtained from measurements performed during five nonconsecutive days. The results shown are the mean ± SD of the parameters for each day. The overall mean ± SD is given in the final row.

4.2.4 Discussion

While analyzing the results presented in the previous section it is important to keep in mind that NLLS regression is highly susceptible to outliers and incorrect initial parameter estimates. Unfortunately, the outliers in the measurement are difficult to remove, given that these outliers may be present in the form of uneven oscillation amplitudes, not just noise in the signal. Synthetic OMW, such as the one shown in figure 4.4, present smooth, even envelope profiles, yet the measured data hardly follow this constant increase and decrease in oscillation amplitudes.

The modelled OMW shown in figures 4.8, 4.9, 4.13, and 4.14 show how the result tends to follow the overall shape of the synthetic case, but is not able to account for larger amplitudes at higher cuff pressures, or to properly centre the location of the maximum amplitude. The first effect may perhaps lead one to conclude that a P-V or compliance function that does not

TABLE 4.6: Parameter estimates for a single individual over the course of 5 non-consecutive days, using equation4.12 in both trials.

D#	Model	a [mmHg^{-1}]	b	$c \times 10^{-2}$ [mmHg^{-1}]	$(d \times L)/C_c$ [mmHg]	$C_{a,max} \times 10^{-3}$ [cm^3/mmHg]
1	DRZ1	$2.83 \pm 2.38 \times 10^{-4}$	9.12 ± 8.06	7.85 ± 1.32	2.92 ± 1.84	8.59 ± 0.64
	DRZ2	$3.15 \pm 4.38 \times 10^{-1}$	27.47 ± 38.57	6.69 ± 0.50	2.00 ± 0.66	8.64 ± 1.82
2	DRZ1	$4.41 \pm 3.07 \times 10^{-4}$	5.41 ± 3.07	8.75 ± 0.88	3.87 ± 1.62	11.21 ± 0.46
	DRZ2	$8.32 \pm 8.50 \times 10^{-1}$	76.25 ± 77.67	8.08 ± 0.86	1.70 ± 1.03	10.13 ± 1.61
3	DRZ1	$4.05 \pm 4.07 \times 10^{-4}$	10.67 ± 9.34	7.51 ± 0.59	3.18 ± 2.56	8.22 ± 5.85
	DRZ2	$8.01 \pm 12.85 \times 10^{-1}$	117.08 ± 100.66	6.82 ± 0.28	1.01 ± 0.32	7.29 ± 2.27
4	DRZ1	$1.31 \pm 2.22 \times 10^{-3}$	105.53 ± 222.46	7.86 ± 0.47	6.73 ± 6.08	12.90 ± 3.43
	DRZ2	$9.48 \pm 9.61 \times 10^{-1}$	87.28 ± 88.37	7.86 ± 0.33	1.54 ± 0.74	11.31 ± 1.49
5	DRZ1	$1.66 \pm 1.37 \times 10^{-4}$	2.66 ± 1.37	8.02 ± 0.91	9.11 ± 11.28	7.61 ± 1.40
	DRZ2	1.18 ± 1.36	107.84 ± 122.76	7.53 ± 0.36	1.01 ± 0.36	7.57 ± 1.75
	DRZ1	$5.81 \pm 11.61 \times 10^{-4}$	32.59 ± 114.14	8.02 ± 0.85	5.46 ± 6.07	10.01 ± 3.41
	DRZ2	$8.48 \pm 9.55 \times 10^{-1}$	84.55 ± 86.03	7.49 ± 0.71	1.45 ± 0.72	9.22 ± 2.25

TABLE 4.7: Parameter estimates for a single individual over the course of 5 non-consecutive days using equation 4.13 in both trials.

D#	Model	$a_B \times 10^{-2}$ [mmHg^{-1}]	$b_B \times 10^{-2}$ [mmHg^{-1}]	$V_o/C_c \times 10^{-1}$ [mmHg]	$C_{a,max} \times 10^{-3}$ [cm^3/mmHg]
1	BBS1	6.72 ± 2.10	2.72 ± 0.46	10.10 ± 2.83	6.45 ± 0.79
	BBS2	0.43 ± 0.04	1.75 ± 0.37	18.99 ± 2.21	0.81 ± 0.06
2	BBS1	5.82 ± 1.32	13.26 ± 8.96	14.61 ± 2.04	8.37 ± 1.38
	BBS2	0.46 ± 0.04	24.80 ± 3.22	24.89 ± 5.35	1.14 ± 0.21
3	BBS1	7.08 ± 1.28	12.37 ± 13.65	9.80 ± 3.04	6.78 ± 1.60
	BBS2	0.44 ± 0.03	2.29 ± 0.29	18.10 ± 4.30	0.79 ± 0.13
4	BBS1	5.95 ± 0.51	3.17 ± 0.39	16.35 ± 1.98	9.71 ± 1.21
	BBS2	0.46 ± 0.01	2.43 ± 0.42	27.66 ± 3.14	1.27 ± 0.17
5	BBS1	5.93 ± 0.51	5.74 ± 2.98	12.37 ± 1.48	7.32 ± 0.94
	BBS2	0.43 ± 0.01	2.45 ± 0.33	18.95 ± 3.43	0.80 ± 0.14
	BBS1	6.22 ± 1.11	7.22 ± 7.34	13.13 ± 3.19	7.95 ± 1.65
	BBS2	0.44 ± 0.03	2.31 ± 0.41	22.36 ± 5.32	1.00 ± 0.26

decrease rapidly towards zero at negative transmural pressures is better suited to describe the observed OMW. That is, if one remembers the different models of arterial mechanics that were presented in figure 4.1, the model obtained from Ursino and Cristalli's publication ([6]), for instance, assumes that the volume of the artery does not fully decrease to zero at the same negative transmural pressures as the rest of the models. This observation makes sense if one considers that the other models describe a point in the artery segment that fully collapses and reduces its volume to zero at moderately negative P_t. In an OBPM the oscillations observed at higher cuff pressures, associated with larger negative values of P_t, originate because the artery does not fully collapse through the entire length of the cuff. Certainly, a model that accounts for this bias in the arterial volume may adjust better for oscillations of higher amplitudes on this high cuff pressure end of the measurement.

The shift in the location of the point of maximum amplitude in the oscillations is not critical in all cases. An interesting thing to point out in this case, however, is how this shift in the maximum amplitude relates to the estimates of BP obtained from the regression, especially considering that the BP estimates in an OBPM depend on the location of certain amplitudes in the OMWE. This means that, although BP estimates can be obtained directly from the regression, either from the FS extreme values or from the estimates of DBP and PP, a future interesting analysis may include obtaining BP estimates from the modelled OMW through the MAR algorithm and comparing those to the estimates obtained from the regression. Perhaps this comparison could further confirm if the parameter estimates from the regression are correct, or it could instead be related to how the cuff estimates are different from intra-arterial values. The latter stems from the fact that the APW is part of equation 4.11, and this is a value that is measured intra-arterially.

P-V and C_a functions obtained with the parameter estimates from the regression are very similar to what was expected, except for those obtained with model BBS2 shown in figure 4.16. The P-V function in the other three cases follows the expected sigmoidal shape, and maximum compliance values are within the expected order of magnitude when compared to the values obtained when using the parameters in the literature, as observed in figure 4.1. It is interesting to observe that the case of model BBS2 is slightly better at fitting the oscillations on the high cuff pressure end than the other three models, so this might reinforce the notion that a P-V or C_a function that doesn't fully decrease to zero at negative transmural pressures may offer an advantage in the regression. Overall, the most significant difference between

the estimated arterial mechanics for the three cases that had the expected shapes seems to be the assumed dimensions of the artery, as one can appreciate from figure 4.18, and from the values of the parameters related to the amplification of the function in table 4.1, such as $(d \times L)/C_c$ and V_o/C_c.

The regressions involving equation 4.13 resulted in a BP estimate closer to the measured BP. This result is not necessarily an indicative of a better/worse fit, which is why the difference between estimated and measured values was purposefully not identified as an error in the measurement. As mentioned above, the APW considered in these models is assumed to be representative of intra-arterial values, and cuff measurements often misrepresent these values. It is not unreasonable to accept that an APW of different extreme values compared to the final BP estimate is responsible for the observed OMW.

It is important to mention, however, that in the case of the first trial, where the APW was estimated as a FS, in some measurements the resulting FS would tend to the limits imposed on its values. This indicates that the limits were perhaps too restrictive, and different estimates might have been obtained if they were expanded or removed altogether, although results with unreasonable values would still have been discarded. Another important observation is the fact that the estimate of MAP in the case of model DRZ1 for most of the OMW obtained from the measurements sampled at 10 kSps resulted in 85 mmHg. This is a strange occurrence, especially considering that the initial guess vectors had this value set at the MAP calculated for each individual, and only one had a MAP of $\sim$ 85 mmHg. At the moment there is no explanation of why this was the case, but perhaps it is also somehow related to the limits imposed on the FS. Since all measurements were decimated to a sampling frequency of 100 Sps the possibility that the sampling rate had any influence on this result is discarded. Since this result was not observed in the case of BBS1, we could also discard the effect that manual deflation has on the data.

The value of function S does not change significantly if one equation or another is used for arterial mechanics in a same trial, although the removal of the FS constants from the parameter vector significantly improved its value as expected. This confirms that the frequency of the oscillations plays a major role in the success of the regression. Unfortunately, the values of S are several orders of magnitude bigger than those of the perfect fits in the synthetic case, which, although expected, indicate that the parameter estimates may be far from their true values. We can still affirm, however, that the results from the second trial

may be closer to the real values than the results from the first trial, and that the procedure greatly benefits from having a measured APW used as input to the model. Even if this is not possible, there may be a more effective way to construct the APW than what is proposed in this work, that avoids the sudden discontinuities in pulse amplitude.

It can be observed in tables 4.4 through 4.7 that there is a very wide spread for some of the parameter estimates between individuals. The most consistent estimates appear to be those for constants c and d where equation 4.12 was used, assuming that L and C_c are constant for all volunteers, and constants a_B and V_o where equation 4.13 was used, once more assuming that C_c is constant for all volunteers. Somewhat surprising is the fact that maximum arterial compliance, $C_{a,max}$ appears to be consistent for all individuals, inferred from the lower spread of values around the mean. In the case of equation 4.12 perhaps the values of constants a and b are not necessarily a good point of reference, since one may compensate for the other in order to fit the constraint placed on them. The case of the second trial with equation 4.13, or BBS2, was already observed to result in a poor representation of arterial mechanics, therefore the accuracy of those parameters is put into question.

Nevertheless, a positive result is observed in the fact that maximum arterial compliance seems to tend towards a specific value depending on subject. This is observed not only in the estimates of the four different volunteers in tables 4.4 and 4.5, but also in those for a single individual over the course of several days, as shown in tables 4.6 and 4.7. These last two results for a single individual show that overall the spread of values is not too large over the 5 days, so it would be an interesting follow up experiment to perform an OBPM on the rest of the volunteers over an extended period of time. If this same trend is observed, then the correct estimates of the parameters is not a critical result. Similar to the case of BP, the important observation would be the trend in the value collected over an extended period of time. Some of these parameters, such as those that present less spread in their values, can be observed over time and deviations in their values could potentially be associated to an underlying modification of the arterial mechanics.

4.2.5 Conclusions

The result of the regressions presented in this chapter offer a positive first approach to validating a mathematical model of the physical phenomena occurring during an OBPM. The comparison between measured and modelled data show that, while the model may not

account for all possible variations in the measured OMW, the mathematical expression seems to be able to reproduce most of the measured waveform, particularly on the diastolic end. At this stage in the development of the mathematical model we cannot conclusively validate one model over the other, however we can appreciate how this simple set of equations serve as a good basis to describe the observed phenomena.

Some improvements could be implemented in the model and in the processing of the data for more successful regressions. For instance, considering cuff compliance as constant may have a greater influence in the results than expected, and a function dependent on transmural pressure may be better suited. This would mean, however, that equation 4.11 is no longer valid and a different derivation would be required. Another possibility to avoid modifying the equation could be to limit the analysis to the OMW obtained exclusively at high cuff pressures where cuff compliance is more likely to be constant. This will also have the advantage of resulting in pressure pulses of consistent shape, which, although not presented in this work for not being of immediate interest to the analysis, has been observed to change as cuff pressure decreases, mostly owed to wave reflections.

Overall, the use of equation 4.12 without including the APW in the regression seems to be the most promising option. It results in lower values of S when compared to the cases where the FS constants are estimated, and in a better representation of arterial mechanics compared to the use of equation 4.13. The inconsistency in constants a and b for different individuals may be overlooked and the rest of the constants can be used as reference to track variations in arterial mechanics. It would appear that the inclusion of more constant parameters to the regression model may have been beneficial, giving the model more freedom to adjust to the measured data. It is also possible that this model has better success owed to the fact that it does not assume maximum compliance at zero P_t.

Measured data can also be modified to a certain extent to simplify the regression. Outliers in the form of oscillations with higher/lower amplitudes than the neighbouring oscillations are already adjusted as discussed in Chapter 2. Perhaps more results from that chapter can be extended to the present analysis, like using one of the OMWEs discussed previously to smoothen the amplitude profile and simplifying the regression process. It was already observed that the use of different OMWE provided more accurate estimates of BP, so normalizing the oscillation amplitudes to a Gaussian envelope, for example, may improve the expected results.

Finally, the most important implication for the results of this chapter is the possibility of verifying the influence arterial mechanics have on BP estimates through the MAR algorithm. This assumption is based on the work of Ursino and Cristalli mentioned at the start of this chapter, and is overall the greatest contribution intended of this work. Once an improved model is derived based on the observations discussed above and more effective regressions are obtained, the relationship between the obtained parameters and the features of the MAR algorithm can be directly analyzed from measured data. The results of such a study could potentially help us improve this algorithm and the overall accuracy of oscillometric devices, which is the overall goal of the work done in this chapter.

Chapter 5

Physics-Based Mathematical Model and Regression Analysis of the Auscultation Method

In this chapter we arrive at the final component of the analysis of the two most popular BP measurement methods. The true origin of Korotkoff sounds is hard to pinpoint, as research and evidence over the years have demonstrated. Undeniably, these are a product of the interaction between fluid mechanics, arterial wall mechanics, and wave transmission along the viscoelastic brachial artery. However, this interaction is a formidable mathematical and physical problem that can only be solved if certain simplifications are made when deriving the descriptive models.

Similar to the case of oscillometry, several mathematical models have been developed and numerically solved to generate synthetic KS. The models have been successful in their purpose of creating traces that resemble KS and that also have frequency characteristics proper to KS. However, the complexity of these models makes it hard to compare them directly to measured data. Likewise, the complexity of the data means that no simple function can be fitted to it and characteristic parameters are usually approximated from *in vitro* measured data.

The objective set for this chapter in the introduction was, thus, to obtain a deeper understanding of this phenomena involved in the generation of KS, and it is believed that this can be accomplished by validating a physics-based model with measured data. Similar to the work in chapter 4, the author believes that the best approach is of a practical nature, which means applying a simple model that can be readily compared to measured auscultation

sounds without requiring a significant computational cost.

In this chapter the author intends to do so by following the approach of assuming that KS are generated by arterial wall mechanical properties. In particular, the model derived here will be based on the one proposed by Babbs [103], where it is assumed that KS are generated by vibrations of the arterial wall.

In the following section we will first be introduced to this model and how KS are assumed to be generated. A simple modification to the model is also proposed by the author of the present text, based on previous observations done of the arterial mechanics, and both representations will be compared afterwards to measured data by means of a NLLS regression. In this case, we shall see that testing the model on synthetic cases first is of particular relevance to determining the best way to interpret the results and selecting the appropriate solutions.

The final sections of this chapter include the discussion of the results, and how they align with the objectives of this thesis. That is, commentary is given on the possibility of validating this model, on possible additional considerations, and on the implication that the obtained parameters have for overall cardiovascular health. Just as in the case of chapter 4, the regressions performed in this chapter may provide us with information of parameters related to the brachial artery, which are ordinarily obtained by specialized procedures such as ultrasound.

5.1 Harmonic Oscillator Model

The premise of this idea, as stated by Babbs in his publication, is that KS are generated due to transient vibrations of the arterial wall caused by a change in elastic response to the forces applied to it. This is due to the nature of the artery, which becomes more rigid in the region where P_t reaches large positive vales to prevent rupture from high internal pressures, and is easily deformed when under compression. These features can be verified by any rubber tube or elastic band: they offer more resistance to stretching, yet require minimal effort in comparison to make opposite ends come in contact.

We can make a visual distinction between these two regions of different elastic response by the shape of the arterial cross-section. Where the artery is stiffer, we can think of it as a cylinder, with a circular cross-sectional shape. Where the artery is more easily deformed it

adopts a cross-sectional form closer to an ellipse, then resembles an hourglass before opposite sides come into contact, and it ultimately flattens. The point that connects these two regions is called the buckling point. Babbs states that once the artery crosses the buckling point as it is changing from its elliptical to its circular shape it suffers a sudden deceleration, which is responsible for the vibrations that give origin to the KS.

To describe this motion mathematically, we can consider a section of the arterial wall, and assume it moves along a single horizontal axis, as exemplified by the red square in the diagram in figure 5.1. For simplicity any longitudinal or torsional stretching effects, as well as wave transmission are ignored. We can identify the buckling point as a distance along this axis that marks the location where the artery shifts from circular to elliptical (and vice-versa) cross-sectional area. This distance is labeled x_b on the figure, and we can now differentiate the two regions depending on whether the movement is occurring at $x < x_b$ or at $x > x_b$.

The section of wall can be thought of as a mass attached to a couple of springs and, since biological tissues are viscoelastic materials, to a dashpot to represent its viscosity. In each region separated by the buckling point only one of the springs is compressed at the time. That is, as once can see in the diagram in figure 5.1, when the artery is at $x > x_b$, only the spring represented by k_1 is compressed. In the region where $x \leq x_b$, only the spring represented by the constant k_2 is compressed. For simplicity, it is assumed that the viscosity of the wall remains constant throughout the entire movement, therefore there is no separate constant for the dashpot in either region.

The system is driven by an oscillating force which in this case is originated by the transmural pressure. That is, the driving force is the result of the interaction between internal and external forces applied to the arterial wall originated by the internal arterial pressure and the external cuff pressure. Including these observations into a harmonic oscillator equation we can write:

$$m\ddot{x} = F_D + F_{S1} + F_t(t) \text{ for } x > x_b \tag{5.1a}$$

$$m\ddot{x} = F_D + F_{S2} + F_t(t) \text{ for } x \leq x_b \tag{5.1b}$$

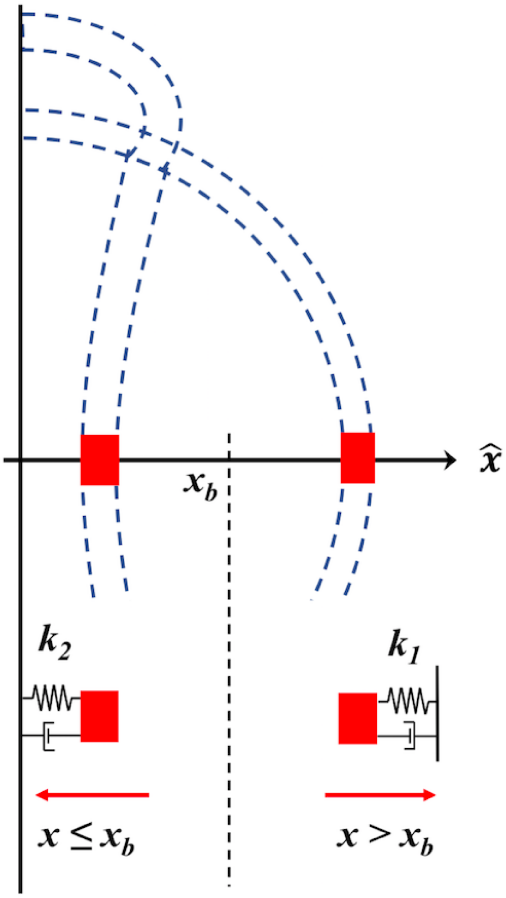

FIGURE 5.1: Diagram of the movement of a single point on the arterial wall along a horizontal axis and its representation as an oscillating mass attached to a couple of springs and dashpots.

where m represents the oscillating mass, F_{S1} and F_{S2} are the two restoring forces corresponding to the two spring constants mentioned above, respectively, F_D is the restoring force of the viscous component, and F_t the force originating from transmural pressure, P_t. The solution to this equation represents the position of the section of arterial wall along the axis, and, as we shall see, the first derivative is used as a surrogate for sound pressure.

A first approximation of the restoring force F_{S1} is of a linear elastic force, $F_{S1} = -k_1(x - x_b)$, for $x > x_b$, which was proposed by Babbs in his work. Under normal pressure ranges, without the influence of an external cuff, this linear force is a good approximation. However, one might recall from the models of arterial mechanics (figure 4.1) that the rate of increase in arterial volume (or cross-sectional area) is fast near zero P_t, but very quickly slows down and becomes almost constant past the point where $P_t \sim$ DBP.

This clearly indicates that the restoring force is not constant throughout the whole range of positive transmural pressures, but that it has a rather gradual increase as we move further away from $P_t = 0$. To convey this, in this work we now propose that we consider the arterial wall in this region as a "hard" spring, which includes additional terms in the Taylor series expansion of the force, such that $F_{S1}(x) = -k_1(x - x_b) - k_3(x - x_b)^3$, where k_3 must be a positive constant to prevent an unstable system. The difference between the two approximations is shown in figure 5.2. Both cases will be considered in this analysis to compare which approach is more effective.

The restoring force, F_{S2} is small for most of the distance $x < x_b$, and then approaches an infinitely large value when the opposite walls come in contact. The force in this case can be described by an equation of the form

$$f(x) = -a\frac{x - x_b}{x}, \tag{5.2}$$

such that

$$F_{S2} = -k_2(x - x_b) = -a\frac{x - x_b}{x}. \tag{5.3}$$

This last expression implies that in this case k_2 is not necessarily constant, but rather a function of the position of the arterial wall: $k_2(x) = a/x$.

The damping force, F_D, is naturally dependent on the velocity of the arterial wall. As mentioned above, it has the same expression for both regions, $F_D = -\beta\dot{x}$, where β is the

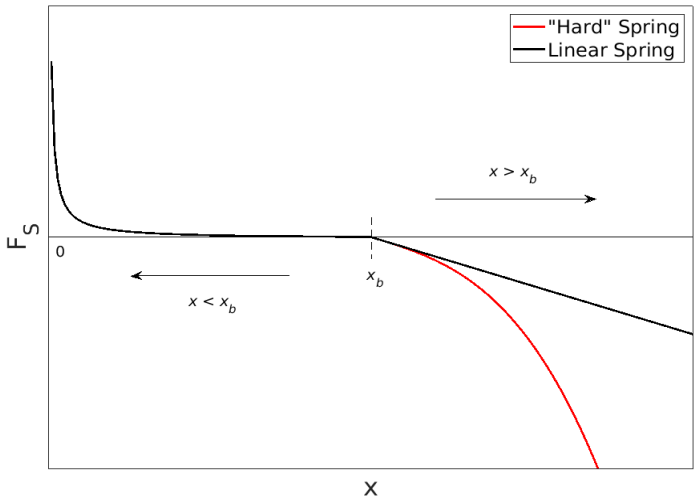

FIGURE 5.2: Restoring forces in the regions where $x < x_b$ and $x > x_b$.

viscosity of the arterial wall. The driving force F_t has already been established to correspond to the transmural pressure P_t acting on a section of arterial wall of area A. Rewriting equation 5.1 to include the constants discussed above results in:

$$m\ddot{x} = P_t A - \beta\dot{x} - k_1(x - x_b) - k_3(x - x_b)^3 \qquad \text{for } x > x_b \tag{5.4a}$$

$$m\ddot{x} = P_t A - \beta\dot{x} - k_2(x - x_b) \qquad \text{for } x \leq x_b \tag{5.4b}$$

where the equation reduces to the linear case when $k_3 = 0$.

5.1.1 Complete Expression of the Harmonic Oscillator Equation

The constants associated to each term in equation 5.4 can be further related to arterial wall parameters. The derivation for the spring constants k_1 and k_2 is included in Appendix D. The derivation is based on Babbs' work, which results in spring constants

$$k_1 = \frac{Eh}{r_o} \cdot \delta\theta L \tag{5.5}$$

and

$$k_2 = 4\frac{E}{\pi^2} \cdot \frac{h^2}{r_o^2} \cdot \delta\theta L, \tag{5.6}$$

where E is the Young's modulus of the arterial wall, h its thickness, r_o the neutral radius of the artery, $\delta\theta$ the angle that defines the section of arterial wall, and L the length of arterial wall.

Constant a from equation 5.2 is solved from its established relationship to spring constant k_2:

$$\frac{a}{x} = 4\frac{E}{\pi^2} \cdot \frac{h^2}{r_o^2} \cdot \delta\theta L, \tag{5.7}$$

however, a special consideration must be made given that the position x is in the denominator. The initial position of the arterial wall is located at $x = 0$, yet this condition results in a division by zero and an equation that diverges. This would eliminate the initial position as a solution and result in an error when attempting to solve the equation by computational means. To avoid this, we can assume that the asymptote is located at a distance beyond $x = 0$, and express this as

$$\frac{a}{x + \eta} = 4\frac{E}{\pi^2} \cdot \frac{h^2}{r_o^2} \cdot \delta\theta L, \tag{5.8}$$

where we assume that $\eta << r_o$. At the point of maximum flattening, where $x = 0$:

$$a = 4\frac{E}{\pi^2} \cdot \frac{h^2}{r_o^2} \cdot \eta\delta\theta L. \tag{5.9}$$

In his publication, Babbs recognized the need to include the term η in the equation and assumed that $\eta = h$. In this case we shall assume the same equality.

The arterial wall in this case was assumed to be represented by a single viscous component for both regions. The change in elastic properties in these two cases is in part due to how the wall's components (elastin, collagen, smooth muscle fibres) are recruited differently to take on the burden of the forces applied to the wall. This means that, potentially, the viscosity of the wall could also be different for both regions. However, in the normal state of the artery the wall is positioned at $x > x_b$, and mechanics in this state are believed to dominate over those in the region where $x < x_b$. There is also more information available of the artery

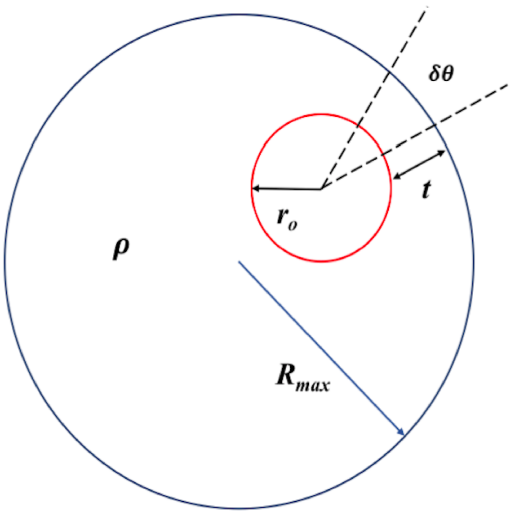

FIGURE 5.3: Cross-sectional diagram of the arm and the relative location of the brachial artery. R_{max} is the radius of the arm.

under normal conditions, therefore, for simplicity, the viscous component of the artery wall will be taken as that occurring at $x > x_b$. This means that the viscosity can be related to arterial wall parameters in an analogous way to the spring constant k_1:

$$\beta = D\frac{h}{r_o}\delta\theta L \tag{5.10}$$

where D is the damping modulus.

The area A over which the transmural pressure acts can be expressed as $r_o L\delta\theta$, such that $F_t = P_t r_o \delta\theta L$. The mass term in equation 5.4 was calculated by Babbs assuming the artery wall moves a section of the surrounding tissue as well. In Babbs' derivation, however, he assumes the artery and the arm are concentric, which in reality is not the case. In this work, we instead assume that the artery is not concentric and that the mass the arterial wall section displaces is much smaller than what Babbs assumed. An expression for the mass can be calculated from the volume of tissue located directly above the section of arterial wall, as shown in figure 5.3.

The arterial wall displaces a volume of tissue defined by the arc length $r_o\delta\theta$ of width t and length L. The effective mass for the harmonic oscillator can then be expressed as

$$m = \rho t r_o \delta\theta L \tag{5.11}$$

where ρ is the lumped density of the tissue.

Finally, the buckling point, x_b is believed to occur at the position of the neutral radius of the artery, r_o. Setting $x_b = r_o$ and substituting equations 5.5, 5.6, 5.10, and 5.11 in equation 5.1, along with the expression for the driving force, the common variable $\delta\theta L$ is eliminated to give the final expression for the harmonic oscillator equation:

$$\ddot{x} = \frac{1}{\rho t r_o}\left[P_t(t) r_o - D\frac{h}{r_o}\dot{x} - E\frac{h}{r_o}(x - r_o) - \gamma(x - r_o)^3\right] \text{ for } x > r_o \tag{5.12a}$$

$$\ddot{x} = \frac{1}{\rho t r_o}\left[P_t(t) r_o - D\frac{h}{r_o}\dot{x} - \frac{4E}{\pi^2}\frac{h^3}{r_o^2}\frac{x - r_o}{x + h}\right] \text{ for } x \leq r_o. \tag{5.12b}$$

Where the case of the hard spring is marked by the inclusion of the term $\gamma(x - r_o)^3$ to the equation effective in the region $x > r_o$, where we assume that

$$\gamma = \frac{k_3}{L\delta\theta}, \tag{5.13}$$

and which simplifies to the linear spring when $\gamma = 0$.

5.2 Model Fitting to Auscultation Data

5.2.1 NLLS Regression and Parameter Ranges

Similar to the case of the OMW the harmonic oscillator model can be fitted to measured auscultation data to confirm the validity of the model and to obtain approximate values of the parameters in the equation. Once more, a non-linear least squares (NLLS) regression is an ideal method to perform this fit. As a reminder, for this regression the measured data is compared to simulated data generated by the equation in the model, and the difference between each point in the two vectors is calculated. The goal is to minimize the sum of the squared differences, or the function

$$S = \sum_{i=1}^{N} \varepsilon_i^2 = \sum_{i=1}^{N} [y_i - f(x_i, \vec{\beta})]^2, \tag{5.14}$$

which was also used in chapter 4. This minimization is accomplished by adjusting the value of the parameters in the vector $\vec{\beta}$, and the process, being an iterative process, requires an initial parameter value guess to start the search in the region of this guess.

In this case the measured variable vector, y_i, is the sound vector that contains the KS, which is measured in volts. The vector $f(x_i, \vec{\beta})$ will be generated from the harmonic oscillator equation 5.12. The voltage output of a capacitor microphone, such as the one the One Digital Stethoscope is based on, is directly proportional to the velocity of movement of the plate. As this plate is in direct contact with the skin, it moves at the same rate as the tissue that the artery displaces. Therefore, the velocity of the harmonic oscillator, obtained from integrating equation 5.12 once, and multiplied by a proportionality constant, becomes the vector $f(x_i, \vec{\beta})$.

The parameters in the vector $\vec{\beta}$ are, thus, the arterial wall variables that define the harmonic oscillator equation, namely the Young's (E) and damping (D) moduli, the neutral radius (r_o) and thickness (h) of the artery, the constant associated to the non-linear spring case (γ), the tissue properties of density (ρ) and thickness (t), and the proportionality constant that relates voltage to velocity. The variable associated to the driving force, P_t, is not included in the parameters since this will be an input to the model obtained from measured data, which will be discussed in the following sections.

The initial guess vector, $\vec{\beta}_0$, and the limiting values for the parameters can be determined from previously reported experimental results. While most measurements have not been performed under the same conditions as the experiment in this work, the values obtained will be helpful in establishing limits and selecting correct answers.

For instance, Babbs mentions that Young's modulus is commonly obtained for an artery under normal pressure conditions, but that it might be up to four times greater than what can be measured when the artery collapses. Values of E can range from 0.5 to 8 $\times 10^6$ dyne/cm^2 under normal conditions, according to his publication, and Nichols *et al* mention in their book E ranges between 2 and 8 $\times 10^6$ dyne/cm^2 [128]. They also indicate, in a summary of previous studies, that the value of E of the brachial artery was higher in males than in females, and that higher pulse pressure present in diabetic subjects also tended to increase the value of E [129]. Overall, we can consider values of the Young's modulus varying from

approximately 0.1 - 8 $\times 10^6$ dyne/cm^2.

To obtain a range of possible damping modulus values, Babbs cites the results of several studies likewise mentioned in Nichols *et al*'s book. Arterial viscosity is dependent on vibration frequency, so the value of D is approximated by arterial wall response to frequencies of 60 Hz, assuming these are the representative frequencies of KS. Babbs identifies a range for D from $\sim$ 286 dyne-s/cm^2 to 845 dyne-s/cm^2. However, we have previously identified in chapter 2 that some KS may have central frequencies higher than 100 Hz, therefore the range for D may be expanded. Following Babbs approach, and using the results in Lawton's publication [130], the damping modulus at 100 Hz may be as low as 170 dyne-s/cm^2, for an $E = 1.4 \times 10^6$ dyne/cm^2.

Values for the neutral pressure radius found by Babbs are mostly within the range of 0.15 to 0.2 cm. Tomiyama *et al* found upper-arm brachial artery diameters of 3.93 ± 0.49 mm [131], Arnold *et al* report brachial diameters of 4.53 ± 0.09 mm [132], Maruhashi *et al* diameters in the range of $2.39 - 6.62$ mm [133], and van der Heijden-Spek *et al* reported brachial artery diameters in men of 4.52 ± 0.48 mm and in women of 3.68 ± 0.48 mm [134]. These reported diameters suggest that brachial artery radius may be within the range of $0.12 - 0.33$ cm.

Babbs considered for his simulations an arterial wall thickness of 0.03 cm, and a neutral radius of 0.2 cm, which results in a ratio $h/r_o = 0.15$. Nichols *et al* indicate that this ratio for an artery under physiologic pressure is in the range $0.06 - 0.16$ [128], and in some research mentioned in their book, this ratio was higher in females than in males. Pedley reports in his book that this ratio is roughly the same for every large artery, and ranges between $0.12 - 0.16$ [135]. Considering the limits for the neutral radius, working limits for arterial wall thickness could be within $\sim 0.07 - 0.53$ mm, although its actual value would be dependent on that of the neutral radius to maintain the ratio h/r_o within appropriate values.

The parameter in the hard spring approximation, γ, is not usually mentioned in the literature, since most experiments measure arterial mechanics under normal pressure conditions where elasticity is assumed linear. The exact relation to the other arterial parameters has also not been established to give an idea of the expected values. However, based on the rest of the constant values, it was determined that the order of magnitude of this constant has to be approximately $> 10^7$ for it to have any real effect in the arterial wall's elastic properties. The larger magnitude of this constant is in agreement with common fits to data done with

polynomial functions; the greater the order of the polynomial, the greater the value of the constants associated to the higher order terms.

Tissue properties vary depending on the individual. Between the brachial artery and the outer layer of skin one may find veins, nerves, muscle, fat and skin. Each of these tissues has its own density, and the thickness of some of these will vary between individuals. For this reason, and to minimize computational time, the density and thickness variables were lumped into a single parameter. Density of the aforementioned tissues is approximately 1 g/cm^3, and the artery is believed to be located around 50% of the arm's radius, so these values can be used in the initial guess vector.

Regression of Synthetic Data

Given the complexity of the data and the number of parameters in the model, preliminary tests were performed on a series of synthetic data generated with equation 5.12, similar to what was done with synthetic oscillometric data in chapter 4. In this case, these tests served a couple of purposes: first, to verify if the equation converges successfully for different combinations of parameters, and second, to verify if the inverse solution to the problem is unique and, if not, how much error will there be in the estimate.

Synthetic sound data were created using equation 5.12. The same transmural pressure was used in all cases: an arterial pressure waveform, P_a, was generated for a BP or 120/80 mmHg and an oscillation frequency of 1 Hz, equivalent to 60 bmp. Cuff pressure, P_c, was modelled as a linear function with a maximum pressure of 140 mmHg and a deflation rate of 3 mmHg/s. The total duration was of 30 seconds and two sampling rates were tested: 1 and 10 kSps. Different combinations of the constants in equation 5.12 were used, starting with those used by Babbs in his publication, and each constant was kept within the limits discussed above.

To obtain velocity and position of the arterial wall, equation 5.12 was integrated with the use of a 4^{th} order Runge-Kutta (RK4) method. Initial tests showed that the sampling rate of 1 kSps was not as effective in obtaining a satisfactory result of the integration as the rate of 10 kSps. The use of the smaller sampling rate made the integration more sensitive to changes in the constants and to the time-step used in the RK4 method. This made it difficult to obtain velocity vectors that resembled measured KS. The higher sampling rate, on the other hand, was less sensitive to the different combinations of constants and integration was

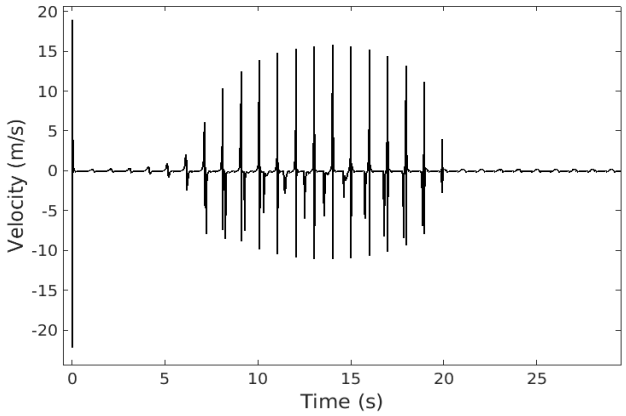

FIGURE 5.4: Synthetic velocity.

successful on most of the attempts. It was later found that this was related to the time-step, since ideally it had to be of the same order as the inverse of the sampling rate, and the smaller sampling rate resulted in a larger time-step. Given that the RK4 method is sensitive to the time-step used, the smaller it is, the more accurate the integration. For this reason, it was decided that synthetic data would be generated only at a sampling rate of 10 kSps, and ten sets were created for the linear spring case. For the non-linear spring case the same constants were used as in the linear case, and only the parameter γ was included and varied in each set.

An example of the velocity obtained from the integration in a linear spring case is plotted in figure 5.4. This is similar to the trace reported by Babbs in his publication. To further make this trace resemble measured data a 6^{th} order Butterworth bandpass filter was applied from 50 to 400 Hz. From comparing measured data to the filtered synthetic data, it was clear that the synthetic data had to be additionally multiplied (or divided) times a constant, so its amplitude would approximate that of the measured data. This constant corresponds to the proportionality constant mentioned above related to capacitor microphones that converts m/s into V, and which will be referred to as constant G in the remainder of the chapter. The result is shown in figure 5.5. The first 0.2 s of the signal were also multiplied times zero to remove the large jump observed at the start in figure 5.4. The non-linear spring case was similar.

The first purpose of the synthetic experiments was fulfilled and the equation was verified

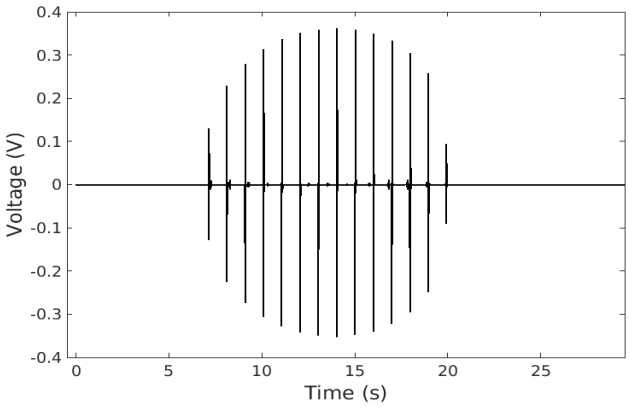

FIGURE 5.5: Synthetic sound obtained by applying a 6^{th} order Butterworth filter between 40 - 500 Hz to the velocity shown in figure 5.4.

to converge for different combinations of parameters, not just those set by Babbs. One thing that became evident while testing different combinations, however, was the fact that the method was most sensitive to the combination of the values of the ratio h/r_o and Young's modulus, E. It was observed that, usually, if the ratio and E had values on the lower end of the allowed limits at the same time, the equation would likely not converge. In the non-linear spring approach, the inclusion of the parameter γ was not found to significantly affect the results, and the only limitation observed was the same one just discussed for the linear case.

Results like the one in figure 5.5 were then used as surrogate for measured data. That is, the NLLS regression would be performed on these synthetic sounds to verify if the regression returned a unique solution composed of the predetermined constants used to generate the sounds, or if there were multiple solutions. Similar to the procedure in chapter 4, several different initial guess vectors, $\vec{\beta}_0$, were used to start the search. To effectively sample a wide range of combinations in the whole space of possible values, the vectors $\vec{\beta}_0$ were also randomly generated with the use of a Latin hypercube sample matrix.

A parameter estimate vector is obtained for each initial guess, however not all of these vectors are correct solutions of the regression. Given that the goal of the regression is to minimize the value of S, vectors of parameter estimates can be selected based on its value. Results of the regression showed that there was a significant separation between values of S: some cases had values > 1, sometimes of orders of magnitude up to 10^4, and other cases were

significantly < 1, of orders of magnitude 10^{-6} and below for the linear case, and 10^{-4} and lower for the non-linear case. Parameter estimate vectors associated to these values of $S << 1$ were plotted on top of the solution to verify if the fit was correct. Visual inspection confirmed these combinations of parameters faithfully reproduce the original synthetic sounds. The second objective of this experiment is partly confirmed, that is, that the solution is not unique. We can, therefore, expect to encounter a similar situation once the regression is applied to the experimentally measured data.

How can we, thus, select the correct answer in the experimental data from all the resulting vectors? While we may not be able to have complete certainty that one or another is the right answer, we can still determine how much error is in the approximation by looking at the distribution of the results obtained with the synthetic case. For example, the histograms in figure 5.6, obtained from estimates of one of the synthetic sets produced with the linear spring approach, show that most of the estimates tend to group around a certain value. The mean of the values, marked by the red vertical line, is close to the original value of the parameter used to produce the synthetic sounds, marked by the purple vertical line, and in some sets they overlap (where only the red line is visible). In six out of the ten sets the original parameter values were within three standard deviations, marked by the yellow vertical lines, of the mean of the estimates, for all seven values shown in the histogram.

It may also be difficult to appreciate at a first glance, but the estimates of Young's modulus E and the ratio h/r_o differ from the correct values in the 6^{th} and 8^{th} decimal figure, respectively. This is only an indication of the algorithm being unable to produce the exact value; we can assume these estimates were correct for both parameters. The estimates of the ratio h/r_o were calculated after the regression, from the individual pair of estimates for h and r_o.

The remaining four cases were similar to what is shown in figure 5.7. In these cases, the mean of most of the parameter estimates was close to the real value, except for those of the neutral radius r_o and the wall thickness h, which are outside the three SD distance. It is interesting to see, however, that the estimate of the ratio h/r_o is correct. This indicates that it is perhaps the value h/r_o and not the individual parameters what is important for the model to converge, or at least that the value of one of the parameters is compensated by the value of the other.

Overall, the information in figures 5.6 and 5.7 indicates that in the experimental data,

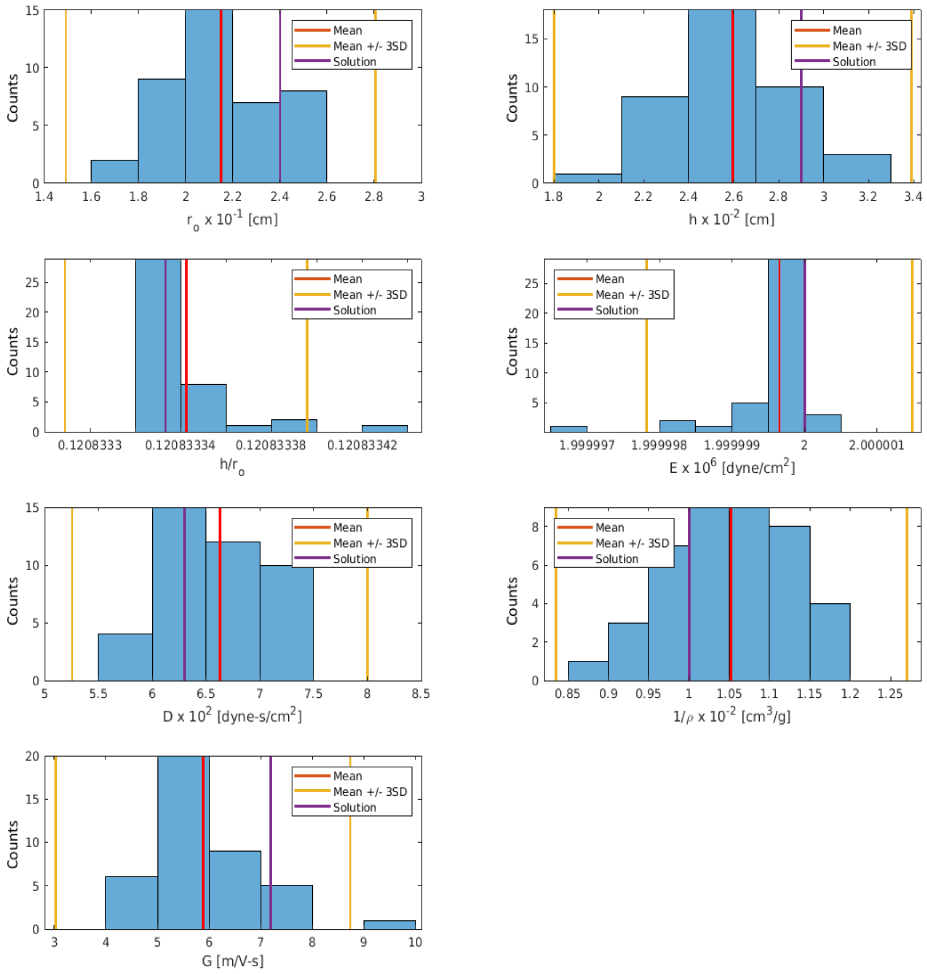

FIGURE 5.6: Distribution of the parameter estimates obtained from the regression of a synthetic data set in the linear spring approach (blue bars). The red vertical lines mark the mean of the estimates. The yellow vertical lines mark a separation of ±3 SD from the mean. The purple line marks the original value of the parameter used to generate the synthetic case. True parameter values are within the ±3 SD range.

when using the linear spring approach, the correct value of each parameter will most likely be within three SD of the mean of the estimates. The only exception is for parameters r_o and h when analyzed individually; their ratio h/r_o is the value with a higher probability of being correctly estimated.

In the case of the non-linear spring approach the error in the estimates decreases. This can be observed in figures 5.8 and 5.9, which have the same original values of the parameters as the results shown in figure 5.6 and 5.7, respectively. Using the non-linear spring approach all the means of the parameter estimates are within two SD of the correct solution. The ratio h/r_o and Young's modulus E are also correctly estimated, just as in the linear spring case. This result was observed in all ten sets of synthetic data. It is likely, thus, that by using the non-linear approach, we could expect to find the correct value of each parameter in the experimental data within two SD of the mean of the estimates.

As a final observation, table 5.1 gives a comparison of the mean $\pm$ SD of the values of the function S for each set of synthetic data and for each case of linear and non-linear springs. The non-linear approach gives larger values of S in comparison with the linear approach, yet their overall values are significantly small, so this difference is not necessarily indicative of a less effective regression in the former approach. The higher value in the function S for the non-linear approach should have been expected given that there is an additional parameter to estimate and that the equation is less stable given the non-linearity.

With these results we have established the second part of the second objective set for these synthetic cases. From what is observed in the distributions discussed above, we can now have an idea of how to filter the estimates in the experimental data in order to have higher confidence in the results obtained. Naturally, experimental results will have a higher error in all estimates, but this experiment with synthetic data serves as a guide for those cases.

As a final observation, it is interesting to comment that there was another test performed on synthetic data where one of the parameters was expressed in a different way. The ratio h/r_o can be identified to be a common factor in several of the terms in equation 5.12, and values of this ratio are more commonly measured than wall thickness by itself. For this reason, in this separate test the ratio was included as a parameter instead of the wall thickness h. The result was the inability of obtaining successful regressions in all but one of the synthetic sets, and a similar failure when it was tried in one experimental measurement. The only

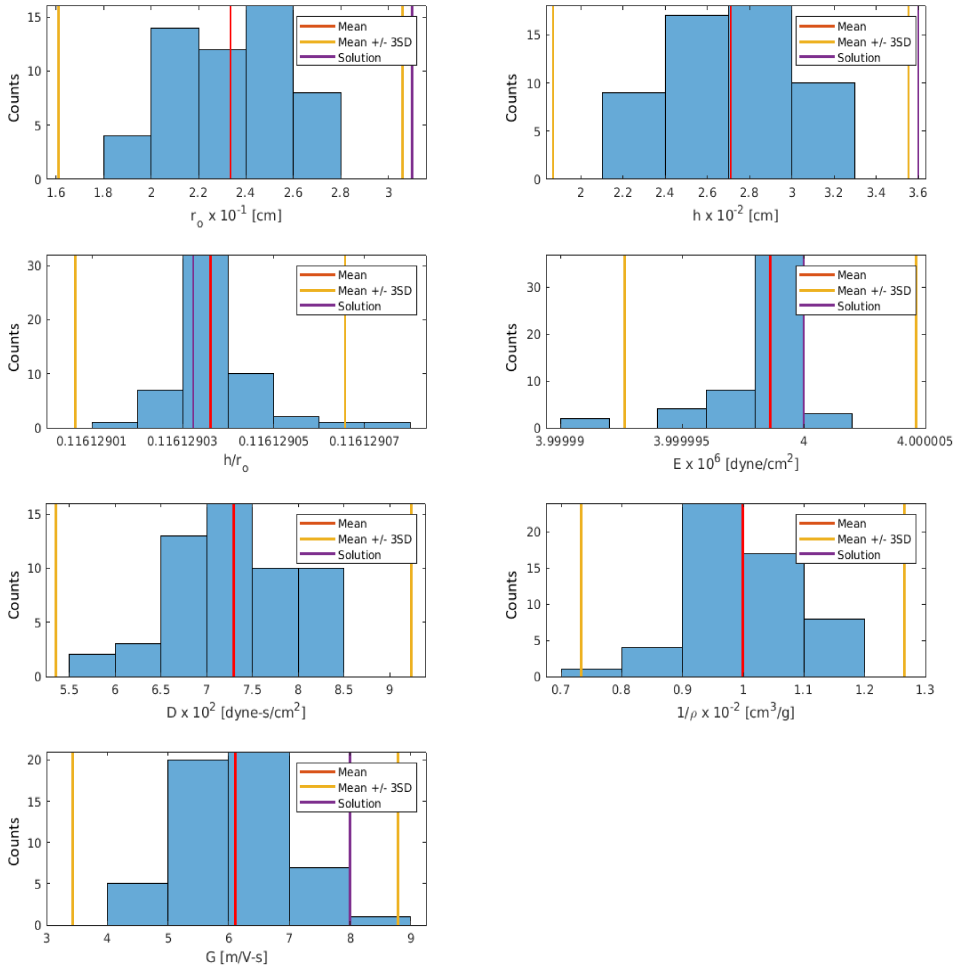

FIGURE 5.7: Distribution of the parameter estimates obtained from the regression of a synthetic data set in the linear spring approach (blue bars). The red vertical lines mark the mean of the estimates. The yellow vertical lines mark a separation of ±3 SD from the mean. The purple line marks the original value of the parameter used to generate the synthetic case. True parameter values of r_o and h are outside the ±3 SD range.

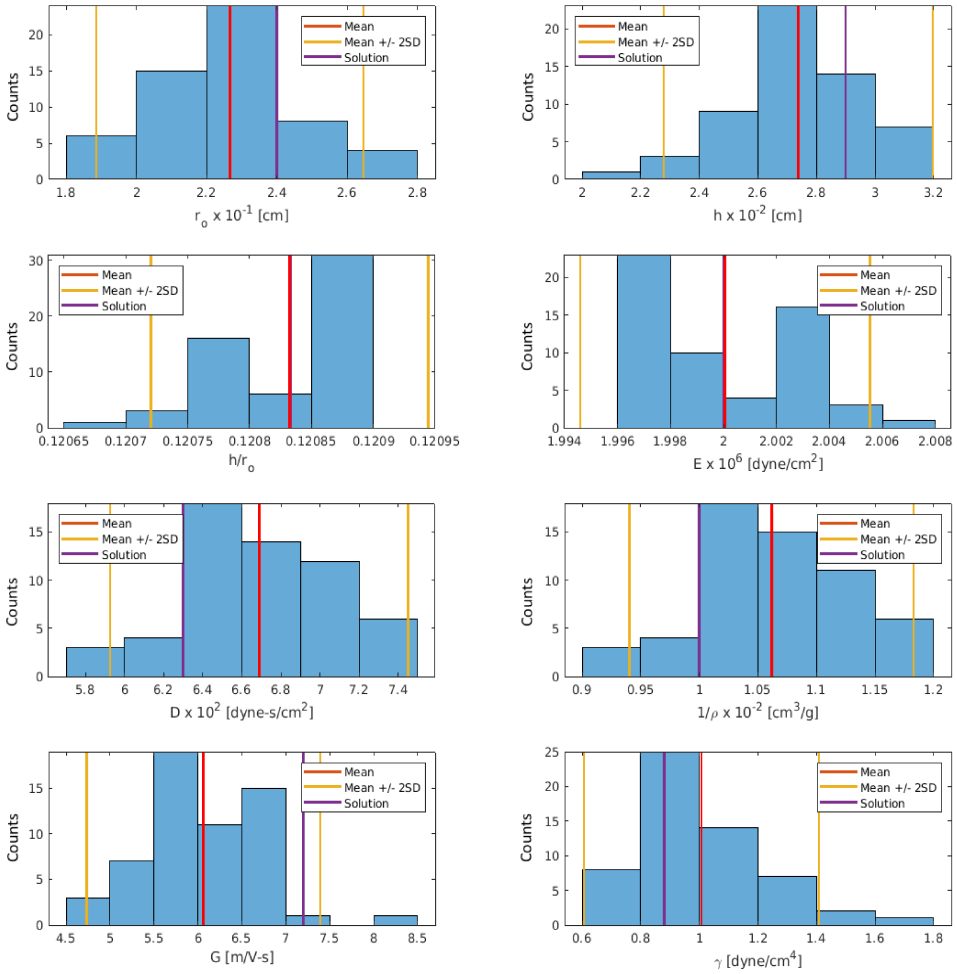

FIGURE 5.8: Distribution of the parameter estimates obtained from the regression of the synthetic data set in 5.6 in the non-linear spring approach (blue bars). The red vertical lines mark the mean of the estimates. The yellow vertical lines mark a separation of ±2 SD from the mean. The purple line marks the original value of the parameter used to generate the synthetic case. True parameter values are within the ±2 SD range.

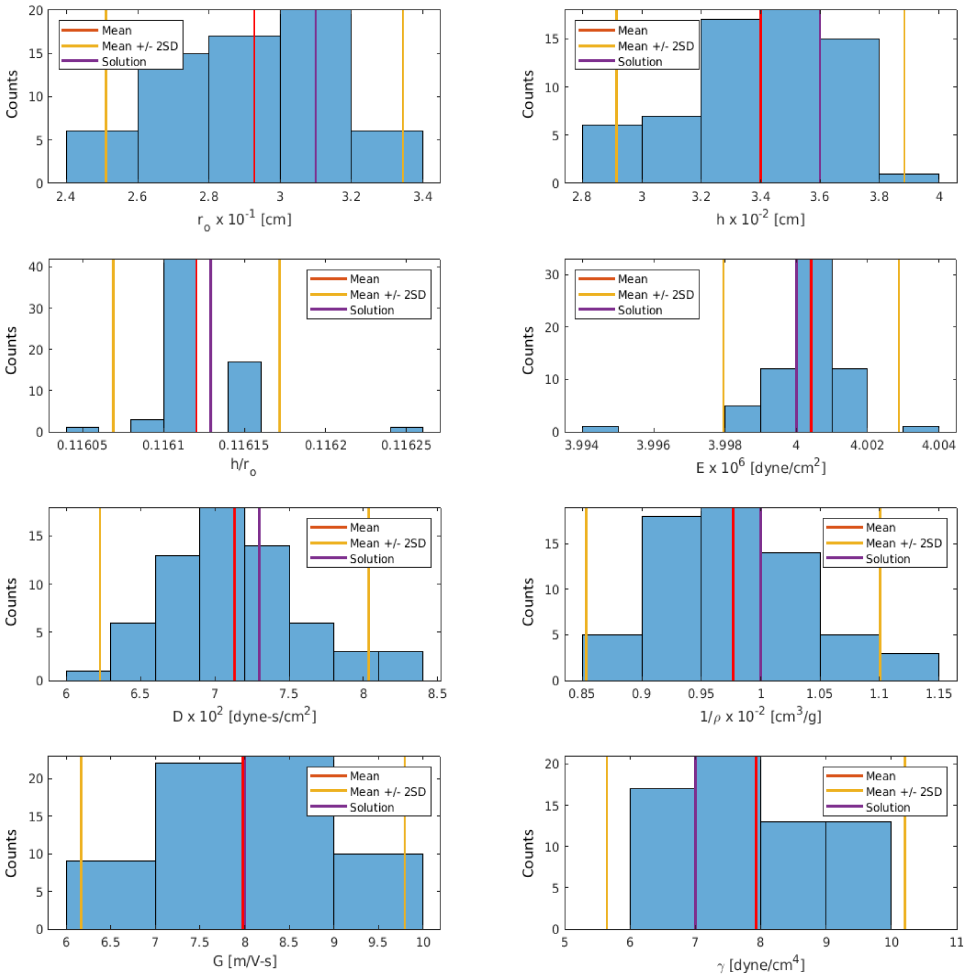

FIGURE 5.9: Distribution of the parameter estimates obtained from the regression of the synthetic data set in 5.7 in the non-linear spring approach (blue bars). The red vertical lines mark the mean of the estimates. The yellow vertical lines mark a separation of ±2 SD from the mean. The purple line marks the original value of the parameter used to generate the synthetic case. True parameter values are within the ±2 SD range (unlike the linear case).

TABLE 5.1: Mean ± SD of the value of the function S for each set, divided by linear and non-linear spring approach. Function S is in units of V^2.

Set #	Linear	Non-Linear
1	$0.88 \pm 2.10 \times 10^{-12}$	$0.72 \pm 1.36 \times 10^{-9}$
2	$5.25 \pm 8.07 \times 10^{-6}$	$2.22 \pm 2.19 \times 10^{-8}$
3	$0.41 \pm 1.29 \times 10^{-10}$	$2.32 \pm 1.73 \times 10^{-4}$
4	$0.64 \pm 1.44 \times 10^{-11}$	$0.81 \pm 2.28 \times 10^{-5}$
5	$0.27 \pm 2.15 \times 10^{-9}$	$1.63 \pm 2.38 \times 10^{-6}$
6	$2.41 \pm 5.39 \times 10^{-12}$	$1.12 \pm 1.49 \times 10^{-4}$
7	$4.57 \pm 9.94 \times 10^{-11}$	$0.72 \pm 1.35 \times 10^{-4}$
8	$0.39 \pm 1.14 \times 10^{-11}$	$8.70 \pm 8.19 \times 10^{-5}$
9	$0.52 \pm 1.54 \times 10^{-11}$	$0.54 \pm 1.04 \times 10^{-4}$
10	$0.17 \pm 1.01 \times 10^{-12}$	$3.69 \pm 5.53 \times 10^{-5}$

synthetic set that had several solutions and a small value of S was that formed with the constants used by Babbs. For the rest of the synthetic sets the estimates obtained would not reproduce the sound signal, and had large values of S, and would only succeed when the initial guess vector used was the exact solution. Any deviation, even a 1% deviation, from the original values would make the regression fail.

It is still unclear why the use of the ratio as a parameter affected the regression to this magnitude, but the author believes that these results point to the fact that equation 5.12 is most sensitive to this particular relationship. Also, the parameter r_o appears by itself in other terms in the equation, and locking the ratio h/r_o as a single parameter imposes an extra limitation on the value of r_o. This limitation likely skews the search of parameter estimates in an incorrect direction, making the regression fail. This, however, does not explain why the regression only works for the original case in Babbs' work; perhaps he accidentally found the most ideal combination of parameters possible.

5.2.2 Data Processing

The data used in the NLLS regression discussed in this chapter is part of the same data set that was used in chapters 3 and 4. Based on the observations in the previous section, however, the analysis in this chapter was limited to the measurements collected at a sampling

rate of 10 kSps. There were a total of 25 measurements collected from 5 individuals, which consisted of simultaneous sound and pressure measurements. Systolic pressures ranged from 108.89 - 138.03 mmHg, with mean ± SD of 121.71 ± 7.05 mmHg. Diastolic pressures ranged from 57.36 - 96.16 mmHg, and mean ± SD of 72.06 ± 9.17 mmHg. Pressures were obtained with the algorithm proposed in chapter 3.

Sound data was processed in the same way as in the final section of chapter 3: the bias in the data was first removed by subtracting the mean of the signal, then bandpass filtered with a 6^{th} order Butterworth bandpass filter, with edge frequencies of 50 and 400 Hz, and had mains and carrier frequencies attenuated by 10 dB with a Chebishev Type II bandstop filter.

In general, there is a consistent amount of base noise in the signal, as well as a few spontaneous voltage peaks that correspond to noise artifact. To prevent these from confounding the fitting process, it was decided that only the sections of the signal corresponding to KS would be maintained, and the rest of the signal would be reduced to zero. This process was simplified by the automated KS detection method proposed in chapter 3. The results from that chapter were directly applied here to identify the voltage oscillations that corresponded to KS. Some KS detection results had to be manually adjusted for those measurements that had errors in their BP estimation.

From the synthetic data obtained in the previous section, it was observed that the KS oscillations generated by equation 5.12 have a short duration after the original velocity signal is band-pass filtered. In the interest of simplifying the process and improving the fit of the model to the measured data, the sections corresponding to KS were limited to a duration of 110 ms. The segments were determined by 10 ms of signal before the maximum positive amplitude, and the following 100 ms including the maximum amplitude point. A close-up of a few of these oscillations is shown in figure 5.10 where we can appreciate how the rest of the signal was reduced to zero. Data of this form will now serve as the vector y_i from equation 5.14 in the NLLS regression.

The variables involved in the transmural pressure, that is, baseline pressure and the APW, can be in part obtained from the measured oscillometric data and in part from the fit. The baseline pressure was previously obtained so it can be directly used as input to the model. The arterial pressure waveform, on the other hand, could be considered as another unknown parameter, modelled as a Fourier Series as in the previous chapter, with a new set of constants

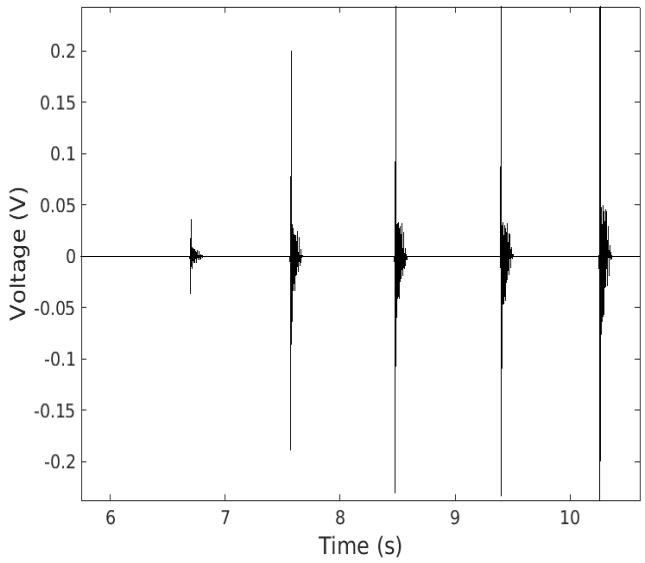

FIGURE 5.10: Sound signal with KS segments of 110 ms duration $\neq 0$.

to be determined by the fit. This, however, would hinder the performance of the regression considering that the amount of parameters would almost double.

Another thing to consider is that setting the frequency of the FS as a fixed parameter would also affect the regression. The results in chapter 4 have already demonstrated the effect that modelling the APW as a FS has on the regression of data like this, where there are minor period or frequency variations between individual oscillations. Given that the pressure oscillations of the APW are directly responsible for the production of KS, then we can safely assume that the frequency of the KS is directly related to the frequency of the APW. Fixing the frequency of the APW by modelling it as a FS would therefore require a fixed frequency of the KS, which is not observed in the measured data.

A proposed solution to this frequency issue is to use the OMW as a surrogate for P_a. Based on the discussion on chapter 4 it is evident that the OMW follows the frequency of the APW and, even though arterial and cuff compliances modify the amplitude of the pulses, it is expected that these changes will not significantly affect the regression. This decision to use the OMW also provides the advantage of avoiding an increase in the amount of parameters in the regression, so as to avoid an increase in computation time.

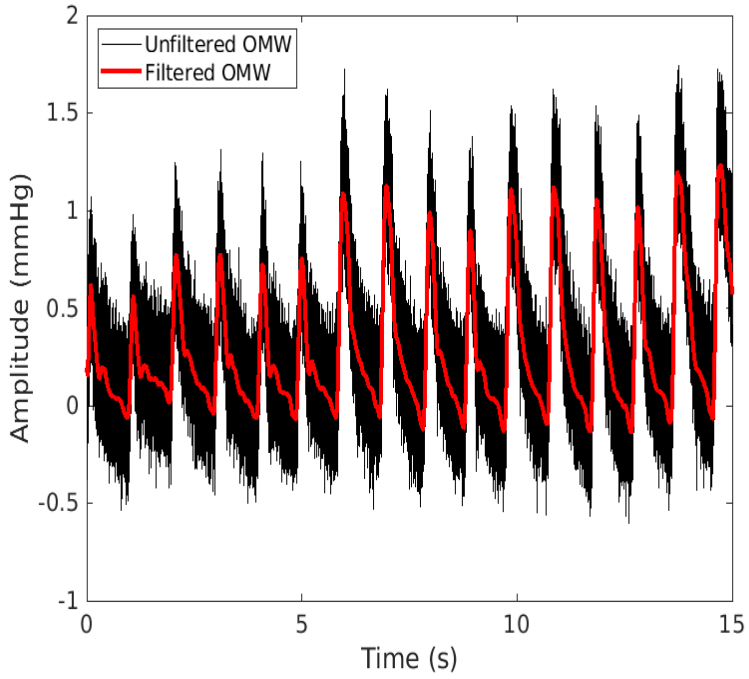

FIGURE 5.11: Unfiltered OMW (black) and filtered OMW (red) obtained from a low-pass filter attenuating frequencies above 10 Hz.

The OMW was obtained in the same way as described in chapter 4, from subtraction of the baseline pressure, and in order to use it as input to the present model, it was first filtered to remove as much of the noise in the signal as possible. A low-pass filter with upper frequency limit at 10 Hz and 60 dB attenuation for frequencies above 15 Hz was implemented in a zero-phase digital filtering process. This type of filtering process specifically preserves the phase of the unfiltered data. The result of applying this filter is shown in figure 5.11, where the filtered OMW (red) is superimposed on the unfiltered OMW (black) to demonstrate the magnitude of noise removal and the preservation of the phase.

Afterwards, the filtered OMW is normalized so that all the pulses have an amplitude of 1, which was done by first subtracting the lower envelope from the signal, and then dividing each point by the upper envelope. This process is exemplified in figure 5.12. The APW can be obtained by multiplying the normalized OMW times the pulse pressure and by adding the DBP. However, instead of fixing these values in the data they were set as the last pair

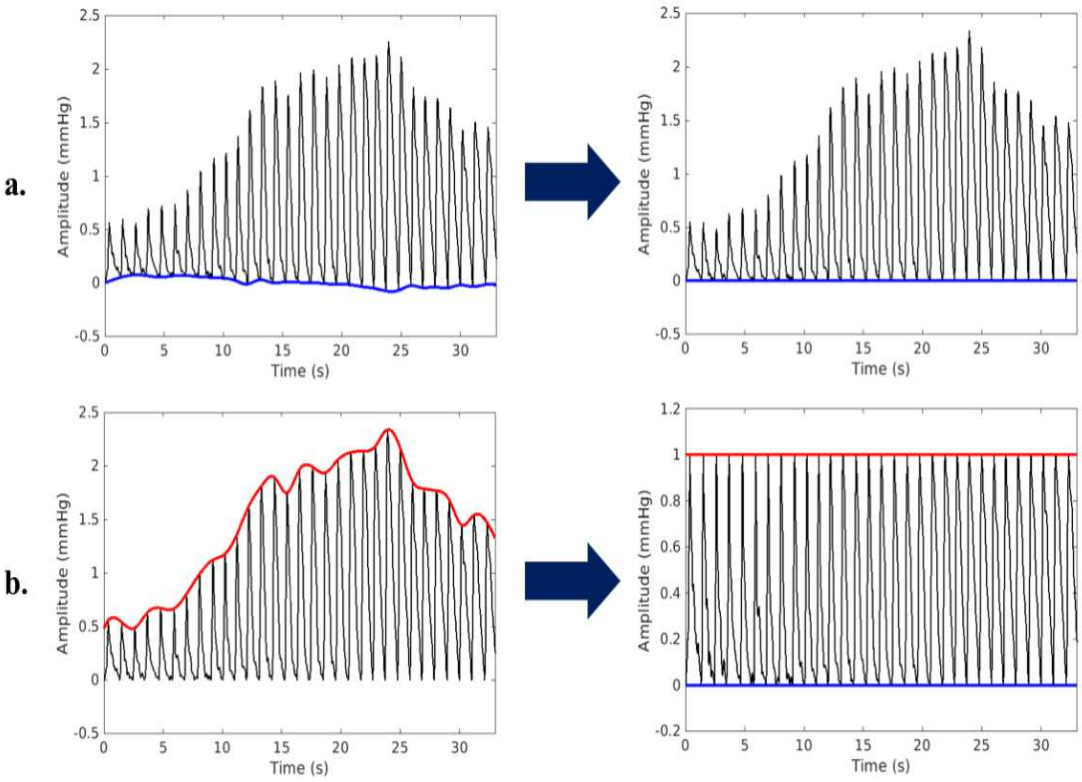

FIGURE 5.12: a.Subtraction of the lower envelope of the OMW. b.Normalization of the OMW by division of each point by the corresponding point in the upper envelope.

of parameters to be determined by the fit. By doing so, the regression will also provide estimates of BP, which will be helpful in choosing correct solutions and in determining the accuracy of the fit.

Just as in the synthetic data, both cases of linear and non-linear spring were tested by removing or including the term containing the constant γ in the equation, respectively. The algorithm developed for the synthetic case was applied here as well, first integrating equation 5.12 with an RK4 numerical integration method, then applying the 6^{th} order Butterworth bandpass filter, and finally reducing to zero the sections of the vector that do not correspond to KS. The matrix of initial guess vectors was also generated with the use of a LHSM and 300 combinations were sampled. The NLLS regression was solved in Matlab using the function "*lsqcurvefit*".

The limits for the possible values described in previous sections were extended in the experimental data in both directions, allowing the regression to sample lower and higher values than expected. This was done considering that the data where these limits were determined from were measured under far different conditions than those in this experiment. Also, no constraints were set on the relationship between the values of r_o and h, given the observations in the previous section of the sensitivity of the regression to their ratio.

5.2.3 Results

Of the 25 sets of measured data, two were excluded from analysis because the OMW could not be satisfactorily converted to APW. A few different tests were performed initially to determine the best way to construct the initial guess vectors and the method that would be followed to establish an automated selection of correct results. The parameter vector, $\vec{\beta}$, was composed of the constants found in equation 5.12 and of the BP variables PP and DBP, which as mentioned above, are respectively multiplied and added to the normalized OMW to give it proper APW values. Of these parameters, the former were always randomly generated with the LHSM. The remaining two, PP and DBP, were fixed to the measured values in one case and to the population mean in another case.

The first observation that was evident was that fixing the PP and DBP to population means resulted in larger values of S compared to the cases where these values were fixed to their corresponding measured values. The other observation, and ultimately why the approach of fixing the values to population means was discarded, was that the estimated

values of PP and DBP had a certain error with respect to the measured values, and this was reflected in the KS plotted with the corresponding parameters. The error in PP and DBP would be acceptable if the voltage spikes matched those of the measured audio, indicating only that an APW of different values could be responsible for the observed sounds. In this case, both the estimates and the modelled KS under/over estimated measured values, indicating that the model corresponds to a different value of BP.

Once it was determined that PP and DBP would be fixed to the measured values in $\vec{\beta}_0$, the regression was carried on and an initial visual inspection of the data was performed, to determine the best way to automate the selection of the correct results. This step was perhaps the most important one, given that, even though there was a resulting set of parameters for each $\vec{\beta}_0$, some would plot a solution like the one in figure 5.13. This example is clearly incorrect, even though the set of parameters estimated from the regression are within reasonable values. Once these cases were removed, it was found that the remaining cases that could potentially be correct solutions all had very similar values of S, which also, as expected, were the lowest values of S of the whole set of 300 potential solutions. This led to determine that an initial filter to automatically select correct solutions was to keep only those solutions with a value of S within $\pm$ 10% of the lowest value obtained for the corresponding measurement.

A second visual inspection of the remaining solutions had then to be performed to locate and remove cases like the one in figure 5.14. The KS plot in 5.14a could, at a glance, be a candidate for a correct solution. The plot of arterial wall position in 5.14b, on the other hand, shows that there is a jump on the position at the start of the measurement and afterwards the oscillations never return near zero. This is unexpected behaviour, particularly at high cuff pressures as observed in this example, considering that at this point in the measurement the arterial wall should completely collapse. Removal of these types of results had to be done manually, as there was no relevant feature of the parameter set that could be identified for selection. It is possible that an algorithm that recognizes this error in wall position could be written, but that was beyond the author's abilities at the time.

Only the solutions with BP estimates within $\pm$1 mmHg of the measured BP were selected for analysis. This step could have been performed for the case where the initial guess for PP and DBP was not the measured value, but in the end it was decided this would not be the case for two reasons: the first is that setting the initial guesses near the solution was more likely to produce a solution that passed the filters described above, therefore producing a

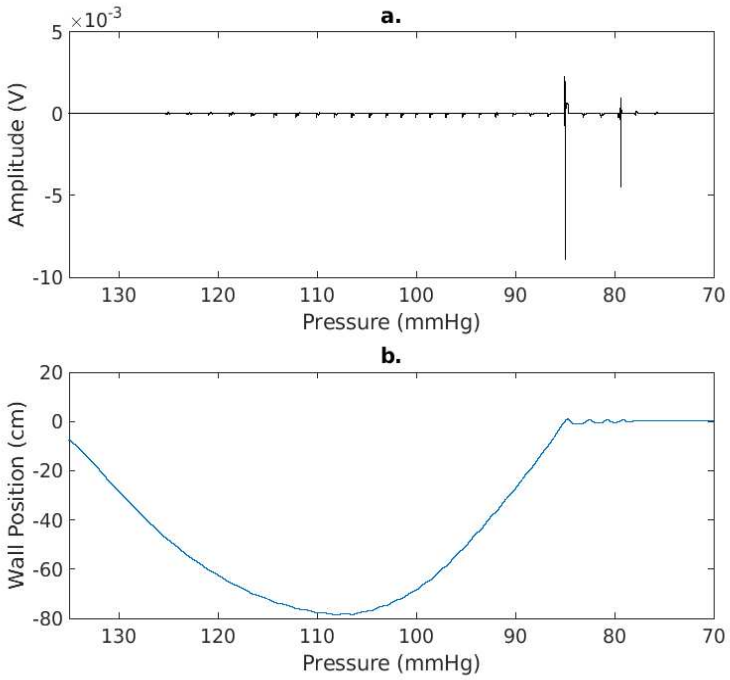

FIGURE 5.13: Incorrect solution to the NLLS regression. a. Plot of the audio vector generated with the estimated parameters. b. Plot of the arterial wall position generated with the estimated parameters.

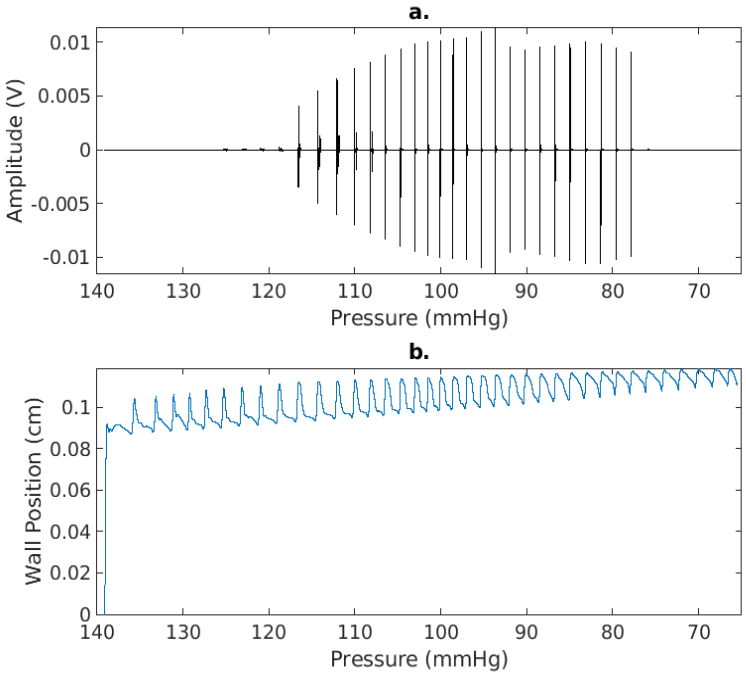

FIGURE 5.14: Incorrect solution to the NLLS regression. a. Plot of the audio vector generated with the estimated parameters. b. Plot of the arterial wall position generated with the estimated parameters.

larger quantity of solutions for a better statistic analysis. The second reason is that in order to obtain a successful NLLS regression, as mentioned before, the initial guess should ideally be near the correct value of the parameter. Given that we have little to no knowledge of the rest of the parameters related to the H.O. equation, it was in the best interest of the analysis that the regression was set up in a way that made it more effective from the start.

Finally, from the remaining set of solutions, only those with values $0.01 < h/r_o < 0.2$ were kept for analysis. These limits are beyond those stated above, but it was decided that, given that there exists the possibility of having some error in the measurement from different experimental conditions, it was better to allow for minor differences in this value. In all cases, except for one, there were sufficient solutions remaining to calculate the mean and SD of the estimates.

One example of the sound and position vectors obtained for one of the subjects in the linear spring approach is shown in figure 5.15. Figure 5.15a is the measured sound data and figure 5.15b the simulated sound data obtained from using one of the vectors of parameter estimates. Figure 5.15c corresponds to the simulated position of the arterial wall. In all three figures BP is marked by the vertical dashed lines: in figure 5.15a the lines represent BP measured with auscultation, 116.58/57.64 mmHg, and in figures 5.15b and 5.15c the lines represent the estimated BP, 116.89/57.94 mmHg. In figure 5.15c the horizontal line represents the estimated value of the zero pressure radius, $r_o = 0.19$ cm.

Figure 5.16 shows the same results as in figure 5.15, for the same measurement, but with the model assuming a non-linear elastic artery wall. The BP marked in figure 5.16b and c is 116.53/57.99 mmHg and the zero pressure radius marked in figure 5.16 is now 0.21 cm.

In both results shown in figures 5.15 and 5.16 a small beat can be observed at SBP, and at DBP sounds cease completely. These points coincide with the first transition of the arterial wall position past the buckling point, or neutral radius, and the first oscillation where the artery wall no longer crosses this point.

Histograms of the parameter estimate distribution for a different measurement are shown in figure 5.17 and 5.18 for the linear spring approach and the non-linear spring approach, respectively. The red vertical line in both cases indicates the mean of the estimates. In the case of figure 5.17 the black lines mark three SD since, as a reminder, in the results obtained from the synthetic data in the linear spring case it was proved that the correct estimate is most likely to be within these values. Likewise, in figure 5.18 the black vertical lines indicate

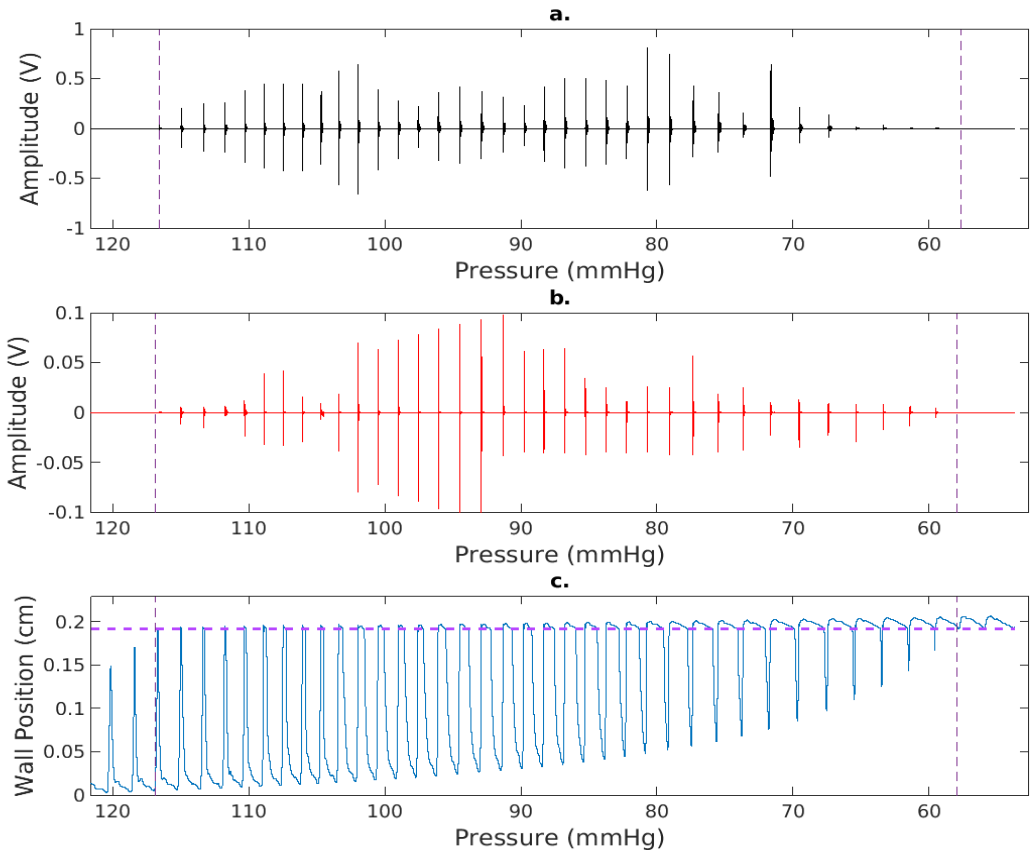

FIGURE 5.15: a.Measured auscultation data with vertical lines marking BP = 116.58/57.64 mmHg. b.Simulated sound obtained from the fit results, assuming a linear elastic artery wall, and vertical lines marking BP = 116.89/57.94 mmHg. c.Simulated wall position obtained from the fit results, vertical lines mark BP = 116.89/57.94 mmHg, and horizontal dashed line a zero pressure radius $r_o = 0.19$ cm.

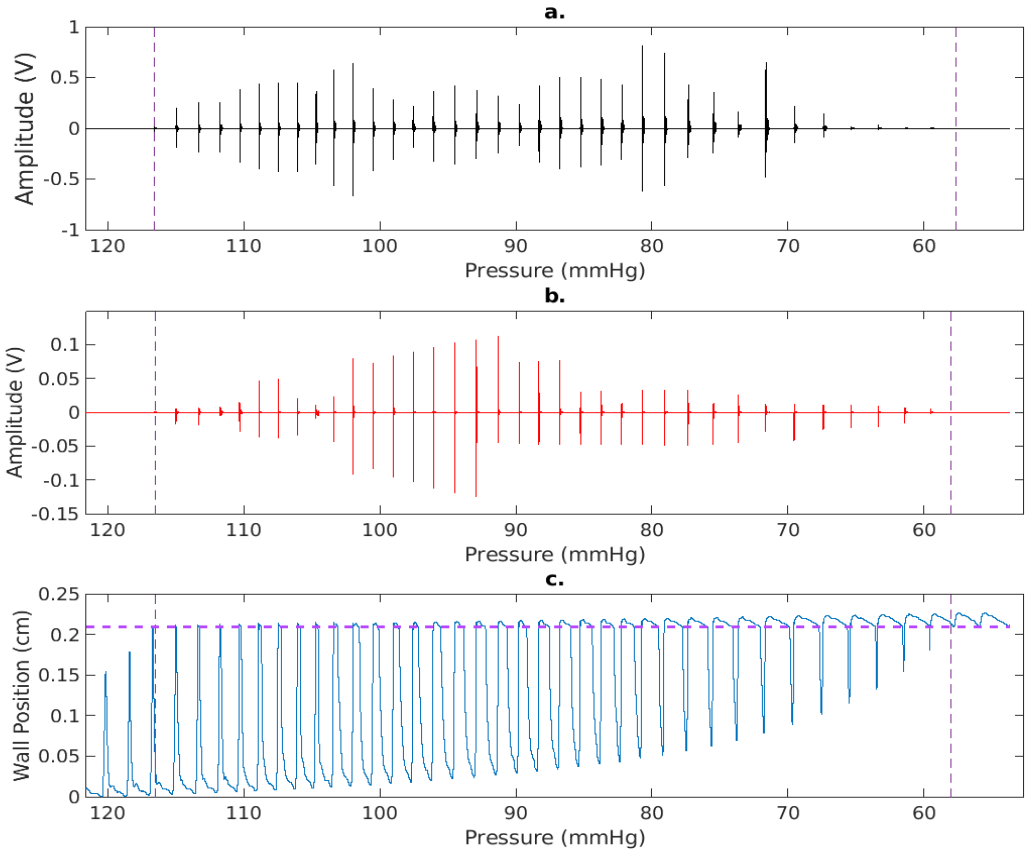

FIGURE 5.16: a.Measured auscultation data with vertical lines marking BP = 116.58/57.64 mmHg (same measurement as figure 5.15). b.Simulated sound obtained from the fit results, assuming a non-linear elastic artery wall, and vertical lines marking BP = 116.53/57.99 mmHg. c.Simulated wall position obtained from the fit results, vertical lines mark BP = 116.53/57.99 mmHg, and horizontal dashed line a zero pressure radius $r_o = 0.21$ cm.

two SD since it was shown in the synthetic cases that in the non-linear spring approach the mean of the estimates was within this distance of the correct value.

It can be observed that the mean minus the determined number of SD results in negative values for a few parameters in the linear case, and for the non-linear spring constant γ in the non-linear spring case. This is not surprising, considering that there is a greater uncertainty for the parameters in the linear spring approximation. The smaller uncertainty for the non-linear spring approximation results in uncertainty limits that are mostly within measured values, indicating that it is likely that one of the obtained estimates is close to the real solution. As for those with uncertainties outside the proper limits, caution must be exercised when considering these results, and perhaps more adjustments to the model and subsequent regressions will result in better estimates.

The results are summarized in tables 5.2 and 5.3 for the parameters directly related to arterial wall properties, that is, r_o, h, their ratio h/r_o, E, D, and γ for the non-linear case in table 5.3. Figures 5.19 through 5.24 are a visual representation of this information in tables 5.2 and 5.3.

Following the reasoning applied to the histograms presented previously, the values are given as mean $\pm$ 3SD and mean $\pm$ 2SD, respectively, considering that table 5.2 shows the results for the linear spring case and table 5.3 those for the non-linear spring case. That is, we continue to assume that, just as in the synthetic data, the correct values in these regressions on experimental data are within the corresponding number of SD.

The mean value of the function S for each case is also given in the last column of the tables. Its SD was considered irrelevant and not included, given how the results were specifically chosen based on those that had the most similar values of S. Even though the measurements are grouped by volunteer (V), the values of the function S are not the same in all their measurements since each corresponds to a completely different sound vector. The regression works differently for each so it is natural that these values are different.

Figures 5.25 through 5.29 show the comparison between the mean of the estimates obtained from the linear *vs* non-linear elastic wall.

5.2.4 Discussion

As observed in figure 5.10 the complexity of each individual KS oscillation is certainly one of the main factors that complicates the effectiveness of the regression. The model in its

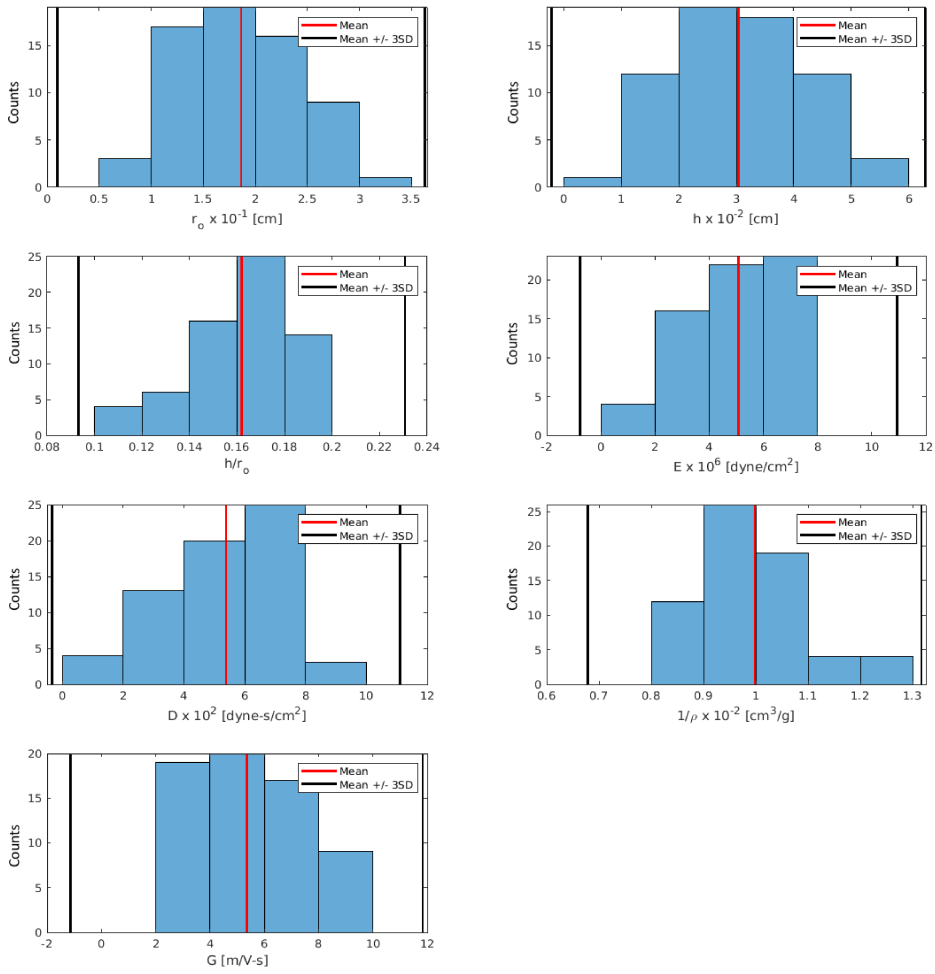

FIGURE 5.17: Distribution of the parameter estimates obtained from the regression of a measured data set in the linear spring approach (blue bars). The red vertical lines mark the mean of the estimates. The black vertical lines mark a separation of ±3 SD from the mean.

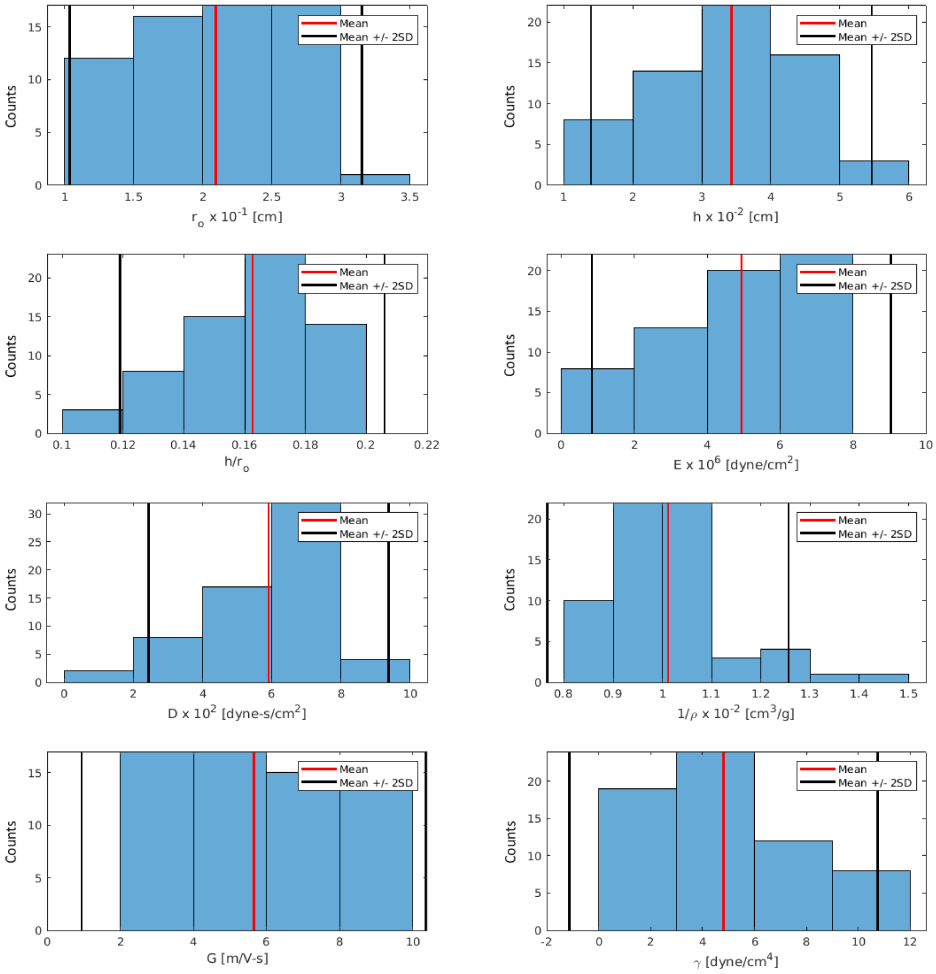

FIGURE 5.18: Distribution of the parameter estimates obtained from the regression of the measured data set in figure 5.17 in the non-linear spring approach (blue bars). The red vertical lines mark the mean of the estimates. The black vertical lines mark a separation of ± 2 SD from the mean.

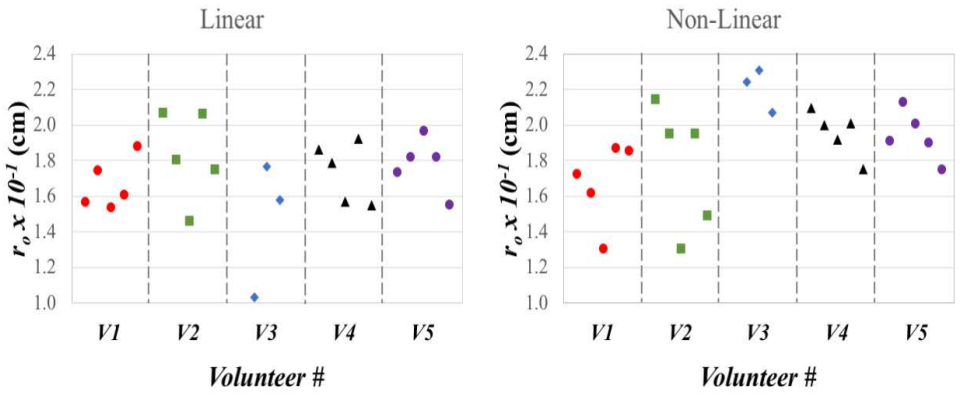

FIGURE 5.19: Mean of the estimates of the neutral radius r_o for each measurement, grouped by volunteer V where the measurement originated from.

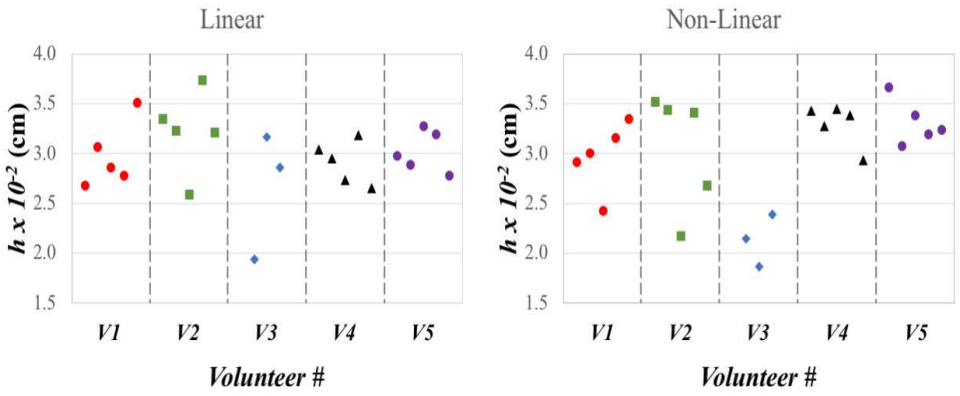

FIGURE 5.20: Mean of the estimates of wall thickness h for each measurement, grouped by volunteer V where the measurement originated from.

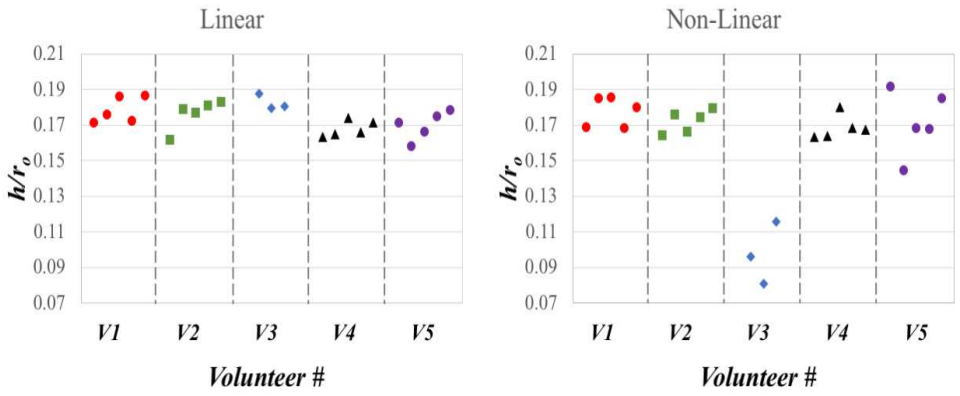

FIGURE 5.21: Mean of the estimates of the ratio h/r_o for each measurement, grouped by volunteer V where the measurement originated from.

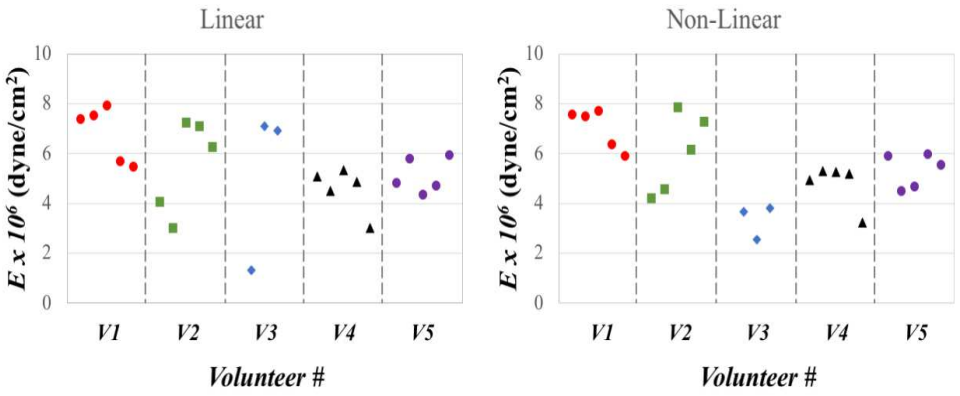

FIGURE 5.22: Mean of the estimates of Young's modulus E for each measurement, grouped by volunteer V where the measurement originated from.

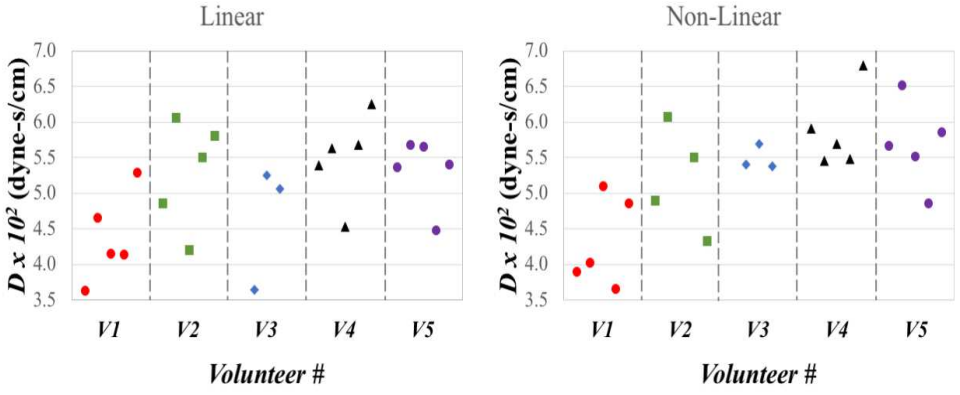

FIGURE 5.23: Mean of the estimates of the damping modulus D for each measurement, grouped by volunteer V where the measurement originated from.

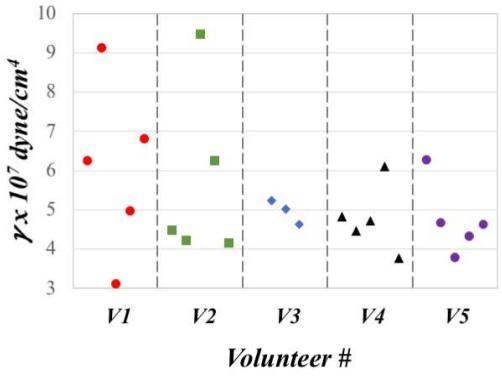

FIGURE 5.24: Mean of the estimates of the non-linear spring constant γ for each measurement, grouped by volunteer V where the measurement originated from.

TABLE 5.2: Mean ± 3SD of the estimated arterial wall parameter values for the case of a linear elastic artery wall, and mean of the function S.

V #	$r_o \times 10^{-1}$ cm	$h \times 10^{-2}$ cm	h/r_o –	$E \times 10^6$ dyne/cm^2	$D \times 10^2$ dyne-s/cm^2	S V^2
	1.55 ± 1.58	2.68 ± 2.99	0.17 ± 0.05	7.40 ± 2.60	3.63 ± 5.00	227.76
	1.75 ± 1.59	3.07 ± 2.65	0.18 ± 0.04	7.54 ± 0.84	4.65 ± 6.44	338.36
1	1.54 ± 1.97	2.86 ± 3.63	0.19 ± 0.03	7.94 ± 0.32	4.14 ± 5.59	106.99
	1.61 ± 2.06	2.77 ± 4.10	0.17 ± 0.07	5.68 ± 6.78	4.14 ± 5.06	150.25
	1.88 ± 1.45	3.51 ± 2.69	0.19 ± 0.03	5.46 ± 5.41	5.29 ± 7.22	114.43
	2.07 ± 1.73	3.35 ± 2.98	0.16 ± 0.06	4.07 ± 6.25	4.86 ± 5.15	457.32
	1.81 ± 1.37	3.23 ± 3.04	0.18 ± 0.07	3.01 ± 7.80	6.06 ± 6.39	270.19
2	1.46 ± 1.47	2.59 ± 2.58	0.18 ± 0.05	7.25 ± 2.65	4.20 ± 7.35	187.33
	2.06 ± 1.80	3.73 ± 3.19	0.18 ± 0.03	7.09 ± 3.50	5.50 ± 7.33	170.31
	1.75 ± 2.09	3.21 ± 3.95	0.18 ± 0.06	6.28 ± 5.43	5.81 ± 7.35	214.04
	1.03	1.93	0.19	1.32	3.65	93.22
3*	1.76 ± 1.74	3.17 ± 3.35	0.18 ± 0.06	7.11 ± 2.83	5.26 ± 6.62	59.08
	1.58 ± 1.18	2.86 ± 2.43	0.18 ± 0.03	6.93 ± 4.29	5.06 ± 5.06	22.74
	1.86 ± 1.76	3.04 ± 3.25	0.16 ± 0.07	5.08 ± 5.85	5.39 ± 5.72	263.66
	1.79 ± 1.52	2.95 ± 3.31	0.16 ± 0.07	4.48 ± 6.32	5.64 ± 7.04	115.64
4	1.57 ± 1.93	2.73 ± 3.81	0.17 ± 0.07	5.34 ± 4.67	4.53 ± 5.22	124.68
	1.92 ± 1.73	3.19 ± 3.24	0.16 ± 0.07	4.84 ± 5.66	5.68 ± 5.38	8.27
	1.55 ± 1.36	2.65 ± 3.18	0.17 ± 0.08	3.00 ± 6.34	6.25 ± 7.10	19.66
	1.74 ± 1.73	2.97 ± 4.00	0.17 ± 0.09	4.83 ± 5.09	5.37 ± 3.99	100.00
	1.82 ± 1.61	2.88 ± 3.03	0.16 ± 0.08	5.81 ± 6.27	5.68 ± 4.70	67.90
5	1.97 ± 1.77	3.28 ± 3.07	0.17 ± 0.06	4.34 ± 6.18	5.66 ± 4.63	51.17
	1.82 ± 1.88	3.19 ± 3.95	0.17 ± 0.08	4.71 ± 8.36	4.48 ± 6.16	105.62
	1.56 ± 1.57	2.78 ± 3.04	0.18 ± 0.04	5.96 ± 5.76	5.41 ± 6.10	38.26

*The measurement represented in the first row had a single set of parameters that complied with all the selection filters, and therefore it was not possible to calculate a SD.

TABLE 5.3: Mean ± 2SD of the estimated arterial wall parameter values for the case of a non-linear elastic artery wall, and mean of the function S.

V #	$r_o \times 10^{-1}$ cm	$h \times 10^{-2}$ cm	h/r_o –	$E \times 10^6$ dyne/cm^2	$D \times 10^2$ dyne-s/cm^2	$\gamma \times 10^7$ dyne/cm^4	S V^2
1	1.72 ± 0.97	2.91 ± 1.82	0.17 ± 0.04	7.56 ± 1.62	3.90 ± 2.49	6.25 ± 7.09	225.85
	1.62 ± 0.62	3.00 ± 1.39	0.18 ± 0.01	7.51 ± 0.94	4.03 ± 2.81	9.14 ± 2.85	329.79
	1.31 ± 0.25	2.43 ± 0.46	0.19 ± 0.01	7.71 ± 0.46	5.09 ± 5.25	3.11 ± 2.57	105.04
	1.87 ± 0.90	3.15 ± 1.85	0.17 ± 0.04	6.39 ± 3.80	3.66 ± 2.77	4.98 ± 6.43	150.83
	1.86 ± 0.99	3.35 ± 1.70	0.18 ± 0.02	5.92 ± 2.99	4.86 ± 4.33	6.81 ± 6.70	116.49
2	2.14 ± 1.02	3.52 ± 1.91	0.16 ± 0.05	4.20 ± 3.84	4.90 ± 2.87	4.47 ± 6.49	456.58
	1.95 ± 1.13	3.43 ± 2.11	0.18 ± 0.02	4.56 ± 5.65	6.08 ± 5.48	4.21 ± 7.47	270.70
	1.30 ± 1.10	2.17 ± 2.15	0.16 ± 0.03	7.88 ± 0.31	3.17 ± 1.08	9.47 ± 0.48	190.29
	1.96 ± 1.11	3.41 ± 2.07	0.17 ± 0.03	6.17 ± 3.73	5.50 ± 4.66	6.25 ± 7.55	169.33
	1.49 ± 0.61	2.68 ± 1.59	0.18 ± 0.04	7.29 ± 1.92	4.33 ± 6.97	4.16 ± 6.60	216.90
3	2.24 ± 1.04	2.14 ± 1.58	0.10 ± 0.07	3.67 ± 4.34	5.40 ± 4.07	5.24 ± 5.79	93.99
	2.31 ± 1.08	1.87 ± 1.57	0.08 ± 0.07	2.54 ± 4.06	5.69 ± 3.81	5.03 ± 5.89	57.78
	2.07 ± 1.05	2.39 ± 1.76	0.12 ± 0.07	3.82 ± 4.55	5.37 ± 3.52	4.64 ± 6.09	21.79
4	2.10 ± 1.06	3.43 ± 2.04	0.16 ± 0.04	4.94 ± 4.10	5.91 ± 3.48	4.81 ± 5.94	263.32
	2.00 ± 1.09	3.28 ± 2.34	0.16 ± 0.05	5.30 ± 4.25	5.45 ± 3.74	4.45 ± 5.79	116.18
	1.92 ± 0.91	3.45 ± 1.96	0.18 ± 0.03	5.25 ± 3.45	5.69 ± 3.41	4.72 ± 5.97	124.05
	2.01 ± 0.95	3.39 ± 1.82	0.17 ± 0.03	5.18 ± 3.16	5.47 ± 3.71	6.09 ± 6.11	8.25
	1.75 ± 0.81	2.93 ± 1.50	0.17 ± 0.03	3.22 ± 4.66	6.79 ± 4.47	3.77 ± 6.24	19.71
5	1.92 ± 1.01	3.67 ± 2.11	0.19 ± 0.03	5.89 ± 2.96	5.67 ± 4.15	6.27 ± 6.05	99.16
	2.13 ± 0.81	3.08 ± 1.59	0.14 ± 0.04	4.48 ± 3.87	6.51 ± 3.05	4.67 ± 6.47	66.55
	2.01 ± 0.98	3.39 ± 1.98	0.17 ± 0.04	4.68 ± 4.69	5.51 ± 3.95	3.78 ± 6.86	51.45
	1.90 ± 0.94	3.19 ± 1.95	0.17 ± 0.06	5.97 ± 4.06	4.86 ± 3.93	4.32 ± 7.52	104.85
	1.75 ± 1.03	3.24 ± 2.12	0.18 ± 0.03	5.54 ± 3.19	5.86 ± 4.07	4.62 ± 7.38	38.14

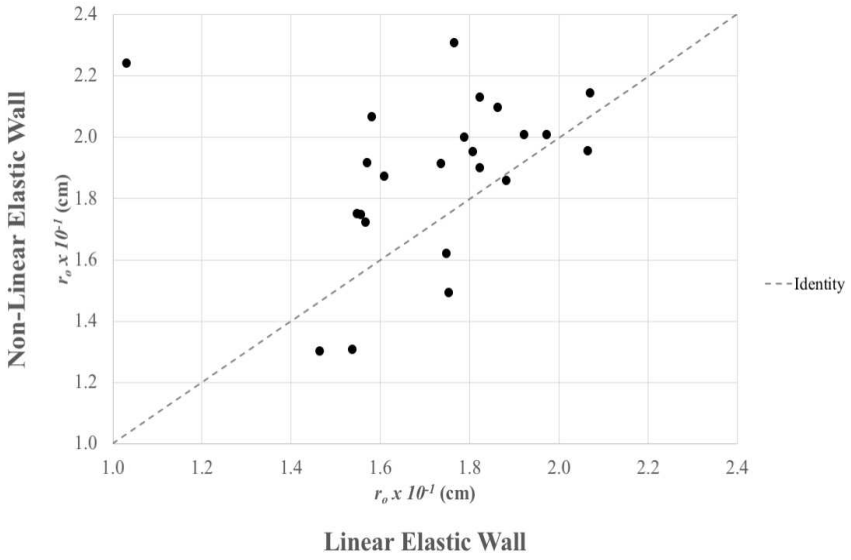

FIGURE 5.25: Comparison of the mean of the estimates of the neutral radius r_o obtained from the linear elasticity approach (abscissa) *vs* the non-linear elasticity one (ordinate).

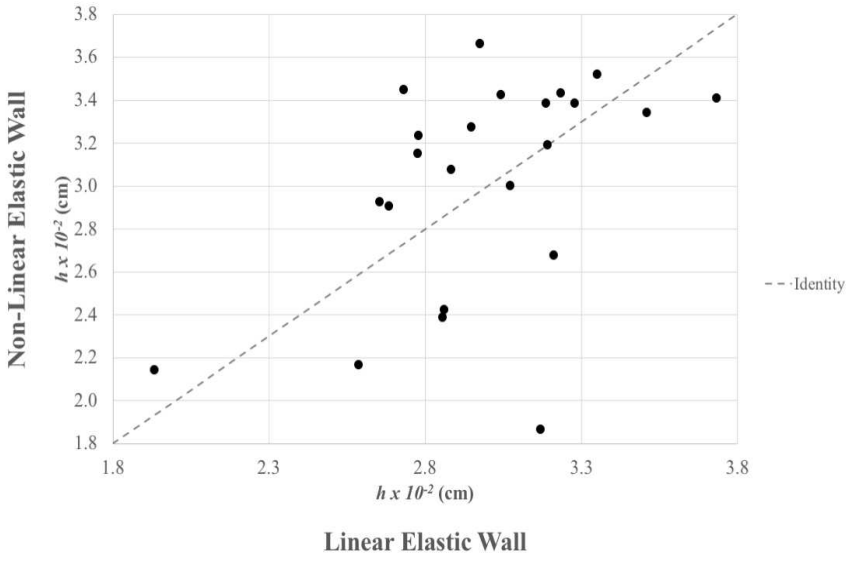

FIGURE 5.26: Comparison of the mean of the estimates of wall thickness h obtained from the linear elasticity approach (abscissa) *vs* the non-linear elasticity one (ordinate).

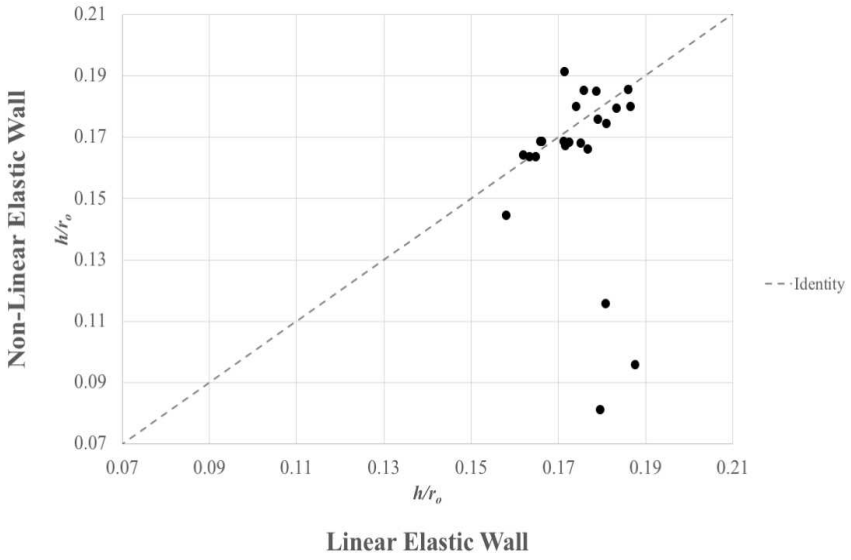

FIGURE 5.27: Comparison of the mean of the estimates of the ratio h/r_o obtained from the linear elasticity approach (abscissa) *vs* the non-linear elasticity one (ordinate).

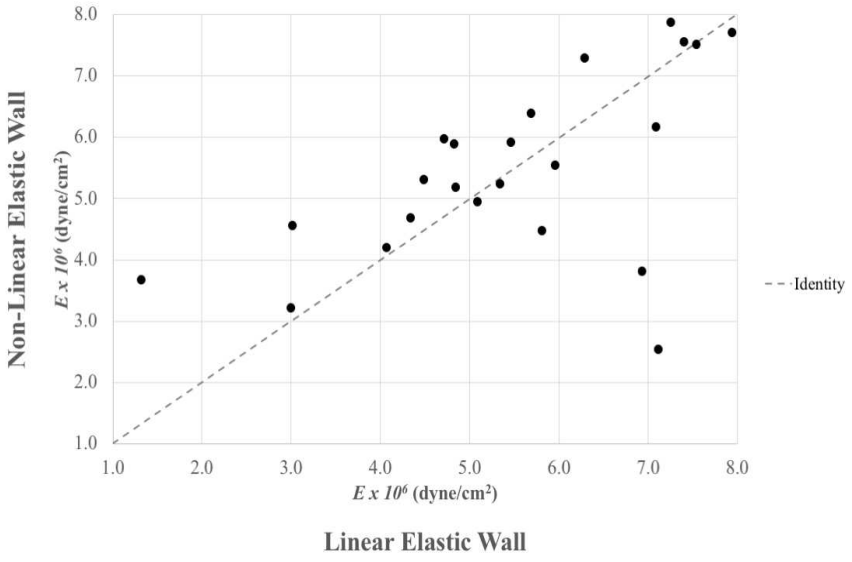

FIGURE 5.28: Comparison of the mean of the estimates of Young's modulus E obtained from the linear elasticity approach (abscissa) *vs* the non-linear elasticity one (ordinate).

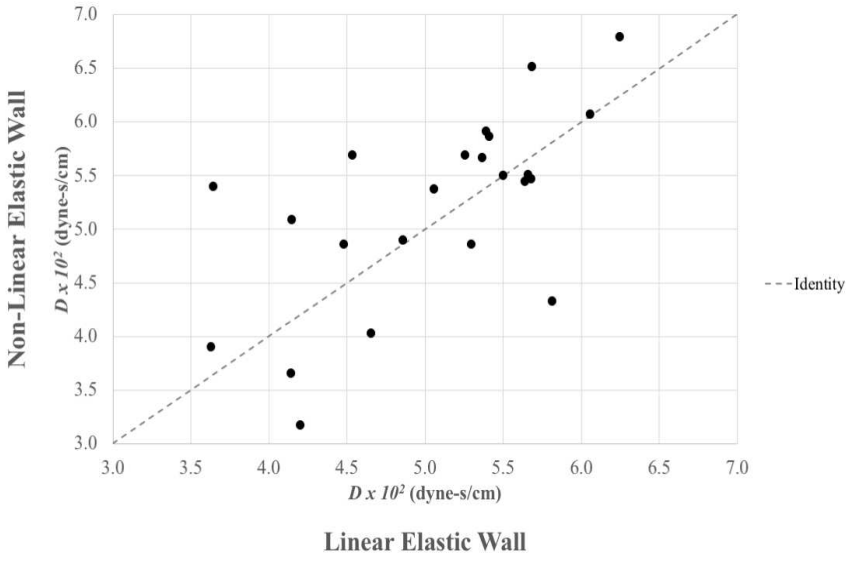

FIGURE 5.29: Comparison of the mean of the estimates of the damping modulus D obtained from the linear elasticity approach (abscissa) *vs* the non-linear elasticity one (ordinate).

present form is only able to reproduce oscillations that decay exponentially, such as would be expected of an ideal damped harmonic oscillator. The oscillations in each KS follow a far more elaborate shape. Perhaps by analyzing these oscillations individually an improvement on the model can be suggested. It is interesting, nevertheless, to observe how the sound vectors produced by the regressions, as shown in figures 5.15 and 5.16, have varying amplitude in each KS. Perhaps if this variation were periodic or followed a certain pattern in the measured data, the model would be able to adjust to this variation with more ease.

It is also interesting to confirm that, from the distributions in figures 5.17 and 5.18, the estimates of the parameters follow similar distributions to those of the synthetic data. It is also important to remind us of what the synthetic cases revealed about the accuracy of the estimates; in the linear spring approach, the true value of the parameters was determined to most likely be within ±3SD of the mean of the estimates, while in the non-linear spring approach, these limits reduced to ±2SD. These inaccuracies are reflected in these histograms and we can see how in the linear spring approach they extend to values outside of those estimated by the regression, similar to the synthetic cases. We should also remember that in the linear-spring approach, in some cases it was possible that the true value of some of the parameters was outside of these limits as well, as shown in figure 5.7 for parameters r_o and h.

In the non-linear spring approach the accuracy limits of ±2SD shown in the histograms in figure 5.18 are mostly within obtained parameter estimates. Similar to the linear case, the possibility exists that some of the parameter true values fall outside estimates and the designated accuracy limits. However, what is shown in this case may give us more confidence in the parameter estimates obtained with this approach. One must point out as well that the value of the function S was many orders of magnitude smaller in the synthetic cases than in the experimental cases. Lowering the value of this function by including corrections to the model may significantly improve the estimates and the inaccuracies in both approaches.

A detailed observation of the results shown in tables 5.2 and 5.3 or figures 5.19 through 5.24 reveals how the mean of the estimates of certain parameters tends to be around a certain value depending on the individual they were obtained from. It is interesting to see how this is mostly the case of the most sensitive parameters discussed above: the ratio h/r_o and each of the two variables separately, and Young's modulus E, and that for variable D this is more evident in the non-linear spring approach. This is a promising result in the potential use of

this technique to obtain estimates of these parameters specific to each individual.

Another particular observation from these tables is how the value of the function S is almost the same in both linear and non-linear spring approaches. This is perhaps not surprising, considering that both equations were required to reproduce the same data, and that both are capable of producing the exact same vibrations by adjusting the value of the parameters accordingly.

The comparison between the mean of the estimates for each parameter in the linear and non-linear case, as observed in figures 5.25 through 5.29 shows that similar values are obtained for the parameter estimates in both approaches, although the non-linear spring assumes slightly larger and thicker arteries.

Overall, the estimates of the parameters were within expected ranges. The values of the constants ρ and G are not shown, since they are not particularly relevant to the elastic properties of the arterial wall, but the results for these constants were similar to those of the results that are included. Unfortunately in this case the conversion factor G of the stethoscope used was not available, yet this is perhaps the easiest value to obtain and verify. In a future experiment a microphone of known characteristics can be used and the data measured in V can be converted to m/s before the regression to avoid the inclusion of additional parameters to account for conversion factors.

In a future analysis, other terms of the harmonic oscillator equation can be also be rewritten as functions of the arterial wall position, such as the damping force, which is not necessarily the same in the two regions separated by the point of buckling, as assumed here. Allowing the damping modulus to vary accordingly, for instance by separating it into two constants, one for each region like in the case of the spring constant, may certainly improve the model where the occurrence of KS is concerned. However, while discussing the possible value ranges of this parameter it was pointed out that it also depends on the vibration frequency: the damping modulus increases as the frequency decreases. This means that the description of the arterial wall's viscosity is far more complicated than what is presented here, especially considering the variation in main frequency components of the KS at each phase.

It is also important to note that we also assumed that the wall could be described by a Kelvin-Voigt element (spring and dashpot in parallel). The literature suggests that a non-degenerate model, where a Kelvin-Voigt element is connected in series with a spring, may

be better suited to describe biological tissues. This model was not applied in this case since it expresses a more complex relationship between elastic and viscous elements, and the goal was to keep the overall harmonic oscillator model simple.

Another observation is that sound segments of 110 ms were used in the present experiment, yet it was mentioned in chapter 3 that the duration of each KS varies as the measurement progresses. Both the algorithm and the model can potentially be adapted to adjust to these duration variations, although this might be a more complicated issue to address.

Finally, it was mentioned previously that estimates of BP obtained from cuff measurements are different than values measured intra-arterially. This means that, while KS estimate BP at certain locations, the underlying APW most likely has a different amplitude and DBP. In the context of this experiment this possibility was tested, but ultimately discarded for reasons described above. However, it is possible that the use of the OMW as a surrogate for APW could have affected these estimates. Another option would have been to sample a larger number of initial guess vectors so that the probability of finding correct solutions with different values of BP increased. However, given the number of results per measurement and the need to manually analyze individual cases is a formidable task, so this option is not really applicable, until a better selection algorithm is written.

5.2.5 Conclusions

We might say, thus, that the results obtained in this section show that, even though the measured signal was complex, a simple harmonic oscillator model is useful as a first approach to describe the phenomena observed in the generation of KS. It is, by no means, a fully accurate description of the origin of KS, but it certainly gives a potential relationship between the sounds and arterial wall characteristics and mechanics. Clearly the model has room for improvement, but in its present form it has the advantage of being easy to apply to a routine measurement in a non-linear regression without a large computational cost.

Similar to the case of the models in chapter 4, at this stage unfortunately we cannot conclusively validate this model, although this model is perhaps a better description of the observed phenomena than those used to describe the OMW in chapter 4. The comparison is not straightforward, considering that different values are compared in the regressions, but in the case of the model presented in this chapter the values of function S are considerably low.

At a glance, there is no significant difference in the results obtained by the two approaches compared here. Computationally speaking, the linear spring case was certainly less demanding, although the difference was not significant. The most significant contribution stemming from the non-linear spring case is the level of confidence in the results. This non-linear consideration allows the algorithm to converge more often to solutions that are closer to the true value of the parameters.

The results in this thesis also show that it is very likely that arterial wall mechanics play a bigger role in the generation of KS, and that fluid dynamics and wave transmission may have a secondary role in their origin. This on the basis that, even though their effects were neglected, the model seems to be able to replicate the observed phenomena. The initial model proposed by Babbs is therefore an excellent first approach and a great basis to further build on.

It is important to emphasize once more that the coincidence in the mean of parameter estimates per individual is a promising result. Including this method in automated auscultation would mean obtaining in a single measurement information of arterial wall mechanics that are otherwise not easily accessible. Similar to BP, a record of these parameters can be maintained over time, and variations in their values can potentially be traced to an alteration of the arterial wall and to cardiovascular health. A follow-up experiment would involve obtaining measurements of the same individuals over an extended period of time and comparing the obtained parameter estimates.

Finally, we can conclude that, although the objective of validating a physics-based mathematical model in this chapter was not fully accomplished, the foundations for a modified version of the model used here are set, and the results point towards a favourable result. The secondary objective of possibly obtaining information on parameters that are otherwise not easy to measure *in vivo* during a cuff measurement, nevertheless seems to have been confirmed. The accuracy of some of these estimates can still be verified by other measurement techniques, such as arterial tonometry or ultrasound, but at the moment they reflect reasonable values and seem to be subject dependent.

Next steps in this research are to improve the expression of the forces involved in the model. The damping force is the ideal candidate based on the discussion above. The next objective should be to derive an expression where the damping modulus is determined by the frequencies present in each KS. Additional terms in the elastic force could also be included,

although deriving first an expression for the associated constants in terms of arterial wall properties is highly recommended to limit the number of parameters in the regression.

Chapter 6

Conclusions

The work presented in this thesis shows an analysis on the most commonly used methods to estimate BP indirectly. The importance of this measurement was well established from the start, as well as the clinical relevance of the ±5 mmHg limit in the accuracy of the estimates. In an age where biotelemetry is available in devices as simple as a watch, and there is increased awareness of the necessity of a healthy lifestyle, technologic and scientific advances on this topic are of the utmost importance.

The findings of this work can be summarized as follows:

- The work on oscillometric measurements and the main algorithms used to estimate BP discussed in chapter 2 provided some background and insight into the many advantages and shortcomings this method has. Evidence was provided on how minor changes to the processing of the oscillometric data can lead to significant differences in BP estimates between devices, and an analysis on the different representations of one of the most important components of the method, the OMWE, led to recommendations on how the accuracy of a device operating under these principles could be improved.

  A most important result was the observation that the design that has the best accuracy for the population as a whole will not always have the best performance for a number of individuals in this population.

- Chapter 3 presents an analysis of the auscultation method for estimating BP from the perspective of psychoacoustics. This analysis of KS and the way they are perceived by human hearing in contrast to masking sounds present in the measurement has not been described previously, to the author's knowledge. The findings on the *SNR* of individual

sound segments containing KS gives additional proof of the reason why this method is particularly challenging, especially for the determination of DBP.

The culminating result in this chapter was the design of an algorithm that can automate the auscultation method based on human response to sound.

- Chapters 4 and 5 present results of a NLLS regression on measured oscillometric and auscultation data, respectively. In each chapter the derivation of a physics-based mathematical model that describes the observed phenomena is detailed, and these models are used in the regression to obtain information on parameters that are relevant to the mechanics of the brachial artery.

  – The work in chapter 4 relates to the method of oscillometry and to a simple mathematical expression of the OMW. Two different arterial compliance functions were tested in the regression, and that proposed by Drzewiecki and his colleagues was found to have more promising results. The parameters obtained in the regression described in this chapter may provide information of the artery's compliance, which is useful in estimating the degree of arterial stiffness.

  – The model described in chapter 5 attempts to give a possible explanation to the origin of KS, and is based on the work done by Charles F. Babbs. The response of the arterial wall to external forces is believed to be responsible for the origin of these sounds. The original work describes this motion as a linear harmonic oscillator, and the author's contribution to this model is to consider the wall as a non-linear spring in the region where the arterial cross-section has a circular shape. The results of the regression show that both approaches have distinct advantages, such as computation time and level of confidence in the estimates. The parameters found in this regression give information of the arterial wall's elastic properties and dimensions.

Overall it can be concluded that the objectives set for this project were fulfilled and that this work offers an important contribution to the advancement of cuff-based BP measurement methods. The study presented in chapter 2 done in collaboration with colleagues from the Department of Medicine confirms the need for extensive work on the method of oscillometry. The work presented here offers the suggestions of working with different data representations

and a combination of such to achieve better accuracy in the BP estimates. Hopefully, these suggestions, included in the author's publication as well, can be implemented to some degree or considered in the design of future automated oscillometric devices.

A most important contribution is included in the work described in chapter 3 related to the study of Korotkoff sounds under a psychoacoustical perspective. This is a novel analysis presented by the author that offers an insight into how the human observer is able to perceive and distinguish the sounds that define the BP measurement method through auscultation. More important is the resulting suggestion of an algorithm that can automate this procedure based on these findings, which is particularly relevant since it has the potential of estimating BP in the same manner as a human observer.

The results of the NLLS regressions in chapters 4 and 5 are also promising, particularly because evidence was obtained on how a simple routine cuff BP measurement can provide more information on a subject's cardiovascular health without the need of additional complicated equipment. Results in both methods also offer guidance on which models seem most effective in describing the observed phenomena, and on how these models can be improved to provide better estimates and better fits to measured data.

The work presented in this thesis also opens new possibilities of extending the research in the area. For instance, an immediate implementation on all fronts is clearly the recruitment of more volunteers and collaborators. At the moment, except for what is presented in chapter 2, most of the work in this thesis was collected and analyzed by the author alone. The study on KS perception and subsequent algorithm would greatly benefit of a collaborative effort with experts in auscultation.

The research presented in chapters 4 and 5 can likewise be benefited from a more extensive pool of volunteers and follow-ups spanning longer periods of time. The use of more sophisticated computational methods could also be another important contribution to the results presented here. One such example is the Finite Element Modelling (FEM), which is a powerful tool in computational physics. In previous research related to cardiovascular applications, and particularly to the measurement of BP, FEM has been used to analyze blood flow and pulse wave propagation in the arteries [136], to determine the effect that cuff pressure has on the upper arm [137], and to aid in the design of new devices that can measure BP noninvasively [138–140].

In the present context of verifying the physics in the cuff BP measurement methods

FEM would offer a more detailed insight into the process. A model could potentially be constructed, perhaps borrowing and combining ideas of the models and equations used in the references cited in the previous paragraph. However, modelling the complete process is challenging considering the nonlinear behaviour of the materials involved, particularly the arterial wall. One might notice in the many articles available that modelling of the arterial dynamics is limited to cases where the artery is fully open and where only minimal pressure is applied to it compared to the full range of pressures applied by a cuff. On the other hand, other literature focusing on the effect of greater cuff pressures does not deal with the arterial response to these pressures.

A great advantage of FEM is the capability of the method of building as complex or as simple models as the research requires. For example, the simulation software COMSOL (COMSOL, Inc., Burlington, MA) offers an application exercise that analyzes the response of the arterial wall to axial stretching, when the wall is modelled with two of its layers and described as an anisotropic hyperelastic material [141]. This, however, means increasing computational time and resources, and introducing a large number of equations. While possible, this would defeat the purpose of obtaining a simple model that can be potentially implemented in a small device. On the other hand, making simplifications on the model to make the process more efficient could be akin to having a resulting set of equations than can be solved by simpler numerical methods, such as what is already presented in this work.

Certainly FEM applied to the cuff methods is a most interesting problem, and one that would be highly recommended as a follow-up to the research presented here. This analysis would be directed mostly towards obtaining a more detailed description of the physics involved in cuff measurements, rather than a more immediate application to routine measurements as intended in this work. Unfortunately, since the application of this method is outside the author's current capabilities and the necessary training is not possible due to time constraints, this will remain as a recommendation for future research.

As a final conclusion, it is important to point out how the main goal of this thesis was to further our knowledge of the two BP measurement methods that serve as a foundation for cardiovascular health, and to provide tools and suggestions for the improvement of current device development. The work presented here offers a couple of distinct and promising avenues of research that can help verify the theories established over the years related to the physical processes occurring in each BP measurement method. Most importantly, this

work offers tools that can be immediately applied to current research in the form of potential improvements and a better reference for newly developed devices.

This work also offers the possibility of obtaining significant information of a subject's cardiovascular condition from a simple, routine measurement. While this information is not, at present, a tool on which physicians rely to make diagnostics and treatment decisions, the simplicity and practicality of the implementation of these algorithms allows this analysis to be performed without hindering the procedure. It is possible that in the future, with enough information to solidly implement the results of this thesis in cuff-based devices, more options will become available to improve the accuracy of the methods in benefit of healthcare.

Bibliography

[1] C. E. Bos and E. de Boer. "Masking and Discrimination". *The Journal of the Acoustical Society of America* 39 (1966), pp. 708–715.

[2] *Acoustics - Normal equal-loudness-level contours*. International Standard ISO 226:2003(E). ISO, 2003.

[3] Satoru Hayashi et al. "Numerical Simulation of Noninvasive Blood Pressure Measurement". *Journal of Biomechanical Engineering* 128 (2006), pp. 680–687.

[4] C. F. Babbs. "Oscillometric measurement of systolic and diastolic blood pressures validated in a physiologic mathematical model". *Biomedical Engineering OnLine* 11.1 (2012).

[5] Gary Drzewiecki, Rush Hood, and Howard Apple. "Theory of the Oscillometric Maximum and the Systolic and Diastolic Detection Ratios". *Annals of Biomedical Engineering* 22 (1994), pp. 88–96.

[6] Mauro Ursino and Cristina Cristalli. "A Mathematical Study of Some Biomechanical Factors Affecting the Oscillometric Blood Pressure Measurement". *IEEE Transactions on Biomedical Engineering* 43.8 (1996), pp. 761–778.

[7] Gary Drzewiecki et al. "Mechanics of the Occlusive Arm Cuff and Its Application as a Volume Sensor". *IEEE Transactions on Biomedical Engineering* 40.7 (1993), pp. 704–708.

[8] World Health Organization. *The top 10 causes of death.*
https://www.who.int/news-room/fact-sheets/detail/the-top-10-causes-of-death
Last checked: July,2021.

[9] Eleni Rapsomaniki et al. "Blood pressure and incidence of twelve cardiovascular diseases: lifetime risks, healthy life-years lost, and age-specific associations in 1.25 million people". *The Lancet* 383 (2014), pp. 1899–1911.

[10] Melanie K. Haroun et al. "Risk Factors for Chronic Kidney Disease: A Prospective Study of 23,534 Men and Women in Washington County, Maryland". *Journal of the American Society of Nephrology* 14 (2003), pp. 2934–2941.

[11] Michiaki Nagai, Satoshi Hoshide, and Kazuomi Kario. "Hypertension and Dementia". *American Journal of Hypertension* 23.2 (2010), pp. 116–124.

[12] Ernesto L. Schiffrin et al. "Hypertension and COVID-19". *American Journal of Hypertension* 33.5 (2020), pp. 373–374.

[13] Raymond Pranata et al. "Hypertension is associated with increased mortality and severity of disease in COVID-19 pneumonia: A systematic review, meta-analysis and meta-regression". *Journal of the Renin-Angiotensin-Aldosterone System* 21 (2020), pp. 1–11.

[14] Chao Gao et al. "Association of hypertension and antihypertensive treatment with COVID-19 mortality: a retrospective observational study". *European Heart Journal* 41 (2020), pp. 2058–2066.

[15] Christopher E. Clark et al. "COVID-19 and hypertension: risks and management. A scientific statement on behalf of the British and Irish Hypertension Society". *Journal of Human Hypertension* (2021).

[16] Colin G. Weaver et al. "Healthcare Costs Attributable to Hypertension Canadian Population-Based Cohort Study". *Hypertension* 66.3 (2015), pp. 502–508.

[17] Emelia J. Benjamin et al. "Heart Disease and Stroke Statistics - 2017 Update". *Circulation* 135 (2017), e146–e603.

[18] DW Jones et al. "Measuring blood pressure accurately: New and persistent challenges". *JAMA* 289.8 (2003), pp. 1027–1030.

[19] L. A. Geddes. "Counterpressure: The Concept that Made the Indirect Measurement of Blood Pressure Possible". *IEEE Engineering in Medicine and Biology Magazine* 17.6 (1998), pp. 85–87.

[20] G. L. Pressman and P. M. Newgard. "A Transducer fo the Continuous External Measurement of Arterial Blood Pressure". *IEEE Transactions on Bio-Medical Electronics* 10.2 (1963), pp. 73–81.

[21] Takayuki Sato et al. "Accuracy of a Continuous Blood Pressure Monitor Based on Arterial Tonometry". *Hypertension* 21 (1993), pp. 866–874.

[22] J. Penaz. "Photoelectric Measurement of Blood Pressure, Volume and Flow in the Finger". *Digest of the 10th International Conference on Medical and Biological Engineering*. 1973, pp. 102–104.

[23] E. R. Nye. "The Effect of Blood Pressure Alteration on the Pulse Wave Velocity". *British Heart Journal* 26 (1964), pp. 261–265.

[24] Brian Gribbin, Andrew Steptoe, and Peter Sleight. "Pulse Wave Velocity as a Measure of Blood Pressure Change". *Psychophysiology* 13.1 (1976), pp. 86–90.

[25] Paul A. Obrist et al. "Pulse Transit Time: Relationship to Blood Pressure and Myocardial Performance". *Psychophysiology* 16.3 (1979), pp. 292–301.

[26] Robert A. Allen et al. "The Covariation of Blood Pressure and Pulse Transit Time in Hypertensive Patients". *Psychophysiology* 18.3 (1981), pp. 301–306.

[27] James D. Lane et al. "Pulse Transit Time and Blood Pressure: An Intensive Analysis". *Psychophysiology* 20.1 (1983), pp. 45–49.

[28] Ramón C. Hermida et al. "2013 Ambulatory Blood Pressure Monitoring Recommendations for the Diagnosis of Adult Hypertension, Assessment of Cardiovascular and other Hypertension-associated Risk, and Attainment of Therapeutic Goals". *Chronobiology International* 30.3 (2013), pp. 355–410.

[29] Rajiv Agarwal and Robert P. Light. "The Effect of Measuring Ambulatory Blood Pressure on Nighttime Sleep and Daytime Activity - Implications for Dipping". *Clinical Journal of the American Society of Nephrology* 5 (2010), pp. 281–285.

[30] Yali Zheng et al. "Wearable Cuff-less PTT-based System for Overnight Blood Pressure Monitoring". *35th Annual International Conference of the IEEE EMBS*. 2013, pp. 6103–6106.

[31] Simi Susan Thomas et al. "BioWatch: A Noninvasive Wrist-Based Blood Pressure Monitor That Incorporates Training Techniques for Posture and Subject Variability". *IEEE Journal of Biomedical and Health Informatics* 20.5 (2016), pp. 1291–1300.

[32] Chang-Sei Kim et al. "Ballistocardiogram as Proximal Timing Reference for Pulse Transit Time Measurement: Potential for Cuffless Blood Pressure Monitoring". *IEEE Transactions on Biomedical Engineering* 62.11 (2015), pp. 2657–2664.

[33] Zhihao Chen et al. "Noninvasive Monitoring of Blood Pressure Using Optical Ballistocardiography and Photoplethysmography Approaches". *35th Annual International Conference of the IEEE EMBS*. 2013, pp. 2425–2428.

[34] Chang-Sei Kim et al. "Ballistocardiogram-Based Approach to Cuffless Blood Pressure Monitoring: Proof of Concept and Potential Challenges". *IEEE Transactions on Biomedical Engineering* 65.11 (2018), pp. 2384–2391.

[35] Yuriy Kurylyak, Francesco Lamonaca, and Domenico Grimaldi. "A Neural Network-based Method for Continuous Blood Pressure Estimation from a PPG Signal". *IEEE Instrumentation and Measurement Technology Conference*. 2013.

[36] Xiaoman Xing and Mingshan Sun. "Optical blood pressure estimation with photoplethysmography and FFT-based neural networks". *Biomedical Optics Express* 7.8 (2016), pp. 3007–3020.

[37] Rong-Chao Peng et al. "Cuffless and Continuous Blood Pressure Estimation from the Heart Sound Signals". *Sensors* 15 (2015), pp. 23653–23666.

[38] Vikram Chandrasekaran et al. "Cuffless Differential Blood Pressure Estimation Using Smart Phones". *IEEE Transactions on Biomedical Engineering* 60.4 (2013), pp. 1080–1089.

[39] J. Smith et al. "Application of Flexible Flat Panel Display Technology to Wearable Biomedical Devices". *Electronics Letters* 51.17 (2015), pp. 1312–1314.

[40] Jae-Woong Jeong et al. "Capacitive Epidermal Electronics for Electrically Safe, Long-Term Electrophysiological Measurements". *Advanced Healthcare Materials* 3.5 (2013), pp. 642–648.

[41] Clementine M. Boutry et al. "A Sensitive and Biodegradable Pressure Sensor Array for Cardiovascular Monitoring". *Advanced Materials* 27 (2015), pp. 6954–6961.

[42] Ningqi Luo et al. "Flexible Piezoresistiv Sensor Patch Enabling Ultralow Power Cuffless Blood Pressure Measurement". *Advanced Functional Materials* 26 (2016), pp. 1178–1187.

[43] Umesh Sharath et al. "Blood Pressure Evaluation Using Sphygmomanometry Assisted by Arterial Pulse Waveform Detection by Fiber Bragg Grating Pulse Device". *Journal of Biomedical Optics* 18.6 (2013), p. 067010.

[44] Maynard Ramsey III. "Noninvasive automatic determination of mean arterial pressure". *Medical and Biological Engineering and Computing* 17.1 (1979), pp. 11–18.

[45] Paul Muntner et al. "Measurement of Blood Pressure in Humans A Scientific Statement From the American Heart Association". *Hypertension* 73 (2019), e35–e66.

[46] Kara A. Nerenberg et al. "Hypertension Canada's 2018 Guidelines for Diagnosis, Risk Assessment, Prevention, and Treatment of Hypertension in Adults and Children". *Canadian Journal of Cardiology* 34 (2018), pp. 506–525.

[47] Sante D. Pierdomenico and Franco Cuccurullo. "Prognostic Value of White-Coat and Masked Hypertension Diagnosed by Ambulatory Monitoring in Initially Untreated Subjects: An Updated Meta-Analysis". *American Journal of Hypertension* 24.1 (2011), pp. 52–58.

[48] Thomas G. Pickering et al. "Task Force V: White-coat hypertension". *Blood Pressure Monitoring* 4 (1999), pp. 333–341.

[49] Paolo Verdecchia et al. "White Coat Hypertension and White Coat Effect Similarities and Differences". *American Journal of Hypertension* 8.8 (1995), pp. 790–798.

[50] David Conen and Fabian Bamberg. "Noninvasive 24-h ambulatory blood pressure and cardiovascular disease: a systematic review and meta-analysis". *Journal of Hypertension* 26.7 (2008), pp. 1290–1299.

[51] Margaret A. Piper et al. "Diagnostic and Predictive Accuracy of Blood Pressure Screening Methods With Consideration of Rescreening Intervals: A Systematic Review for the U.S. Preventive Services Task Force". *Annals of Internal Medicine* 162.3 (2015), pp. 192–204.

[52] Alison M. Ward et al. "Home measurement of blood pressure and cardiovascular disease: systematic review and meta-analysis of prospective studes". *Journal of Hypertension* 30.3 (2012), pp. 449–456.

[53] Athanasios E. Raptis, Mark W. Spring, and Giancarlo Viberti. "Comparison of blood pressure measurement methods in adult diabetics". *The Lancet* 349 (1997), pp. 175–176.

[54] Frans J. van Ittersum et al. "Determinants of the limits of agreement between the sphygmomanometer and the SpaceLabs 90207 device for blood pressure measurement in healthy volunteers and insulin-dependent diabetic patients". *Journal of Hypertension* 16.8 (1998), pp. 1125–1130.

[55] Nicole M. van Popele et al. "Arterial Stiffness as Underlying Mechanism of Disagreement Between an Oscillometric Blood Pressure Monitor and a Sphygmomanometer". *Hypertension* 36.4 (2000), pp. 484–488.

[56] Gert A. van Montfrans. "Oscillometric blood pressure measurement: progress and problems". *Blood Pressure Monitoring* 6.6 (2001), pp. 287–290.

[57] L. A. Geddes and R. Tivey. "The Importance of Cuff Width in Measurement of Blood Pressure Indirectly". *Cardiovascular Research Center Bulletin* 14.3 (1976), pp. 69–79.

[58] Ethel M. Frese, Ann Fick, and H. Steven Sadowsky. "Blood Pressure Measurement Guidelines for Physical Therapists". *Cardiopulmonary Physical Therapy Journal* 22.2 (2011), pp. 5–12.

[59] Jennifer Ringrose et al. "Effect of overcuffing on the accuracy of oscillometric blood pressure measurements". *Journal of the American Society of Hypertension* (2015), pp. 1–6.

[60] Paolo Palatini et al. "Rectangular cuffs may overestimate blood pressure in individuals with large conical arms". *Journal of Hypertension* 30.3 (2012), pp. 530–536.

[61] John N. Amoore. "Extracting oscillometric pulses form the cuff pressure: does it affect the pressures determined by oscillometric blood pressure monitors?" *Blood Pressure Monitoring* 11.5 (2006), pp. 269–279.

[62] Vojko Jazbinsek et al. "Influence of Different Presentations of Oscillometric Data on Automatic Determination of Systolic and Diastolic Pressures". *Annals of Biomedical Engineering* 38.3 (2010), pp. 774–787.

[63] John N. Amoore et al. "Automatic blood pressure measurement: the oscillometric waveform shape is a potential contributor to differences between oscillometric and auscultatory pressure measurements". *Journal of Hypertension* 26.1 (2008), pp. 35–43.

[64] Dingchang Zheng, Roberto Giovannini, and Alan Murray. "Asymmetrical Oscillometric Pulse Waveform Envelopes in Normotensive and Hypertensive Subjects". *Computing in Cardiology* 37 (2010), pp. 377–380.

[65] Paolo Salvi. "Pulse Waves. How Vascular Hemodynamics Affects Blood Pressure." Springer, 2012. Chap. Pulse Wave Analysis.

[66] Amir M. Benmira et al. "Systolic peak foot-to-apex time interval, a novel oscillometric technique for systolic blood pressure measurement". *Journal of Hypertension* 35.5 (2017), pp. 1002–1010.

[67] Ahmadreza Argha et al. "Blood Pressure Estimation From Beat-by-Beat Time-Domain Features of Oscillometric Waveforms Using Deep-Neural-Network Classification Models". *IEEE Access* 7 (2019), pp. 113427–113439.

[68] Branko G. Celler et al. "GMM-HMM-Based Blood Pressure Estimation Using Time-Domain Features". *IEEE Transactions on Instrumentation and Measurement* 69.6 (2020), pp. 3631–3641.

[69] L. A. Geddes et al. "Characterization of the Oscillometric Method for Measuring Indirect Blood Pressure". *Annals of Biomedical Engineering* 10.6 (1982), pp. 271–280.

[70] P. D. Baker, D. R. Westenskow, and K. Kück. "Theoretical analysis of non-invasive oscillometric maximum amplitude algorithm for estimating mean blood pressure". *Medical & Biological Engineering & Computing* 35.3 (1997), pp. 271–278.

[71] Jiankun Liu, Jin-Oh Hahn, and Ramakrishna Mukkamala. "Error Mechanisms of the Oscillometric Fixed-Ratio Blood Pressure Measurement Method". *Annals of Biomedical Engineering* 41.3 (2013), pp. 587–597.

[72] Mohamad Forouzanfar et al. "Ratio-Independent Blood Pressure Estimation by Modeling the Oscillometric Waveform Envelope". *IEEE Transactions on Instrumentation and Measurement* 63.10 (2014), pp. 2501–2503.

[73] Seddigheh Baktash et al. "Characteristic Ratio-Independent Arterial Stiffness-Based Blood Pressure Estimation". *IEEE Journal of Biomedical and Health Informatics* 21.5 (2017), pp. 1263–1270.

[74] Jiankun Liu et al. "Patient-Specific Oscillometric Blood Pressure Measurement: Validation for Accuracy and Repeatability". *IEEE Journal of Translational Engineering in Health and Medicine* 5 (2017).

[75] Mariana Alvarado Alvarez et al. "Optimum waveform envelopes and amplitude ratios in oscillometric blood pressure estimation". *Blood Pressure Monitoring* 26 (2021), pp. 53–59.

[76] *Non-invasive sphygmomanometers - part 2: clinical investigation of automated measurement type.* ANSI/AAMI/ISO 81060-2:2013. Arlington, VA: Association for the Advancement of Medical Instrumentation: Association for the Advancement of Medical Instrumentation, 2013.

[77] Branko G. Celler et al. "Novel methods of testing and calibration of oscillometric blood pressure monitors". *PLoS ONE* 13.8 (2018), e0201123.

[78] GS Stergiou et al. "Unreliable oscillometric blood pressure measurement: prevalence, repeatability and characteristics of the phenomenon". *Journal of Human Hypertension* 23 (2009), pp. 794–800.

[79] Harold N. Segall. "How Korotkoff, the Surgeon, Discovered the Auscultatory Method of Measuring Arterial Pressure". *Annals of Internal Medicine* 83.4 (1975), pp. 561–562.

[80] David Wingfield et al. "Terminal digit preference and single-number preference in the Syst-Eur trial: influence of quality control". *Blood Pressure Monitoring* 7 (2002), pp. 169–177.

[81] David M. Howard and Jamie A. S. Angus. "Acoustics and Psychoacoustics". Fifth. Routledge, 2017. Chap. Introduction to Hearing.

[82] Dean S. Picone et al. "Accuracy of Cuff-Measured Blood Pressure Systematic Reviews and Meta-Analyses". *Journal of the American College of Cardiology* 70.5 (2017), pp. 572–586.

[83] Ernest P. McCutcheon and Robert F. Rushmer. "Korotkoff Sounds an Experimental Critique". *Circulation Research* 20.2 (1967), pp. 149–161.

[84] Horace Marshall Korns. "The Nature and Time Relations of the Compression Sounds of Korotkov in Man". *American Journal of Physiology - Legacy Content* 2 (1926), pp. 247–264.

[85] Simon Rodbard and Jan Ciesielski. "Duration of Arterial Sounds". *The American Journal of Cardiology* 8.1 (1961), pp. 18–21.

[86] Robin C. Cozby and Reza R. Adhami. "Low-Frequency Korotkoff Signal Analysis and Application". *IEEE Transactions on Biomedical Engineering* 40.10 (1993), pp. 1067–1070.

[87] L. A. Geddes, W. A. Spencer, and H. E. Hoff. "Graphic Recording of the Korotkoff Sounds". *American Heart Journal* 57.3 (1959), pp. 361–370.

[88] John Allen et al. "Characterization of the Korotkoff sounds using joint time-frequency analysis". *Physiological Measurement* 25 (2004), pp. 107–117.

[89] R. W. Ware and W. L. Anderson. "Spectral Analysis of Korotkoff Sounds". *IEEE Transactions on Bio-Medical Engineering* 13.4 (1966), pp. 170–174.

[90] Alan H. Maurer and Abraham Noordergraaf. "Korotkoff sound filtering for automated three-phase measurement of blood pressure". *American Heart Journal* 91.5 (1976), pp. 584–591.

[91] Donald P. Golden Jr. et al. "Development of a Korotkov Sound Processor for Automatic Identification of Auscultatory Events – Part I: Specification of Preprocessing Bandpass Filters". *IEEE Transactions on Biomedical Engineering* 21.2 (1974), pp. 114–118.

[92] James C. Fletcher et al. *Apparatus and Method for Processing Korotkov Sounds*. United States Patent no. 3,814,083. 1974.

[93] L. A. Geddes. *The Direct and Indirect Measurement of Blood Pressure*. Year Bood Medical Publishers, Inc., 1970.

[94] Joseph Erlanger. "Studies in Blood Pressure Estimation by Indirect Methods III. The Movements in the Artery under Compression during Blood Pressure Determinations". *American Journal of Physiology* 55.1 (1921), pp. 84–158.

[95] M. Shimizu and Y. Tanida. "On the mechanism of Korotkoff sound generation at diastole". *Journal of Fluid Mechanics* 127 (1983), pp. 315–339.

[96] Simon Rodbard. "The Significance of the Intermediate Korotkoff Sounds". *Circulation* 8 (1953), pp. 600–604.

[97] Amiram Ur and Michael Gordon. "Origin of Korotkoff sounds". *American Journal of Physiology* 218.2 (1970), pp. 524–529.

[98] Ramon L. Lange, Robert P. Carlisle, and Hans H. Hecht. "Observations on Vascular Sounds: The "Pistol-Shot" Sound and the Korotkoff Sound". *Circulation* 13 (1956), pp. 873–883.

[99] D. Chungcharoen. "Genesis of Korotkoff sounds". *American Journal of Physiology* 207.1 (1964), pp. 190–194.

[100] Morton E. Tavel et al. "Korotkoff Sounds Observations on Pressure-Pulse Changes Underlying Their Formation". *Circulation* 39 (1969), pp. 465–474.

[101] Max Anliker and K. R. Raman. "Korotkoff Sounds at Diastole – A Phenomenon of Dynamic Istability of Fluid-Filled Shells". *International Journal of Solids and Structures* 2 (1966), pp. 467–491.

[102] G. M. Drzewiecki, J. Melbin, and A. Noordergraaf. "The Korotkoff Sound". *Annals of Biomedical Engineering* 17.4 (1989), pp. 325–359.

[103] Charles F. Babbs. "The origin of Korotkoff sounds and the accuracy of auscultatory blood pressure measurements". *Journal of the American Society of Hypertension* 9.12 (2015), pp. 935–950.

[104] Paul Y. Ertel et al. "Stethoscope Acoustics: II. Transmission and Filtration Patterns". *Circulation* 34 (1966), pp. 899–909.

[105] Lukasz J. Nowak and Karolina M. Nowak. "Acoustic characterization of stethoscopes using auscultation sounds as test signals". *The Journal of the Acoustical Society of America* 141.3 (2017), pp. 1940–1946.

[106] William C. Cushman et al. "Effect of Back Support and Stethoscope Head on Seated Blood Pressure Determinations". *American Journal of Hypertension* 3.3 (1990), pp. 240–241.

[107] Chengyu Liu et al. "Comparison of stethoscope bell and diaphragm, and of stethoscope tube length, for clinical blood pressure measurement". *Blood Pressure Monitoring* 21.3 (2016), pp. 178–183.

[108] Lukasz J. Nowak and Karolina M. Nowak. "Sound differences between electronic and acoustic stethoscopes". *BioMedical Engineering OnLine* 17.104 (2018).

[109] *Thinklabs One Digital Stethoscope*
https://www.thinklabs.com/filtering
Last checked: May 2021.

[110] Leo L. Beranek. "Acoustics". American Institute of Physics, Inc., 1996. Chap. Hearing, Speech Intelligibility, and Psychoacoustic Criteria.

[111] R. H. Randall. "An Introduction to Acoustics". Dover Publications, 2005. Chap. Speech and Hearing.

[112] H. Fastl and E. Zwicker. *Psychoacoustics. Facts and Models*. Third. Springer, 2007.

[113] Walt Jesteadt, Craig C. Wier, and David M. Green. "Intensity discrimination as a function of frequency and sensation level". *The Journal of the Acoustical Society of America* 61.1 (1977), pp. 169–177.

[114] Sung Jun Hong et al. "Automatic assessment of blood pressure for Korotkoff sond on th basis of human hearing threshold". *Blood Pressure Monitoring* 22 (2017), pp. 364 –370.

[115] Bruce S. Alpert. "The Accutension Stetho, an automated auscultatory device to validate automated sphygmomanometer readings in individual patients". *Journal of Human Hypertension* 32 (2018), pp. 455–459.

[116] Guang Chu et al. "Validation of a smartphone auscultatory blood pressure kit Accutension XYZ-110 in adults according to the ANSI/AAMI/ISO 81060-2:2013 standard". *Blood Pressure Monitoring* 22 (2017), pp. 290 –294.

[117] Jeary R. Vogt. *Blood Pressure Measuring System with Korotkoff Sound Detector*. United States Patent no. 3,450,131. 1969.

[118] Klaus Berger, Karl-Heinz Affeldt, and Lutz Böttcher. *Method and Apparatus for Measuring Blood Pressure by Instantaneous Comparison of Multiple Frequency-Range Components of Korotkoff Noise*. United States Patent no. 4,534,361. 1985.

[119] Tsutomu Ichinomiya, Toshio Kusunoki, and Tomohiro Kami. *Blood Pressure Measuring Apparatus*. United States Patent no. 4,417,587. 1983.

[120] William J. Kaspari, Herman Wong, and Joseph L. Kirch. *Blood Pressure Measuring Apparatus*. United States Patent no. 4,058,117. 1977.

[121] Yuqi Wang et al. "Improving Auscultatory Blood Pressure Measurement With Electronic and Computer Technology: The Visual Auscultation Method". *American Journal of Hypertension* 22.6 (2009), pp. 624–629.

[122] Ahmadreza Argha and Branko G. Celler. "Blood Pressure Estimation Using Time Domain Features of Auscultatory Waveforms and Deep Learning". *Annual International Conference of the IEEE Engineering in Medicine and Biology Society*. IEEE Engineering in Medicine and Biology Society. IEEE, 2019.

[123] Fan Pan et al. "A novel deep learning basd automatic auscultatory method to measure blood pressure". *International Journal of Medical Informatics* 128 (2019), pp. 71 –78.

[124] H. H. Hardy and R. E. Collins. "On the pressure-volume relationship in circulatory elements". *Medical & Biological Engineering & Computing* 20 (1982), pp. 565 –570.

[125] Jan M. Meinders and Arnold P.G. Hoeks. "Simultaneous assessment of diameter and pressure waveforms in the carotid artery". *Ultrasound in Medicine & Biology* 30.2 (2004), pp. 147 –154.

[126] Linda A. Taylor and John H. Gerrard. "Pressure-radius relationships for elastic tubes and their applications to arteries: Part 1 - Theoretical relationships". *Medical & Biological Engineering & Computing* 15 (1977), pp. 11 –17.

[127] NIST. *NIST/SEMATECH e-Handbook of Statistical Methods, http://www.itl.nist.gov/div898/handbook/. Last checked: July 8, 2021.*

[128] Wilmer W. Nichols, Michael F. O'Rourke, and Charalambos Vlachopoulos. "McDonald's Blood Flow in Arteries. Theoretical, Experimental and Clinical Principles". 6^{th} Edition. Taylor & Francis Group, 2011. Chap. Properties of the arterial wall: theory.

[129] Wilmer W. Nichols, Michael F. O'Rourke, and Charalambos Vlachopoulos. "McDonald's Blood Flow in Arteries. Theoretical, Experimental and Clinical Principles". 6^{th} Edition. Taylor & Francis Group, 2011. Chap. Properties of the arterial wall: practice.

[130] Richard W. Lawton. "Measurements on the Elasticity and Damping of Isolated Aortic Strips of the Dog". *Circulation Research* 3 (1955), pp. 403 –408.

[131] Yuuki Tomiyama et al. "Accurate quantitative measurements of brachial artery cross-sectional vascular area and vascular volume elastic modulus using automated oscillometric measurements: comparison with brachial artery ultrasound". *Hypertension Research* 38 (2015), pp. 478–484.

[132] J. Malcolm O. Arnold et al. "Large Artery Function in Patients with Chronic Heart Failure. Studies of Brachial Artery Diameter and Hemodynamics". *Circulation* 84.6 (1991), pp. 2418 –2425.

[133] Tatsuya Maruhashi et al. "Brachial artery diameter as a marker for cardiovascular risk assessment: FMD-J study". *Atherosclerosis* 268 (2018), pp. 92 –98.

[134] Janneke J. van der Heijden-Spek et al. "Effect of Age on Brachial Artery Wall Properties Differs From the Aorta and Is Gender Dependent. A Population Study". *Hypertension* 35 (2000), pp. 637 –642.

[135] T. J. Pedley. "The Fluid Mechanics of Large Blood Vessels". Cambridge University Press, 1980. Chap. Physiological introduction.

[136] Pranali Choudhari and M. S. Panse. "Finite Element Modeling and simulation of arteries in the human arm to study the aortic pulse wave propagation". *Procedia Computer Science* 93 (2016), pp. 721 –727.

[137] *An investigation into the upper arm deformation under inflatable cuff*. IMECE2008-67009. 2008.

[138] Shivam Kohli, Anish Saini, and Ajesh J. Pillai. "MEMS based Capacitive Pressure Sensor Simulation for Healthcare and Biomedical Applications". *International Journal of Scientific & Engineering Research* 4.12 (2013), pp. 1855 –1862.

[139] Aaron M. Zakrzewski and Brian W. Anthony. "Noninvasive Blood Pressure Estimation Using Ultrasound and Simple Finite Element Models". *IEEE Transactions on Biomedical Engineering* 65.9 (2018), pp. 2011 –2022.

[140] Tse-Yi Tu and Paul C.-P. Chao. "Optimal Design of a New Strain-Type Sensor for Cuff-Less Blood Pressure Measurement via Finite Element Modeling and Taguchi Method". *IEEE Sensors Journal* 19.22 (2019), pp. 10355 –10364.

[141] COMSOL. *COMSOL Multiphysics, Arterial Wall Viscoelasticity, https://www.comsol.com/model/arterial-wall-viscoelasticity-42821 Last checked: November 23, 2021.*

Appendix A

Optimum Waveform Envelopes and Amplitude Ratios in Oscillometric Blood Pressure Estimation

Optimum waveform envelopes and amplitude ratios in oscillometric blood pressure estimation

Mariana Alvarado Alvarez[a], Raj Padwal[b], Jennifer Ringrose[b], Afrooz Jalali[b], Wayne Hiebert[a,c]

Objective **To determine if, when using the oscillometric method, there is a specific range of amplitude ratios in the fixed-ratio algorithm that will result in blood pressure estimates that consistently fall within a mean error ≤5 mmHg and a SD of the error <8 mmHg. Additionally, to apply different representations of the oscillometric waveform envelope to verify if this will affect the accuracy of the results.**

Methods **SBP and DBP were obtained using the fixed-ratios method applied to a dataset of 219 oscillometric measurements obtained from 73 healthy volunteers and compared to their corresponding auscultation values. Ratio and envelope analysis were done on Matlab (The MathWorks, Inc., Natick, Massachusetts, USA).**

Results **Depending on the envelope representation, ratios between 0.44–0.74 for systolic pressure and 0.51–0.85 for diastolic pressure yield results within the limits mentioned above. When a set of optimum envelope representations and ratios are selected based on population mean, the highest percentage of subjects presenting blood pressure estimates within the limits were 72.6% for systolic and 69.9% for diastolic.**

Conclusion **The range of ratios presenting optimum results appears to be independent of the degree of arterial stiffness given the wide range of ages of the subjects in the study. Different representations of the oscillometric waveform envelope may improve the accuracy of the method. However, there remains a considerable percentage of the population with unreliable results. It is therefore important to only use devices that have been properly validated according to standard protocol.** ***Blood Press Monit*** **26: 53–59**

Blood Pressure Monitoring 2021, **26**:53–59

Keywords: auscultation, oscillometric waveform envelope, oscillometry, pressure

Departments of [a]Physics, [b]Medicine, University of Alberta and [c]Nanotechnology Research Centre, National Research Council Canada, Edmonton, Alberta, Canada

Correspondence to Mariana Alvarado Alvarez, MSc, Department of Physics, University of Alberta, 116 St. and 85 Ave., Edmonton, Alberta T6G 2R3, Canada
Tel: +15053107913; e-mail: malvarad@ualberta.ca

Received 4 May 2020 **Accepted** 4 August 2020

Introduction

Cardiovascular diseases are the leading cause for death and disability worldwide [1], and raised blood pressure (BP), or hypertension, is a key risk factor [2]. The use of traditional auscultation for BP depends on proper training and use of accurate devices to avoid the different sources of error that affect this method [3].

Automated noninvasive BP measurement, particularly oscillometric blood pressure measurement (OBPM), has therefore become the method recommend over traditional auscultation [4,5], as it may prevent many of the human-sourced errors in the measurement, reduce the risk of white-coat effect, and can collect multiple readings for averaging. Ambulatory BP measurement and home BP measurements are generally based on OBPM and are stronger predictors of cardiovascular events than current clinic measurements [6–8].

Despite its many advantages, the OBPM also has some documented shortcomings that could mean that this method is not adequate for its target population: oscillometric devices perform poorly in the elderly, in patients with diabetes, and in those with increased arterial stiffness [9–12]. This can most likely be traced back to the way oscillometric devices process the data they collect to estimate BP. Unfortunately, the detailed inner workings of most commercial devices are proprietary and not available for public scrutiny.

During an oscillometric procedure, pressure oscillations are detected in a cuff similar to the one used in auscultation. These oscillations, or their envelope, can be expressed as a function of the approximately linear deflation pressure and are known as the oscillometric waveform, or the oscillometric waveform envelope (OMWE). An algorithm can then relate BP to this OMWE.

The method of filtering the pulses from the original signal to construct the OMWE has been found to alter the shape of the envelope [13,14]. The shape of the OMWE also affects the estimation of BP, particularly in complex

Supplemental Digital Content is available for this article. Direct URL citations appear in the printed text and are provided in the HTML and PDF versions of this article on the journal's website, www.bpmonitoring.com.

1359-5237 DOI: 10.1097/MBP.0000000000000485

envelope shapes [15], or in wider envelopes, such as those present in subjects with documented hypertension when compared to those of normotensives [16]. Additionally, two algorithms popularly discussed in literature for BP estimation, the slope-based and the fixed-ratio algorithms, depend on the shape of the OMWE; the former estimates BP based on the location of the maximum slopes of the envelope, while the latter on locations of the envelope where the height is of a certain ratio of the maximum amplitude.

In this study, we analyze other options for the presentation of the OMWE and we focus primarily on efficiency of the fixed-ratio algorithm. The ratios that define this algorithm are empirically determined and are thus not representative of all subjects. Therefore, we set out to answer the question of whether there are certain ratios that will consistently yield accurate results for a sample population, and if there are ways of improving this method.

Methods

Study subjects/data collection

Data were collected in a convenience sample of 73 healthy subjects at the University of Alberta, in Edmonton, Alberta, Canada. University of Alberta Research Ethics Board approval was obtained prior to enrolling subjects. BP measurement was performed in standardized fashion following the International Standard Organization (ISO) 2013 protocol [17]. Subject ages ranged from 19 to 79 years and BPs ranged from 82 to 155 mmHg for SBP, 51 to 93 mmHg for DBP, and 24 to 88 mmHg for pulse pressure. General subject characteristics are presented in Table 1.

Cuff size was chosen according to arm circumference (based on the closest approximation to 40% of arm circumference width) and cuffs were connected to a custom made oscillometric device, by which oscillometric measurements were made. Two trained observers who were blinded to each other's results performed auscultation simultaneously with a mercury column and a dual earpiece stethoscope while a third observer ensured measurements were within 4 mmHg. A total of five auscultatory measurements and four oscillometric measurements were taken in alternate fashion on the same arm beginning with auscultation. The first two measurements were discarded and not used for analysis. The mean of the auscultatory measurements for the two observers was first calculated; next, the average of the auscultation measurements taken immediately before and after each oscillometric reading was taken and used in the analysis to compare to each oscillometric reading. Therefore, a total of three oscillometric measurements and corresponding auscultatory comparisons were obtained for each subject, for a total of 219 BP comparisons.

Table 1 Baseline characteristics

Variable	Mean ± SD or no. (%)
Age (years)	51 ± 18
Female	46 (63)
Weight (kg)	72.1 ± 14.2
Arm circumference (cm)	30.5 ± 3.7
SBP (mmHg)	115 ± 16
DBP (mmHg)	69 ± 8
Pulse pressure (mmHg)	46 ± 14

Applying the fixed-ratio method

The complete procedure, from filtering to estimating BP via the fixed-ratio method was done using Matlab functions (The MathWorks, Inc., Natick, Massachusetts, USA) and original code written for Matlab as well. The oscillometric waveform from each individual measurement was obtained by reconstructing the baseline deflation pressure and subtracting it from the original pressure signal. The resulting waveform was leveled to zero to have the absolute amplitudes of the pulses expressed as functions of the baseline deflation pressure. Outliers were identified and replaced using a function, which uses statistics of a seven-point window to identify these outliers, and then replaces them by doing a linear interpolation between the two neighboring points.

There are several ways to obtain the OMWE to estimate BP; the exact method that each commercial device uses is not usually disclosed, and most likely not uniform across devices. Some devices obtain the envelope directly after extracting the OMW from the peak-to-peak amplitude from each pulse, while others average a few pulses at certain pressures [13]. Another method to do this is by performing a linear interpolation between each maximum peak of the oscillations when they are expressed as absolute amplitudes. In this study, we use this latter method, and we also fit three other different functions to these peaks, selected because of their closeness-of-fit to an OMWE distribution and smoother profiles. These functions were polynomials of sixth and eigth degree and a Gaussian function.

We defined the systolic ratio (SR) and the diastolic ratio (DR), according to Geddes *et al.* [18], as a SR = A_s/A_m and a DR = A_d/A_m, where A_s and A_d were defined as the amplitude of the oscillations where auscultatory SBP and DBP were located, expressed as ratios of the amplitude of the maximum oscillations, A_m, which has been previously identified as mean arterial pressure.

First, we used Geddes *et al.*'s 'typical' ratios of 0.55 for systolic and 0.82 for diastolic to examine the ability of each of the four methods of fitting the oscillometric envelope to derive BP values close to the auscultatory reference standard for an individual with a BP of 118/80 mmHg (the subject with the BP closest to what Geddes defined as typical: 120/80 mmHg).

Second, given that Geddes *et al.* also reported a range of ratios, noting that the results were dependent on the BP of the subject, we tested a range of SRs and DRs for each envelope. The four envelopes were fitted to each of the 219 OMWs obtained from the study; SBP was calculated for each ratio in a range of SRs going from 0.28 to 0.89 sampled in increments of 0.01. Likewise, DBP was calculated for each ratio in a range of DRs from 0.3 to 0.99 sampled in increments of 0.01. The resulting BP values were then compared to the true auscultation values and the error was calculated for each as the auscultation minus the oscillometric value. The mean of the error (ME) and the SD of the error (SDE) were obtained for the study sample and were plotted against a reference of a ME within ±5 mmHg and a SDE <8 mmHg. These limits are within ISO standards [17] and are of clinical relevance for diagnosis and treatment.

Third, the effect of the choice of ratios was also analyzed for individual subjects. Instances of prevailing error in the oscillometric method for some patients have been reported [19] so it was considered of interest to verify the average error incurred per subject. For this purpose, the ratios with the lowest ME were chosen as the ratios under which an oscillometric device would hypothetically operate.

Using these ratios SBP and DBP were determined for each of the three oscillometric measurements taken per subject. The errors between these three results and their corresponding auscultatory values were averaged to obtain the ME for each subject. Three distributions of the absolute errors were analyzed: ME ≤ 5mmHg, 5 < ME ≤ 10 mmHg, and ME ≥ 10 mmHg. The analysis was done with respect to the complete sample and by age group. The age groups were divided by tertiles: the first group ranging from 19 to 40 years, the second group from 41 to 62 years, and the third group from 63 to 79 years. There is a total of 24 subjects included in the first two groups and 25 subjects in the last group. See Table, Supplemental Digital Content 1, *http://links.lww.com/BPMJ/A123*, for summarized age and BP characteristics of the age groups.

Results

Figure 1 shows a sample diagram of the OBPM process for a subject with BP of 118/80 mmHg. In Fig. 1c the SBP/DBP (error) obtained with each envelope were 105/77 (+13/+3) mmHg for linear interpolation; 110/74 (+8/+6) mmHg for the sixth-degree polynomial; 107/75 (+11/+5) mmHg for the eight-degree polynomial; and 115/73 (+3/+7) mmHg for the Gaussian function.

Figure 2 shows the ME and SDE results determined for the range of ratios sampled for, plotted with the limits of ±5 mmHg for ME and 8 mmHg for SDE marked with dashed horizontal lines. The ratios that correspond to a ME close to zero for the four different envelopes ranged from 0.54 to 0.63 for SRs, and 0.62 to 0.75 for DRs. The ranges that comply with the limits marked in Fig. 2 are summarized in Table 2.

The SR and DR from each envelope selected to represent the results from a hypothetical commercial device are presented in Table 3.

Figure 3 shows a comparison of the percentage of subjects from the complete sample with absolute ME ≤ 5 mmHg, > 5 and ≤ 10 mmHg, and > 10 mmHg, depending on OMWE representation. The percentages are the values written atop each bar. The same analysis with respect to the number of subjects in each age group was obtained (see Figure, Supplemental Digital Content 2, *http://links.lww.com/BPMJ/A124*, which shows the percentage of subjects from each age group with absolute ME ≤ 5 mmHg, > 5 and ≤ 10 mmHg, and > 10 mmHg. Top for SBP and bottom for DBP).

Discussion

In summary, the results of this analysis indicate that:

(1) The method of constructing the final OMWE leads to variation in BP estimation;
(2) results where the ME falls within ±5 mmHg and SDE <8 mmHg are obtained in the middle of a wide range of fixed ratios in all cases of OMWE construction; and
(3) for individual subject sequential measurements, the common method of linear interpolation is most effective in estimating SBP, but an eight-degree polynomial performed better in the case of DBP.

From what is presented in Fig. 1 it is clear that a single set of fixed ratios does not fit every individual, even if these ratios had been previously determined for a similar BP. This confirms that the choice of ratios not only depends on BP alone, but on a combination of other physiological factors. Different mathematical models of the oscillometric BP measurement method have been proposed to determine the greatest contributors to its inaccuracy for different populations. These models agree in general that pulse pressure and arterial stiffness play a major role in the effectiveness of the method [20–23].

However, once the range of ratios was sampled, the linear behavior of the ME for the ratios indicates that there is indeed a limited range centered around 60% of the maximum for SBP and 70% of the maximum for DBP, as seen in Fig. 2, which will consistently yield results within ME and SDE limits for the sample. The sample includes a relatively wide range of pulse pressures, and arterial stiffness is a natural occurrence in older patients, so these parameters may not affect the results of this method in the specific case of a healthy population.

Additional potential contributors to variability include different diseases (e.g. vascular disease, chronic kidney disease, obesity) and altered physiological states (e.g. advanced age, pregnancy), however, the sample

Fig. 1

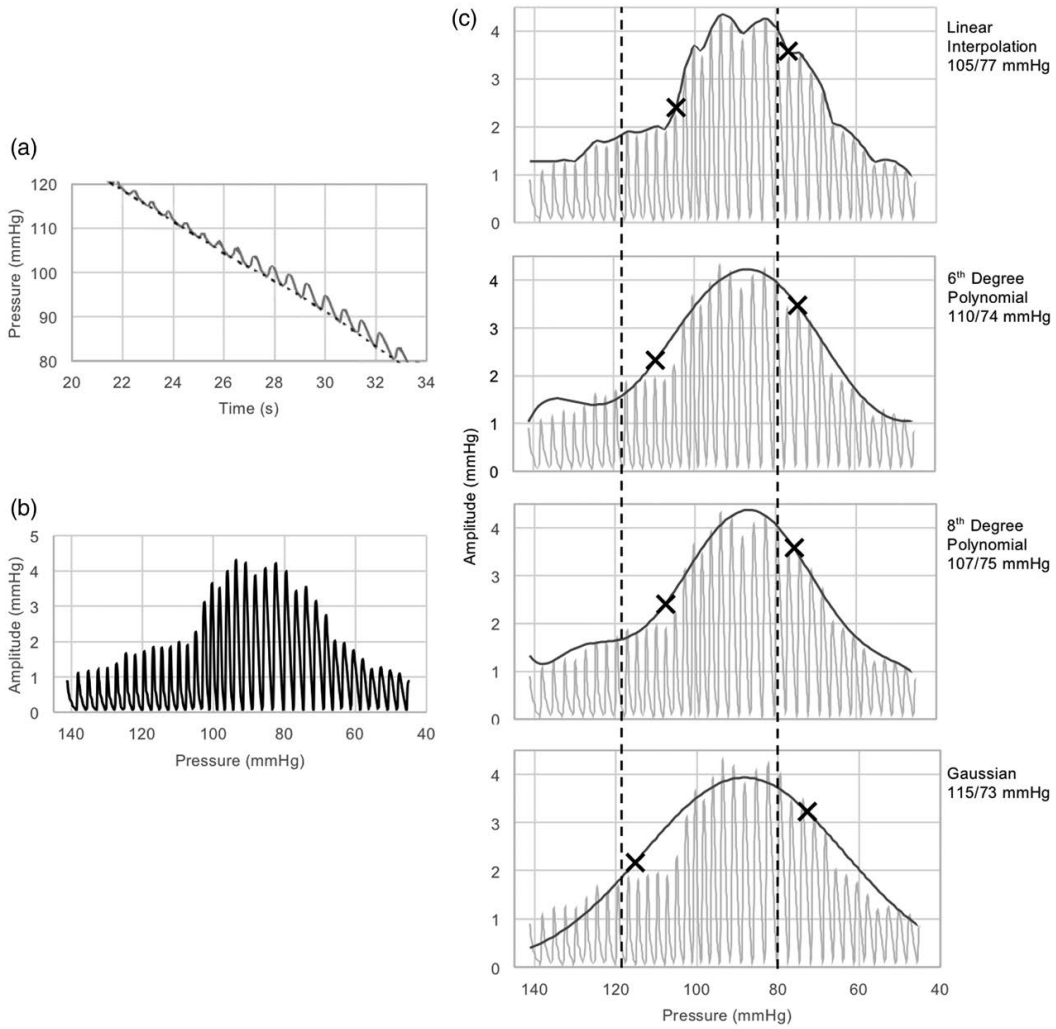

Visual schematic of the OMW extraction and OMWE fit for different envelope functions. (a) Original signal (solid) with reconstructed baseline (dashed) showing oscillations between SBP and DBP. (b) Leveled OMW as function of baseline pressure. (c) Different functions fitted to the OMW. Dashed vertical lines indicate an auscultatory BP of 118/80 mmHg; cross markers indicate estimated BP obtained for each envelope using a SR of 0.55 and a DR of 0.82. BP, blood pressure; DR, diastolic ratios; OMWE, oscillometric waveform envelope; SR, systolic ratios.

examined in the present study was comprised of healthy subjects; thus, the findings would not be able to confirm or disprove the effect of these factors.

The different functions used to fit an OMWE to the waveforms, unlike the linear interpolation, present a well-defined maximum and have smooth profiles on both high- and low-pressure sides. These features were expected to improve on MAP location and subsequent SBP and DBP estimation. As expected, the location of the maximum amplitude is shifted by each function, an example of which can be seen in Fig. 1. Unfortunately, this study did not collect information on the subjects' true MAP, so the magnitude of this shift is unknown.

The ME exhibits an approximately linear behavior within the limits for both the SRs and DRs, and for all four envelopes, while the SDE is always below the accepted limit for the ranges of interest. Although the behavior of the SDE across the range of fixed ratios is highly irregular for both SBP and DBP (Fig. 2c and d), the Gaussian function results in the lowest and most consistent systolic SDE, within the 8 mmHg limit across the entire range of fixed ratios.

Fig. 2

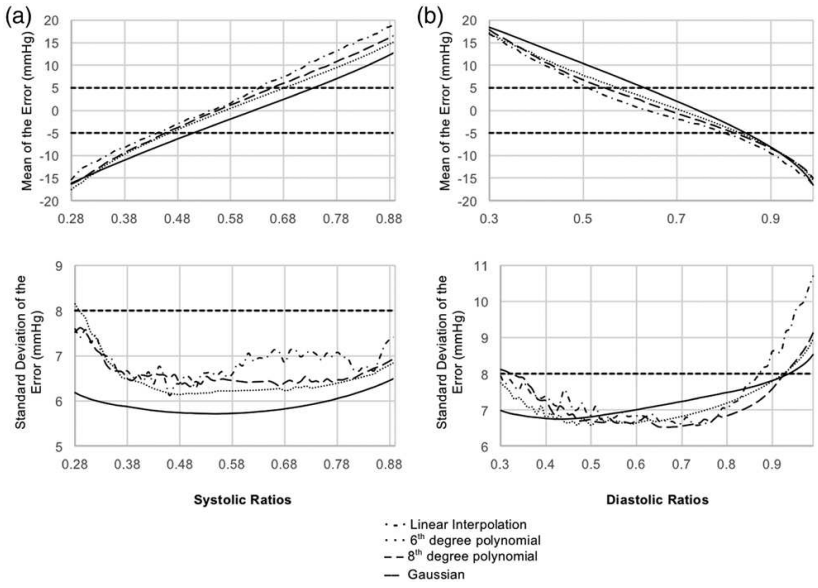

Mean of the error (ME) and SD of the error (SDE) obtained for all four envelopes for a sampled range of (a) systolic ratios (SR), and (b) diastolic ratios (DR).

Table 2 Accurate amplitude ratios

Envelope function	Systolic ratios	Diastolic ratios
Linear Interpolation	0.44–0.63	0.51–0.81
6th-degree polynomial	0.46–0.69	0.57–0.84
8th-degree polynomial	0.45–0.66	0.54–0.83
Gaussian	0.50–0.74	0.62–0.85

Ranges of systolic and diastolic ratios which produce population mean error within ±5 mmHg and SD of the error <8 mmHg.

Once an ideal ratio is established for each envelope, the methods perform similarly, with the exception that the lowest values for SDE were obtained with the Gaussian envelope for SBP and with the eight-degree polynomial for DBP, which indicates that a mix of methods may be required to achieve optimal accuracy. The value of these results depends on the practicality of implementing a mixed-method approach.

The intra-individual analysis demonstrates that optimum population results do not imply accuracy for all individuals. The SRs of choice result in close to three-quarters of the population with average SBP estimates within acceptable error, with the linearly interpolated envelope performing better than the other three functions. The DRs of choice have results close to those of the SRs, of these the eight-degree polynomial envelope performed better than the other three envelopes. In both cases, however, there is almost one-quarter of the population with unreliable results. Because these findings demonstrate variability within an individual over a sequence of readings, they must primarily represent minute-to-minute physiologic changes and a greater understanding of this variability is needed to optimize oscillometric BP accuracy.

A look at the different age groups confirms that some representations of the OMWE are better suited for certain populations. It is interesting to note that the second age group (41–62 years) had the lowest accuracy for SBP, and the third group (63–79 years) had the lowest accuracy for DBP. Mean SBP and PP increase respectively by age group as expected, although there is not a significant difference in mean DBP between the last two groups. These observations reveal that for this population sample in particular arterial stiffness might not be a major factor in the accuracy of the method.

The primary limitation of this analysis is that it focused on healthy individuals recruited at a single center in Canada and, therefore, the results should be extrapolated with caution to broader populations.

In conclusion, we have determined that results with ME within ±5 mmHg and SDE <8 mmHg can be obtained within a moderately tight range of ratios for SBP and DBP. These ranges appear to be independent of pulse pressure and arterial stiffness, but possibly limited to

Table 3 Select ratios

Envelope function	SR	ME ± SDE (mmHg)	DR	ME ± SDE (mmHg)
Linear interpolation	0.54	0.0 ± 6.6	0.64	−0.1 ± 6.9
6th degree polynomial	0.57	0.0 ± 6.2	0.71	−0.1 ± 6.8
8th degree polynomial	0.56	0.2 ± 6.5	0.68	0.0 ± 6.5
Gaussian	0.62	−0.2 ± 5.7	0.74	0.2 ± 7.3

SR and DR chosen for each envelope along with corresponding ME and SDE statistics.
DR, diastolic ratios; ME, mean of the error; SDE, SD of the error; SR, systolic ratios.

Fig. 3

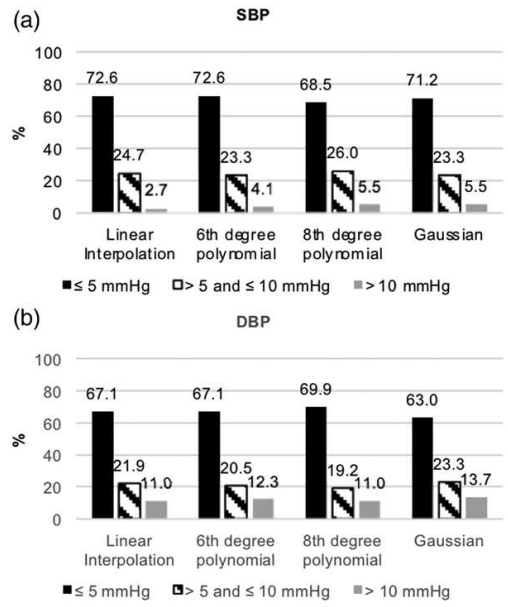

Percentage of subjects from the total sample with individual absolute absolute mean error ≤ 5 mmHg, > 5 and ≤ 10 mmHg, and > 10 mmHg. (a) Results for SBP and (b) results for DBP.

only healthy populations. We have also confirmed that an additional factor that affects the accuracy of the fixed ratio oscillometric method is the function used to construct the final OMWE, and that a possible improvement to the method would be the use of a combination of functions. Further studies are recommended to verify if these findings extend to healthy populations in general, and if there exist similar outcomes for populations with varying conditions. This might result in devices with customizable ratios that can be set by the user depending on their condition. The extent to which this can be practically implemented in a given device remains to be determined.

It is unlikely that commercial devices operate based on this method alone, but rather on a combination of algorithms. Therefore, results presented here may serve as an additional consideration in the design of a device. As previously mentioned, this information is not usually disclosed, so it is important to use only those devices that have been properly validated according to standard protocol [24,25]. This ensures the device has been submitted to rigorous testing and provides reliable measurements, regardless of the algorithm on which it is based.

Acknowledgements

We thank Sangita Sridar, Chief Technology Officer, mmHg Inc., for providing the custom oscillometric blood pressure measurement device and Dr. Alexander Kobryn, Senior Research Officer, National Institute for Nanotechnology, National Research Council Canada, for his help.

M.A.A. was supported by a CONACyT scholarship, Mexico.

Conflicts of interest

R.P., J.R. and A.J. are co-founders of mmHg Inc., a blood pressure measurement start-up. For the remaining authors, there are no conflicts of interest.

References

1 World Health Organization. A global brief on Hypertension. Document number: WHO/DCO/WHD/2013.2 Geneva, Switzerland. http://www.who.int.
2 Rapsomaniki E, Timmis A, George J, Pujades-Rodriguez M, Shah AD, Denaxas S, *et al*. Blood pressure and incidence of twelve cardiovascular diseases: lifetime risks, healthy life-years lost, and age-specific associations in 1·25 million people. *Lancet* 2014; **383**:1899–1911.
3 Kallioinen N, Hill A, Horswill MS, Ward HE, Watson MO. Sources of inaccuracy in the measurement of adult patients' resting blood pressure in clinical settings: a systematic review. *J Hypertens* 2017; **35**:421–441.
4 Canadian Hypertension Education Program. The 2015 Canadian Hypertension Education Program recommendations for blood pressure measurement, diagnosis, assessment of risk, prevention, and treatment of hypertension. *Can J Cardiol* 2015; **32**:549–568.
5 Pickering TG, Hall JE, Appel LJ, Falkner BE, Graves J, Hill MN, *et al*.; Subcommittee of Professional and Public Education of the American Heart Association Council on High Blood Pressure Research. Recommendations for blood pressure measurement in humans and experimental animals: part 1: blood pressure measurement in humans: a statement for professionals from the Subcommittee of Professional and Public Education of the American Heart Association Council on High Blood Pressure Research. *Hypertension* 2005; **45**:142–161.
6 Conen D, Bamberg F. Noninvasive 24-h ambulatory blood pressure and cardiovascular disease: a systematic review and meta-analysis. *J Hypertens* 2008; **26**:1290–1299.
7 Piper MA, Evans CV, Burda BU, Margolis KL, O'Connor E, Whitlock EP. Diagnostic and predictive accuracy of blood pressure screening methods with consideration of rescreening intervals: a systematic review for the U.S. Preventive Services Task Force. *Ann Intern Med* 2015; **162**:192–204.
8 Ward AM, Takahashi O, Stevens R, Heneghan C. Home measurement of blood pressure and cardiovascular disease: systematic review and meta-analysis of prospective studies. *J Hypertens* 2012; **30**:449–456.

9 Raptis AE, Spring MW, Viberti G. Comparison of blood pressure measurement methods in adult diabetics. *Lancet* 1997; **349**:175–176.
10 van Ittersum FJ, Wijering RM, Lambert J, Donker AJ, Stehouwer CD. Determinants of the limits of agreement between the sphygmomanometer and the SpaceLabs 90207 device for blood pressure measurement in health volunteers and insulin-dependent diabetic patients. *J Hypertens* 1998; **16**:1125–1130.
11 van Popele NM, Bos WJ, de Beer NA, van Der Kuip DA, Hofman A, Grobbee DE, Witteman JC. Arterial stiffness as underlying mechanism of disagreement between an oscillometric blood pressure monitor and a sphygmomanometer. *Hypertension* 2000; **36**:484–488.
12 van Montrfrans GA. Oscillometric blood pressure measurement: progress and problems. *Blood Press Monit* 2001; **6**:287–290.
13 Amoore JN. Extracting oscillometric pulses from the cuff pressure: does it affect the pressures determined by oscillometric blood pressure monitors? *Blood Press Monit* 2006; **11**:269–279.
14 Jazbinsek V, Luznik J, Mieke S, Trontelj Z. Influence of different presentations of oscillometric data on automatic determination of systolic and diastolic pressures. *Ann Biomed Eng* 2010; **38**:774–787.
15 Amoore JN, Lemesre Y, Murray IC, Mieke S, King ST, Smith FE, Murray A. Automatic blood pressure measurement: the oscillometric waveform shape is a potential contributor to differences between oscillometric and auscultatory pressure measurements. *J Hypertens* 2008; **26**:35–43.
16 Zheng D, Giovannini R, Murray A. Asymmetrical oscillometric pulse waveform envelopes in normotensive and hypertensive subjects. *Comput Cardiol* 2010; **37**:377–380.
17 Association for the Advancement of Medical Instrumentation. *ANSI/AAMI/ISO 81060-2:2013 non-invasive sphygmomanometers - part 2: clinical investigation of automated measurement type*. Arlington, VA: Association for the Advancement of Medical Instrumentation; 2013. Available at www.aami.org. [Accessed 10 August 2013]
18 Geddes LA, Voelz M, Combs C, Reiner D, Babbs CF. Characterization of the oscillometric method for measuring indirect blood pressure. *Ann Biomed Eng* 1982; **10**:271–280.
19 Stergiou GS, Lourida P, Tzamouranis D, Baibas NM. Unreliable oscillometric blood pressure measurement: prevalence, repeatability and characteristics of the phenomenon. *J Hum Hypertens* 2009; **23**:794–800.
20 Ursino M, Cristalli C. A mathematical study of some biomechanical factors affecting the oscillometric blood pressure measurement. *IEEE Trans Biomed Eng* 1996; **43**:761–778.
21 Babbs CF. Oscillometric measurement of systolic and diastolic blood pressures validated in a physiologic mathematical model. *Biomed Eng Online* 2012; **11**:56.
22 Liu J, Hahn JO, Mukkamala R. Error mechanisms of the oscillometric fixed-ratio blood pressure measurement method. *Ann Biomed Eng* 2013; **41**:587–597.
23 Talts J, Raamat R, Jagomägi K, Kivastik J. An influence of multiple affecting factors on characteristic ratios of oscillometric blood pressure measurement. 15th NBC on Biomedical Engineering & Medical Physics, IFMBE Proceedings. 2011; **34**:73–76.
24 ISO 81060-2:2018(E) Non-invasive sphygmomanometers – part 2: clinical investigation of intermittent automated measurement type. Available at www.iso.org. [Accessed 27 July 2020].
25 ISO 81060-2:2018/AMD 1:2020 Non-invasive sphygmomanometers – part 2: clinical investigation of intermittent automated measurement type – Amendment 1. Available at www.iso.org. [Accessed 27 July 2020].

Appendix B

Performance of the Algorithm Proposed to Automate Auscultation in Simulated Noisy Environments

The algorithm proposed to automate the measurement of BP through auscultation was developed considering the masking of a narrow-band sound by another narrow-band sound (noise). This applies to the mostly ideal case where the recorded measurement contains only electronic noise originated by the stethoscope. In order to address the possibility of other sources of noise in the signal, such as noise from a busy clinic, a separate analysis of masking of sounds is required. Namely, how a sound that is no longer narrow-band in its frequency spectrum affects our perception of KS, how it affects the auditory threshold of these KS, and how we can define a new set of *DL* between noise and test sounds. This would, of course, imply that the goal is now to develop a new algorithm specific to this new situation.

The algorithm in its current format can also be tested under these conditions, which would be akin to testing the performance of a potential device under different situations, even if they were not the intended use of the device. In this section, the author presents results of a couple of tests done on the algorithm that intend to simulate the case of a noisy environment. Measurements directly collected in a noisy environment with the setup used in chapter 3 were not available. Therefore, background noise was added after the fact to one of the original measurements used in said chapter.

The measurement used was selected from the 60 measurements used in chapter 3 on the basis that BP was correctly estimated with the algorithm, which made it an ideal control candidate. Two types of background noise were added to the original soundtrack: a segment

of a heavy metal song and helicopter sounds. The background sounds have the same duration as the original measurement, and the mixing and rendering of tracks was done with the free audio software Audacity. The resulting track were saved as a ".wav" file that could be played back and also processed in Matlab.

Ideally, when the stethoscope is placed in contact with the skin there should be no gaps in this contact to create a perfectly closed acoustic system. In reality, however, this is not the case, so external noise can be picked up by the stethoscope head-piece, which is the situation we are assuming with these examples. Additionally, even if the stethoscope detects external sounds, these will not be detected faithfully in terms of quality (frequency and amplitude of the original source), but they will rather appear attenuated or "muffled".

At present, it is difficult to gauge to what extent will external sounds be attenuated during a measurement with the Thinklabs One electronic stethoscope used for the analyses in this thesis. For this reason, before the mixing and rendering of the tracks, the background noise was separately attenuated at different levels to analyze the effect that each sound intensity had on the algorithm.

This attenuation was accomplished with the "Amplify" option in Audacity, and attenuations of -10, -15, -20 and -25 dB with respect to the original intensity were selected. Figures B.1a and B.2a show the comparison between the amplitude of the original segments of song and helicopter sounds, respectively, and their different attenuation options. Figures B.1b and B.2b show how their respective frequency spectrums compare after the application of a 6^{th} order Butterworth band-pass filter between the frequencies of 50 and 400 Hz with the Matlab software. From these figures we can already identify the presence of a larger number of harmonics in our background noises, other than the more specific mains and carrier frequencies present in our original measurements.

Figures B.3 and B.4 show the same type of information as figures B.1 and B.2, but now in this case we have the measured auscultation sounds mixed with the two types of background noise. Figures B.3a and B.4a represent the amplitude of the original measurement (labelled "Original") and the amplitude of the measurement mixed with the song and helicopter sounds attenuated to different levels, respectively. Figures B.3b and B.4b are the corresponding frequency spectrums after a 6^{th} order Butterworth band-pass filter has been applied between the frequencies of 50 - 400 Hz with the Matlab software.

To compare the performance of the algorithm to observer response, the mixed tracks

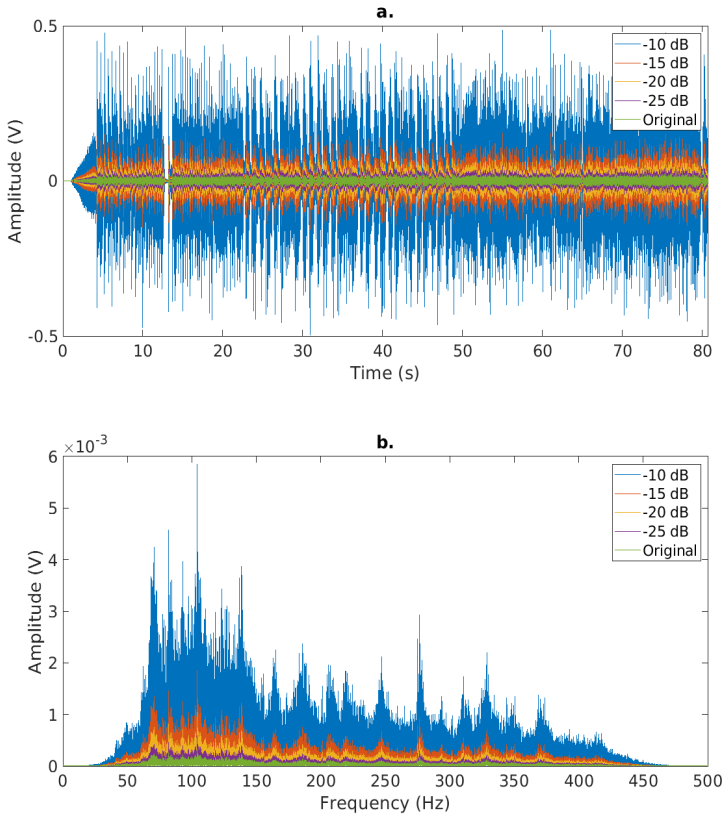

FIGURE B.1: a. Comparison of the original amplitude of the song segment and its different levels of attenuation. b. Frequency spectrum of the different song representations in a. after being band-pass filtered between 50 - 400 Hz by a 6^{th} order Butterworth band-pass filter.

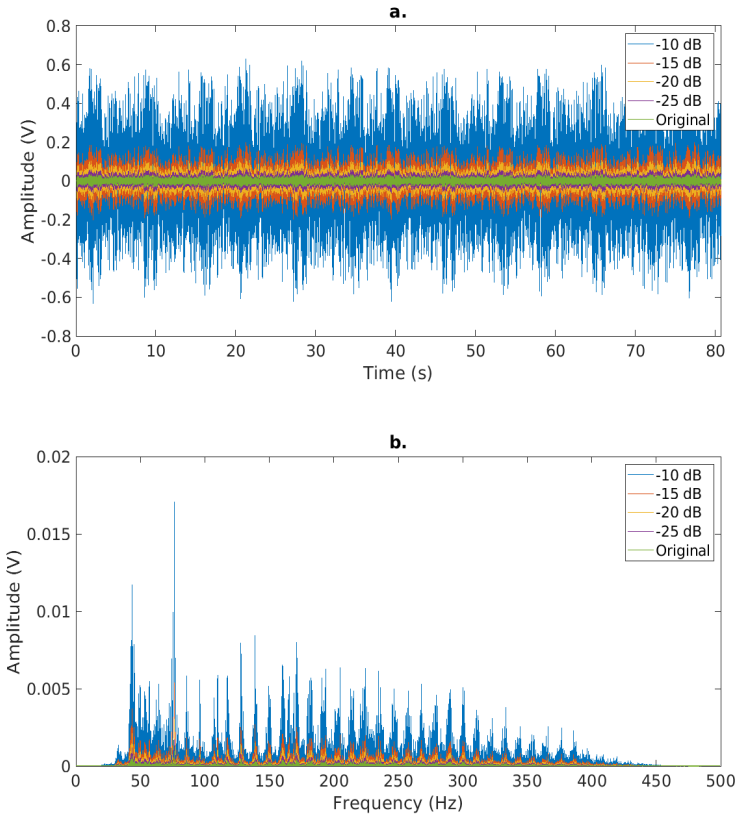

FIGURE B.2: a. Comparison of the original amplitude of the helicopter sounds segment and its different levels of attenuation. b. Frequency spectrum of the different sound representations in a. after being band-pass filtered between 50 - 400 Hz by a 6^{th} order Butterworth band-pass filter.

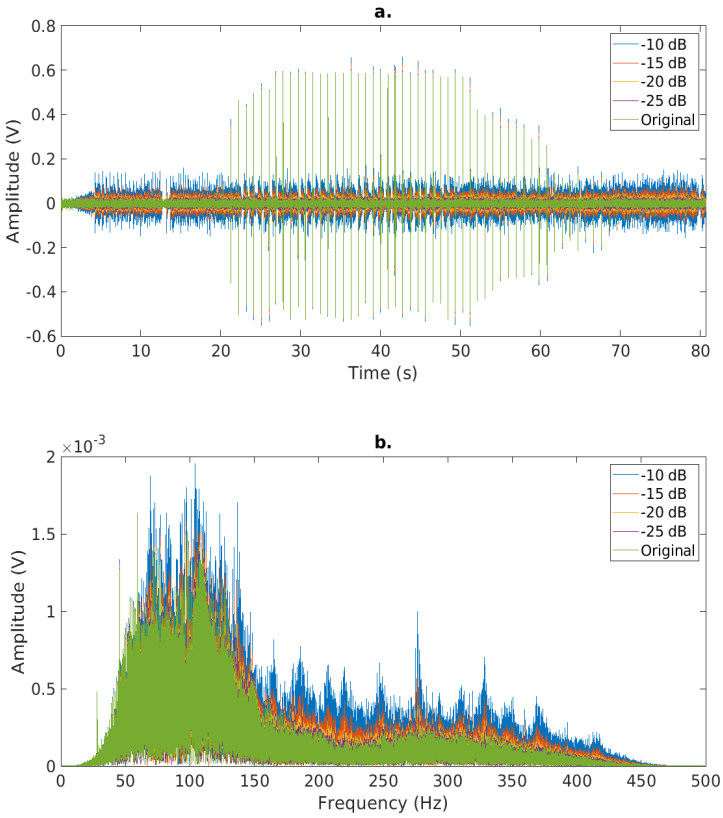

FIGURE B.3: a. Comparison of the original measurement and the different levels of attenuation of the measurement and song mix. b. Frequency spectrum of the different representations in a. after being band-pass filtered between 50 - 400 Hz by a 6^{th} order Butterworth band-pass filter.

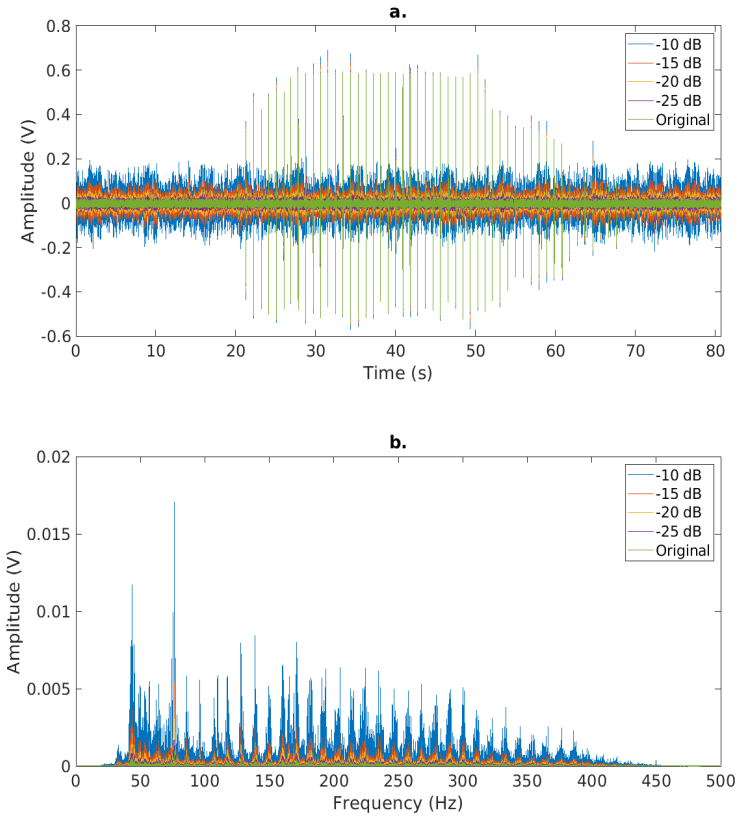

FIGURE B.4: a. Comparison of the original measurement and the different levels of attenuation of the measurement and helicopter sounds mix. b. Frequency spectrum of the different sound representations in a. after being band-pass filtered between 50 - 400 Hz by a 6^{th} order Butterworth band-pass filter.

TABLE B.1: Comparison between BP estimates of the observer and the algorithm for the measurement mixed with the song segment at different levels of attenuation. The true values of BP for the original measurement are given in the second row.

	SBP [mmHg] 96.51		DBP [mmHg] 48.04	
Level of Attenuation	Observer	Algorithm	Observer	Algorithm
-10 dB	93.76	N/A*	61.14	N/A*
-15 dB	93.76	94.74	55.82	56.56
-20 dB	95.65	94.74	51.02	52.55
-25 dB	96.51	94.74	51.02	49.34

*N/A = estimate could not be obtained.

were played in the Audacity software to identify how a human observer (the author) would estimate BP in these conditions. The tracks were high-pass filtered with a cut-off frequency of 50 Hz and a roll-off of 36 dB per octave with this software, and then low-pass filtered with a cut-off frequency of 400 Hz and a roll-off of 36 dB per octave, to mimic the band-pass filtering applied with Matlab. All tracks were listened to at the same volume level used in the development of the algorithm. This also confirmed that the noise is still perceived at the -25 dB level of attenuation.

The algorithm was finally applied in the same way that was presented in chapter 3, following the same steps of data processing and BP selection. Table B.1 shows the comparison between observer and algorithm estimates of BP for the case where the measurement was mixed with the song. Table B.2 shows this same comparison for the case where the measurement was mixed with the helicopter sounds. The true value of BP for this measurement is 96.51/48.04 mmHg for reference.

In the track where the song was mixed with the measurement SBP estimates from the observer were closer to the real value, while DBP estimates were closer in half of the measurements. In the case of the helicopter sounds mixed with the measurement we can see that the algorithm performed just as the observer in the SBP estimates, while the DBP estimates also had closer estimates in half the measurements.

From these results we can make a few observations:

TABLE B.2: Comparison between BP estimates of the observer and the algorithm for the measurement mixed with the helicopter sounds at different levels of attenuation. The true values of BP for the original measurement are given in the second row.

	SBP [mmHg] 96.51		DBP [mmHg] 48.04	
Level of Attenuation	Observer	Algorithm	Observer	Algorithm
-10 dB	94.74	94.74	62.20	56.56
-15 dB	94.74	94.74	56.56	54.22
-20 dB	94.74	94.74	51.02	53.52
-25 dB	95.54	95.54	51.02	54.22

1. As mentioned above, there is no real way to determine the extent of the background sound's intensity as recorded by the stethoscope during a real measurement. A real possibility is that the background noise that an operator is detecting comes from a deficient seal of the ear cavity by the ear-piece of the stethoscope. In this case, the stethoscope head-piece would not detect this sound and the results of the algorithm would be affected to a lesser extent. On the other hand, an example collected by the author with the original measurement setup may give some indication of whether the noise levels examined in this Appendix are appropriate. This example is shown in figure B.5, which is the case of a sound that the volunteer made during the measurement. The section of measurement represented in figure B.5 is no the lower pressure end and we can see, by comparison to figures B.3a and B.4a, that the amplitude of this sound is significantly smaller and does not obscure the information of the nearby KS. This is to say that, if this is the amplitude of a sound originating from the actual volunteer, then it is possible that the cases presented here of higher noise amplitude could represent at least the case of a busy clinic.

2. Even though the estimates of SBP from the observer were better in the case where the song was mixed into the measurement, it is possible that these measurements are biased. Previous knowledge of the song by the author of this thesis proved to be distracting while listening to the audio, but it may have also helped distinguish KS from the song's

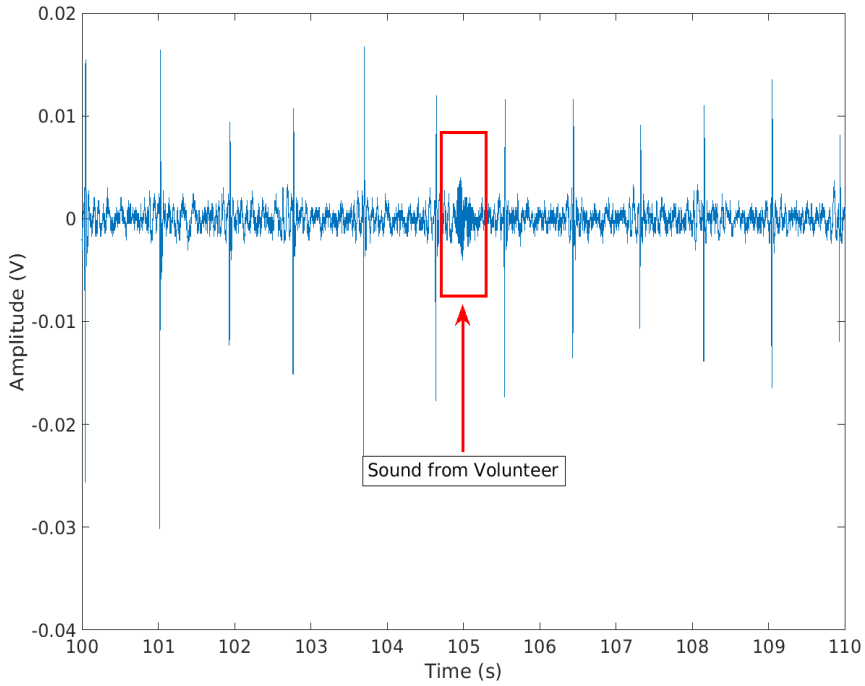

FIGURE B.5: Instance of a recorded sound produced by the volunteer during the measurement.

content. The fact that both algorithm and observer performed equally in the helicopter case at least for SBP estimation, may serve as confirmation of this.

3. The repetitive nature of the helicopter sounds may have similarly influenced the observer's judgement, although it is difficult to identify if the influence was positive or negative.

These observations demonstrate how the different type of frequency content considered in these examples has a different effect on human perception of KS. Nevertheless, further analysis of cases like the ones studied here may help us define these effects and a new method to process and interpret the measured data.

Finally, it is important to point out how, despite the less than ideal conditions that the algorithm was subject to here, the BP estimates are not far from those of a human observer in most of the cases. The accuracy of the estimates compared to the true value of BP is not

ideal, particularly that of DBP, yet the algorithm still accomplishes its goal of mimicking human response to a certain extent. It is possible that improving the algorithm for these types of situations may only require setting an additional number of frequency filters to obtain a "cleaner" signal.

Appendix C

Application of the Algorithm Proposed to Automate Auscultation to Measurements from the BIHS

The algorithm proposed to automate the measurement of BP through auscultation presented in chapter 3 should, ideally, be self sufficient. This means that, since its based on the observer's ability to perceive test sounds above the base noise of the stethoscope, here considered as the masking noise, then the algorithm should be applicable regardless of instrumentation (type of stethoscope) used. To verify this, the algorithm was applied to a set of measurements collected by the British and Irish Hypertension Society (BIHS).

These measurements are publicly available as YouTube© videos grouped in a playlist in the BIHS account, and a link to the videos, as well as a pdf with information on each measurement, is included in the BIHS webpage[1]. Permission to use them was obtained by electronic communication (e-mail). They consist of 29 measurements obtained from individuals with varying cardiovascular conditions, such as atrial fibrillation or tachycardia, and were intended to serve as interactive tutorials to teach how to apply the method of auscultation. The videos consist of the basic components of a manual measurement of BP through auscultation: the mercury manometer is shown with the height of the mercury column progressively decreasing, and the audio is a record of the sounds coming through a stethoscope.

Given the nature of the videos, once they are converted to files that can be processed in Matlab, the vectors produced only contain information of the sound amplitude measured in

[1]https://bihsoc.org/resources/bp-measurement/bp-measurement-auscultatory-tutorials/ *Last checked: January 12, 2022*

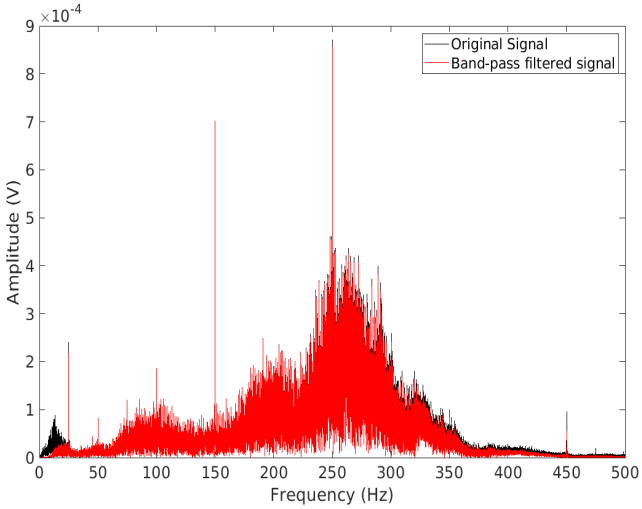

FIGURE C.1: Frequency spectrum of the full auscultation measurement (black) and the spectrum that remains (red) after the band-pass filter with edge frequencies between 20 and 400 Hz is applied.

volts. There is no corresponding pressure vector, so the only correlation that can be made to the measured BP is through the time vector. To do this, careful inspection of the videos and the obtained vectors must be made to ensure the right sound segments are chosen as KS, and furthermore, that the times corresponding to SBP and DBP are properly identified. These values were identified using the document provided by the BIHS, which includes the correct BP values for each measurement.

Three examples of the application of the proposed algorithm to these measurements are discussed below. The data was processed with some minor modifications. The bias in the signal is equally removed from the sound vector by subtracting its mean. Afterwards, the 6^{th} order Butterworth band-pass filter was modified to now have edge frequencies between 20 and 400 Hz, instead of 50 - 400 Hz as in chapter 3. An example of how this filter modifies the frequency spectrum of the data is shown in figure C.1. This was considered to be a better range of frequencies given that there is no information available on the type of stethoscope used to collect the measurements, nor on the method used to digitize them. Therefore, the lower frequency of the band-pass filter corresponds to the lowest frequency a human can perceive.

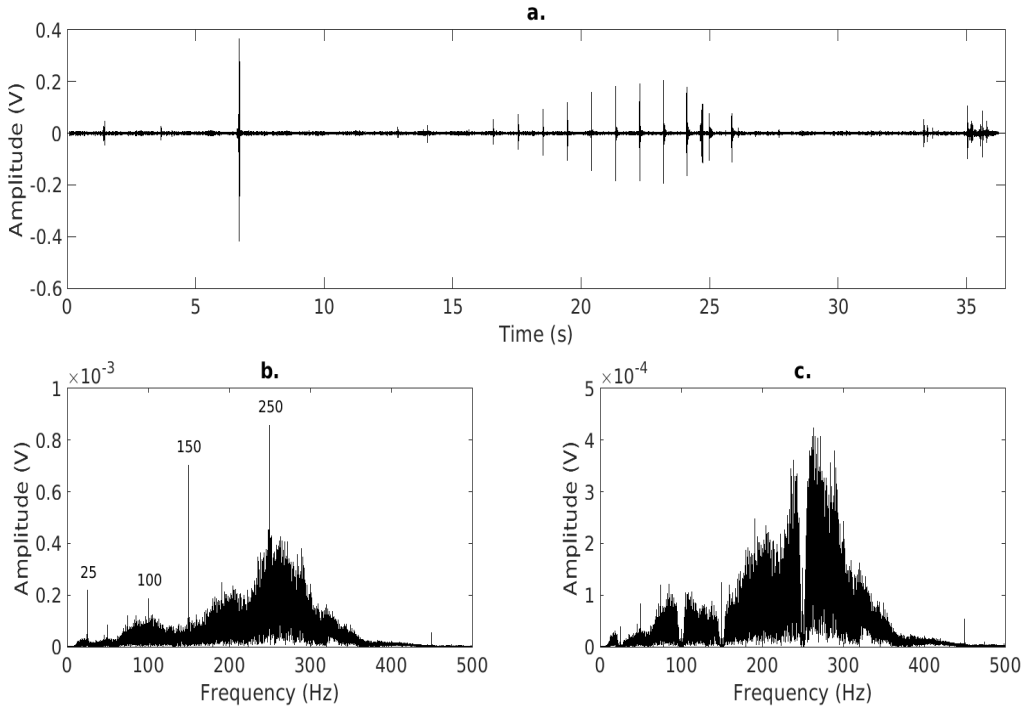

FIGURE C.2: a.Sound vector of the measurement labelled as BP11. b.Frequency spectrum of BP11 with the prominent frequencies of 25, 100, 150 and 250 Hz labelled. c.Frequency spectrum of BP11 after the labelled frequencies have been attenuated 15 dB with a Chebyshev Type II filter.

It was observed that these measurements also contained prominent frequency peaks at the mains and carrier frequencies as shown in figure C.2. In this case, however, we can see that these frequencies are different than those present in the measurements from chapter 3. The reason behind this is that the mains frequency in the European continent is 50 Hz instead of 60 Hz as in the American continent. Despite these differences, this doesn't really affect the algorithm since, as we may remember, in the training set the mains and carrier frequencies were manually selected and attenuated. In the case shown in figure C.2 the frequencies of 25, 100, 150 and 250 Hz were attenuated 15 dB using a Chebyshev Type II filter.

Once these filters were applied to the data, the rest of the procedure followed the same steps as in chapter 3. The sound vector was segmented into smaller sections. Those sections containing voltage amplitudes above the 0.5 mV threshold were used for analysis, resized

to 400-ms long segments, and the test and masking sounds were identified in each of these segments. Finally, their *SNR* was calculated for a bandwidth of 40 Hz centred at the test sound's highest energy frequency, and the *DL* of 4.2 dB was used to classify the sounds as audible and inaudible. The same criteria to locate SBP and DBP were applied to these measurements, and this selection was not affected by the lack of a baseline pressure since it only depends on the temporal relationship between segments identified as KS.

Figure C.3 shows the first example of how the algorithm estimated BP for the measurement labelled BP1 by the BIHS. Measured BP = 170/120 mmHg, and the document includes the following comment for this measurement:

> "Phase 1 is clearly heard at 170mmHg and auscultatory sounds continue until 120mmHg (*although with less amplification 122 mmHg may be the last sound heard*). This patient is in sinus rhythm. It is important to remember that the cuff pressure should be reduced at a rate of 2-3mmHg per second or per pulse beat. This cuff has been released too quickly".

For this measurement the frequencies 50, 100, 150, 200, 230 and 300 Hz were attenuated 15 dB with the Chebyshev filter and the sound vector was initially segmented into sections of 500-ms duration. SBP in this case was determined to be located at/near a time of 14.44 s, and the last audible Korotkoff sound is at/near 28.09 s. We can see from figure C.3 that the algorithm correctly located BP in this case.

The second example shown in figure C.4 corresponds to the case labelled BP5. In this case BP = 178/122 mmHg, and the comments for this measurement are as follows:

> "The subject is in atrial fibrillation. This column demonstrates the difficulties of estimating blood pressure in arrhythmias. In atrial fibrillation, stroke volume and hence blood pressure vary depending on the preceding pulse interval. Thus blood pressure will be a rough estimate which can perhaps be improved upon only by repeated measurements. A very soft sound can be detected at 120 mmHg with amplification."

In this case the frequencies 25, 50, 150, and 250 Hz were attenuated 10 dB and because of the irregular heartbeat, the sound vector was segmented into 400-ms long segments to avoid losing as much information as possible. The location of SBP was determined to be at/near a

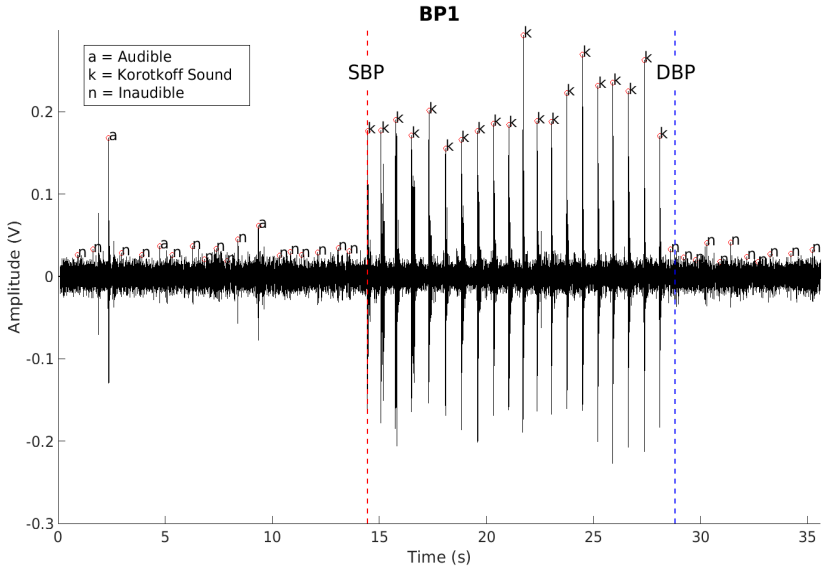

FIGURE C.3: Visual representation of the result obtained with the proposed algorithm for measurement BP1.

time of 13.94 s, and the last audible Korotkoff sound at/near 35.96 s. Unfortunately, in this case the algorithm located SBP at a time of 11.90 s, although it correctly located the last audible KS.

The third and final example is the one labeled as BP11, where BP = 104/86 mmHg, and the only comment for this case is: "The subject is in sinus rhythm". This is the same case shown in figure C.2, and the results of the algorithm are given in figure C.5. This sound vector was segmented into 700-ms long sections.

In this case SBP is located at/near a time of 16.59 s, and the last audible KS at/near 25.86 s. The algorithm correctly identified SBP, and while it also correctly classified the last audible KS as audible, the previous sound was classified as inaudible, causing the algorithm to ultimately locate DBP at the incorrect position. At a glance, one might infer why this was the case, however, a close-up of this is shown in figure C.6.

The sound segment that was incorrectly classified as inaudible, which corresponds to peak #26 shown in figure C.6a, contains two large voltage peaks. Because of the separation of the peaks with respect to those before and after, the second peak was selected as the test sound, making the preceding one as part of the masking sound. This, naturally, resulted in a

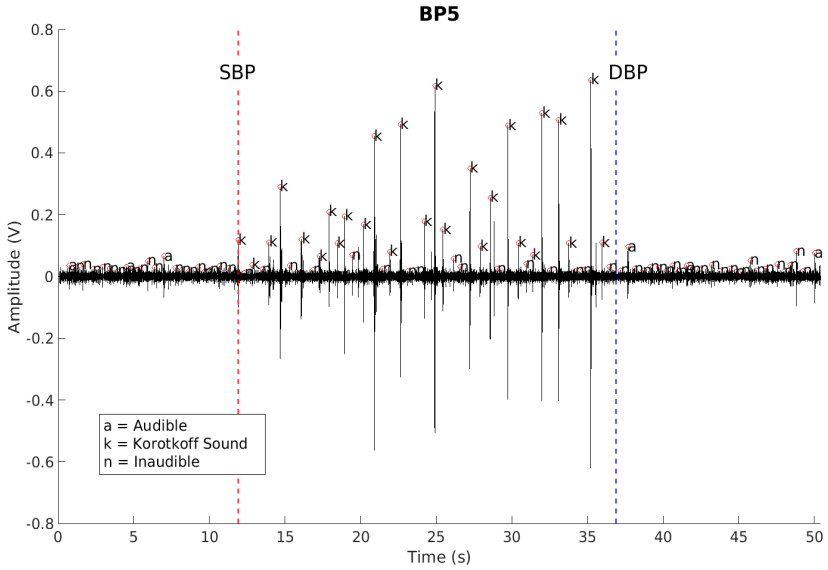

FIGURE C.4: Visual representation of the result obtained with the proposed algorithm for measurement BP5.

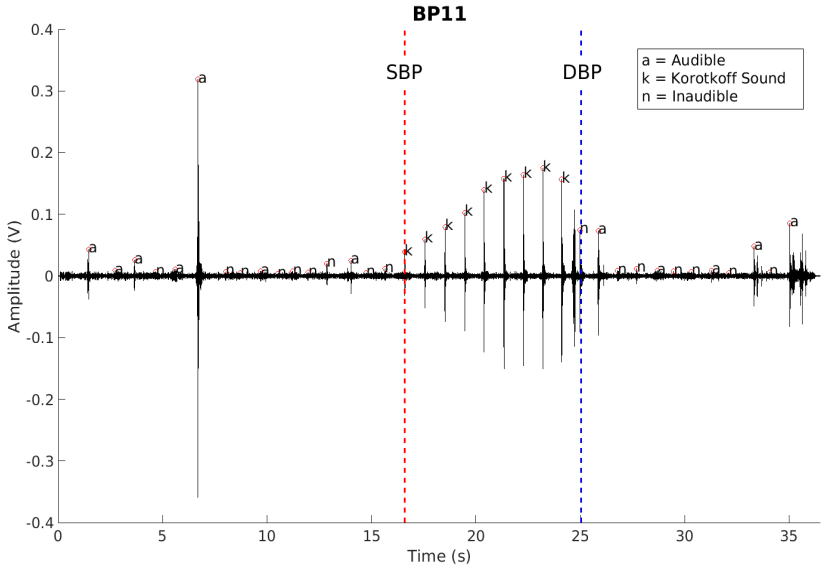

FIGURE C.5: Visual representation of the result obtained with the proposed algorithm for measurement BP5.

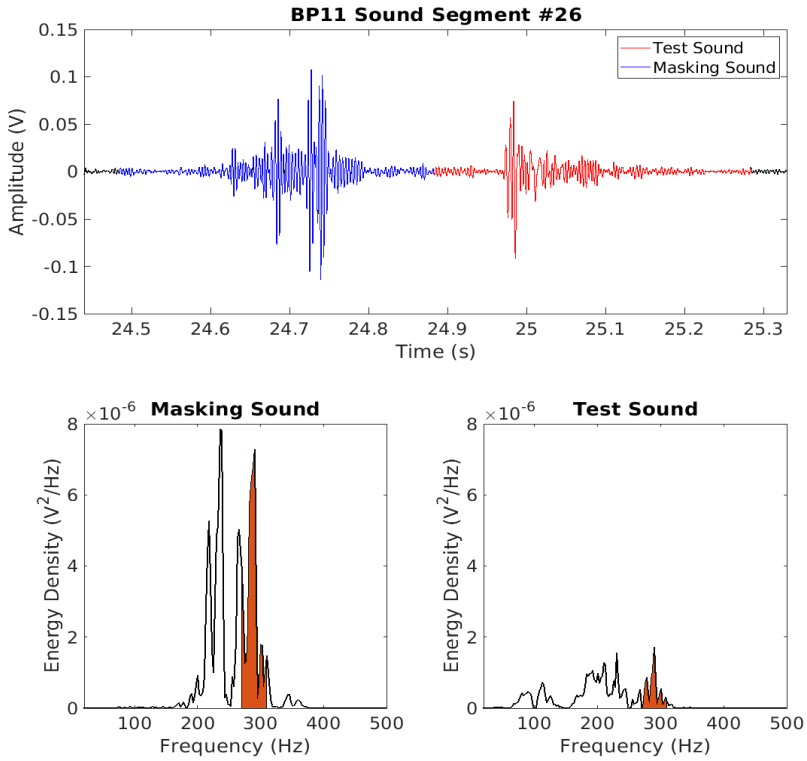

FIGURE C.6: a.Sound segment labelled as #26 for measurement BP11. Masking sound is coloured in blue and test sound in red. b.Energy density of the masking sound with the bandwidth used in the *SNR* marked by the coloured area. c.Energy density of the test sound. Relevant bandwidth is also represented by the coloured area.

SNR = -7.67. The energy density of the two sounds is shown in figures C.6b for the masker, and C.6c for the test sound. The masking sound is actually more energetic that the test sound.

The results presented in this Appendix show that the algorithm, in principle, can be applied to different instances of auscultation recordings. Measurement BP1 represents an ideal case, where the algorithm provides accurate results of BP, provided some adjustments are made first to accommodate for some differences. Situations present in case BP11 like that shown in figure C.6 are common, and it is very likely that these "double peaks" also affected some of the measurements discussed in chapter 3. A fail-safe set of instructions can

be added to the algorithm in the future for it to be able to deal with these cases where there is a very energetic peak selected as the masker. Overall the method works for case BP11, since the rest of the segments and SBP were correctly classified and located.

Measurement BP5 represents a more challenging situation, although the comments provided by the BIHS on this case already state that the value of BP given is but a rough estimate. In general, automated devices are not suited for subjects with atrial fibrillation, where the judgement of an expert is necessary. Nevertheless, the proposed algorithm obtained the answer for SBP given by the BIHS. It may be worth exploring the psychoacoustics of other cases of atrial fibrillation to determine if the relations used in this algorithm to identify SBP apply equally to this cardiovascular condition. At the moment, the algorithm in cases of atrial fibrillation could be a useful visual aid for the operator to identify audible sounds and make a more informed decision on the estimate of BP.

In conclusion, we can see that the proposed algorithm is mostly independent of instrumentation. The subject of frequency content and individual cardiovascular condition are certainly variables that should not be an obstacle for its performance. However, assuming the proposed algorithm is implemented into an automated device, the stethoscope or microphone used in the device would be fully characterized, so the filtering of the right frequencies would no longer be an issue. Another important thing to point out is how measurement BP1 corresponds to an individual with hypertension. The document from the BIHS doesn't explicitly state it, but a BP of 170/120 mmHg is well above the threshold of what is considered normal pressure. This indicates that the algorithm also performs accurately for hypertensive subjects, which is usually challenging in automated oscillometric devices. Other cardiovascular conditions need to be addressed more carefully, but it is possible that with further research a version of this algorithm can be catered specifically to different types of populations.

Appendix D

Spring Constants

Spring constant k_1 can be related to arterial wall parameters by considering the artery to be an elastic cylinder. Its cross-sectional area is a circular shell, like the one shown in figure D.1, of thickness h and neutral radius, r_o. Because of the curvature of the tube, the internal angular strain, $\sigma_{\theta\theta}$, produces radial strain, σ_{rr}, directed towards the centre of the artery. If the artery is in equilibrium, from basic trigonometry the strains are related as

$$\sigma_{rr} \cdot A_{rr} + 2 \cdot \sigma_{\theta\theta} \cdot \sin\left(\frac{\delta\theta}{2}\right) \cdot A_{\theta\theta} = 0 \tag{D.1}$$

where A_{rr} is the area perpendicular to the direction where strain σ_{rr} is directed, ansd $A_{\theta\theta}$ is the area perpendicular to $\sigma_{\theta\theta}$.

If we are considering a segment of length L the areas are: $A_{rr} = r_o\delta\theta L$ and $A_{\theta\theta} = hL$. With the small angle approximation, $sin(\delta\theta/2) \approx \delta\theta/2$, and substituting the areas in equation D.1, we arrive at a simple relationship between the strains:

$$\sigma_{\theta\theta} = \frac{r_o}{h}\sigma_{rr}. \tag{D.2}$$

Using the stress-strain relationships for an elastic solid given by

$$\varepsilon_{xx} = \frac{1}{E}[\sigma_{xx} - \nu(\sigma_{rr} + \sigma_{\theta\theta})] \tag{D.3a}$$

$$\varepsilon_{rr} = \frac{1}{E}[\sigma_{rr} - \nu(\sigma_{\theta\theta} + \sigma_{xx})] \tag{D.3b}$$

$$\varepsilon_{\theta\theta} = \frac{1}{E}[\sigma_{\theta\theta} - \nu(\sigma_{xx} + \sigma_{rr})] \tag{D.3c}$$

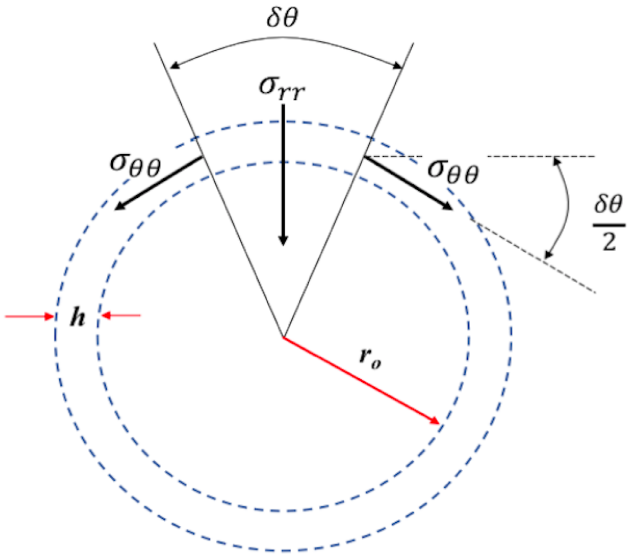

FIGURE D.1: Angular and radial strains in a section of arterial wall.

where E is Young's modulus and ν Poisson's constant, and the assumption that there is no movement in the longitudinal direction x, that is, that $\sigma_{xx} = 0$ and $\varepsilon_{xx} = 0$, we have

$$\varepsilon_{\theta\theta} = \frac{\sigma_{rr}}{E} \cdot \frac{r_o}{h}, \tag{D.4}$$

where we have assumed that the ratio $r_o/h >> \nu$.

The angular strain will also cause a change in the artery's radius from its neutral radius, r_o, to a radius $r_o + \Delta r$. The angular strain can, therefore, be expressed in the change in arc length that results from this change in radius:

$$\varepsilon_{\theta\theta} = \frac{(r_o + \Delta r)\delta\theta - r_o\delta\theta}{r_o\delta\theta} = \frac{\Delta r}{r_o}. \tag{D.5}$$

Substituting this in equation D.4, and solving for the stress:

$$\sigma_{rr} = \frac{Eh}{r_o^2}\Delta r \tag{D.6}$$

which we can finally relate to a force applied in the radial direction on the perpendicular area A_{rr} mentioned above as

$$F_{rr} = \frac{Eh}{r_o} \cdot \delta\theta L \cdot \Delta r, \tag{D.7}$$

and from this expression relate the spring constant k_1 to the parameters of the arterial wall:

$$k_1 \approx \frac{Eh}{r_o} \cdot \delta\theta L. \tag{D.8}$$

When the artery is deformed by an external pressure and its cross-sectional area resembles an ellipse or hourglass, the restoring force F_{S2} can be assumed to arise from bending moments that result from the external force and from the compression and extension of the arterial wall. When the artery flattens, the curving of the arterial wall at the extremes of the "ellipse" will result in perpendicular compressive stresses below the neutral axis, as shown in figure D.2 by the arrows labeled as σ_C, and in perpendicular tensive stresses above the neutral axis, labelled σ_T in figure D.2. These stresses will shorten or lengthen the wall, respectively, causing a change in arc length at these sections.

Based on the scheme in figure D.2, we assume that the neutral axis of the wall is located a distance y from the zero P_t radius, r_o. The plane parallel to this neutral axis will not suffer any change in length from the stresses. The strain relative to this segment can be expressed as

$$\varepsilon = \frac{r_o\delta\theta - (r_o + y)\delta\theta}{(r_o + y)\delta\theta} = \frac{y}{r_o + y}, \tag{D.9}$$

which, from equation D.3, is related to the stresses by

$$\sigma = E \cdot \varepsilon_{\theta\theta} = E\frac{y}{r_o + y} \tag{D.10}$$

where once more we consider no stress in any of the other two directions. The moment generated by this stress is $r\sigma dA$, where r refers to the distance where the force σdA is applied at. The area dA is considered for a wall segment of length L. The moment here will therefore be equal to

$$M = \int_0^h (r_o + y) \cdot E\frac{y}{r_o + y} \cdot L dy = \frac{1}{2}ELh^2. \tag{D.11}$$

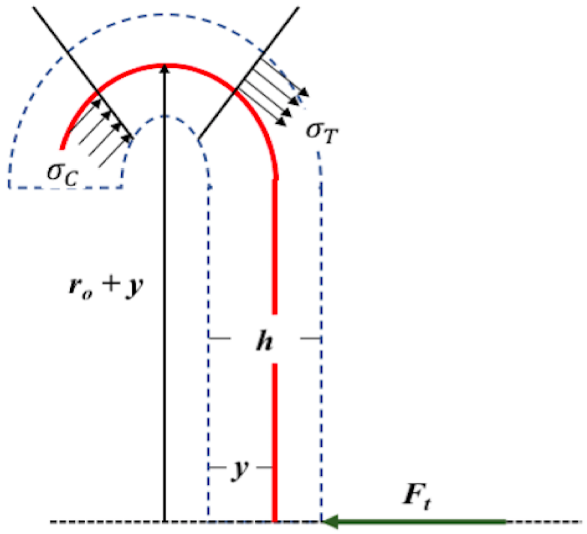

FIGURE D.2: Stresses and forces generating bending moments in the arterial wall.

The compressing force $F_t = P_t A$ is assumed to be distributed along the straight portion of the artery wall, but replaced by an equivalent force at the centre, as shown in figure D.2. The moment originating from this force is calculated as

$$M = \int_0^{\pi r_o/2} y P_t L dy = \frac{1}{2} \cdot P_t L \cdot \frac{\pi^2}{4} r_o^2. \tag{D.12}$$

The balance of moments gives an expression for the pressure P_t in terms of arterial parameters:

$$P_t = \frac{4E}{\pi^2} \cdot \frac{h^2}{r_o^2}. \tag{D.13}$$

As stated above, the pressure P_t is the result of the force F_t applied over an area A. This area, in turn, can be written as $A = r\delta\theta L$ for a segment of the wall, such that $F_t = P_t \delta\theta L r$. This is reminiscent of the expression for any force applied at a distance r: $F(r) = kr$, where the spring constant is then $k = P_t \delta\theta L$, or using equation D.13:

$$k_2 \approx 4\frac{E}{\pi^2} \cdot \frac{h^2}{r_o^2} \cdot L\delta\theta. \tag{D.14}$$